

MEASUREMENT AND MODELING OF INTRAVEHICULAR CHANNELS FOR
MULTIANTENNA COMMUNICATION

by

Alyssa Magleby Richards

A dissertation submitted to the faculty of
The University of Utah
in partial fulfillment of the requirements for the degree of

Doctor of Philosophy

Department of Electrical and Computer Engineering

The University of Utah

May 2011

Copyright © Alyssa Magleby Richards 2011

All Rights Reserved

The University of Utah Graduate School

STATEMENT OF DISSERTATION APPROVAL

The dissertation of Alyssa Magleby Richards
has been approved by the following supervisory committee members:

<u>Cynthia M. Furse</u>	, Chair	<u>10/29/2010</u> Date Approved
<u>Behrouz Farhang Boroujeny</u>	, Member	<u>10/29/2010</u> Date Approved
<u>Neal Patwari</u>	, Member	<u>10/29//2010</u> Date Approved
<u>Rong Rong Chen</u>	, Member	<u>10/29//2010</u> Date Approved
<u>Osama S. Haddadin</u>	, Member	<u>10/29//2010</u> Date Approved

and by Gianluca Lazzi, Chair of
the Department of Electrical and Computer Engineering

and by Charles A. Wight, Dean of The Graduate School.

ABSTRACT

Wireless communication has become an essential part of everyday life. The hunger for more data, more phone calls, more video, and more access in more places, including vehicles, is growing massively. Communication in vehicles is particularly challenging because of their extremely high multipath environment. In addition, there is significant interest in reducing the number of wires in vehicles to reduce weight, complexity, maintenance, etc. and replace them with wireless systems. Preliminary research shows that MIMO systems take advantage of the extreme multipath environment found in aircraft and other vehicles and also provides more consistent channel capacity than SISO systems.

The purpose of this research was to quantify complex channels (including the aircraft/vehicle environment) and their relation to other environments, evaluate MIMO in aircraft, provide design constraints for accurately modeling complex channels, and provide information to predict optimum antenna type and location to enable communication in aircraft/cars/buses/ships/trains/etc. and other extreme channels. The ability to evaluate and design MIMO technologies from the guidelines in this paper is potentially transformative for aircraft safety – enabling a new generation of location specific monitoring and maintenance.

Average measured capacity was found to be between 18 and 21 bits/s/Hz using a 4x4 array of antennas, and had no direct relation to the size of the channel. Site-specific

capacity showed a multipath rich channel, varying between 15 to 23 bits/s/Hz. The capacity decreased for increasing measurement distance, with exceptions near reflective objects that increase multipath. Due to these special circumstances for site-specific locations within complex channels, it is recommended that 3D ray tracing be used for modeling as it is more accurate than commonly used statistical models, within 1.1 bits/s/Hz. This showed that our 3D ray tracing is adaptable to various environments and gives a more accurate depiction than statistical models that average channel variations. This comes at the cost of greater model complexity. If increased complexity is not desirable, Nakagami 1.4 could be used as the next most accurate model.

Design requirements for modeling different complex channels involve a detailed depiction of channel geometry, including height, width, length, shape (square, cylindrical, slanted walls, etc.), large windows, and reflective objects inside the channel space, especially those near the transmitter. Overall, the multipath rich channel found in vehicles is an excellent environment for MIMO systems. These complex channels can be simulated accurately without measurement and before they are even built using our site-specific 3D ray tracing software combined with a detailed signal model to incorporate antenna effects.

I dedicate this dissertation to my parents, Marvin and Patricia Magleby, and to my loving
husband, Aaron.

TABLE OF CONTENTS

ABSTRACT.....	iii
LIST OF TABLES	ix
ACKNOWLEDGMENTS	x
Chapter	
1 INTRODUCTION.....	1
1.1 The Need for Wireless in Vehicles.....	1
1.2 Contributions	5
1.2.1 Channel Measurement and MIMO System Evaluation	6
1.2.2 MIMO Channel Model for Complex Environments.....	7
1.2.3 MIMO Network System Design Specifications	8
1.3 Summary	9
1.4 Publications	12
1.5 References	12
2 WIRELESS COMMUNICATION FOR SENSOR NETWORKS	16
2.1 The Need for Wireless Sensor Networks in Aircraft and Other Vehicles	16
2.2 Communication Systems for Aircraft	16
2.2.1 Spread Spectrum Sensing System.....	17
2.2.2 Ultra Wideband (UWB)	20
2.2.3 Multiple Input, Multiple Output (MIMO).....	21
2.3 Prior Measurements and Simulations	26
2.4 Complex Channel Modeling	29
2.4.1 Statistical Models.....	31
2.5 Why MIMO for Wireless Sensor Networks.....	34
2.6 References	34
3 TOOLS AND PRELIMINARY STUDIES	41
3.1 SISO Measurements in Multipath Channels	41
3.2 MIMO Simulations in Hyper-Rayleigh Channel.....	43
3.3 Multiantenna Test Bed for Channel Measurement	47

3.4	3D Ray Tracing Software.....	51
3.4.1	Initial Validation of 3D Ray Tracer for Aircraft.....	57
3.4.2	Initial Power Mappings	60
3.4.3	Extension to MIMO	62
3.5	Reflective and Lossy Obstacles Within the Channel.....	65
3.5.1	Seat Measurements	65
3.5.2	Wall Simulations.....	68
3.6	Summary	69
3.7	References	69
4	3D SIMULATION OF WIRELESS CHANNEL IN SMALL AIRCRAFT	72
4.1	Abstract	72
4.2	Introduction	72
4.3	3D Ray Tracing Software.....	76
4.4	Quantification of the Aircraft Communication Environment	83
4.5	Variation of Parameters	91
4.5.1	Number of Facets.....	91
4.5.2	Site Specific Obstacles.....	92
4.5.3	Maximum Allowed Reflections.....	93
4.5.4	Electromagnetic Parameters	94
4.6	Conclusion.....	95
4.7	Acknowledgment.....	97
4.8	References	97
5	MEASUREMENT AND SIMULATION OF THE MULTIAN TENNA COMMUNICATION CHANNEL ON A SHUTTLE BUS	101
5.1	Abstract	101
5.2	Introduction	102
5.3	Bus Measurements and Mapping	104
5.4	Model Accuracy	111
5.5	Other Modeling Techniques.....	116
5.6	Conclusion.....	121
5.7	Acknowledgment.....	122
5.8	References	123
6	WIRELESS CHANNEL MEASUREMENTS AND MODELING IN A HELICOPTER	126
6.1	Abstract	126
6.2	Introduction	126
6.3	Quantification of the Bell OH-58A Helicopter Wireless Channel	128
6.4	3D Ray Tracing Modeling.....	134
6.5	Statistical Models.....	139
6.6	Conclusion.....	142

6.7	Acknowledgment	143
6.8	References	143
7	COMPLEX CHANNEL MEASUREMENT AND MODELING FOR THE DESIGN OF WIRELESS SYSTEMS.....	146
7.1	Abstract	146
7.2	Introduction	147
7.3	Complex Channel Measurement	149
7.3.1	Rockwell T-39 Sabreliner.....	150
7.3.2	Beech Baron 58P.....	151
7.3.3	2004 Thomas Bus 110YN	154
7.3.4	Bell OH58 Helicopter.....	155
7.3.5	Underground Cement Tunnel	157
7.3.6	Basement Concrete Tunnel.....	159
7.4	Complex Channel Modeling	163
7.5	Conclusion.....	167
7.6	Acknowledgment	168
7.7	References	168
8	CONCLUSION AND FUTURE WORK	171
8.1	Contributions	171
8.1.1	3D Ray Tracing Model.....	171
8.1.2	Quantification of Vehicular Channels.....	172
8.1.3	Comparison to Statistical Models	175
8.2	Future Work	177
8.3	References	178
	APPENDIX: 3D RAY TRACING TUTORIAL.....	180

LIST OF TABLES

2.1: Electromagnetic spectrum for aircraft communication and navigation equipment combined with frequencies for personal electronic devices (PED) (overlapping frequencies with bold outline).....	18
3.1: K values for environments with various levels of multipath	43
3.2: K and Δ values for channel models	44
3.3: MIMO test bed system parameters.....	49
3.4: Parameter grouping for ray tracing software	54
3.5: Chair loss measurements in anechoic chamber.....	68
5.1: Statistics on absolute error (bits/s/Hz) of capacity comparisons for various channel models, with the minimum for each category in bold and italics.	120
7.1: Average measured capacity for complex channels in relation to transmitter location and distance.	163
7.2: Average error, maximum error and percent of locations error was best (minimum) for complex channels simulated with various modeling techniques.	166

ACKNOWLEDGMENTS

I would like to first thank my advisor, Dr. Cynthia Furse, for all the guidance and encouragement she has given me throughout my college career because I would not be where I am without her. She has helped me develop skills and confidence in teaching, mentoring and conducting research. She saw the capacity in me to succeed when I could not see it myself, giving me the motivation to finish what I started. She has prepared me well for whatever my future may hold.

I thank my committee members, Osama Haddadin, Behrouz Farhang-Boroujeny, Neal Patwari, and Rong-Rong Chen, for patience through my slow progress, and their help in making this a better dissertation through their content recommendations and research suggestions.

Much thanks to my measurement team, James Nagel and Sai Ananthanarayanan. Not only were they key to all of the measurements taken, but also gave me encouragement during difficult times, and helped me gain better understanding through our collaboration and discussion. Our measurements would also not have been possible without the help of Randy Chesley, Utah State University, Logan Airport and the University of Utah Transportation services and I thank each of them for allowing us to come and measure their vehicles.

This work was supported by the US Air Force Research Laboratories (AFRL) through a grant from Universal Technologies Corporation and the National Science

Foundation under grant ECCS-0823927. Permission to reproduce work submitted to the IEEE Transactions on Vehicular Technology, and the Journal of Microwave and Optical Technology Letters is gratefully acknowledged.

I also thank my family and friends for their continued love and support in this endeavor. I especially thank my husband for his support, encouragement and for taking such good care of me through this long and difficult process. I dedicate my dissertation to them.

CHAPTER 1

INTRODUCTION

1.1 The Need for Wireless in Vehicles

Future communication systems hold promise for streaming video to mobile handsets, coupled with real-time interaction with that video, personalized data transmission and medical assessment on the fly. The generation of personalized remote access, interaction, assessment, and control has barely scratched the surface of its planned potential. Communication and information – the keys to power and wealth in this generation – are no longer anchored to expensive, government-controlled infrastructures, but can be quickly deployed throughout countries and global communities who have been isolated and limited for generations. Notwithstanding the massive social implications of this new communication environment, the hunger for more data, more phone calls, more video, more access is growing massively, challenging the availability of spectral resources and infrastructure. Traditional communication systems are nearing their maximum potential and cannot provide the linkages needed for future generations of ‘screaming’ video, voice, and data transmission. Paradigm shifts are needed in order to achieve the anticipated worldwide demand for immediate personalized broadband communication, and to squeeze the most out of the fledgling wireless infrastructure in developing countries. A new concept showing great promise for improving

communication in complex channels is using Multiple-Input Multiple-Output (MIMO) systems which employ multiple antennas to extract multiple effective channels from the rich multipath scattering present in most environments. There is somewhat of a debate in scholarly circles about the differences between MIMO and multiantenna systems, but they will be used interchangeably throughout this paper.

Our initial interest in MIMO communication for complex channels stems from a critical safety application that has been the focus of much of our previous research¹. Aging electrical wiring systems have been identified as an area of critical national concern [1][2][3]. For aircraft, where both preventative and responsive maintenance are taken very seriously, aging wiring is a very expensive problem. Electrical wiring problems in the US Navy cause an average of two in-flight fires every month, more than 1,077 mission aborts, and over 100,000 lost mission hours each year [3]. Each year the Navy spends from one to two million man-hours finding and fixing wiring problems [4]. A majority of the man hours spent locating faults are on intermittent faults that occur in flight but are not easily replicated on the ground. TWA 800 and SwissAir 111 are now infamous crashes caused by intermittent faults on electrical wiring. Both of these aircraft had multiple intermittent precursors to the in-flight short circuits and subsequent explosions that caused their demise. One new method of locating these faults is Spread Spectrum Time Domain Reflectometry (SSTDR), which is capable of locating intermittent electrical faults on live aircraft wiring, in flight, with an accuracy of +/- 1 foot (the length of an aircraft interior panel) in less than 5 ms (the duration of an

¹ Much of this introduction and certain segments of this paper were written as part of a group effort in preparing and submitting a joint NSF proposal in Feb 2008. The tasks described in this paper represent my contributions to the proposed work effort.

intermittent wet arc). [5] This technology, now sponsored by NSF, USAF, Navair, NASA, FAA, and others, is being commercialized by LiveWire Test Labs, a university spin-off company, in partnership with several companies who build aircraft components.

Another method is Vernier Time Domain Reflectometry that was integrated into a prototype chip for intermittent fault location [6]. Current data links for these devices are either infra-red (for the AFCB) or hard-wired (for the remote power distribution systems or Smart Connector). A wireless data link is needed for the widespread deployment of the Smart Connectors and Arc Fault Circuit Breakers, shown in Figure 1.1, into regions of the aircraft that are otherwise inaccessible.

The major challenge of retrofitting old aircraft with sensors is how to collect the data. Wire fault location sensors are not the only sensors of interest. Aircraft maintainers would like to add numerous pressure, temperature, vibration, fuel quantity, and moisture/chemical sensors. Aircraft that are 20 years old today were designed about 30 years ago. Aircraft being designed today have an expected life span of 100 years.



Figure 1.1: Smart Connectors (Left) and Arc Fault Circuit Breakers (right, approx. 1” square) are two applications currently being commercialized. Current data links are infrared or hard-wired. Wireless communication will enable large-scale deployment in regions of the aircraft that are otherwise inaccessible.

Electronics have/will continue to progress over that time, and there are many compelling reasons to retrofit new technology into old aircraft. The major challenge is the data link to control sensors or to enable the sensors to control other things.

Wireless data transfer in aircraft has been identified as a ‘transformative’ technology for aviation. Yet, as we all know, cell phones and other wireless devices have not been allowed on aircraft until the recent addition and limited use of WiFi [7][8]. The industry is pursuing wireless prospects, but so far all are limited by the extreme multipath channels in aircraft. It was observed in [9] that spread spectrum communication was extremely limited in aircraft because of the multipath channels, but ultra wideband communication was effective. However, [10] has documented problems with ultra wideband communication interfering with aircraft radios, even when operated at approved, ‘safe’ levels.

In order to add wireless communications, we must be able to overcome the challenge of the extreme multipath environment. Due to the aforementioned difficulties with ultra wideband and spread spectrum communication in aircraft, we have chosen to explore MIMO for our wireless communication. The design of an optimal (or even a sufficient) MIMO system depends heavily on the accuracy of the channel model. MIMO has been extensively used in other multipath channels, but little has been done to characterize its use in complex channels such as aircraft and other vehicles. Today’s models do not include an accurate representation of non-Gaussian, ultrareflective, depolarizing, and highly lossy channels seen in many personal communication channels, body-worn or implanted medical communication channels, highly reflective and lossy (‘hyper-Rayleigh’) channels common in vehicular communication for sensor networks

inside aircraft, cars, buses, trains, ships, etc., most wireless ad-hoc network environments, or the human body scattering channel for medical imaging. This research provides an advanced channel model for MIMO as well as a characterization of several complex channels measured with a MIMO system. This will enable specialized MIMO design for each application, providing a far greater probability of initial success for the deployed systems. As MIMO theory advances, so must its validation tools. The theory developed in this research and other recent work was verified on an enhanced MIMO test bed that can measure the effects of the complex channel, number, orientation, type, polarization and spacing of antennas [12][13][14].

1.2 Contributions

The purpose of this research was to quantify complex channels (including the aircraft/vehicle environment) and their relation to other environments, evaluate MIMO in aircraft, provide design constraints for how to accurately model these complex channels, and provide information to assist in predicting which antenna type and location are best to enable communication in aircraft/cars/buses/ships/trains/etc. and other extreme channels. The ability to evaluate and design MIMO technologies from the guidelines in this paper is potentially transformative for aircraft safety – enabling a new generation of location-specific monitoring and maintenance. And once we can evaluate and optimize MIMO for the complex aircraft channel, we can also study and hopefully optimize other complex channels, as well – reflective and lossy channels with multiple sensors interacting in wireless ad hoc networks indoors or outdoors (including tunnels, culverts, stream beds, etc.) or the human body, where MIMO may be used to enhance microwave

breast cancer detection [11]. These applications provide a good cross section of the multitude of complex channels where MIMO may excel. This dissertation will focus on the intravehicle application. We have chosen to focus on intravehicular links because they have extreme multipath (much like a reverberation chamber) and (if the aircraft is flying) significant electromagnetic noise, which noise effects are explored in a joint research effort with this paper [26][27].

1.2.1 Channel Measurement and MIMO System Evaluation

MIMO research (ours included) is wedded in either theory or measurement with only limited cross section of the two. One of my goals in this research was to characterize MIMO capacity performance in complex channels through measurement and analysis. Preliminary measurements with our initial single-antenna system test bed showed sufficient multipath that we expected MIMO would work well in this environment. In coordinating research, enhancements were made to the MIMO test bed to enable taking measurements in a variety of complex channels to validate the modeled signal, noise and interference theories [13]. The updated test bed is described in section 3.3. Measurements taken with this system will be used to validate our 3D MIMO ray tracing software and evaluate in which situations it is more beneficial than statistical models.

MIMO performance in aircraft will be obtained using complex channel matrices. We wish to determine appropriate channel matrices for intravehicle and other highly-lossy complex multipath channels. We will include channel effects using the comprehensive detailed signal model (DSM) from previous work [14]. We will simulate

MIMO performance in each complex channel and compare with common statistical channel models (Gaussian, Weibull, Nakagami) as well as measured data.

We used the MIMO test bed to complete the characterization of MIMO communication in a selection of complex channels. Intravehicle communication was tested using several aircraft, a bus, a helicopter, and two tunnels. I have also quantified the critical factors in the simulation tools, in order to prescribe the simplest possible approaches for modeling complex channels.

1.2.2 MIMO Channel Model for Complex Environments

One of the goals of this research was to adapt a comprehensive MIMO capacity model (also referenced as the detailed signal model (DSM)) to selected complex channels. Channel models represent how the multipath environment impacts the MIMO capacity. Channel models are environment specific. For general MIMO applications the channels have been assumed to be Rayleigh or Gaussian, however these are not sufficient for modeling the intravehicle environment (which has a varying range of fading statistics anywhere from Ricean to hyper-Rayleigh, depending on the vehicle and location within it), ad-hoc networks (non-Gaussian), or scattering within the human body (highly lossy). Thus we will evaluate the accuracy of a new site-specific 3D ray tracing software (detailed in section 3.4) as an alternative to the statistical models that only provide an average for the whole channel. The 3D ray tracing model will be compared with the Gaussian model [23] and other statistical models that have been used for channels with severe multipath, including Weibull [20], Nakagami [22], and hyper-Rayleigh [15].

Another goal was to quantify and evaluate MIMO performance in complex intravehicle channels. The Gaussian, Weibull, Nakagami, and hyper-Rayleigh channel models for complex channels available in the SISO literature have been converted to their MIMO counterparts. These channels were then integrated with the MIMO capacity equation (part of the DSM) to evaluate the capacity and SNR of complex channels. The noise models are also being evaluated in these complex channels, using the methods developed in coordinating research [27]. The DSM is MIMO simulation software that was created to include the antenna effects of directivity, antenna efficiency, antenna radiation pattern, mutual coupling, rotation, and polarization agility on capacity. The DSM has been shown to accurately predict MIMO performance using various 2D channel models [17]. This will be used to evaluate MIMO performance in aircraft in comparison to the hyper-Rayleigh [15] and other statistical channel models. The inputs to the DSM include channel parameters that make up the channel matrix, such as K factor, noise effects, path gain, angles of arrival and departure, etc. The output of the DSM simulation is a CDF capacity curve. Simulated capacities have been compared with the capacity obtained using the normal Gaussian model to determine if the differences in system design justify the need for these complex models, and to improve flexibility for simulation as the Gaussian model is strongly based on K values obtained from measurement.

1.2.3 MIMO Network System Design Specifications

An evaluation of MIMO performance in various complex channels will provide some of the tools necessary to design a wireless sensor network for aircraft. Channel

capacity and network coverage have been used as a basis for Grade of Service (GOS) requirements for telephony services [24] and are a natural way of showing the performance of wireless networks. Channel capacity can be defined as an upper bound on the rate of reliable transfer of data across a communication channel. Network coverage can be obtained by looking at the level of capacity available at different site-specific locations within a network's transmission range and making sure this capacity is above minimum requirements. These parameters will be used in the analysis and quantization of the complex vehicular channels studied in this paper. Complex channels will also be compared with one another to determine if a generic MIMO system could be designed or if each channel requires specific design constraints. This information will assist in optimizing channel performance and providing the best placement of sensors in a complex enclosed environment.

1.3 Summary

This dissertation first provides a detailed explanation of the adaptation of a new 3D modeling software which uses ray tracing to accurately model site-specific locations in complex vehicular environments [32][26]. It then provides quantification of three vehicular channels using multiantenna measurement and from this develops a parameterization of each environment to show what level of detail is required to obtain accuracy. It offers a comparison of the site-specific 3D modeling to various common statistical models and details appropriate circumstances in which to use each. It concludes with an analysis of the three complex channel environments described in this

research along with several other vehicular channels measured in concurrent research to determine common system modeling and design parameters.

The format of this dissertation is as follows:

Chapter 2 explores the need for wireless networks in vehicles, as well as what has been done thus far to quantify aircraft and other complex channels and discusses the attempts to communicate wirelessly in this environment. It then describes state of the art technologies related to this application, including Ultra Wideband (UWB) and Multiple-Input Multiple-Output (MIMO) systems. It also details the reasoning behind our focus on a site-specific model for MIMO.

Chapter 3 describes tools and preliminary research used as a basis for later measurement and analysis. This includes a full description of our key measurement tool, the MIMO system test bed, as well as our new simulation tool, 3D ray tracing software. It describes initial verification of our adaptation of the 3D ray tracing software, as well as other preliminary studies involving the reflective or lossy obstacles inside vehicles.

Chapter 4 discusses a site-specific 3D ray tracing modeler which uses the triangular grid method to improve computational efficiency, decreasing the CPU time needed to only 25%-30% of what is required for typical ray tracing methods [32]. It has been validated and used to estimate location specific channel performance in 2D indoor/outdoor environments as well as the 3D environment of a stairwell [32][33][26]. This ray tracer has been adapted to simulate the reflections that occur inside an aircraft fuselage. This information is used to develop a channel matrix and site specific capacity predictions. Preliminary research has shown that multiantenna systems use spatial diversity to take advantage of extreme multipath environments [34][14], such as those

found in aircraft. Additionally, for ideal multiantenna systems, capacity grows linearly with increasing antenna element count without requiring additional bandwidth [35]. Thus the 3D software has been extended to simulate both single and multiantenna systems in order to facilitate development of both types of systems and explore the advantages of each. The site-specific model described in this dissertation provides significant improvements in accuracy of estimating the channel matrix over traditional statistical models. Capacity predictions in the fuselage are also compared for varying input parameters of the ray tracing software to see which of these parameters have significant impact on accuracy. [28]

Chapter 5 describes the measurement and modeling of a 2004 Thomas Bus 110YN. It includes the application of a site-specific 3D modeling software [36] that uses ray tracing to accurately estimate the location specific capacity of a complex channel in a shuttle bus with severe multipath and fading. Research has shown that this modeling software accurately describes the complex channel found in aircraft [26][26] and tunnels [27] and is applied to a public transportation bus to show its adaptability and accuracy in different environments. [29]

Chapter 6 discusses a measurement campaign to evaluate the complex wireless channel in a Bell OH-58A helicopter. The measurement system involved the use of a 4x4 antenna array to measure the channel capacity at points throughout the helicopter. 3D software was then used to simulate the same channel and compared to measurement to find what factors were most important in the ray tracing simulation to obtain accuracy. This chapter provides an analysis of the wireless channel found in a small vehicle, such as a helicopter and how the configurable parameters of the 3D ray tracing software affect

channel modeling accuracy when compared to measured capacity. It then demonstrates the improved accuracy of the 3D ray tracing method over commonly used statistical models at the cost of increased modeling complexity. [29]

Chapter 7 discusses the measurement, modeling, and analysis of a variety of complex channels, including tunnel, bus, and aircraft. Measurements were made using a multiantenna test bed [12][13] in order to take advantage of the extreme multipath environments found in these channels. 3D ray tracing software [36] was used as the main method of modeling, but also compared to other common statistical models including Gaussian [23], hyper-Rayleigh [15], Weibull [20] and Nakagami [22]. This chapter provides an analysis of similarities, differences and trends for this group of complex channels to evaluate design parameters and constraints that may be applied to designing such systems. [31]

1.4 Publications

The work in this paper has been presented at IEEE Antennas and Propagation Systems conferences in 2008 [37] and 2009 [26] and has been submitted for publishing in various journals. [13][25]-[31]

1.5 References

- [1] NASA, "Wiring integrity research (WIRE) pilot study A0SP-0001-XB1," August 2000.
- [2] NSTC, "Review of federal programs for wire system safety," *White House Report*, November, 2000.
- [3] Jerome Collins, "The challenges facing U.S. Navy aircraft electrical wiring systems," *9th Annual Aging Aircraft Conference*, March 2006.

- [4] M. A. Dornheim, "New rules and hardware for wiring soon to emerge," *Aviation Week & Space Technology*, April, 2001.
- [5] P. Smith, C. Furse, and J. Gunther, "Analysis of spread spectrum time domain reflectometry for wire fault location" *IEEE Sensors Journal*, Volume: 5, Issue: 6, 2005, Page(s): 1469 – 1478.
- [6] Chirag Sharma, Reid Harrison, and Cynthia Furse, " Low-power STDR CMOS sensor for locating faults in aging aircraft wiring," *IEEE Sensors Journal*, Volume 7, Issue 1, Jan. 2007 Page(s):43 – 50.
- [7] WiFi in the sky. [Online] Available: <http://www.physorg.com/news5047.html>, [Accessed: July 8, 2005].
- [8] Gareth Halfacree, "Delta to fit WiFi to all aircraft," [Online] Available: <http://www.bit-tech.net/news/2008/08/06/delta-to-fit-wifi-to-all-aircraft/1>, [Accessed: August 6, 2008].
- [9] A. Ameti, R. Fontana, E. Knight, and E. Richley, "Ultra wideband technology for aircraft wireless intercommunication systems (AWICS) design," *IEEE Aerospace and Electronic Systems Magazine*, Vol. 19, No. 7, Page(s): 14–18, 2004.
- [10] Jay J. Ely, Gerald L. Fuller, and Timothy W. Shaver, "Ultra wideband electromagnetic interference to aircraft radios," *Digital Avionics Systems Conference*, 2002.
- [11] D. W. Bliss and K. W. Forsythe, "MIMO radar medical imaging: self-interference mitigation for breast tumor detection," *Fortieth Asilomar Conference on Signals, Systems and Computers*, Page(s): 1558-1562, Oct.-Nov. 2006
- [12] D. Palchak and B. Farhang-Boroujeny, "A software defined radio test bed for MIMO systems," *Proceedings of the SDR 06 Technical Conference and Product Exposition*, Orlando, FL, Nov. 2006.
- [13] J. Nagel, A. Magleby, S. Ananthanarayanan, C. Furse, "Measured multiuser MIMO capacity in aircraft," accepted for publication in *IEEE Antennas and Propagation Magazine*.
- [14] D. Landon and C. Furse, "The MIMO transmission equation," *IEEE Antennas and Propagation Symposium (APS)*, San Diego, CA, July 7-11, 2008.
- [15] J. Frolik, "A case for considering hyper-Rayleigh fading channels," *IEEE Transactions on Wireless Communications*, Vol. 6, No. 4, Page(s): 1235–1239, 2007.

- [16] David G. Landon and Cynthia M. Furse, "Recovering handset diversity and MIMO capacity with polarization-agile antennas," *IEEE Trans. Antennas and Propagation*, Vol. 55, No. 11, Page(s): 3333–3340, Nov. 2007.
- [17] David Landon "Polarization misalignment and the design and analysis of compact MIMO arrays," PhD Dissertation, University of Utah, Salt Lake City, UT, 2007.
- [18] David G. Landon and Cynthia M. Furse, "Channel matrix normalization corrections to demonstrate MIMO's capacity dependence on realistic cross-polarization and branch-power-ratios," in preparation for *IEEE Transactions on Vehicular Technology*.
- [19] M. Lupupa and M.E. Dlodlo, "Performance of MIMO system in Weibull fading channel-channel capacity analysis," *IEEE EUROCON*, Page(s): 1735-1740, July 2009.
- [20] I.Y. Abualhaol and M.M. Matalgah, "Capacity analysis of MIMO system over ideally independent distributed Weibull fading channels," *IEEE International Conference on Communication*, Page(s): 5003-5008, June 2007.
- [21] D. Matolak and A. Chandrasekaran, "Aircraft intravehicular channel characterization in the 5 GHz band," in *Integrated Communications, Navigation and Surveillance Conference*, 2008. ICNS 2008, Page(s): 1–6, 2008.
- [22] G. Fraidenraich, O. Leveque, and J. Cioffi, "On the MIMO channel capacity for the Nakagami-m channel," *IEEE Transactions on Information Theory*, Vol. 54, no. 8, Page(s): 3752–3757, 2008.
- [23] I. Telatar et al., "Capacity of multiantenna Gaussian channels," *European Transactions on Telecommunications*, Vol. 10, No. 6, Page(s): 585–596, 1999.
- [24] ITU-T Study Group 2, *Teletraffic Engineering Handbook* [Online] Available: <http://www.com.dtu.dk/teletraffic/handbook/telenook.pdf>, [Accessed: August 27 2010].
- [25] Alyssa Magleby, Cynthia Furse, and Z. Q. Yun, "3D Ray Tracing for Intravehicle MIMO," *IEEE/URSI Antennas and Propagation Symposium*, Charleston, SC, June 1-5, 2009.
- [26] Sai Ananthanarayanan, Alyssa Magleby Richards, and Cynthia Furse, "Measurement and modeling of multiantenna systems in aircraft," submitted to *Journal of Aerospace Computing, Information, and Communication*, June 2010.
- [27] Sai Ananthanarayanan, Alyssa Magleby, and Cynthia Furse, "Measurement and modeling of interference for multiple antenna system," *Microwave and Optical Technology Letters*, Volume 52, Issue 9, pages 2031–2037, September 2010.

- [28] Alyssa Magleby Richards, Sai Ananthanarayanan, and Cynthia Furse, "3D simulation of the wireless channel in small aircraft," submitted to *IEEE Transactions on Vehicular Technology* October 2010.
- [29] Alyssa Magleby Richards, Sai Ananthanarayanan, and Cynthia Furse, "Measurement and simulation of the multiantenna communication channel on a shuttle bus," in preparation for *IEEE Transactions on Vehicular Technology*.
- [30] Alyssa Magleby Richards, Sai Ananthanarayanan, and Cynthia Furse, "Wireless channel measurements and modeling in a helicopter," submitted to *Microwave and Optical Technology Letters* October 2010.
- [31] Alyssa Magleby Richards, Sai Ananthanarayanan, and Cynthia Furse, "Complex channel measurement and modeling for the design of wireless systems," in preparation for *IEEE Transactions on Vehicular Technology*.
- [32] S. Lim, Z. Yun, J. Baker, N. Celik, H. Youn, and M. Iskander, "Radio propagation in stairwell: measurement and simulation results," *IEEE Antennas and Propagation Society International Symposium*, Charleston, SC, June 2009.
- [33] C. Takahashi, Z. Yun, M. F. Iskander, et al. "Propagation-prediction and site-planning software for wireless communication systems" *IEEE Antennas and Propagation Magazine*, Vol. 49, No. 2, April 2007.
- [34] V. R. Anreddy and M. A. Ingram, "Capacity of measured Ricean and Rayleigh indoor MIMO channels at 2.4 GHz with polarization and spatial diversity," *IEEE Wireless Communications Networking Conference 2006*, Vol. 2, Page(s): 946-951.
- [35] G.J. Foschini and M.J. Gans, "On limits of wireless communications in a fading environment when using multiple antennas," *Wireless Personal Communications* Vol. 6, Page(s): 311-355, Mar 1998.
- [36] Z. Yun, Software package called "3D ray tracing for radio propagation modeling," last updated Dec. 2009, unpublished.
- [37] A. Magleby and C. Furse, "Predicted MIMO performance in intravehicle channels," *IEEE Antennas and Propagation Society International Symposium*, San Diego, CA, Page(s): 1-4, 2008.

CHAPTER 2

WIRELESS COMMUNICATION FOR SENSOR NETWORKS

2.1 The Need for Wireless Sensor Networks in Aircraft and Other Vehicles

The hunger for more data, more phone calls, more video, and more access in more places is growing massively, challenging the availability of spectral resources and our current infrastructure. For example, monitoring aircraft safety and health has become a major priority. Current planes are being retrofitted for a variety of sensors including moisture, vibration, temperature, chemical, engine wear and electrical faults. New planes are being constructed with these sensors already in place. Using wired sensor systems adds unnecessary weight and potential electrical failure points, which has brought an extreme interest in wireless sensor networks [39][40][41][83]. A potential solution to this situation would involve enabling wireless communication in presently built structures, such as aircraft, cars, buses, ships, trains and other extreme channels, as well as improving the capacity achievable in these complex channels and improving the design of wireless communication for future vehicles.

2.2 Communication Systems for Aircraft

Present wireless aircraft systems that have been developed without interfering with existing aircraft systems include smoke detection [39], video security [40],

emergency lighting control [41], WiFi [85][88] and other sensors [41][42]. A proposed wireless system for aircraft, called Aircraft Wireless Intercommunications Systems (AWICS), involves the use of ultrawideband signals for communication in order to free up crew members from the cumbersome cables that connect their headsets to the aircraft [87]. There are no other known intraaircraft wireless communication systems, but there are still frequency ranges available for use in developing other wireless communications that will not interfere with aircraft operation. Frequencies for aircraft communication are detailed in Table 2.1 with overlaps in frequency use for the aircraft systems shown with a bold outline, and frequencies used in personal electronic devices (PEDs) highlighted in grey. [55][56]

As we can see from the table, the frequencies of PEDs do no overlap those used by on-board systems, but still have the potential to interfere, thus most PEDs are not permitted to be used in-flight. The exception to that are the frequencies of 2.4 GHz and 5 GHz used for IEEE 802.11, HyperLAN2, and Bluetooth wireless, as well as on-board fire alarms, which have been approved as safe by the Federal Aviation Administration. Most characterizations of aircraft have been performed at these frequencies, however our characterization is performed at 915 MHz, which is in the band for industrial, scientific and medical applications, which we felt appropriately fit our purpose of safety sensor networks.

2.2.1 Spread Spectrum Sensing System

The fault sensing system that triggered our interest in wireless communication on aircraft uses spread spectrum time domain reflectometry (SSTDR) and

Table 2.1: Electromagnetic spectrum for aircraft communication and navigation equipment combined with frequencies for personal electronic devices (PED) (overlapping frequencies with bold outline).

Wireless Signal	Frequency Range
Omega Navigation	10-14 kHz
Automatic Direction Finder	190-1750 kHz
HF	2-30 MHz
Marker Beacon	74.85, 75, 75.15 MHz
VHF Omnidirectional Range Localizer (VOR)	108-118 MHz
VHF Communications	118-136 MHz, 225-399 MHz
Glide Slope	328-335 MHz
Cellular uplink	824-849 MHz
Industrial, Scientific, Medical (ISM)	902-928 MHz
Distance-Measuring Equipment	960-1220 MHz
Traffic alert/collision avoidance system	1030-1090 MHz
Global positioning system	1575 MHz, with 2 MHz bandwidth
Satellite Communications	1529-1661 MHz
PCS Uplink	1.85-1.91 GHz
Wireless IEEE 802.11, HyperLAN2, Bluetooth	2.4 GHz
Industrial, Scientific, Medical (ISM)	2.4-2.485 GHz
Low-range radio altimeter	4.3 GHz
Wireless IEEE 802.11, HyperLAN2, Bluetooth	5 GHz
Microwave landing system	5.03-5.09 GHz
Weather radar	5.4, 9.3 GHz

sequence time domain reflectometry (STDR) techniques to find intermittent faults in live aircraft wiring [43][44][65]. Such faults are undetectable by the usual dead wire testing methods. To begin with, a PN code signal is transmitted on the wire, as shown in Figure 2.1a. The signal is then reflected back to the source by a fault on the cable as shown in Figure 2.1b and c. This reflection is then correlated with the original PN code and the location of the resulting peak is a function of the distance to the fault. This method has been proven to be accurate to within +/- one foot for aircraft wires up to around 300 feet long carrying 28 V DC, 400 Hz AC power signals or Mil Std 1553 data bus signals. The hardware for this system has been programmed into an FPGA [43], and is being prepared for commercial development as a custom ASIC chip that will cost around \$10-\$20 when finished [65]. Spread Spectrum technology was initially considered as a possible transmission method since the fault sensing system already uses spread-spectrum for the sensing signal. However, the study that proved UWB to be a beneficial transmission method (described in Section 2.2.2) also found evidence that spread spectrum signals suffered severe multipath signal degradation within an aircraft cabin [58].

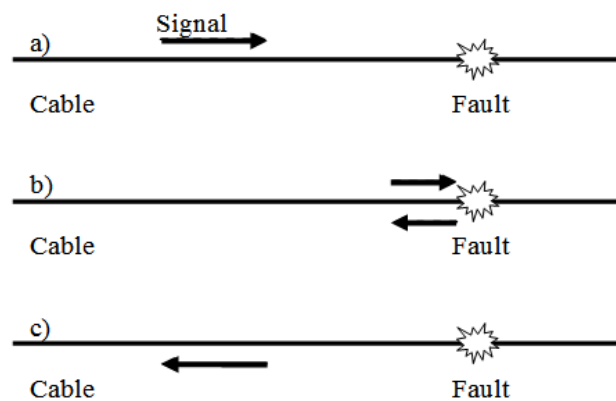


Figure 2.1: Example STDR/SSTD signal reflection. a) Transmission b) Reflection c) Return of signal.

Intraaircraft wireless communication systems will have to satisfy several constraints, which are already satisfied by the fault sensing system. The hardware must be as small as possible, and must work on low power to reduce either frequency of battery. Additionally, all wireless communication must either not interfere with present aircraft systems or be limited to after flight transmission to avoid interference with aircraft operation.

2.2.2 Ultra Wideband (UWB)

Ultra wideband (UWB) technology was recently tested for feasibility of use in a nonfixed-wing aircraft wireless intercommunications system (AWICS) because of its advantages in the aircraft environment. These advantages include low probability of interference (LPI) to onboard systems (such as the Legacy system), robustness to onboard electromagnetic interference, high throughput in a multiuser environment, multipath mitigation, and low probability of detection (LPD). All features except the last are essential in the proposed fault-sensing communication system, as well as other communication applications. UWB advantages are due to the use of large bandwidth waveforms which can be resolved in the time domain from a selection of multipath returns, given short channel dispersion relative to the interarrival times of the UWB pulse. Other advantages (LPD and LPI) are due to a low average power density of the UWB waveform. The AWICS system is also similar to the proposed communication system in size and battery power constraints. The UWB system tested in the study operated at L-band, with a 400 MHz RF bandwidth and 26 dBm of effective radiated power. It was able to operate with a 96 to 100 dB path loss. Time division multiple

access (TDMA) was used to accommodate simultaneous users, which would also be beneficial for the multiple sensors used in the proposed fault sensing communication system. C-band versions of the UWB communications system are under development for other applications such as commercial and home intercom and audio/video distribution systems [87]. Extreme caution must be used, however, in implementing new UWB systems. This is because EMI from UWB systems has been found to interfere with the air traffic control beacon system, the traffic alert/collision avoidance system (TCAS), the instrument landing system (ILS) and glide slope pointers on various fixed-wing aircraft, even when the UWB system was operating within limits set by FCC Part 15.209 [88]. Further research and simulations will be required to find a noninterfering UWB system for fixed wing aircraft.

2.2.3 Multiple Input, Multiple Output (MIMO)

Multiple-input, multiple-output (MIMO) antenna systems, such as the one depicted in Figure 2.2, offer capacity benefits over their more traditional single-input, single-output (SISO) counterparts thus attracting considerable current research [45]-[54]. In theory, MIMO holds promise for extracting orders of magnitude more capacity from a single spectral channel than today's SISO systems. Because of this, 2x2 MIMO systems are in the early stages of commercial deployment. MIMO performance has been shown to depend on a wide range of parameters [47][48] including radiation efficiency [50] [50], correlation [51][52], mutual coupling [53][54][58][59], matching efficiency [58] and polarization misalignment [59]. Previous NSF work (ECS-0524720) resulted in a comprehensive model that included all of these effects plus their coupling and

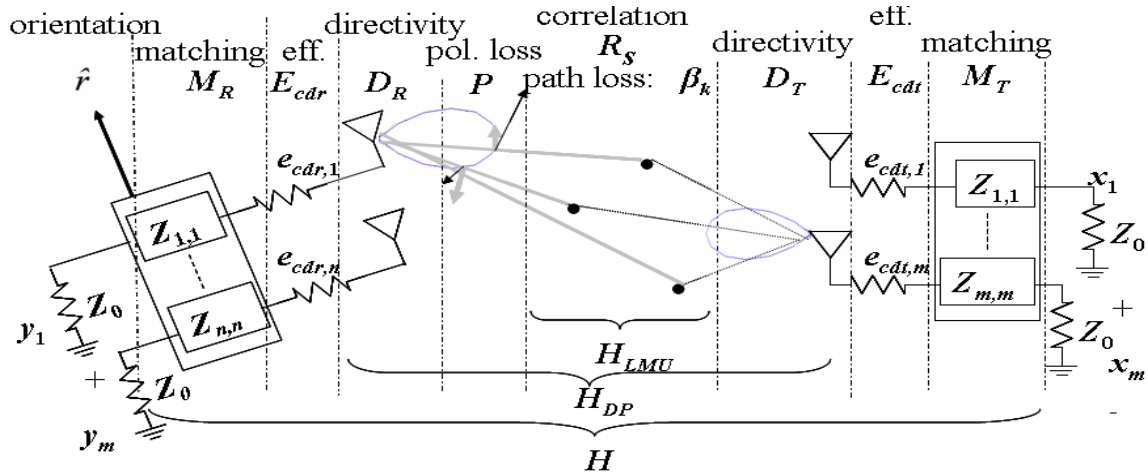


Figure 2.2: A general MIMO system model. M_R is the $n \times n$ impedance matrix describing the receive antenna array with efficiencies E_{cdr} , $e_{cdr,i}$. R_s is the spatial correlation of signals impinging on the receiver—traditionally including the directivity and polarization effects expressed above as D_R and P . Corresponding matrices for the transmit array are subscripted with a T or t . Grouping designator, H_{LMU} , represents a lossless, matched, uncoupled channel matrix and H represents a complete system channel matrix.

interactions. [61][89] The model was verified by basic measurements, which I wish to enhance in this research. Although accurate and effective, the comprehensive model was sufficiently complex that it was very difficult, if not impossible, to extract practical insight from. With the design engineer in mind, a simplified version of the comprehensive model, reminiscent of the widely used Friis Transmission Equation, was developed to provide insight and quick computation, as detailed in Figure 2.2. The theoretical effectiveness of this simplified equation was verified in [89], and its usefulness for design engineers is being tested at L-3 Communications.

Capacity, the principal metric of MIMO systems, expresses the maximum rate at which information can be reliably transferred in a system and is a function of the channel matrix, H . Figure 2.2 shows the many channel and system effects that influence this capacity. Because of the random orientation and compact nature of arrays for complex

channels, their characterization requires an unusually comprehensive formulation of the multiple-input, multiple-output (MIMO) capacity equation.

We were not, of course, the first group to notice MIMO's dependence on multiple parameters. Previous MIMO models have focused on one characteristic in isolation as in [52][59] leaving it to the reader to predict the relative interaction of that characteristic with other excluded effects. Other sources lump multiple loss effects together as a single homogenized effect [50][50], or use coupling matrices in sophisticated Monte-Carlo simulations to compute capacity [54]-[59]. In [61], rotation of the array (as would be typical of a handheld device) was found to have a critical effect on capacity, thus prompting the development of our comprehensive model.

The comprehensive MIMO model in [89] was developed from the network model of [68]. This method uses a voltage-voltage far-field pattern for the i^{th} receive antenna, $E_i^R(AOA)$, and trans-impedance gain pattern for the j^{th} transmit antenna, $e_j^T(AOD)$, as a function of angle-of-arrival (AOA) and angle-of-departure (AOD) to determine the effective signal and hence capacity within the model. Receive and transmit antenna efficiencies, E_{cdr} and E_{cdt} , are also included. The effect of receive array orientation, $\hat{\theta}$, is included through the gain term $E_i^R(AOA, \hat{\theta})$. The polarization loss is the dot product between this quantity and the unit vector describing the polarization of the impinging signal, $\hat{\rho}_T$ [52]. The influence of the channel on channel-system capacity is expressed as a summation of N_p plane waves where the k^{th} plane wave has complex gain (path loss and phase shifts) β_k , and angles of arrival and departure, AOA_k and AOD_k . Thus, the transmit antenna voltages can be expressed as:

$$y = Z_0^{1/2} S_{21} (\mathbf{I} - \mathbf{S}_{RR} S_{11})^{-1} \left(\mathbf{I} + \frac{\mathbf{Z}_{RR}}{Z_0} \right)^{-1} \mathbf{E}_{cdr} \underbrace{\left[\frac{1}{Z_0} \sum_{k=1}^{N_p} E_i^R(AOA_k, \hat{r}) \hat{p}_T \beta_k e_j^T(AOD_k) \right]}_{H_{DP}} \mathbf{E}_{cdt} (\mathbf{I} - \mathbf{S}_{TT}) x \quad (2.1)$$

The channel matrix, H_{DP} , is obtained from measurement, statistical models, or simulation. This is a very comprehensive model for the signal (voltages) received by the antennas. Additional effects, such as more complex channel models, will be added (see Section 2.4) and noise models can be considered along with the signal to determine the comprehensive MIMO capacity. Although accurate and useable, this equation provides minimal insight to guide a design engineer in the development of a MIMO system. All of the terms above are interrelated, which is certainly to be expected in MIMO systems. However, in the interests of obtaining design insight, the comprehensive model above was simplified by extracting the deterministic effects in the comprehensive model in a systematic fashion, evaluating each approximation against the more complete model. The full derivation is too long to include here but has been made available online at [89]. The simplified capacity expression that resulted is given by

$$C_E \approx \underbrace{N \log_2 \left(\frac{P_T}{M \sigma^2} \right)}_{\text{SNR, } N \text{ pathloss}} + \underbrace{\log_2 \prod_{i=1}^N e_{cdr,i}}_{\substack{\text{efficiency} \\ \eta_{cd}}} + \underbrace{\log_2 |M_R M_R^H|}_{\text{matching}} + \underbrace{\log_2 \prod_{i=1}^N \frac{PLF_i}{PLF_{ref}}}_{\eta_{PLF}} + \underbrace{\log_2 \prod_{i=1}^N \frac{D_i}{D_{ref}}}_{\substack{\text{distribute } d \\ \text{directivity} \\ \eta_D}} + \underbrace{\log_2 |R_{s-DP}|}_{\text{channel correlation}} \quad (2.2)$$

The comprehensive model and simplified model were compared in actual engineering designs for 26 MIMO arrays from a broad mix of antenna types (2-4 dipoles, patches, PIFAs, and polarization-agile antenna designs) as shown in Figure 2.3. Agreement is quite good for arrays that are held in fixed rotation (traditional MIMO) or rotated (more realistic for handheld devices). This initial test provided confidence that the simplified model can be used in practice to design MIMO systems. We emphasize here that this simplified model and method is very new, so both in this research and in concert with our engineering colleagues in industry, we will continue to assess its validity and seek out its limitations and problems. For a time, at least, we will use both the comprehensive model and the simplified model in our calculations.

This new comprehensive model (and its simplified adaptation for insight) allows us to predict the signal that is transmitted, propagated within the channel, and received as

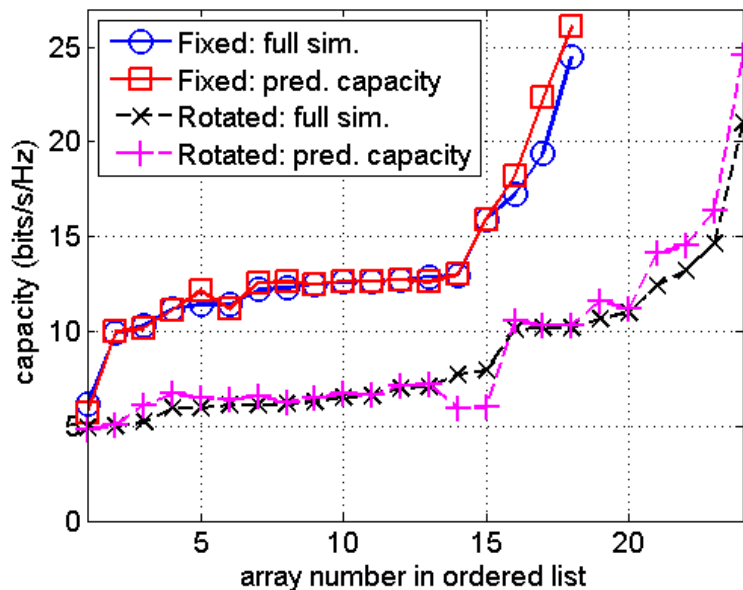


Figure 2.3 Capacity computed for 26 antenna array designs that included 2-4 dipole, patch, PIFA, and polarization-agile antenna designs.

a MIMO capacity. But the true information available in the communication system is a function of both the signal and the noise. A comprehensive model of the noise is under development in other work [90][91] in conjunction with the NSF proposal mentioned previously.

2.3 Prior Measurements and Simulations

Normally, wireless networks are deployed in mobile systems with a constantly changing multipath environment. Sensor networks however are more commonly static and deployed in enclosed cavities, and thus do not always experience the normal fading characteristic defined by Rayleigh fading [94]. Several recent studies evaluate measurements taken in various airframes both in flight and on the ground in an attempt to understand the wireless transmission environment in enclosed cavities [71][79]. Early studies showed the reverberant nature of the inside of an aircraft cabin, which compared well with reverberation chambers [73]-[76].

Later studies have attempted to define the environment using statistical models, and evaluate the effect of inner obstacles (such as chairs, walls, and people). Two studies have shown fading worse than Rayleigh observed on both commercial aircraft and a helicopter [83][93]. The initial study on aircraft was followed up by an extensive study varying antenna location, frequency and polarization in a large transport helicopter. This study found a new type of fading called hyper-Rayleigh, where the received signal is dominated by two constant amplitude signal components with uniformly distributed angles of arrival over $[0, 2\pi)$, this is also referred to as two-wave with diffuse power (TWDP), and is fully described in Section 3.1. The study concluded that hyper-Rayleigh

fading occurred more than 20% of the time in the 915 MHz, 2.4 GHz, and 5.8 GHz ISM bands. It also concluded that using small scale fading models, such as hyper-Rayleigh, enabled analysis of how different diversity methods mitigate severe fades [83].

Other studies found conflicting information about the aircraft channel. One on a Boeing 737-400, found that the channel fading had a much steeper curve, which fit a Ricean CDF for both frequencies and locations measured. They found $K = 12.7$ dB at a frequency of 1.8 GHz along the corridor of the aircraft with and $K = 8.6$ dB at a frequency of 2.1 GHz at the seats of the aircraft. They concluded that the lower K value near the seats was due to the backrests obstructing the path of the ray. They determined that the diffractions by and transmission through backrests, along with multiple reflections off of walls created a complex inner geometry that was best described by a site-specific model [94]. Other studies in mid-size aircraft using single antenna measurements found the aircraft channel to have Weibull [70] or Nakagami-m [72] type distributions.

A study on larger aircraft, namely the Boeing 747, 767 and 777, predicted propagation using Wireless Insite software and compared to measurement data to conclude that internal airplane configuration (including seats, doors, windows, galleys and bathrooms) significantly altered propagation. Simulations of the plane with internal obstacles caused +/- 5 dB fades in the resulting received power (when compared to the empty fuselage) at locations throughout the cabin, and was a better match to measured data. [57] Though Wireless Insite was able to qualitatively predict propagation of electromagnetic signals within airframes to estimate received power, and to assist in the

best placement of transmitters, it is time consuming to run and requires a full Solidworks model of the aircraft as input.

Further studies using single antenna measurements have been performed on aircraft and trains to evaluate the effect of people on wireless signals. All of these have come to similar conclusions that people absorb over 60% of the signal depending on the location and number of passengers in relation to the transmit and receive antennas [77] - [80]. People also significantly increase fade depth by anywhere from 7 dB (going from an empty aircraft to 50% full) to around 10dB (for a full load of passengers) [77], adding to the multipath richness of the channel.

This was promising information, as our goal was to use MIMO on aircraft because it works well in such environments, but we further researched studies on the effect people have when using MIMO to validate our assumptions. We found some promising studies evaluating people in an indoor environment. The first study used an 8 by 8 MIMO system at 2.45 GHz within a small room and evaluated the effect that 4 people moving around had on average channel capacity. They determined that capacity increased from 10.9 bits/s/Hz for the static room case to 12.3 bits/s/Hz for the dynamic room case (with people moving) [81]. Another study used a 4 by 4 MIMO-OFDM system at 5.2 GHz with between 0 and 10 pedestrians walking between line of site (LOS) transmitter and receiver. They found a constant average channel capacity using a fixed SNR, but an increase in dynamic capacity ranging from 0.5 bits/s/Hz for no pedestrians to 5 bits/s/Hz for 10 pedestrians. They also found that the slope of the Ricean CDF decreased proportionally with the number of pedestrians (which is an increase in multipath, approaching the CDF for hyper-Rayleigh). From this, they concluded that

adaptive coding schemes in the MIMO system could overcome this variation [82]. These two studies show that the use of MIMO in the already multipath rich environment found on aircraft and other vehicles could provide a constant or improved capacity with the increased multipath caused by people. They also show that MIMO systems could benefit from adaptive coding schemes, which is not a focus of this paper, but could be included in future work.

Presently, all measurements regarding the environment inside a metal cavity, such as aircraft or other vehicles, have used a SISO communication system. The varying fading characteristics and effects of complex inner geometry depending on the vehicle or channel measured (including seats, walls and people) that were found in these previous studies provide an optimal environment for MIMO. This research aims to expand upon previous SISO evaluations by taking MIMO measurements and comparing them to the SISO baseline to calculate capacity. A MIMO test bench developed at the University of Utah has been used to take these measurements [97] along with MIMO simulation software which includes antenna effects (also referred to as the detailed signal model or DSM) [89] in order to evaluate channel response. Once MIMO has been evaluated for its performance in a cavity through measurement, further simulations could be performed using the DSM in combination with our new 3D ray tracing software [96] as described in Section 2.2.3 and Section 3.4, respectively, to predict optimal placement of transmitters.

2.4 Complex Channel Modeling

The detailed signal model is software that includes antenna effects including radiation efficiency, correlation, mutual coupling, matching efficiency and polarization

misalignment, as detailed in Section 2.2.3. These are essential to accurately calculate multiantenna channel capacity regardless of the channel model used, whether from measurement, statistical models, or simulation [89]. The estimated channel matrix, H , from either the 3D ray tracing software or a statistical model can be combined with the antenna effects to obtain a complete system channel matrix, H_{DSM} .

$$H_{DSM} = \underbrace{Z_0^{1/2} \underbrace{S_{21}(I - S_{RR}S_{11})^{-1}}_{\text{matching}} \left(I + \frac{Z_{RR}}{Z_0} \right)^{-1}}_{M_R} \underbrace{E_{cdr}}_{\text{rad eff}} \underbrace{[H]}_{H_{DP}} \underbrace{E_{cdt}}_{\text{rad eff}} \underbrace{(I - S_{TT})}_{\text{matching}} \quad (2.3)$$

Z_0 is the characteristic impedance, Z_{RR} is the impedance of the receiver, S_{11} and S_{21} represent a matching circuit and transmission circuit for a selected matching approach, S_{RR} and S_{TT} are the scattering parameters of the unloaded transmit and receive arrays respectively. Receive and transmit antenna efficiencies, E_{cdr} and E_{cdt} , are also included. H is the channel scattering matrix created from the model or measurement and includes the channel path loss along with the gain at both the transmitter and receiver and any directivity or polarization losses. This matrix is then combined with estimated channel SNR_r in equation (5) to obtain a multiantenna capacity calculation which includes antenna effects [90].

$$C = \log_2 \det \left[I + \frac{SNR_r N_r}{\| \mathbf{H} \|_{Frobenius}^2} \mathbf{H} \mathbf{H}^H \right] \quad (2.4)$$

The DSM is used in this dissertation to postprocess all measurement, 3D simulation and statistical modeling data.

2.4.1 Statistical Models

Based on the studies described in Section 2.3, we have chosen to compare our measurements and simulations with the statistical models found to best represent the aircraft channel in those studies. Thus Gaussian [97], hyper-Rayleigh [94], Weibull [70], and Nakagami-m [72] distributions will be evaluated in this paper.

2.4.1.1 Hyper-Rayleigh

Hyper-Rayleigh occurs when the received signal is dominated by two constant amplitude signal components with statistically independent phase components uniformly distributed over $[0, 2\pi)$. This is also referred to as two-wave with diffuse power (TWDP). The received voltage is described by the following equations [94].

$$\mathbf{S}_{\text{RT}} = \sum_{i=1}^M \sum_{j=1}^N \left[\frac{1}{Z_0} (E_i^R(\theta, \phi) \beta_1 E_j^T(\theta, \phi) + E_i^R(\theta, \phi) \beta_2 E_j^T(\theta, \phi) + \sigma \sum_{k=3}^{N_p} E_i^R(\theta, \phi) \beta_k E_j^T(\theta, \phi)) \right] \quad (2.5)$$

$$\sigma = \sqrt{\frac{\beta_1^2 + \beta_2^2}{2K}} \quad (2.6)$$

Where σ is the diffuse parameter and K is the Ricean K -factor. The \mathbf{S}_{RT} can be substituted in (2.3) to obtain the channel matrix \mathbf{H} .

2.4.1.2 Weibull

The fading envelope in wireless communication is commonly modeled using the Weibull distribution. Path loss for the Weibull model is described as

$$\beta_k = R_k^{\alpha/2} \exp(j\Theta_k) \quad (2.7)$$

where R_k is the amplitude of the Weibull envelope, Θ_i is the phase, which is uniformly distributed over $[0, 2\pi)$, and α_k is the Weibull fading parameter. The probability density function (pdf) of the Weibull envelope can be written as

$$p_{R_k}(r) = \frac{\alpha_k}{\Omega_k} r^{\alpha_k-1} \exp\left(-\frac{r^{\alpha_k}}{\Omega_k}\right) \quad (2.8)$$

where α_k is the Weibull fading parameter and Ω_k is the average fading power. The severity of fading decreases as α_k increases. This model reduces to the Rayleigh channel

model for $\alpha_k = 2$. [232] Weibull channels with various values of α_k and Ω_k were simulated in coordinating research, with the best capacity estimates obtained for an $\alpha_k = 1.5$ and $\Omega_k = 1$, which were then used for simulations in this paper.

2.4.1.3 Nakagami-m

The Nakagami-m distribution includes an additional parameter than the Gaussian and Weibull models, and thus provides increased flexibility and a better match to most fading channels [72][98]. The Nakagami-m model simplifies to the Rayleigh and uniform distribution on the unit circle for the extreme cases of $m=1$ and $m=\infty$, respectively. The path loss is again modeled as

$$\beta_k = R_k \exp(j\Theta_k) \quad (2.9)$$

where the pdf distribution of R_k is given by

$$p_R(r) = \frac{2m^m r^{2m-1}}{\Omega_m \Gamma(m)} \exp\left(-\frac{mr^2}{\Omega}\right) \quad (2.10)$$

with shape parameter, m , and spread parameter, Γ [72]. The Nakagami was simulated in coordinating research for a range of m values, and the best capacity estimates were obtained for an $m=1.4$, which is used for simulations in this paper.

2.5 Why MIMO for Wireless Sensor Networks

The impetus for this research is the need to communicate with sensors in aircraft for location of intermittent wiring faults, a previous NSF project that has grown into a commercial application. The Smart Connector shown in Figure 1.1 is being commercialized by LiveWire Test Labs in conjunction with Minnesota Defense. Some regions of the aircraft can support infrared links with this device, but most locations of interest are buried deep within the aircraft where a wireless link will be required for retrofit applications. This research addresses some of the unmet demand for communication between future wireless devices by enabling communication in complex channels using MIMO communication strategies. The intravehicle channel was the main focus in this proposal, but the developed methods can be applied to other complex channels. The significant contributions of this research include an evaluation of MIMO in aircraft and other vehicles, quantification of the aircraft/vehicle environment and its relation to other environments, and a parameterization of vehicles for modeling multiantenna communication. These results will further the goals of making the data from each sensor easily accessible in real time, and potentially enabling connectivity mapping of the wires between sensors. The ability to evaluate and design MIMO technologies in this proposal is potentially transformative for aircraft safety—enabling a new generation of location-specific monitoring and maintenance.

2.6 References

- [38] Wireless Smoke Detection. [Online] Available:
<http://www.securaplane.com/smoke2.html>, [Accessed: June 21 2009]

- [39] Securaplane Technologies, Inc. Press Release, "Securaplane technologies awarded Boeing 787 contract for wireless emergency lighting," December 21, 2004. [Online] Available: <http://www.securaplane.com/releases/pr0095.html>, [Accessed: June 21 2009].
- [40] [Online] Available: www.honeywell.com/sites/aero/AircraftSensors.html, [Accessed: June 21 2009].
- [41] E. St. John, "Operational issues wireless overview," Presented at World Airline Entertainment Association Single Focus Workshop, Washington D. C., Nov 19, 2002.
- [42] Jerome Collins and Gail Edwards, "NAVAIR aircraft wiring diagnostic support equipment for multiple maintenance levels." *Aging Aircraft Conference*, Feb 3, 2005.
- [43] Paul Smith, Cynthia Furse, and Jacob Gunther. "Analysis of spread spectrum time domain reflectometry for wire fault location." *IEEE Sensors Journal*, Vol. 5 No. 6, December 2005.
- [44] Cynthia Furse and Randy Haupt, "Down to the wire." *IEEE Spectrum*, February 2001.
- [45] G.J. Foschini and M.J. Gans, "On limits of wireless communications in a fading environment when using multiple antennas," *Wireless Personal Communications*, Vol. 6, Page(s): 311-355, Mar 1998.
- [46] D. Tse and P. Viswanath, *Fundamentals of wireless communication*. Cambridge: Cambridge University Press, 2005.
- [47] M. A. Jensen and J. Wallace, "A review of antennas and propagation for MIMO wireless communications," *IEEE Transactions on Antennas and Propagation*, Vol. 52, Page(s): 2810-2824, Nov 2004.
- [48] R. Vaughan and J. B. Andersen, "Channels, propagation and antennas for mobile communications," The Institution of Electrical Engineers, London, 2003, sections 6.3-4 and chapters 8-9.
- [49] J. Valenzuela-Valdés, M. A. García-Fernández, A. M. Martínez-González, and D. Sánchez-Hernández, "The influence of efficiency on receive diversity and MIMO capacity for Rayleigh-fading channels," submitted for publication in *IEEE Transactions Antennas Propagation*.

- [50] P. S. Kildal and K. Rosengren, "Correlation and capacity of MIMO systems and mutual coupling, radiation efficiency, and diversity gain of their antennas: simulations and measurements in a reverberation chamber," *IEEE Communications Magazine*, Vol. 42, Issue 12, Page(s): 104-112, Dec 2004.
- [51] S. Loyka and A. Kouki, "The impact of correlation on multiantenna system performance: correlation matrix approach," *IEEE Vehicular Technology Conference, 2001*, Vol. 2, Page(s): 533-537, 7-11 Oct 2001.
- [52] J. W. Wallace and M. A. Jensen, "Termination-dependent diversity performance of coupled antennas: network theory analysis," *IEEE Transactions on Antennas and Propagation*, Vol. 52, Page(s): 98-105, Jan 2004.
- [53] Jon W. Wallace and Michael A. Jensen "Mutual coupling in MIMO wireless systems: A rigorous network theory analysis", *IEEE Transactions on Wireless Communication*, Vol. 3, No. 4, C 1317-1325, July 2004.
- [54] C. Waldschmidt, S. Shulteis, and W. Wiesbeck, "Complete RF system model for analysis of compact MIMO arrays," *IEEE Transactions on Vehicular Technology*, Vol. 53, No. 3, Page(s): 579-586, May 2004.
- [55] Tekla S. Perry and Linda Geppert, "Do portable electronics endanger flight?" *IEEE Spectrum*, Page(s):26-33, September 1996.
- [56] Bill Strauss, "The onboard commercial aircraft in-flight RF environment: measurements and implications," *IEEE International Symposium on Electromagnetic Compatibility, 2006*, Vol. 1, Page(s): 234 – 239, 2006.
- [57] Mennatoallah Youssef and Linda Vahala, "Effects of passengers and internal components on electromagnetic propagation prediction inside Boeing aircrafts." *IEEE Antennas and Propagation Society International Symposium 2006*, Page(s): 2161 – 2164, 2006.
- [58] B. K. Lau, S. M. S. Ow, G. Kristensson, and A.F. Molisch, "Capacity analysis of compact MIMO systems," *Vehicular Technology Conference 2005*, Vol. 1, Page(s): 165-17030, May-June 2005.
- [59] S. Ow, "Impact of mutual coupling on compact MIMO systems," M.S. Thesis, Lund University, Sweden, 2005, [Online] Available:
<http://www.es.lth.se/teorel/Publications/TEAT-5000-series/TEAT-5074.pdf>
- [60] Aitan Ameti, Robert J. Fontana, EJ. Knight and Edward Richley, "Ultrawideband technology for aircraft wireless intercommunications systems (AWICS) Design," *IEEE A&E Systems Magazine*, July 2004.

- [61] D. Landon and C. Furse, "MIMO capacity dependence on realistic cross-polarization and branch-power-ratios," *Microwave and Optical Technology Letters*, Vol. 50, No. 5, Page(s): 1384-1388, May 2008.
- [62] David Gesbert, et al. "From theory to practice: an overview of MIMO space-time coded wireless systems," *IEEE Journal on Selected Areas in Communications*, Vol. 21, No. 3, April 2003.
- [63] Susan Karlin. "Take off, plug in, dial up." *IEEE Spectrum*, Page(s): 53-59, August 2001.
- [64] Fred Halsall, *Data communications, computer networks, and OSI*. 4th Edition. Reading, MA: Addison Wesley, 1996.
- [65] Chirag R. Sharma, Cynthia Furse, and Reid R. Harrison. "Low-power STDR CMOS sensor for locating faults in aging aircraft wiring" *IEEE Sensors Journal*, Vol. 7, No. 1, January 2007.
- [66] T. T. Evans. "Wireless communication channels in aircraft," Senior Project, University of Utah, Salt Lake City, UT, 2007.
- [67] D. Dowdle, "Polarization agile antenna for MIMO," M.S. Thesis, University of Utah, Salt Lake City, UT, 2007.
- [68] Matthew L. Morris and Michael A. Jensen, "Network model for MIMO system with coupled antennas and noisy amplifiers", *IEEE Transactions on Antennas and Propagation*, Vol. 53, No.1, Page(s): 545-552, Jan 2005.
- [69] D. Cox, "Antenna diversity performance in mitigating the effects of portable radiotelephone orientation and multipath propagation." *IEEE Transactions on Communications*, Vol. 31, Issue 5, May 1983.
- [70] M. Lupupa and M.E. Dlodlo, "Performance of MIMO system in Weibull fading channel-channel capacity analysis," *IEEE EUROCON*, Page(s): 1735-1740, July 2009.
- [71] I.Y. Abualhaol and M.M. Matalgah, "Capacity analysis of MIMO system over ideally independent distributed Weibull fading channels," *IEEE International Conference on Communication*, Page(s): 5003-5008, June 2007.
- [72] G. Fraidenraich, O. Leveque, and J. Cioffi, "On the MIMO channel capacity for the Nakagami-m channel," *IEEE Transactions on Information Theory*, Vol. 54, No. 8, Page(s): 3752-3757, 2008.

- [73] M. D. Johnson, et al., "Phase II demonstration test of the electromagnetic reverberation characteristics of a large transport aircraft. Dahlgren, Virginia: Naval Surface Weapons Center," *Dahlgren Division*, September 1997.
- [74] G. J. Freyer and M. O. Hatfield, "Aircraft test applications of reverberation chambers," *Proceedings of the IEEE International EMC Symposium*, Page(s): 491-6, 1994.
- [75] M. D. Johnson, et al., "Comparison of RF coupling to passenger aircraft avionics measured on a transport aircraft and in areverberation chamber," *Proceedings of the IEEE International EMC Symposium*, Vol. 2, Page(s): 1047-52, 1998.
- [76] G. J. Freyer, M. O. Hatfield, and M. B. Slocum, "Characterization of the electromagnetic environment in aircraft cavities excited by internal and external sources," *15th Digital Avionics Systems Conference*, Page(s): 327-332, Oct 1996.
- [77] Kathy Weiquan Wang-Hurst, "Analysis of path loss from a transmitter in an aircraft cabin to an exterior fuselage-mounted antenna," M.S. Thesis, Virginia Polytechnic Institute and State University, Blacksburg, VA, 2007.
- [78] Y. Katayama, et al., "Ultrawideband impulse-radio propagation for in-vehicle wireless link," *IEEE 64th Vehicular Technology Conference, 2006*, Page(s): 1-5, Fall. 2006.
- [79] R. Felbecker, W. Keusgen, and M. Peter, "Incabin millimeter wave propagation simulation in a wide-bodied aircraft using ray tracing," *IEEE 68th Vehicular Technology Conference*, Page(s): 1-5, 2008.
- [80] Y. P. Zhang and Y. Hwang, "Theory of the radio-wave propagation in railway tunnels" *IEEE Transactions on Vehicular Technology*, Vol. 47, No. 3, August 1998.
- [81] K. I. Ziri-Castro, W. G. Scanlon, and N. E. Evans, "Prediction of variation in MIMO channel capacity for the populated indoor environment using a Radar cross-section-based pedestrian model," *IEEE Transactions on Wireless Communications*, Vol. 4, Issue: 3, Page(s): 1186 – 1194, 2005.
- [82] H. Tan, J. DasGupta, and K. Ziri-Castro, "Human-body shadowing effects on indoor MIMO-OFDM channels at 5.2 GHz," *Proceedings of the Fourth European Conference on Antennas and Propagation (EuCAP)*, Page(s): 1 – 5, 2010.
- [83] C. Fitzhugh, J. Frolik, R. Ketcham, J. Covell, and T. Meyer, "2.4 GHz multipath environments in airframes," *IEEE Conference on Wireless and Microwave Technology (WAMICON 2005)*, Clearwater, FL, April 7-8, 2005.

- [84] M. Youssef, L. Vahala, and J. H. Beggs, "Electromagnetic propagation of wireless networks in aircraft cabins," *IEEE/ACES International Conference on Wireless Communications and Applied Computational Electromagnetics*, Page(s): 832 – 836, 2005.
- [85] WiFi in the sky. [Online] Available: <http://www.physorg.com/news5047.html>, [Accessed: July 8, 2005].
- [86] Gareth Halfacree, "Delta to fit WiFi to all aircraft," [Online] Available: <http://www.bit-tech.net/news/2008/08/06/delta-to-fit-wifi-to-all-aircraft/1>, [Accessed: August 6, 2008].
- [87] A. Ameti, R. Fontana, E. Knight, and E. Richley, "Ultra wideband technology for aircraft wireless intercommunication systems (AWICS) design," *IEEE Aerospace and Electronic Systems Magazine*, Vol. 19, No. 7, Page(s): 14–18, 2004.
- [88] Jay J. Ely, Gerald L. Fuller, and Timothy W. Shaver, "Ultrawideband electromagnetic interference to aircraft radios," *Digital Avionics Systems Conference*, 2002.
- [89] David Landon and Cynthia Furse, "MIMO transmission equation for array design and analysis," submitted to *IEEE Trans Antennas and Propagation*.
- [90] Sai Ananthanarayanan, Alyssa Magleby Richards, and Cynthia Furse, "Measurement and modeling of multiantenna systems in small aircraft," Submitted to *Journal of Aerospace Computing, Information, and Communication*, June 2010.
- [91] Sai Ananthanarayanan, Alyssa Magleby Richards, and Cynthia Furse, "Measurement and modeling of interference for multiantenna system," accepted for publication in *Microwave and Optical Technology Letters*.
- [92] J. Frolik, "A case for considering hyper-Rayleigh fading channels," *IEEE Transactions on Wireless Communications*, Vol. 6, No. 4, Page(s): 1235–1239, 2007.
- [93] R. Ketcham, J. Frolik, and J. Covell, "Propagation measurement and statistical modeling for wireless sensor systems aboard helicopters," *IEEE Transactions on Aerospace and Electronic Systems*, Vol. 44, No. 4, Page(s): 1609–1615, 2008.
- [94] Nektarios Moraitis, Philip Constantinou¹ Fernando Perez Fontan, and Pavel Valtr. "Propagation measurements and comparison with EM techniques for in-cabin wireless networks," *EURASIP Journal on Wireless Communications and Networking*, 2009.

- [95] D. Palchak and B. Farhang-Boroujeny, "A software defined radio testbed for MIMO systems," *Proceedings of the SDR 06 Technical Conference and Product Exposition*, Orlando, FL, Nov 2006.
- [96] Z. Yun, Software package called "3D ray tracing for radio propagation modeling," last updated Dec 2009, unpublished.
- [97] I. Telatar et al., "Capacity of multiantenna Gaussian channels," *European transactions on telecommunications*, Vol. 10, No. 6, Page(s): 585–596, 1999.
- [98] D. Matolak and A. Chandrasekaran, "Aircraft intravehicular channel characterization in the 5 GHz band," *Navigation and Surveillance Conference, 2008*, Page(s): 1–6, 2008.

CHAPTER 3

TOOLS AND PRELIMINARY STUDIES

In Chapter 2, we reviewed what has been done thus far in the area of wireless communication on aircraft and other vehicles. All the communication systems attempted were using single-input single-output systems, as well as most of the measurement campaigns to characterize the channel, with a limited set of measurements using MIMO systems. They all found the aircraft channel to vary in its multipath at site-specific locations. The simulations of these environments have been limited to either statistical models, which are not site-specific, or SISO simulation software that is site-specific but takes an extensive time to run. In order to accomplish our goals of further characterizing these complex environments and accurately simulating a multiantenna system in a shorter amount of time, we needed new tools. This chapter will discuss our preliminary research and the development of tools which we later use for measurement and simulation of complex channels.

3.1 SISO Measurements in Multipath Channels

To find the range of multipath levels in a variety of multipath environments, path loss was measured for a range of wireless channels using a single-input single-output (SISO) system. This was accomplished using a set of monopole antennas, each with a

gain of 2.15 dBi, designed to transmit and receive at 418, 433, 915, and 2450 MHz. The transmitting antenna was connected to an Agilent E4438C ESG Vector Signal Generator, with power set to 20 dBm, and the receiving antenna was connected to an Agilent E4404B ESA-E Series Spectrum Analyzer. These antennas were placed in a variety of locations, including an anechoic chamber, the hallway of a building, and numerous locations in a passenger car and an A-10 fighter jet. Measured data at each frequency and location was fit to a Ricean curve to find the varying K values, for example, the cockpit to wing data at 915 MHz fit a Ricean $K=-0.07$ dB curve, shown in Figure 3.1. [99]

Sample results for K values from my conference paper [100] are found in Table 3.1. Weak multipath, or low fade depth (around -5 dB), is expressed by a high K value, say above $K=150$ dB. Moderate multipath (fade depth around -20 dB) is expressed in K values between 0 and 10 dB. Extreme multipath (fade depth below -40 dB) occurs at K values below -70 dB [99].

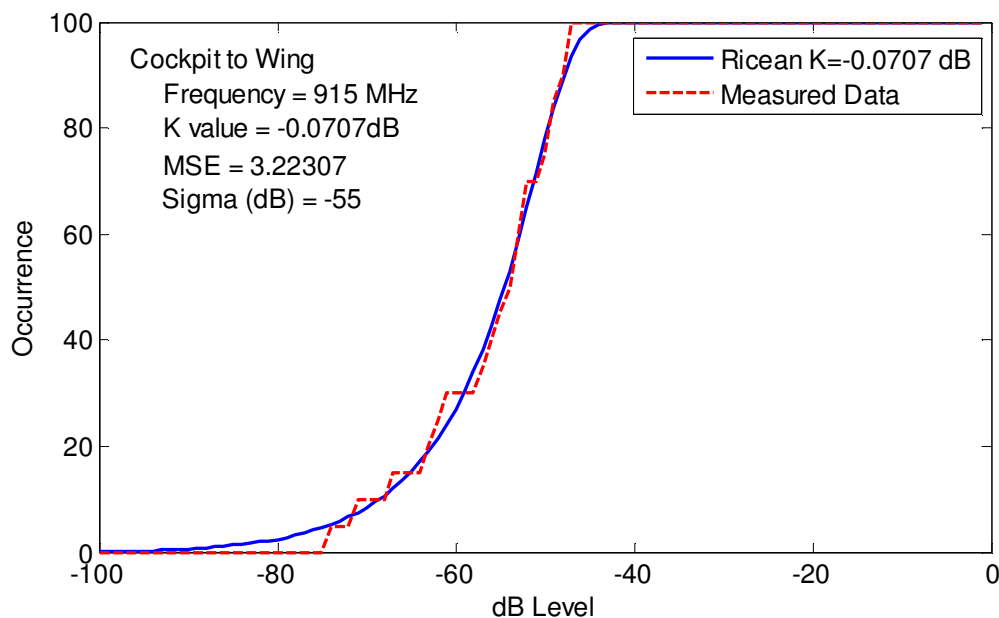


Figure 3.1: Ricean CDF of cockpit to wing at 915 MHz.

Table 3.1: K values for environments with various levels of multipath at 915 MHz [100]

Location	K (dB)	Multipath Level
Anechoic Chamber	200	Low
Aircraft Bay 2 to Bay 3	8	Moderate
Hallway	6	Moderate
Car Passenger Compartment	3	Moderate
Aircraft Cockpit to Wing	0	Moderate
Car Engine Compartment	-70	Extreme
Aircraft Left to Right Wing	-150	Extreme

These measurements verified previous studies that a wide range of K values, associated with moderate to extreme multipath, can be found in small vehicular channels.

3.2 MIMO Simulations in Hyper-Rayleigh Channel

Statistical models thus far have been limited to SISO systems. Previous research resulted in a detailed signal model (DSM) software that used the channel response based on the statistical model to create a channel matrix and combined it with antenna effects to obtain MIMO system capacity [101], as discussed in Section 2.2.3. One of our initial goals was to find the statistical model that best represented the extreme fading found in vehicular channels and simulate the response of these channels with a MIMO system. The first statistical model that considered the severe multipath effects found in vehicles was hyper-Rayleigh [102]. A hyper-Rayleigh channel is described by equation (3.1) with Δ and K values defined by equations (3.2) and (3.3). Hyper-Rayleigh channels occur when the received signal is dominated by two constant amplitude signal components with statistically independent phase components uniformly distributed over $[0, 2\pi)$. This is

also referred to as two-wave with diffuse power (TWDP). The relationship between Δ and K values [102] for this model and the behaviors it exhibits is shown by Table 3.2.

$$V_{received} = \underbrace{V_1 \exp(j\varphi_1) + V_2 \exp(j\varphi_2)}_{\text{specular components}} + \underbrace{\sum_{i=3}^L V_i \exp(j\varphi_i)}_{\text{diffuse component}} \quad (3.1)$$

$$\Delta = \frac{\text{Peak specular power}}{\text{Average specular power}} - 1 = \frac{2V_1V_2}{V_1^2 + V_2^2} \quad (3.2)$$

$$K = \frac{\text{Average specular power}}{\text{Diffuse power}} = \frac{V_1^2 + V_2^2}{2\sigma^2} \quad (3.3)$$

Simulation software was written to evaluate MIMO capacity in various channels using a simplified code based on the detailed signal model (DSM) [100], described in Section 2.2.3. This simplified code created a channel matrix using gain based on the hyper-Rayleigh received signal from equation (3.1) and randomly distributed angles of arrival and departure, which was then combined with estimated antenna effects of directivity, antenna efficiency, antenna radiation pattern, mutual coupling, rotation, and polarization agility. A 2x2 MIMO channel with 0.5λ spacing was simulated over 500

Table 3.2: K and Δ values for channel models

Rayleigh	$K = 0$	NA
Ricean	$K > 0$	$\Delta = 0$
One-wave	$K \rightarrow \infty$	$\Delta = 0$
Two-wave	$K \rightarrow \infty$	$\Delta \geq 1$

trials at varying K factors to compare against SISO measurements described in the previous section. The comparison is shown in Figure 3.2 and Figure 3.3, from my conference paper in [100]. SISO had a greater capacity per antenna than MIMO, but *total* capacity was significantly higher for the MIMO 2x2 system. For the MIMO system, the capacity did not drop below 4.2 bits/Hz/antenna even for strong line of sight K values above 150 dB. A noticeable increase in capacity occurred around $K = 25$ dB, and capacity continued to increase until it maxed out at 5.5 bits/Hz/antenna for 50% abscissa and $K = 8$ dB and stayed close to that capacity for decreasing K values. This shows that varying the K value to match the range of values measured in intravehicle channels appears to have little effect on the capacity of each antenna of a MIMO system assuming hyper-Rayleigh channels.

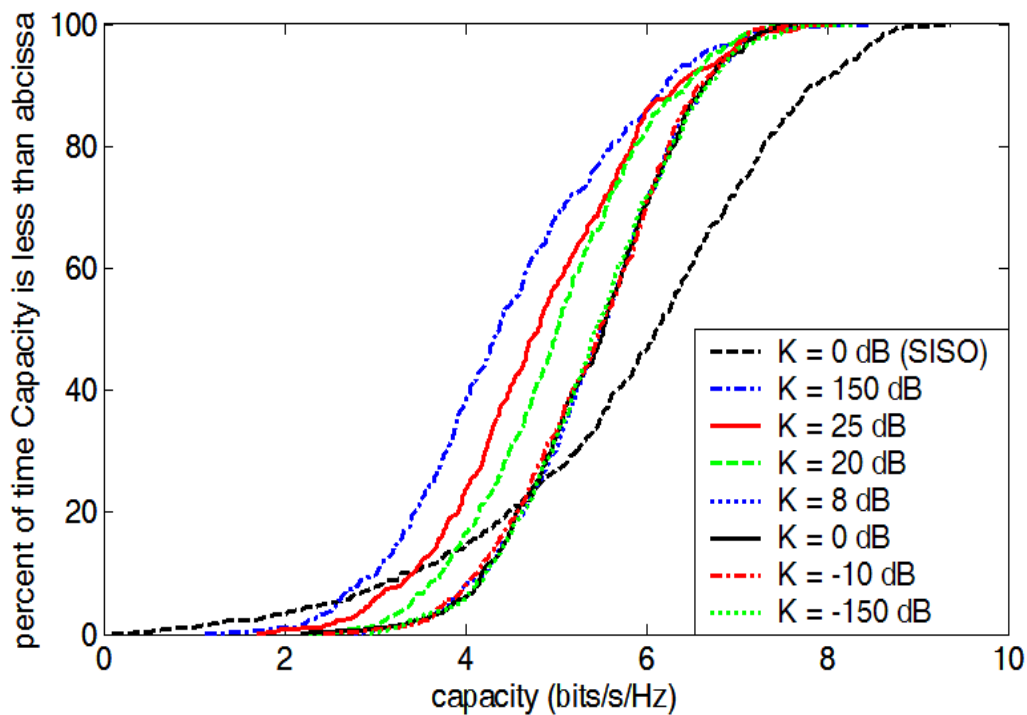


Figure 3.2: Individual antenna capacity CDF of 2x2 MIMO system performance using the hyper-Rayleigh channel (equivalent to SISO performance at different K values)

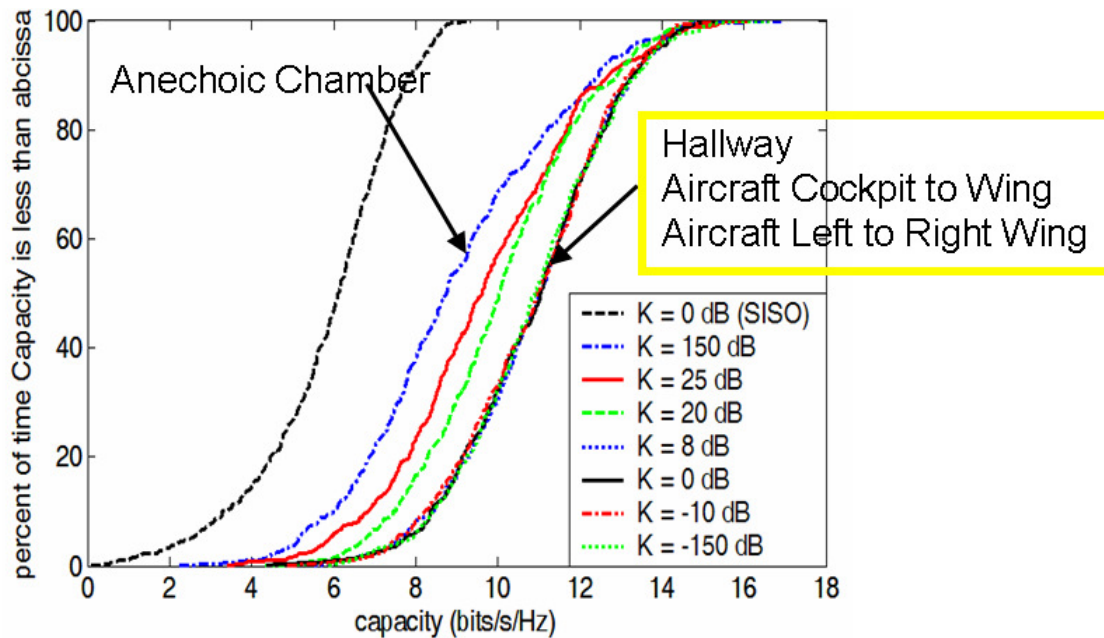


Figure 3.3: Total channel capacity CDF of 2x2 MIMO system using the hyper-Rayleigh channel

The intravehicle channels measured experience moderate to extreme multipath fading, which can be modeled using the hyper-Rayleigh channel [102]. Using this model, MIMO transmission was simulated over the ranges of K values that were seen to occur in vehicles, ranging from 8 dB to -150 dB and compared to strong line of sight values, ranging from 8 dB to 100 dB. MIMO simulations resulted in consistent channel capacity for K values that were measured, which predicts that hyper-Rayleigh may not be detailed enough to differentiate between the wide range of fading that can be found at site-specific locations within complex intravehicular channels. From here, it will be useful to simulate and compare the effects of the channels of interest, and determine what parameters of the MIMO system are most impacted by these channels. This is a completely new application for MIMO systems in a not well-defined channel environment.

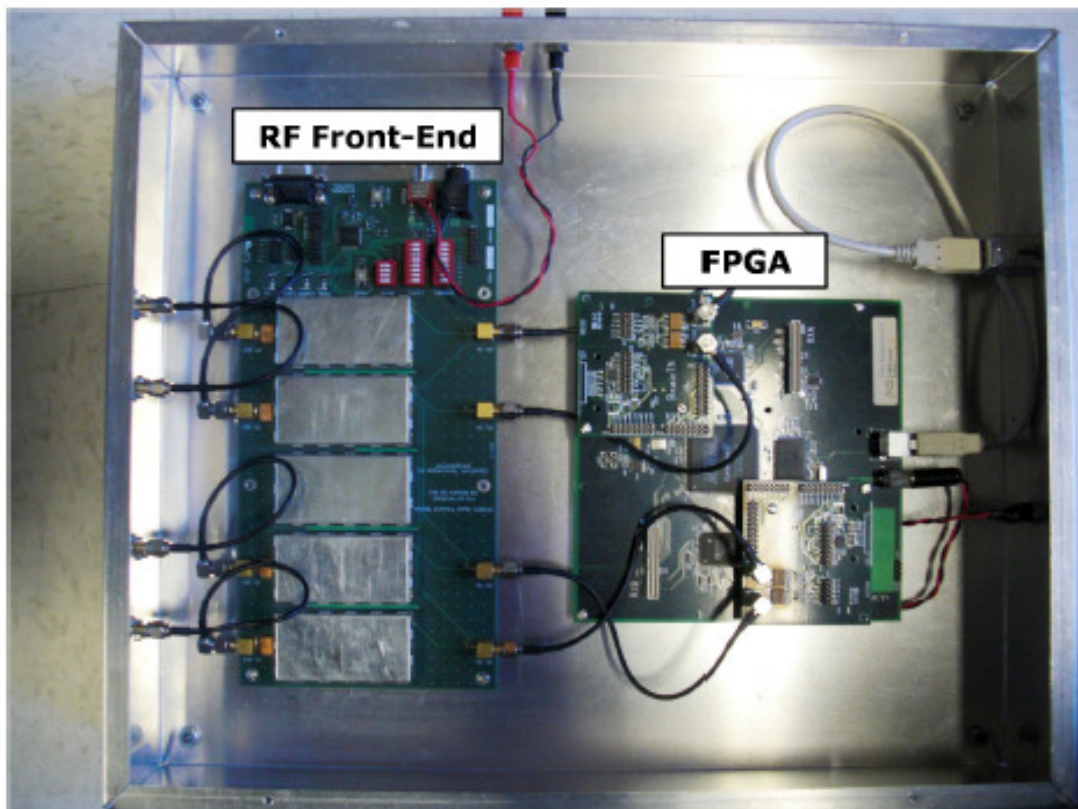
3.3 Multiantenna Test Bed for Channel Measurement

As we were previously limited to characterizing the various channels using SISO measurement, it was necessary to obtain a tool that could measure the channel response of a MIMO system in order to more accurately compare to MIMO simulations. Just such a test bed was created at the University of Utah. It was originally designed in 2006 by David Palchak as a MIMO software defined radio (SDR) measurement system, and details on the original system can be found in [103]. The MIMO test bed was used previously to measure channel capacity for various antenna configurations as well as to test the advantages of polarization agile antennas [105]. This system has now been updated to be used on this project [104].

The software-defined radio (SDR) platform that forms the basis of the test bed consists of antennas connected to an RF front-end which is then connected to a high speed analog-to-digital converter (ADC) when operating as a receiver and a digital-to-analog converter (DAC) when operating as a transmitter, both of which are controlled by a laptop computer. Field programmable gate arrays (FPGA) are used to coordinate parallel data from the ADCs or DACs for a MIMO system. The RF units come from SignalCraft Technologies Inc, with transmit and receive units in separate chassis. The RF front ends each consist of a series of filters, mixers, and amplifiers that convert between RF frequencies and baseband. The system supports a 4x4 single user MIMO (SU-MIMO) array at a center frequency of 915 MHz with a sampling rate of 800 kHz. The antennas were a 8.2 cm spaced 0.25λ monopoles, centered lengthwise on a 38 x 45.7 cm ground plane, starting 10 cm from the edge. [103] Photos of the system are shown in Figure 3.4.



(a)



(b)

Figure 3.4: The University of Utah MIMO Software-defined radio test bed. (a) Complete system. (b) Inside view of chassis with the RF front-end and FPGA

The test bed runs on an open source development kit, the GNU Radio software package, which requires Linux, Matlab, Python and C++. The Universal Software Radio Peripheral (USRP) developed by Ettus Research, LLC operates under the GNU package and acts as the brain of the test bed. Modulation types available on the test bed include BPSK, QPSK, 8-PSK, and 16-QAM. QPSK was used for our measurements without any error correction schemes or feedback (no CSI at the transmitter). Maximum spectral efficiency is 2.5 bits/s/Hz, and the rest of the system parameters are listed in Table 3.3.

Each antenna radiated an average power of around 5 mW, combining to give 20 mW from the entire four-element array. Output power was reduced to 0.5 mW to prevent receiver saturation for transmit locations in proximity to the receive array. Data packets were transmitted based on the 4-QAM modulation scheme using differential encoding with 50 kbps of data per antenna. Each packet started with a simple single antenna preamble of 4000 pseudorandom data bits added to allow phase and timing synchronization by the receiver. The packet then included a multiantenna sequence of 4 x 4000 pseudorandom bits to be used as a training sequence for channel estimation. The

Table 3.3: MIMO test bed system parameters

Parameter	Range
Sample Rate	[0, 1] MHz
Symbol Rate	[0, 125] kHz
Data Bandwidth	[0, 200] kHz
Total Bandwidth	[1, 400] kHz
Center Frequency	[905, 925] MHz

packet terminated with a small payload of text data used to verify proper packet detection in postprocessing. [103]

The received packet of data is then used to create a channel matrix to be used for capacity calculation. To do this, we start with creating a complex M by L matrix named T for the training sequence, which is made up of a set of column vectors following the form

$$T = [t(1) | t(2) | \dots | t(L)] \quad (3.4)$$

Each column vector, $t(i)$, represents an M by 1 vector of complex data symbols that are sent by the transmitter at time i . The resulting N by L matrix of sampled symbols at the k -th receiver is then described as

$$Y_k = H_k T + N_k, \quad (3.5)$$

where N_k is just a matrix of sampled noise with dimensions N by L . Now, since T is known, we can use it to estimate the channel matrix. If we define \tilde{H}_k as the channel matrix estimate, it can be written as

$$\tilde{H}_k = Y_k T^+ = H_k + N_k T^+, \quad (3.6)$$

where T^+ is the Moore-Penrose pseudo inverse of T given by

$$T^+ = (T^H T)^{-1} T^H \quad (3.7)$$

The effects of the noise term N_k are minimal and our approximation, \tilde{H}_k , approaches H_k if the receiver SNR stays relatively large. We can further reduce noise effects by selecting a relatively large L . This is due to the fact that the value $N_k T^+$ acts almost like a correlation between the noise and training sequence. Thus for uncorrelated noise we have $N_k T^+$ approaching 0 as the limit of L approaches ∞ . L can then be chosen as any large value under the condition that the channel remains stationary for the length of the training sequence. All channel matrices for measurements in this paper were estimated using a length $L = 4000$ training sequence of pseudo random data. [103]

3.4 3D Ray Tracing Software

Now that we have the tools to measure and characterize the intravehicle environment, we needed a tool to model the environment, as it is not always economical or even possible to measure these environments. In Section 3.2, we found that the hyper-Rayleigh statistical model was not detailed enough to cover the range of multipath that can be found at site-specific locations within intravehicle channels, which is expected as statistical models average over all sites. Additionally, the hyper-Rayleigh model assumes only two rays in the received signal which does not account for rich multipath environments with more than two paths. There are several numerical models that could be adapted or used to simulate the reflections that occur inside an aircraft fuselage. Full-wave models such as method of moments (MoM), finite integration time domain (FITD), finite difference time domain (FDTD), and others could provide excellent site-specific

channel models [106][107][108] but are very resource and time intensive, making it impractical to use them in this application. Fast 3D and full 3D methods (which combine the shooting and bouncing ray method with an image method) have been used to estimate received power inside aircraft within 10 dBm, but are also resource and time intensive [109]. We chose a site-specific 3D ray tracing model based on a triangular grid method that minimizes computational time by determining which rays arrive at the receive antenna without having to test whether they bounced off every wall in the region [110][111]. The selection criteria, adaptation and detailed description of the site-specific ray tracing model are outlined in this section. The algorithm uses only 25%-30% of what is required for typical ray tracing methods [112] and has been validated in 2D indoor and outdoor environments, and in a 3D environment for reflections in stairwells[110][114]. This ray tracer has been adapted to simulate the reflections that occur inside an aircraft fuselage for both single and multiantenna systems [113]. The output of the 3D ray tracing software includes not only received power, but also path gains along with complex electric fields and angle of arrival and departure (AOA/AOD) information which is used to develop a channel matrix and estimate site-specific capacity performance within the enclosed environment, with input and output parameters as diagramed in Figure 3.5. The software was adapted by making the outside walls sufficiently configurable to represent a fuselage or other vehicle. The software was extended to multiple antennas by postprocessing the single antenna channel data to calculate the additive channel matrix effects from all antenna pairs [111]. The channel is consistent between single measurements, allowing the combination of single sequential measurements to represent one multiple simultaneous measurement.

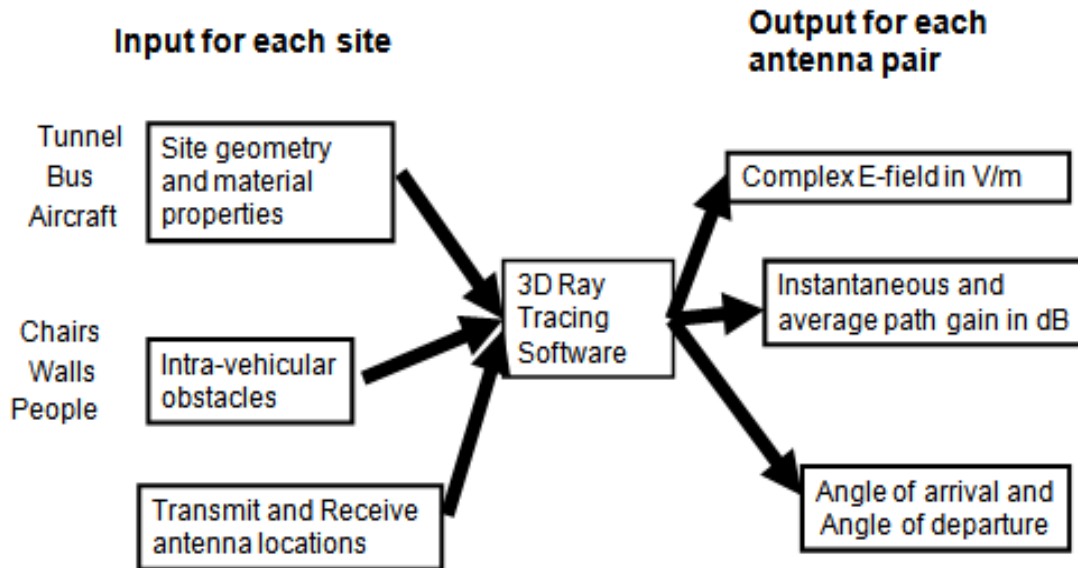


Figure 3.5: Inputs and outputs for 3D software

The 3D ray tracing software is completely configurable to a variety of extreme fading channels found in enclosed environments, such as aircraft. Both flat and curved walls and obstacles in these environments can be represented by faceted rectangular or triangular plates made of a variety of materials, based on material properties for each surface. Preprocessing software is used to create input files for the ray tracer and to make slight adjustments for variations in the configurable environments. The inputs for each enclosed environment include site-specific geometry and material properties of outer walls, location and material properties of intravehicular obstacles, transmit and receive antenna locations, and frequency range. The input parameters are broken down into five groups: reflective surface (size and location of each facet, relative permittivity (ϵ_r) and conductivity (σ) for each reflective surface), lossy surface (size and location of each lossy surface, loss factor in dB), receive and transmit antennas (number of antennas, x-y-

z position of each antenna, repeating number and distance for antenna arrays), and frequency (start frequency, stop frequency and step size), as detailed in Table 3.4, plus a few other inputs that are not part of any specific group for maximum number of reflections allowed and graphic display options.

For simulations in this paper, rectangular facets have been used to represent the simple surfaces such as walls and obstacles found in aircraft and hallways. Triangular facets could be used to model spherical or other complex surfaces. Each aircraft is simulated with five or more faceted sides to represent the cylindrical shape of the fuselage, and flat rectangular surfaces for the front and back of the fuselage, except as otherwise noted. All walls were assumed to be perfect electrical conductors (PEC), except as otherwise noted. Models which include windows use the parameters for glass, with permittivity $4 < \epsilon_r < 10$ F/m, and conductivity $\sigma = 10^{-12}$ S/m [115] for the facet that represents the window. The floor was found to be electrically transparent in [116] for 2.4

Table 3.4: Parameter grouping for ray tracing software

Group	Parameters entered
RefGroup	Reflective surface parameters: number of surfaces, x,y,z position for corners of each surface, relative permittivity (ϵ_r) and conductivity (σ) for each surface
TransGroup	Lossy surface parameters: number of surfaces, x,y,z position for corners of each surface, loss factor in dB
TxGroup	Tx Antenna Parameters: number of antennas, x,y,z position of each antenna, repeating number and distance for antenna arrays
RxGroup	Rx Antenna Parameters: number of antennas, x,y,z position of each antenna, repeating number and distance for antenna arrays
FreqGroup	Frequency Parameters: start frequency, stop frequency and step size

and 5 GHz, and was assumed to be so at 915 MHz as well, for simplification. If there are frequencies where the floor is found to be reflective or lossy, it should be included in the model. Both lossy and reflective internal obstacles such as chairs, reflective walls, etc. can be added by specifying their shape, location, and permittivity/conductivity or the loss factor in dB.

The instantaneous and average path gain along with complex electric fields and angle of arrival and departure for each antenna pair are used to create the 3D channel matrix. Angle of arrival and departure information is combined with antenna gain patterns modeled in CST©, a 3D electromagnetics software which uses Finite Integral Technique (FIT) to simulate specific types of antennas. For multiantenna systems, multiple sets of simulations are postprocessed, which includes incorporating antenna factors using the DSM, to obtain the channel matrix for each antenna pair, which is then used to create the channel matrix, H . The received power can then be estimated from the measured channel response as:

$$P_r = \frac{P_s}{N_r} \| \mathbf{H} \|_{Frobenius}^2 \quad (3.8)$$

where P_r is the received power, H is the channel matrix, N_r is the number of antennas at the receiver, and P_s is the power radiated by the n th antenna. The Frobenius norm is the RMS value of the elements of a matrix. The received SNR can be estimated as:

$$SNR_r = \frac{P_s}{\sigma_w^2 N_r} \| \mathbf{H} \|_{Frobenius}^2 \quad (3.9)$$

where σ_w^2 is the noise variance. The channel matrix obtained from the ray tracing software, referred to as H_{3D} below, can then be combined with the antenna effects using equation (3.10). The estimated SNR_r and complete system channel matrix, H_{DSM} , can then be used to calculate capacity using (3.11) (as detailed in [117]), and further compared to measured capacities.

$$H_{DSM} = \underbrace{Z_0^{1/2} \underbrace{S_{21} (I - S_{RR} S_{11})^{-1}}_{\text{matching}} \left(I + \frac{Z_{RR}}{Z_0} \right)^{-1}}_{M_R} \underbrace{\underbrace{E_{cdr}}_{\text{rad eff}} \underbrace{[H]}_{H_{3D}} \underbrace{E_{cdt}}_{\text{rad eff}} \underbrace{(I - S_{TT})}_{\text{matching}}}_{M_T}}_H \quad (3.10)$$

$$C = \log_2 \det \left[I + \frac{SNR_r N_r}{\| \mathbf{H} \|_{Frobenius}^2} \mathbf{H} \mathbf{H}^H \right] \quad (3.11)$$

For equation (3.10), Z_0 is the characteristic impedance, Z_{RR} is the impedance of the receiver, S_{11} and S_{21} represent a matching circuit and transmission circuit for a selected matching approach, S_{RR} and S_{TT} are the scattering parameters of the unloaded transmit and receive arrays, respectively. Receive and transmit antenna efficiencies, E_{cdr} and E_{cdt} ,

are also included. H is the channel matrix obtained from either the ray tracing software or statistical model, and includes the channel path loss along with the gain at both the transmitter and receiver and any polarization losses. [118]

3.4.1 Initial Validation of 3D Ray Tracer for Aircraft

This section shows our conclusions on the validity of the adaptation of our 3D ray tracing software [113] for preliminary single-input single output (SISO) measurements. Several simulations were run for various configurations, including a tunnel (cement hallway), bus, and aircraft. The standard deviations of error between the measured and simulated values were all calculated around 3 dB, which is good for indoor environments.

The simulations were re-run for several different material properties including dielectric constant (ϵ_r), conductivity (σ), and loss (in dB). Standard deviation of error was sensitive to all of these parameters and was not as affected by other changes in parameters. Measured path loss data was compared to simulated data in Figure 3.6 through Figure 3.8.

All of the path loss simulations showed an increase in loss with an increase in distance from the transmitter, which matched the trend of the measured data, validating that the software was behaving appropriately. Path loss comparisons however, were determined to be an insufficient measurement of channel performance, as it was difficult to extract system loss from the measurements to get an appropriate comparison. This was when we added complex electric field and angle of arrival and departure (AOA/AOD) information to the output of the software, which could be used to estimate channel matrices to calculate capacity for comparing performance.

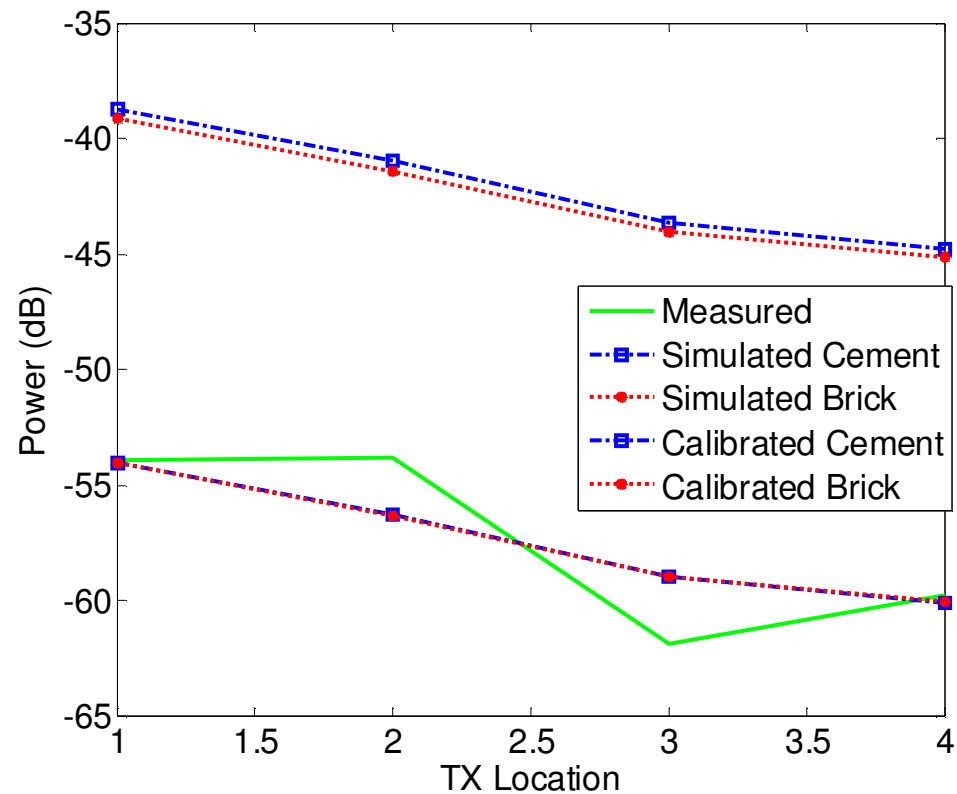


Figure 3.6: Comparison of measured and simulated path loss in a tunnel (cement hallway) for both cement and brick material properties. Standard deviation of error: cement = 2.20 dB, brick = 2.22 dB, showing results are more accurate for the proper material properties.

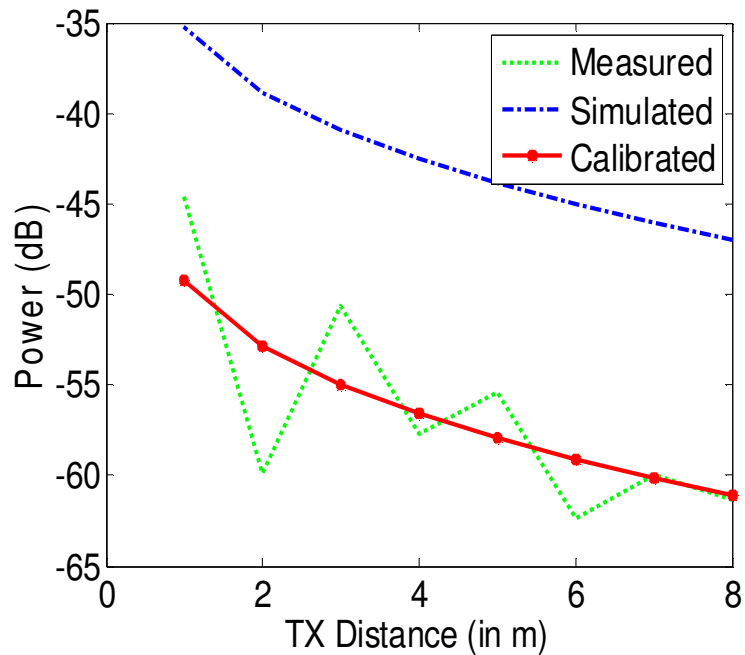


Figure 3.7: Comparison of measured and simulated path loss on a bus. Seat loss was not included in the simulation. Standard deviation of error = 3.92 dB

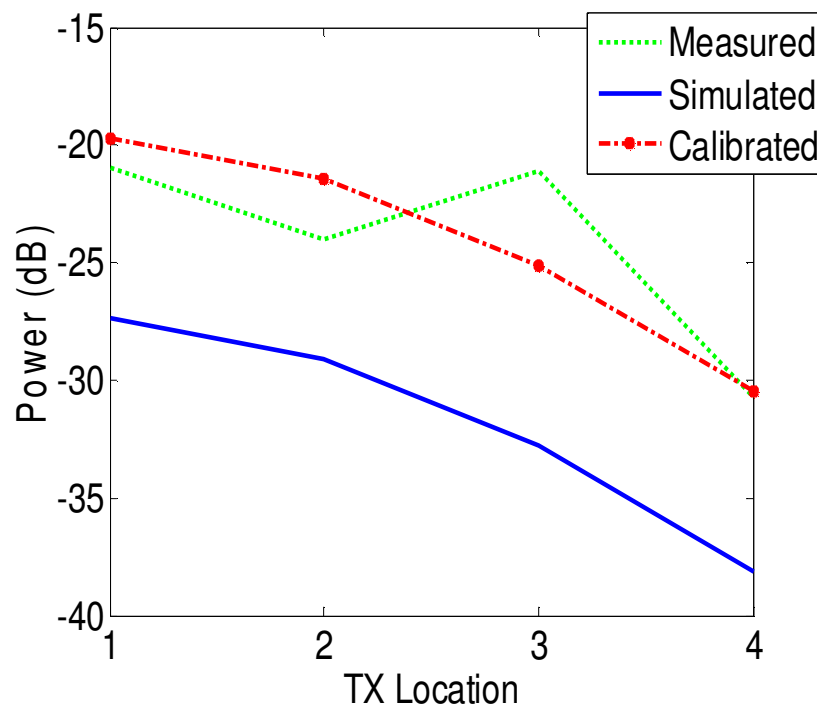


Figure 3.8: Comparison of measured and simulated path loss on an aircraft (beech baron) including loss from seats and cabin separation walls. Standard deviation of error = 2.85 dB

3.4.2 Initial Power Mappings

Before moving on to capacity comparisons, we wished to better understand how the model behaved with received power for different vehicle widths. Following is a comparison of the received power at site-specific locations from the 3D ray tracing simulation. We compared simulations of a 1.1 m diameter by 5.4 m length fuselage with 3 rows of 2 chairs and walls placed at 1.3 m and 4.8 m from the back of a fuselage as depicted in Figure 3.9a) with a 2.2 m diameter by 5.4 m length fuselage with 3 rows of 4 chairs and walls still placed at 1.3 m and 4.8 m from the back of the fuselage as depicted in Figure 3.9b). The chairs and walls were simulated with a loss of 0.1 dB.

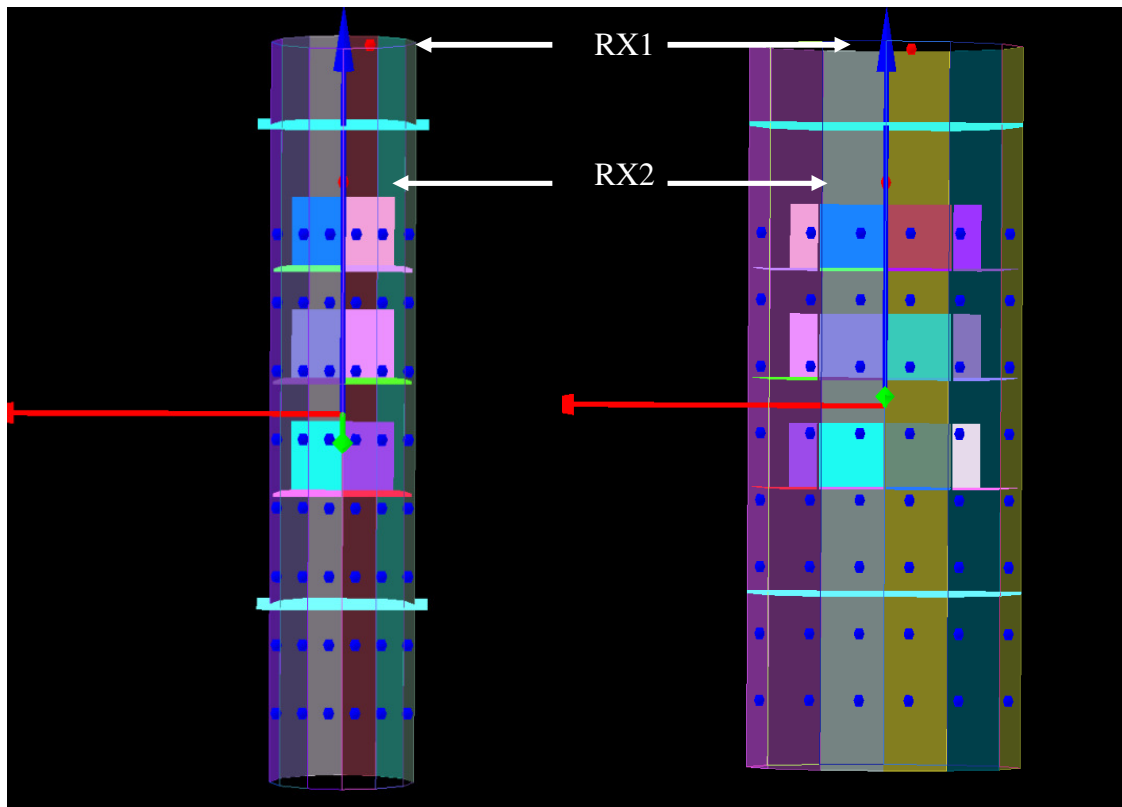


Figure 3.9: 3D simulation of fuselage with chairs. a) 1.1 m diameter fuselage. b) 2.2 m diameter fuselage

Figure 3.10 and Figure 3.11 show the simulated received power at varying distances from the back of each fuselage, with RX1 located at 5.38 m from the back of the fuselage, and at 0.2 m to the right of center width. RX2 is located 4.38 and at center width in the fuselage. The colorbar on the right of the plot shows the received power in dB, the x axis shows the distance in meters from the center of the fuselage ($x = 0$), and the y axis shows the distance from the back of the fuselage, with the 1.3 m and 4.8 m walls denoted by a thick black line. No measurements were taken in the white space. Comparing a) and b) plots from Figure 3.10 and Figure 3.11, there appears to be a tunneling effect. It is clear that for both fuselage diameters that the power dissipates the further it gets from the transmitter, but it stays at a higher level for a longer distance in the narrower fuselage.

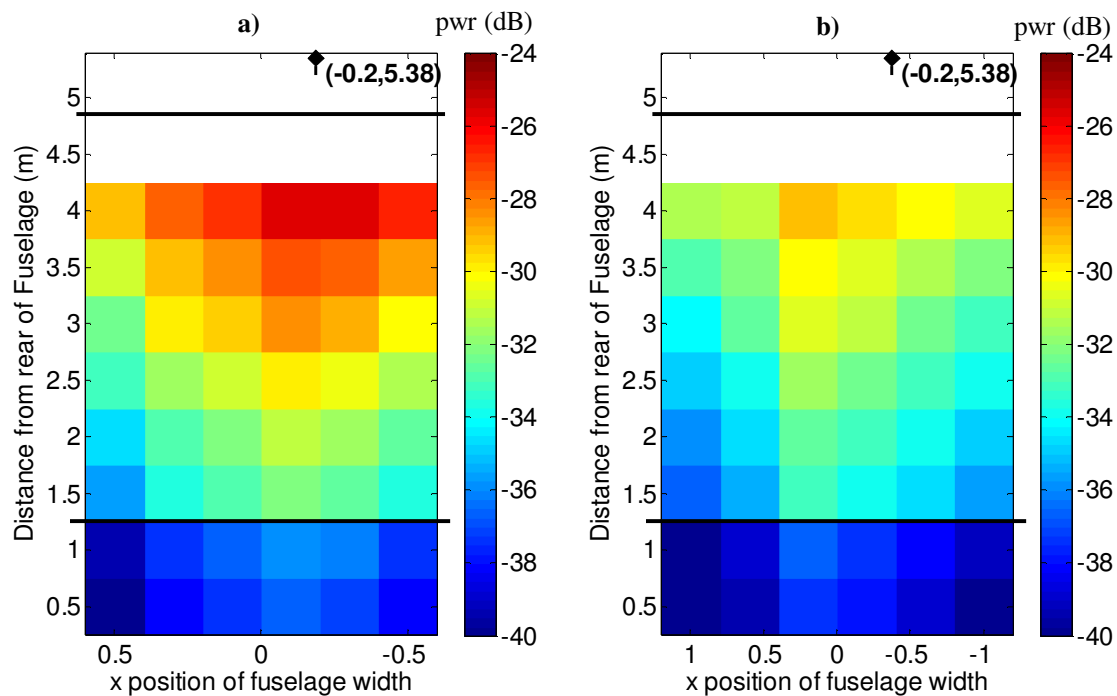


Figure 3.10: Received power mapping for a) RX1 in 1.1 m diameter fuselage. b) RX1 in 2.2 m diameter fuselage

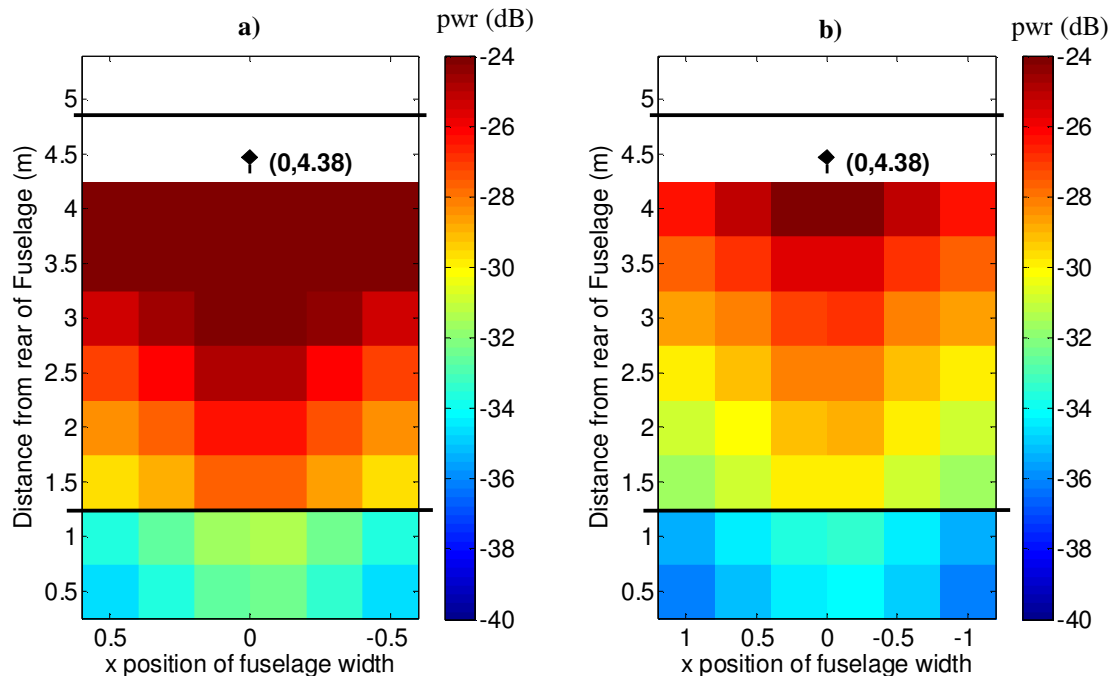


Figure 3.11: Received power mapping for a) RX2 in 1.1 m diameter fuselage. b) RX2 in 2.2 m diameter fuselage

3.4.3 Extension to MIMO

After initial validation of the software, it was then extended for use with multiple antenna systems. The input file takes the start position of the MIMO array, the antenna spacing, and the orientation or direction for as many transmit and receive arrays as needed. The software steps through each antenna pair and calculates all the received rays. Because the channel is consistent between individual simulations, the combination of single sequential simulations represents one multiple simultaneous simulation. The output includes complex electric fields in V/m, instantaneous and averaged received power magnitude, and angle of arrival and departure (AOA/AOD) information for each antenna pair. The output is then processed to calculate the channel matrix, which can then be incorporated into the detailed signal model (DSM) to include multiantenna effects [119]

in order to obtain a full system channel matrix which is used to calculate capacity (as described earlier in Section 3.4). Figure 3.12 through Figure 3.14 show the configuration for a Diamond DA42 Twin Star aircraft with 0.25λ antenna spacing for various locations and orientations throughout the cabin to match what was previously measured with our MIMO test bed.

Once the ray tracing software was capable of simulating multiantenna systems that could be compared to multiantenna measurement, we needed to look at what other factors were required for simulation accuracy.

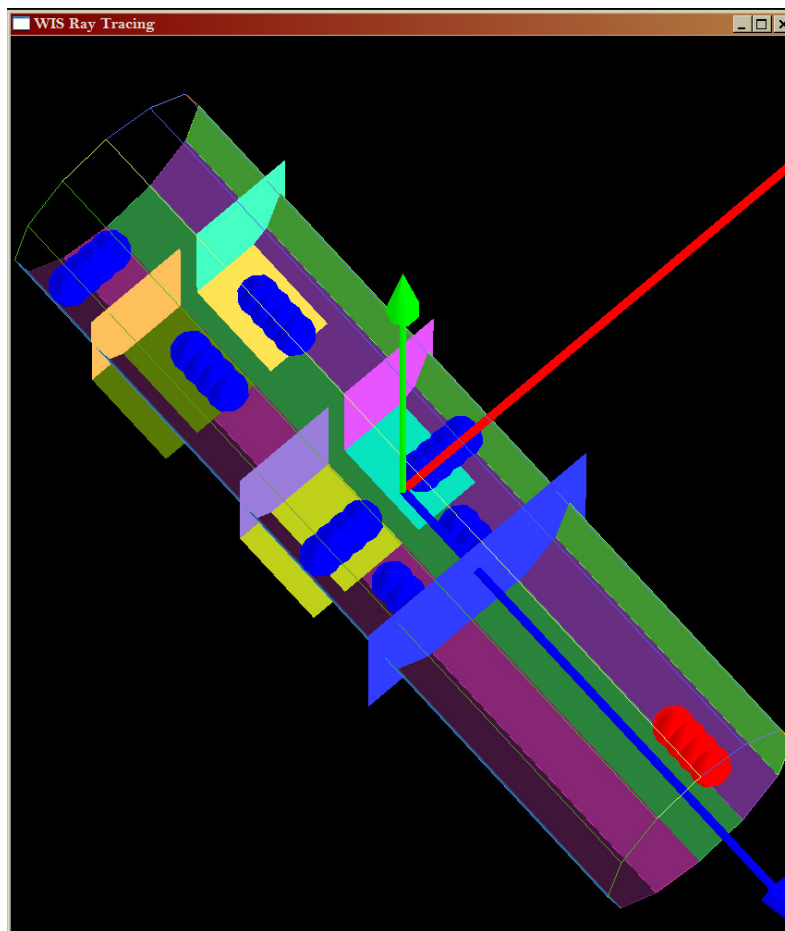


Figure 3.12: Top view of Diamond Twin Star MIMO measurement configuration

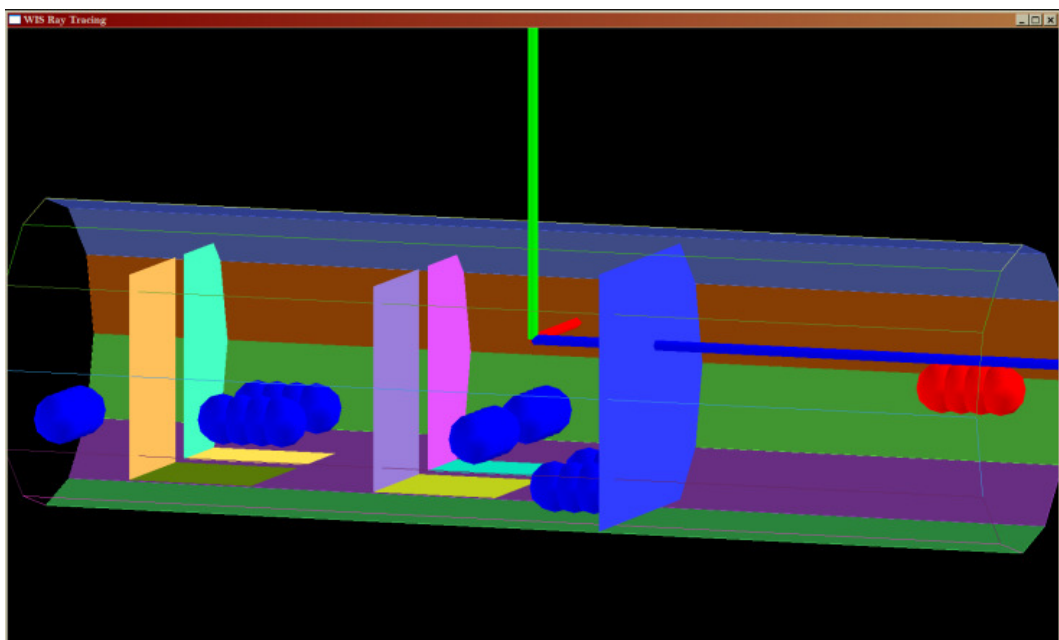


Figure 3.13: Side view of Diamond Twin Star MIMO measurement configuration

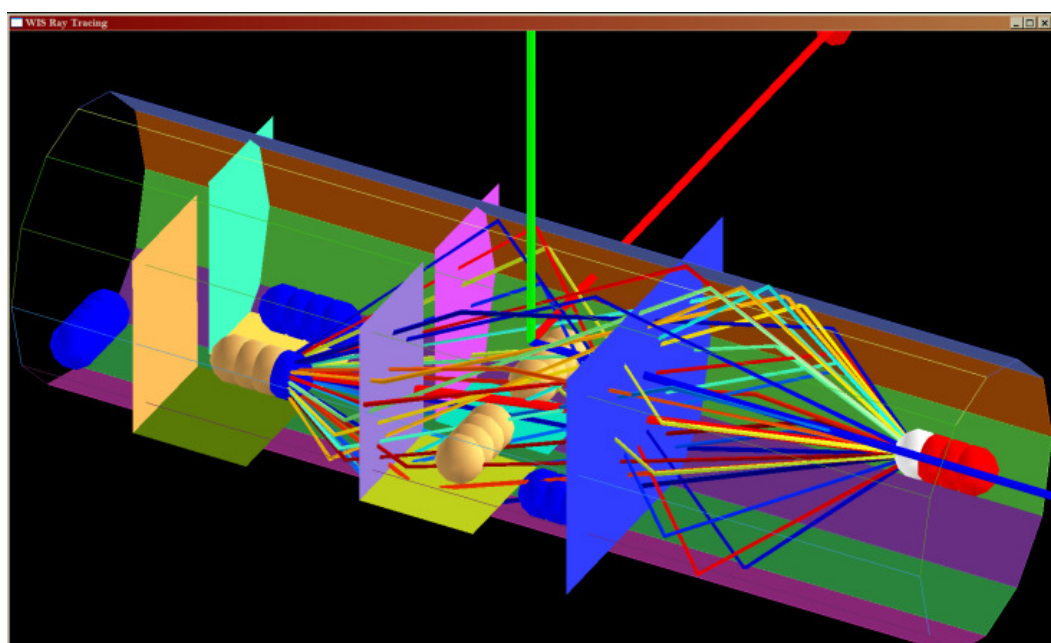


Figure 3.14: Side view of Diamond Twin Star MIMO measurement configuration showing all 2-bounce rays between a pair of MIMO antennas

3.5 Reflective and Lossy Obstacles Within the Channel

In order to accurately model the environment inside aircraft and other vehicular environments, we needed to understand how seats and other obstacles affect the path of the wireless signal. The chairs, walls and other obstacles that may be present within a channel will add reflection, refraction and scattering to the already richly multipath environment, and could have a significant effect on channel performance. Section 2.3 described several studies that quantified many of the parameters of interest. This section discusses additional measurements and analysis that were performed to evaluate how these parameters affect channel simulation in order to accurately model our complex channels of interest.

3.5.1 Seat Measurements

There were a few studies done to attempt to classify the effect of seats [120][121], whether they were lossy or reflective or both, but these were not done at our frequency of interest (915 MHz), and were not all translatable into a measurable power lost in each seat, so we performed a measurement study of our own in an anechoic chamber. The study in [120] developed an equation to calculate the loss due to the backrest of each seat in a Boeing 737–400 aircraft, which resulted in an insertion loss of 9.6 dB at 2.45 GHz, 8.1 dB at 2.1 GHz, and 7.7 dB at 1.8 GHz, respectively. This showed a trend of decreasing loss with decreasing frequency, so we expected our results at our lower frequency of 915 MHz to have a smaller insertion loss.

To measure the path loss of antennas in anechoic chamber we used the same equipment, settings, and 915 MHz antennas as was used for our SISO aircraft

measurements. This equipment included an Agilent E4438C vector signal generator set to 915 MHz, and 20 dBm for the transmitter and an Agilent E4407B spectrum analyzer for the receiver, each connected to a 915 MHz monopole antenna attached to a ground plane, as shown in Figure 3.15.

Antennas were set one meter apart to take the initial measurement for channel loss calculations. We used 10 ft RG 174 cables with a spec loss of 3 dBm/cable for each side of the system. We estimated the antenna gain to be 3 dB and measured a received power of -20.5 dBm +/- 0.1 dBm jitter. We performed another measurement to obtain system loss connecting the cables directly to each other, as shown in Figure 3.16, this time with the vector signal generator set to 915 MHz, and 20 dBm. We measured -5.85 dBm +/- 0.05 dBm jitter when cables were looped, and -5.7 dBm +/- 0.1 dBm jitter when cables were laid out.

Next, we measured chair loss by setting up the antennas one meter apart at approximately one meter elevation (high enough to be mid-back level for the seat), measured received power, then inserted a chair into the path in a manner that blocked line of sight signals, as shown in Figure 3.17 and Figure 3.18, and measured again.

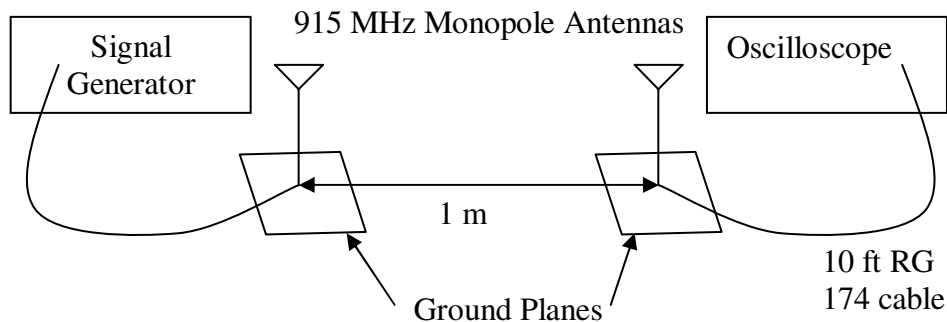


Figure 3.15: SISO equipment setup in anechoic chamber for 1 m measurement at 915 MHz and 2.4 GHz.

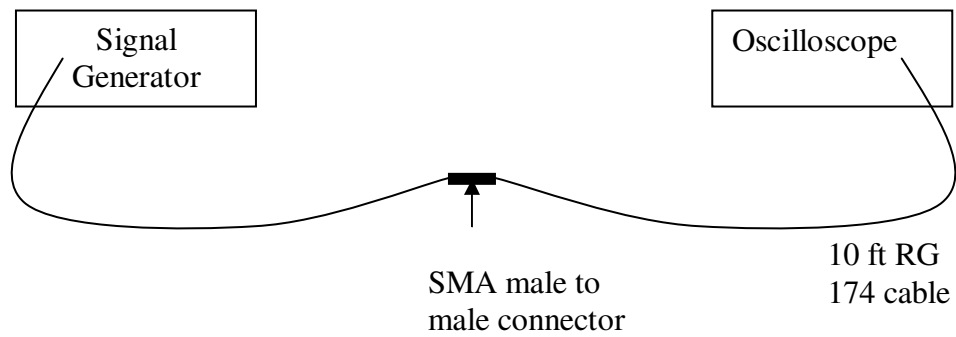


Figure 3.16: SISO equipment setup for system loss measurement.

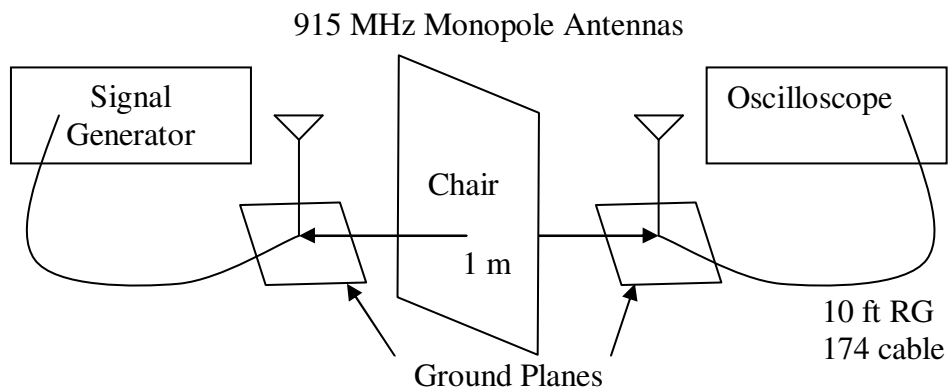


Figure 3.17: SISO equipment setup for chair loss measurement.



Figure 3.18: Photo of SISO equipment setup with and without chair, with red arrows pointing to transmit and receive antennas.

We took measurements for two different types of chairs and for a few different antenna configurations as detailed in Table 3.5. The scope was set to average 100 samples for all measurements in the table.

Comparing the chair measurements at one meter with the line of site measurements at one meter, we concluded that chairs have a 0 to 1.6 dBm loss at 915 MHz, and are almost electrically invisible. These results fit in reasonably with data from previous studies, as it was a much smaller insertion loss for a greatly decreased frequency.

3.5.2 Wall Simulations

Several simulations were run and compared to SISO received power measurements on the Beech Baron and Diamond Twin Star in order to evaluate the loss from walls within the fuselage. The wall loss was varied from 2 to 4 dB, and average error and standard deviation of error for received power were compared. The minimum average and standard deviation were achieved between 2 and 2.8 dB, and thus 2.8 dB was chosen as the standard wall loss for simulation to account for the maximum loss through walls.

Table 3.5: Chair loss measurements in anechoic chamber

Antenna Setup	Frequency	1 m measurement	Leather Chair measurement	Fabric/Metal Chair measurement
Horn to 915 MHz monopole	915 MHz	-16.5 dBm	-15.6 dBm	--
915 MHz Monopole to monopole	915 MHz	-20.4 dBm +/- 0.1 dBm	-20.2 dBm +/- 0.1 dBm	-22 dBm +/- 0.5 dBm

3.6 Summary

With the multiantenna test bed ready for measurement and the ray tracing software capable of simulating multiantenna systems in complex environments including internal obstacles, we now had the tools we needed in order to characterize and analyze multipath environments. Measured and simulated data for a variety of complex channels are compared in the following chapters in order to characterize these channels and show what factors and parameters are required for simulation accuracy.

3.7 References

- [99] T. T. Evans. “Wireless communication channels in aircraft,” Senior Project, University of Utah, Salt Lake City, UT, 2007.
- [100] A. Magleby and C. Furse, “Predicted MIMO performance in intravehicle channels,” *IEEE Antennas and Propagation Society International Symposium*. San Diego, CA, Page(s): 1-4, 2008.
- [101] D. Landon and C. Furse, “The MIMO transmission equation,” (Honorable Mention, student paper contest) *IEEE Antennas and Propagation Symposium (APS)*, San Diego, CA, July 7-11, 2008.
- [102] J. Frolik, “A case for considering hyper-Rayleigh fading channels,” *IEEE Transactions on Wireless Communications*, Vol. 6, No. 4, Page(s): 1235–1239, 2007.
- [103] J. Nagel, A. Magleby, S. Ananthanarayanan, and C. Furse, “Measured multiuser MIMO capacity in aircraft,” accepted for publication in *IEEE Antennas and Propagation Magazine*.
- [104] D. Palchak and B. Farhang-Boroujeny, “A software defined radio test bed for MIMO systems,” *Proceedings of the SDR 06 Technical Conference and Product Exposition*, Orlando, FL, Nov 2006.
- [105] D. Dowdle, “Polarization agile antenna for MIMO,” M.S. Thesis, University of Utah, Salt Lake City, UT, 2007.
- [106] H. L. Blocher, K. Beilenhoff, and J. Wenger, “Simulation of the electromagnetic wave propagation in cars,” *33rd European Microwave Conference, 2003*. Vol. 3, Page(s): 1151 – 1154, 2003.

- [107] M. Heddebaut, V. Deniau, and K. Adouane, "In-vehicle WLAN radio-frequency communication characterization," *IEEE Transactions on Intelligent Transportation Systems*, Vol. 5, Issue: 2, Page(s): 114 – 121, 2004.
- [108] Zhizhang Chen and Shuiping Luo, "Generalization of the finite-difference-based time-domain methods using the Method of Moments," *IEEE Transactions on Antennas and Propagation*, Vol. 54, Issue: 9, Page(s): 2515 – 2524, 2006.
- [109] M. Youssef, L. Vahala, and J. H. Beggs, "Electromagnetic propagation of wireless networks in aircraft cabins," *IEEE/ACES International Conference on Wireless Communications and Applied Computational Electromagnetics*, Page(s): 832 – 836, 2005.
- [110] C. Takahashi, Z. Yun, M. F. Iskander, et al., "Propagation-prediction and site-planning software for wireless communication systems," *IEEE Antennas and Propagation Magazine*, Vol. 49, No. 2, April 2007.
- [111] Alyssa Magleby, Cynthia Furse, and Z. Q. Yun, "3D Ray tracing for intravehicle MIMO," *IEEE/URSI Antennas and Propagation Symposium*, Charleston, SC, June 1-5, 2009.
- [112] Z. Yun, Z. Zhang, and M. F. Iskander, "A ray tracing method based on the triangular grid approach and application to propagation prediction in urban environments," *Proceedings of the IEEE International Symposium on Information Theory (ISIT2004)*, Vol. 50, Page(s): 750–758, May 2002.
- [113] Z. Yun, Software package called "3D ray tracing for radio propagation modeling," last updated Dec. 2009, unpublished.
- [114] S. Y. Lim, Z. Yun, J. M. Baker, N. Celik, H.-S. Youn, and M. F. Iskander "Radio propagation in stairwell: measurement and simulation results," *IEEE Antennas and Propagation Society International Symposium*, Charleston, SC, 2009.
- [115] M. F. Iskander, *Electromagnetic Fields and Waves*. Prospect Heights, IL: Waveland Press, 1992.
- [116] F. Whetten, A. Soroker, D. Whetten, and J. H. Beggs, "802.11 wireless network performances within aircraft cabins." Embry-Riddle Aeronautical University: 2003.
- [117] Sai Ananthanarayanan, Alyssa Magleby Richards, and Cynthia Furse. "Measurement and modeling of multiantenna systems in small aircraft," submitted to *Journal of Aerospace Computing, Information, and Communication*, June 2010.

- [118] Alyssa Magleby Richards, Sai Ananthanarayanan, and Cynthia Furse, “3D simulation of the wireless channel in small aircraft,” submitted to *IEEE Transactions on Vehicular Technology*, October 2010.
- [119] D. Landon and C. Furse, “The MIMO transmission equation,” (Honorable Mention, student paper contest) *IEEE Antennas and Propagation Symposium (APS)*, San Diego, CA, July 7-11, 2008.
- [120] Kathy Weiquan Wang-Hurst, “Analysis of path loss from a transmitter in an aircraft cabin to an exterior fuselage-mounted antenna,” M.S. Thesis, Virginia Polytechnic Institute and State University, Blacksburg, VA, 2007.
- [121] N. Moraitis and P. Constantinou, “Radio channel measurements and characterization inside aircrafts for in-cabin wireless networks.” *IEEE 68th Vehicular Technology Conference-Fall 2008*. Page(s): 1 – 5, 2008.

CHAPTER 4

3D SIMULATION OF WIRELESS CHANNEL IN SMALL AIRCRAFT²

4.1 Abstract

This paper describes the use of 3D ray tracing software for studying the multiantenna channel characteristics in vehicular environments. This software shows improved accuracy over other statistical models. The channel matrix from the ray tracer is postprocessed using a detailed signal model (DSM) that incorporates antenna factors such as radiation pattern, polarization, and matching. The resultant capacity estimation is within 0.5 to 1 bits/s/Hz of measurements for various detailed configurations of the aircraft fuselage. This software can be extremely beneficial in understanding site-specific capacity performance in aircraft, especially when the aircraft or other enclosed channel is difficult to measure or has not yet been built.

4.2 Introduction

Present and proposed wireless communication systems on aircraft carry data from smoke detection systems, in-flight entertainment systems, sensors for wire fault location, chemical sensors, moisture sensors, etc. according to [127], [141], [142], [143]. In order

² Content of this chapter is taken from an article coauthored with Sai Ananthanarayanan P.R. and Dr. Cynthia Furse and submitted to *IEEE Transactions on Vehicular Technology* [28]

to develop wireless communication systems for aircraft, the severe multipath channel found inside aircraft must be well defined. This multipath channel is much more complex than usual indoor/outdoor channels. A common model for the aircraft channel is the hyper-Rayleigh stochastic model. This model is based on a received signal dominated by two constant amplitude signals with angles of arrival uniformly distributed over $[0, 2\pi)$ and is also known as two-wave with diffuse power (TWDP) as described in [122], [127]. Hyper-Rayleigh has been useful for a general understanding of the aircraft environment for single-antenna systems and gives better capacity estimates than some other statistical channel models including IEEE TGn, Kronecker, Weischelberger, and virtual channel models shown in [133]. However, this model was found in [123] to not be accurate enough to describe multiantenna system performance for all types of fading channels. Other effective stochastic models are the Nakagami, log-shadow and Weibull described in [138], even though the latter tends to over-predict the constructive interference of the channel according to [122]. This is particularly problematic in the confined metallic aircraft environment, where the multipath richness of the channel varies considerably between different locations in the aircraft as found in [134], [135], and where multiantenna systems could be advantageous. None of these stochastic models are designed to be used for site-specific modeling, which is particularly important when considering fixed communication points such as sensor networks. Ray tracing, which does enable site-specific modeling, has most commonly been used in modeling indoor/outdoor channels in [125] and [148]. It has also been applied for single input and optical communication in aircraft cabins in [127], [146], [147]. This paper will use a more advanced ray tracing model that includes the reflection and loss effects from

windows, seats and walls, to model multiple antenna communication systems in aircraft. The measurements and simulations are site-specific, using actual aircraft structure geometries. The channel matrix obtained from the ray tracing model is then postprocessed to calculate site-specific channel capacity using a network-theory-based detailed signal model (DSM) for multiantenna systems. This model includes the effects of antenna polarization misalignment, correlation, mutual coupling, and radiation efficiency which were found in [130] to impact multiantenna system performance. Although multiantenna systems have great promise in this application, they will still require improvements in antenna miniaturization, smaller and lower power transceivers, and a thorough understanding of the site specific channel. This paper focuses on understanding the complex channel found in the interior of an aircraft fuselage. An evaluation of the internal compartments of the aircraft, where sensors and control systems may most often be embedded, would require a full-wave 3D modeling method such as the finite-difference time domain method that can consider interactions of the fields with this even more densely packed metallic environment (as the close range spaces are no longer far-field, an assumption required for the ray tracer). The site-specific modeling improvements this paper demonstrates in the fuselage indicate that future work focused on the internal compartments may very well yield similar improvements over statistical channel models in capacity predictions in those areas.

This paper discusses a site-specific 3D ray tracing modeler which uses the triangular grid method to improve computational efficiency, decreasing the CPU time needed to only 25%-30% of what is required for typical ray tracing methods as detailed in [125]. It has been validated and used to estimate location specific channel

performance in 2D indoor/outdoor environments as well as the 3D environment of a stairwell in [124], [126], [131]. This ray tracer has been adapted to simulate the reflections that occur inside an aircraft fuselage. This information is used to develop a channel matrix and site specific capacity predictions. Preliminary research in [123], [130] has shown that multiantenna systems use spatial diversity to take advantage of extreme multipath environments, such as those found in aircraft. Additionally, for ideal multiantenna systems [143], shows that capacity grows linearly with increasing antenna element count without requiring additional bandwidth. Thus the 3D software has been extended to simulate both single and multiantenna systems in order to facilitate development of both types of systems and explore the advantages of each. The site-specific model described in this paper provides significant improvements in accuracy of the channel matrix over traditional statistical models. Capacity predictions in the fuselage are also compared for varying input parameters of the ray tracing software to see which of these parameters have significant impact on accuracy. The site-specific ray tracing model is described in Section 4.3, as well as how to combine it with a network-theory based DSM. Initial validation of the 3D ray tracing model is detailed in Section 4.4. Section 4.4 also evaluates trade-offs between the site-specific and statistical channel models in aircraft. An analysis of how the configurable parameters of the 3D ray tracing software affect its accuracy for predicting capacity at the different locations within the fuselage is given in Section 4.5.

4.3 3D Ray Tracing Software

The selection criteria, adaptation and detailed description of the site-specific ray tracing model are outlined in this section. There are several numerical models that could be adapted or used to simulate the reflections that occur inside an aircraft fuselage. Full-wave models such as method of moments (MoM), finite integration time domain (FITD), finite difference time domain (FDTD), and others found in [139], [140], and [149] could provide excellent site-specific channel models but are very resource and time intensive, making it impractical to use them in this application. Fast 3D and full 3D methods (which combine the shooting and bouncing ray method with an image method) have been used in [127] to estimate received power inside aircraft within 10 dBm, but are also resource and time intensive. We chose a 3D ray tracing model from [126] and [131], which is based on a triangular grid method that minimizes computational time by determining which rays arrive at the receive antenna without having to test whether they bounced off every wall in the region. The algorithm uses 30% or less CPU time than other ray tracing methods and has been validated in 2D indoor and outdoor environments, and in a 3D environment for reflections in stairwells in [124]-[126]. The output of the 3D ray tracing software includes not only received power, but also path gains along with complex electric fields and angle of arrival and departure (AOA/AOD) information which can be used to estimate site-specific capacity performance within the enclosed environment. The software was adapted by making the outside walls sufficiently configurable to represent a fuselage. The software was extended to multiple antennas in [123] by postprocessing the single antenna channel data to calculate the additive channel matrix effects from all antenna pairs. The channel is consistent between single measurements, allowing the

combination of single sequential measurements to represent one multiple simultaneous measurement. The results of the adaptation were initially validated by measurements in two small aircraft, a Diamond DA-42 Twin Star (composite body) and a Beech Baron BE 58P (metallic body), for comparison. These initial comparisons showed excellent agreement of received power trends shifted by as little as 5 dB for the aircraft in [123] and capacity predictions within 1 bit/s/Hz in the tunnels in [150]. Further validation of the adaptation of the 3D software is discussed in this paper using measurements on a medium aircraft, the Rockwell T-39 Sabreliner (metallic body) and using measurements previously taken on the Diamond DA-42 Twin Star (composite body)

The 3D ray tracing software is completely configurable to a variety of extreme fading channels found in enclosed environments, such as aircraft. Both flat and curved walls and obstacles in these environments can be represented by faceted rectangular or triangular plates made of a variety of materials, based on material properties for each surface. Preprocessing software is used to create input files for the ray tracer and to make slight adjustments for variations in the configurable environments. The inputs for each enclosed environment include site-specific geometry and material properties of outer walls, location and material properties of intravehicular obstacles, transmit and receive antenna locations, and frequency range. The input parameters are broken down into five groups: reflective surface (size and location of each facet, relative permittivity (ϵ_r) and conductivity (σ) for each reflective surface), lossy surface (size and location of each lossy surface, loss factor in dB), receive and transmit antennas (number of antennas, x-y-z position of each antenna, repeating number and distance for antenna arrays), and frequency (start frequency, stop frequency and step size), plus a few other inputs that are

not part of any specific group for maximum number of reflections allowed and graphic display options.

For this paper, rectangular facets have been used to represent the simple surfaces such as walls and obstacles found in aircraft and hallways. Triangular facets could be used to model spherical or other complex surfaces. Each aircraft is simulated with 12 faceted sides to represent the cylindrical shape of the fuselage, except as otherwise noted, and flat rectangular surfaces for the front and back of the fuselage. None of the models in this paper include windows, which would result in more power loss than shown here. The floor was found to be electrically transparent in [155] for 2.4 and 5 GHz, and was assumed to be so at 915 MHz as well, for simplification. If there are frequencies where the floor is found to be reflective or lossy, it should be included in the model. Both lossy and reflective internal obstacles such as chairs, reflective walls, etc. can be added by specifying their shape, location, and permittivity/conductivity or the loss factor. All aircraft walls were assumed to be perfect electrical conductors (PEC), except as otherwise noted. Chairs were modeled as two flat surfaces connected at one edge with a loss factor of 0.1 dB, based on transmission measurements made in an anechoic chamber. Lossy walls within the cabin were modeled as a rectangular surface with a loss factor of 2.8 dB, which was found empirically by comparing simulated and measured values with different loss factors for the walls. The various configurations simulated for the Rockwell T-39 Sabreliner (metallic body) are detailed in Figure 4.1, all of which used perfect electrical conductor (PEC) parameters for the outer reflective walls.

Antenna locations should be a small distance from walls to avoid modeling errors, as antennas are modeled as spheres with a small diameter and are seen as embedded in a

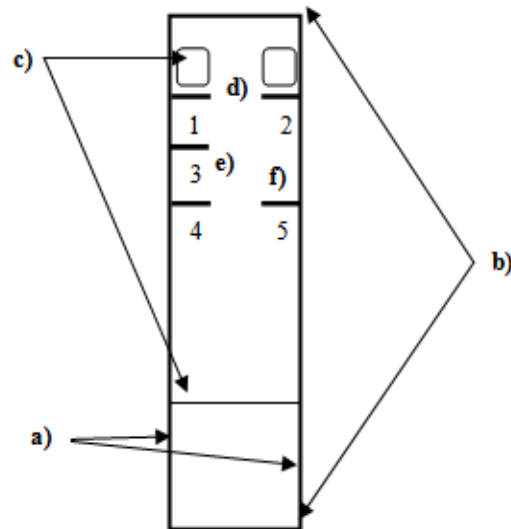


Figure 4.1: Configurations used for 3D ray tracing model of the Sabreliner. a) Fuselage tunnel: includes side walls only, b) Fuselage with endcaps: adds front and back ends, c) Fuselage with lossy obstacles: adds lossy cockpit chairs and back wall d) Cockpit configuration: adds reflective walls 1, 2, e) Half configuration: adds reflective walls 3, 4, f) Full configuration: add reflective wall 5—includes everything in figure.

wall if located too close to one. Our simulation antennas are a minimum of 1 cm from any wall or floor, which is approximately 0.03λ , at our measurement frequency, 915 MHz, with $\lambda = 32.8$ cm. Opposing sides of reflective walls must also be a reasonable distance (again we used 1 cm, or 0.03λ) away from each other to avoid mathematical error. For ray tracing to be effective, measurement distances between transmit and receive antennas should be in the far field, which is approximately $r > 0.167 \lambda$ from [156] (or 5.2 cm). This value should not only be applied to the distance between transmitter and receiver antenna, but also antenna distance from walls (or other reflective objects) to keep reflections in the far field. Distances between transmit and receive antennas were kept at this range, but distances from walls were sometimes smaller. Increasing the distance

would be expected to further improve the accuracy of the simulations discussed in this paper.

We simulated at 915 MHz, chosen to match our available multiple antenna test system, though the software also allows for a range of frequencies. The number of projected rays is limited by specifying a maximum number of bounces before reaching the receiver. Rays that do not reach the receiver within their allotted number of bounces are ignored. The maximum number of projected rays for simulations in this paper is 320, which can be attained when the maximum number of reflections is set to 6 or more. The maximum number of reflections for simulations in this paper was set to 10, unless otherwise noted. Simulations in this paper took from 10 to 30 minutes, depending on CPU RAM and processor speed (from 8G at 2.3 GHz to 512M at 1.5 GHz respectively), number of antennas, and maximum number of reflections allowed.

The instantaneous and average path gain along with complex electric fields and angle of arrival and departure for each antenna pair are used to create the 3D channel matrix. Angle of arrival and departure information is combined with antenna gain patterns modeled in CST©, a 3D electromagnetics software that uses the Finite Integral Technique (FIT) to simulate specific types of antennas. For multiantenna systems, multiple sets of simulations are postprocessed to obtain the channel matrix for each antenna pair, which is then used to create the channel scattering matrix, H . The received power can then be estimated from the measured channel response as:

$$P_r = \frac{P_s}{N_r} \| \mathbf{H} \|_{Frobenius}^2 \quad (4.1)$$

where P_r is the received power, H is the channel scattering matrix, N_r is the number of antennas at the receiver, and P_s is the power radiated by the n th antenna. The Frobenius norm is the RMS value of the elements of a matrix. The received SNR can be estimated as:

$$SNR_r = \frac{P_s}{\sigma_w^2 N_r} \| \mathbf{H} \|_{Frobenius}^2 \quad (4.2)$$

where σ_w^2 is the noise variance. The multiantenna capacity can then be calculated using:

$$C = \log_2 \det \left[I + \frac{SNR_r N_r}{\| \mathbf{H} \|_{Frobenius}^2} \mathbf{H} \mathbf{H}^H \right] \quad (4.3)$$

The antenna affects are incorporated into the channel matrix using:

$$H_{DSM} = \underbrace{Z_0^{1/2} \underbrace{S_{21} (I - S_{RR} S_{11})^{-1}}_{\text{matching}} \left(I + \frac{Z_{RR}}{Z_0} \right)^{-1}}_{M_R} \underbrace{E_{cdr}}_{\text{rad eff}} \underbrace{[H]}_{H_{DP}} \underbrace{E_{cdt}}_{\text{rad eff}} \underbrace{(I - S_{TT})}_{\text{matching}} \quad (4.4)$$

Z_0 is the characteristic impedance, Z_{RR} is the impedance of the receiver, S_{11} and S_{21} represent a matching circuit and transmission circuit for a selected matching approach, S_{RR} and S_{TT} are the scattering parameters of the unloaded transmit and receive arrays respectively. Receive and transmit antenna efficiencies, E_{cdr} and E_{cdt} , are also included. H is the channel scattering matrix created from the model or measurement and includes the channel path loss along with the gain at both the transmitter and receiver and any directivity or polarization losses.

The estimated H and SNR_r from (2) can be used to calculate capacity either by using H directly in (3) or by combining H with the DSM (4) to obtain a complete system channel matrix, H_{DSM} , which is then combined with (4.3) to obtain a capacity calculation which includes antenna effects [133]. We will show in the next section that combining the channel scattering matrix obtained from the model, H , with DSM in (4.4) gives a more accurate capacity from (4.3) than using H alone.

The capacity obtained using the 3D ray tracing channel matrix will be compared to measurements obtained from the Rockwell T-39 Sabreliner and the Diamond DA42 Twin Star in Sections 4.4 and 4.5. The Twin Star is a composite airplane, and the walls were therefore modeled over a range of relative permittivity (ϵ_r) and conductivity (σ) to see how accuracy was affected by material properties. No calibration was required for capacity measurements, as all sampled data were normalized to a unit noise variance at each antenna. This was accomplished by isolating an unused portion of the spectrum and applying the matched filter as if there were actual data. The resultant noise variance was then used as the normalization factor for the antenna. Also, it is common in multi-antenna array measurements to normalize the channel matrices in order to eliminate capacity

variations due to path loss. The resultant capacity after normalization is thus a reflection of the relative multipath richness of the channel, rather than any particular gain due to proximity with the transmitter.

4.4 Quantification of the Aircraft Communication Environment

In this section, we evaluate the need to include antenna effects in multiantenna systems using our DSM to postprocess the 3D channel model, described later in this section. Additionally, due to the widely varying channel inside aircraft, such as that found in [138], we evaluate how a site-specific ray tracing model compares to commonly used statistical and measurement based channel models that are averaged over the aircraft as a whole.

The network-theory-based DSM predicts the capacity of the channel (4.3) by combining the channel matrix created from either site-specific or statistical models with antenna effects (4.4). The DSM includes the capacity-reducing effects of antenna polarization misalignment, correlation, mutual coupling, and radiation efficiency [130]. In order to characterize the intraaircraft channel, Ricean K factors were derived from single-antenna measurements. K factors were found to be in the range from 0 to 15 dB for three different small aircraft, the Rockwell T-39 Sabreliner, Diamond DA-42 Twin Star, and Beech Baron BE 58P [138]. These empirical K factors were combined with a Gaussian distribution to create a channel matrix for the DSM [123][133], and will hereafter be referred to as the K-G model. The hyper-Rayleigh model was also used to create a channel matrix for the DSM. The hyper-Rayleigh model described in [122] assumes the received signal is dominated by two constant amplitude signal components

with uniformly distributed angles of arrival over $[0, 2\pi)$ and uses the same K factor. This is also referred to as two-wave with diffuse power (TWDP).

In this section, we compare the statistical K-G and hyper-Rayleigh models to the site-specific 3D ray tracing model. The K-G and hyper-Rayleigh models are used because they gave better capacity estimates in [133] than several other statistical models including the IEEE TGn 100, Kronecker from [152], Weischelberger from [153], and virtual channel from [152] models for the Beech Baron BE 58P, Diamond DA-42 Twin Star, and Rockwell T-39 Sabreliner aircraft. All of these models are based on statistical averages of the channels within the aircraft. We would expect the site-specific model to provide more accurate results than these simpler statistical models at the cost of an increase in computational complexity.

To quantify the channels on a Rockwell T-39 Sabreliner and a Diamond DA42 Twin Star, capacity measurements were taken with a test bed designed in [154] and updated in [137]. This included a 4x4 system of 0.25λ spaced monopoles at 915 MHz. Data packets were transmitted based on the 4-QAM modulation scheme using differential encoding with 50 kbps of data per antenna. Each packet started with a simple single antenna preamble of 4000 pseudorandom data bits added to allow phase and timing synchronization by the receiver. The packet then transmitted a multiantenna sequence of 4×4000 pseudorandom bits to be used as a training sequence for channel estimation. The packet terminated with a small payload of text data used to verify proper packet detection in postprocessing.

For the Sabreliner, the transmit antenna was placed on the dash of the cockpit for TX1. The receiver was initially placed 2.5 ft from the transmitter, where three

measurements were taken spanning the width of the aircraft. It was then moved in 3.1 ft increments up to 17.5 ft, taking measurements spanning the width of the aircraft at each distance. Two other locations for the transmitter were used—TX2 in the maintenance bay in the rear of the aircraft, and TX3 in the center of the aircraft (location 7). The approximate receiver and transmitter locations are shown in Figure 4.2.

Measurements for TX2 were obtained at receiver locations 7 through 17. These showed an obvious decrease in the receive power as we moved away from the transmitter and a significant loss with TX2 in the maintenance bay. We then modeled the aircraft

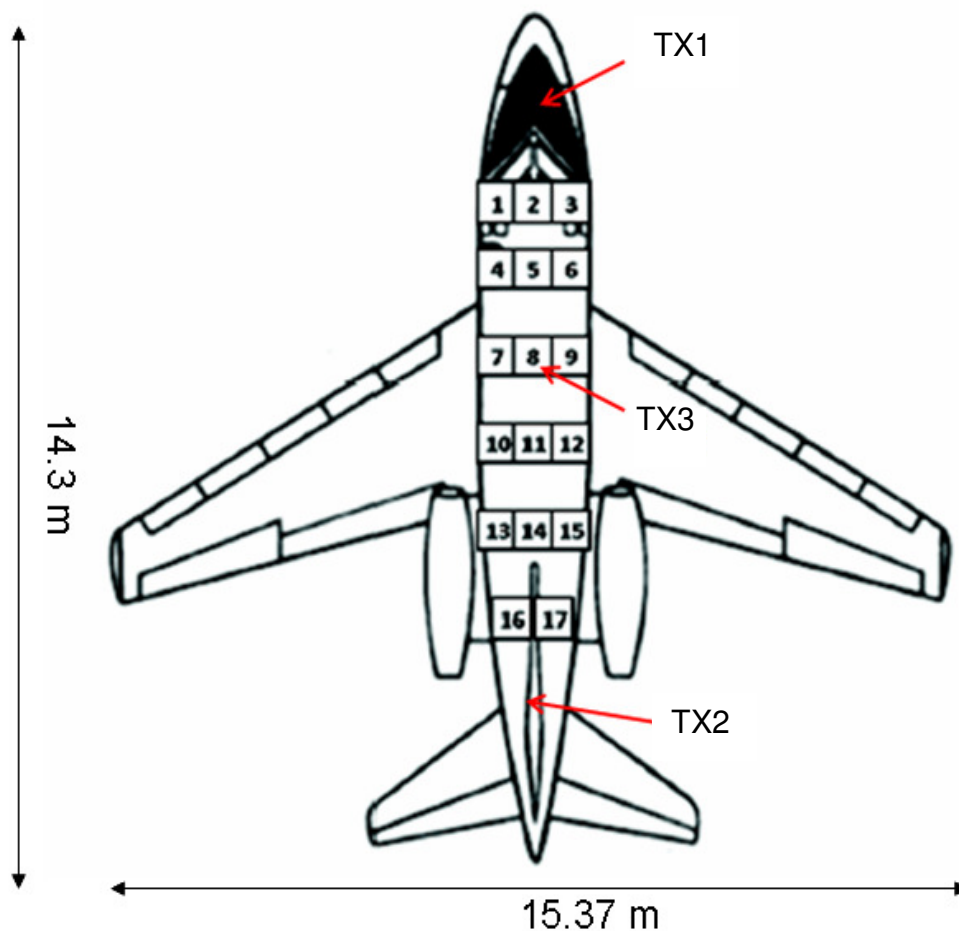


Figure 4.2: Transmitter and receiver locations for multiantenna measurements on the Rockwell T-39 Sabreliner.

using the 3D ray tracing software as detailed in Section 4.3. We used a variety of configurations (shown in Figure 4.1) to evaluate how much 3D modeling detail is required for each site. Then we evaluated whether using the channel matrix from the 3D ray tracing model directly in the capacity equation (3) was as accurate as combining the 3D ray tracing model with the DSM (4) before plugging it into (3). We found that combining the ray tracing channel matrix with the DSM (3D+DSM) decreased the error by 0.5 bits/s/Hz up to 1.3 bits/s/Hz, increasing with the detail of the configuration. For the 3D+DSM, the expected trend that increasing the detail of internal obstacles improves accuracy was seen as the error went from 1.1 bits/s/Hz for the cockpit configuration down to less than 0.5 for the full configuration. Due to this improved accuracy, the rest of the 3D simulations, as well as the K-G and hyper-Rayleigh models analyzed in this paper were postprocessed with the DSM equation.

The measured capacity is shown in Figure 4.3 for TX1 at each receiver location throughout the Sabreliner to illustrate the effect of walls and other obstacles inside the fuselage. The center point at the back of the plane was created by taking an average of locations 16 and 17 to get the value for the location between them. The capacity varies up to 5 bits/s/Hz depending on the receive location. There is a significant loss in capacity just behind wall 4 in Figure 4.3, and a hot spot at the back of the fuselage. These large variations in capacity that depend on the inner geometry of the plane validate the need for site-specific modeling of intraaircraft environments.

We then compared the three most complex configurations from the ray tracing software (see d), e) and f) in Figure 4.1) averaged over all locations to the K-G and hyper-Rayleigh models as shown in Figure 4.4. For transmitter locations 1 and 2, the K-

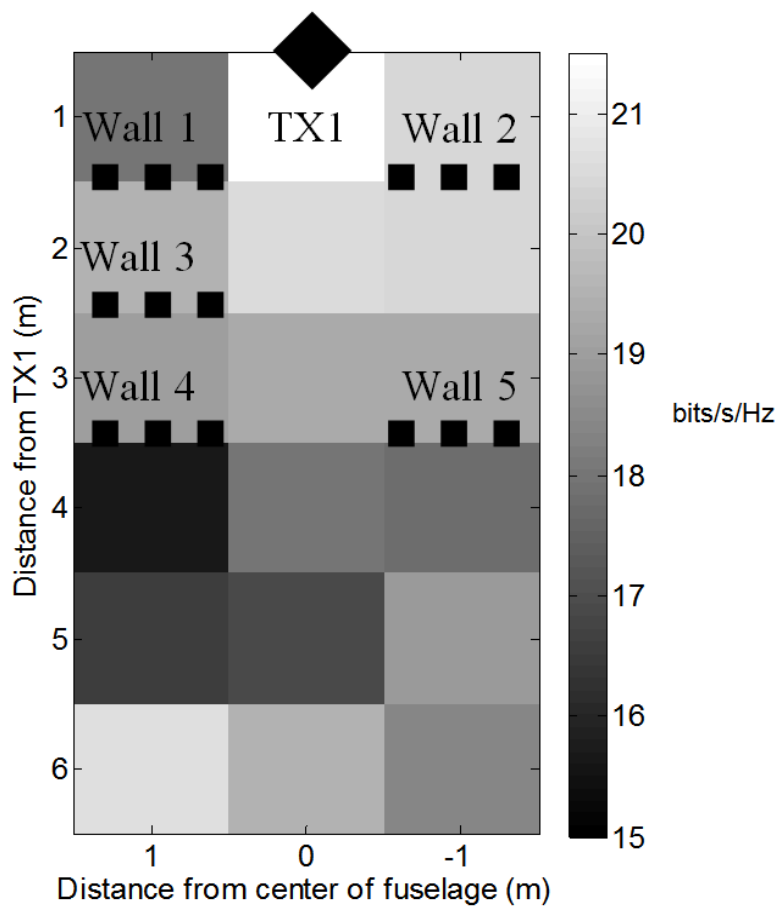


Figure 4.3: Measured capacity for TX1 in the Sabreliner. Location of internal reflective walls and transmitter on the front dash of the cockpit are shown. Each color block represents a receiver location.

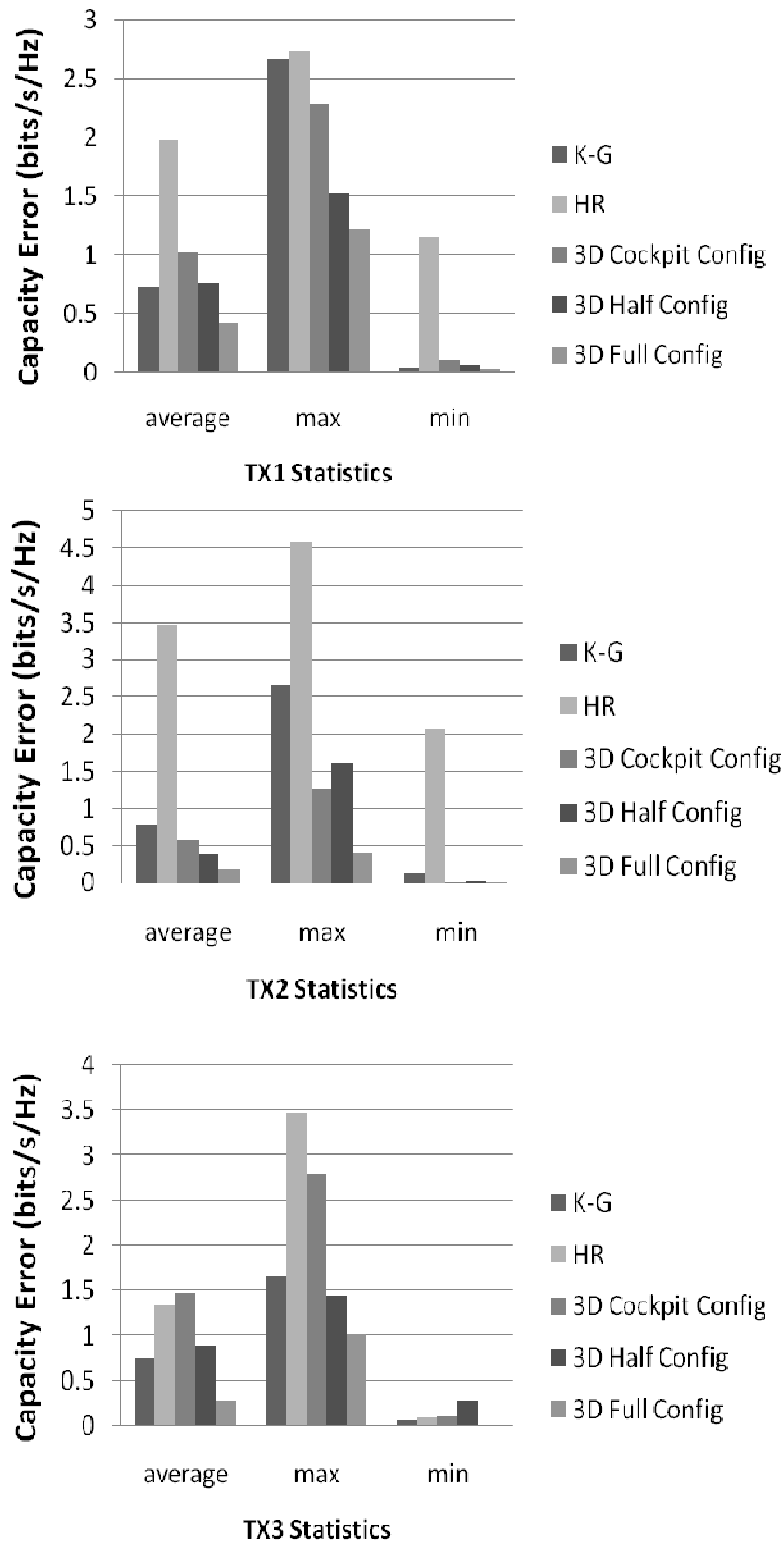


Figure 4.4: Comparison of capacity error statistics over all receiver locations for each transmitter location (TX1, TX2, TX3) in the Sabreliner for the K-G, hyper-Rayleigh, and three configurations of the 3D ray tracing model (see Figure 4.1)

G and 3D models were much more accurate than the hyper-Rayleigh model (designated HR in the graph). For TX3, the least detailed model of the ray tracing software was close to the hyper-Rayleigh, but all the others still had less than half the error of the hyper-Rayleigh. So overall, the hyper-Rayleigh was less accurate, followed by the K-G and simple configurations of the 3D. The Full Config of the 3D model achieved the lowest average and maximum error in each case, with maximum error below 1.3 bits/s/Hz for all transmitter locations. This shows us that the statistical models are representative of a simplified aircraft model, but are significantly less accurate than the 3D ray tracing model for actual aircraft.

We then used the Sabreliner measurements to compare to location specific capacity calculations obtained using the channel matrix based on the hyper-Rayleigh, the K-G, and the 3D ray tracing models. Figure 4.5 shows the error for each model at each

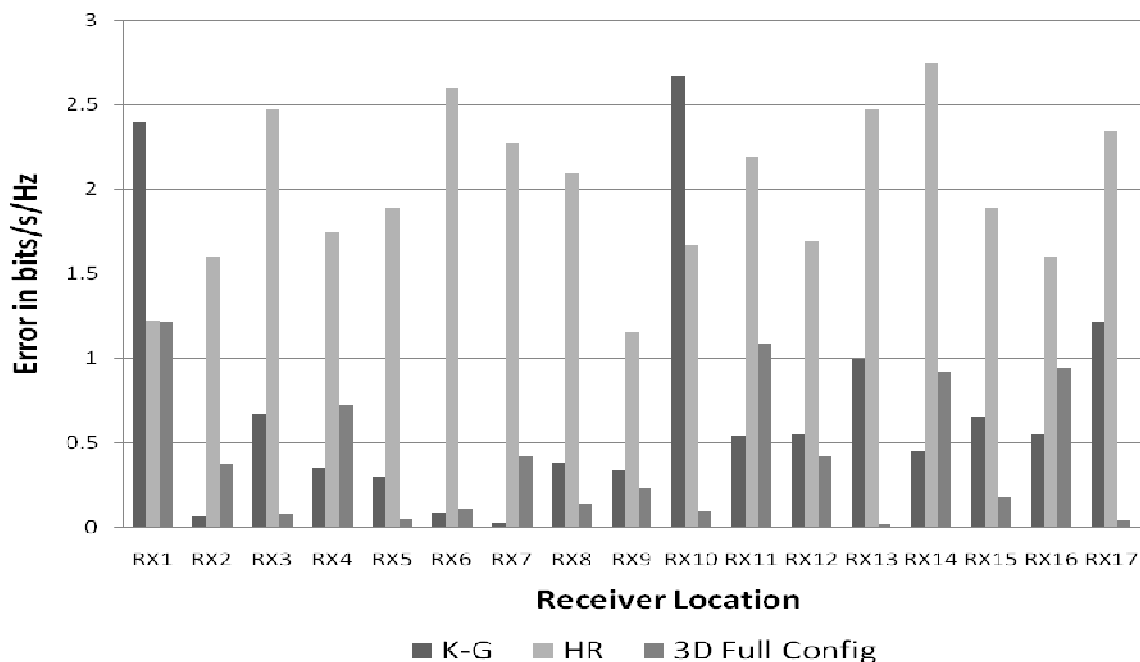


Figure 4.5: Comparison of capacity error for the Gaussian, hyper-Rayleigh and 3D ray tracing models for TX1 at each receiver location in the Sabreliner.

location. The figure shows how hyper-Rayleigh has a consistently greater capacity error by 1 to 3 bits/s/Hz, whereas the K-G and 3D ray tracing are much closer to the actual capacity. The K-G model has an error more than 1 bit/s/Hz at only 3 out of 17 locations, which was expected as it is strongly based on measurement. The 3D ray tracing model outperforms the others with errors as low as 0.02 bits/s/Hz, only becoming greater than 1 bit/s/Hz error at two locations. Its error is always within 1.3 bits/s/Hz.

Overall, the ray tracing model has an average of 0.9 to 1.5 bits/s/Hz less error than the hyper-Rayleigh model and up to 0.3 bits/s/Hz less error than the K-G model, which uses Ricean K factors based on measurements. There are several instances when measuring an aircraft to obtain the K factors needed for statistical analysis is either too expensive or inconvenient (due to grounding a plane during testing, logistics, etc.) or impossible (such as when a plane has not yet been built). So, in addition to considering the difficulty of acquiring measured K values for the K-G model, the improved accuracy of the 3D ray tracing model over the hyper-Rayleigh model shows that the site-specific model provided by the 3D ray tracing software allows for more accurate capacity estimates than statistical models without the need for measurements. Thus the 3D ray tracing software is extremely beneficial in properly analyzing the detailed performance of multiantenna systems in a variety of inraircraft environments at the cost of increased complexity in creating a detailed model and postprocessing 3D simulation data. The following sections describe the important factors for creating an accurate 3D model for the ray tracing software.

4.5 Variation of Parameters

To fully describe the aircraft environment, ray tracing is implemented in a detailed 3D site-specific model. 3D simulations with varying parameters were compared with multiantenna system measurements taken on a Rockwell T-39 Sabreliner as described in Section 4.3, and a DA42 Twin Star described in this section. These comparisons assist in defining an accurate configuration for the 3D ray tracing model. Most of the graphs in this section show the mean or average of the absolute value error, where the error is the difference between the measurement and the simulation. This means that the error shown is a maximum deviation, but does not show whether it was an over or underestimate. On average, hyper-Rayleigh underestimated capacity, whereas the 3D and K-G overestimated it, so hyper-Rayleigh could be used as a minimum achievable capacity and the 3D ray tracer as either a maximum achievable capacity, or just a more accurate estimate.

4.5.1 Number of Facets

The ray tracing software is capable of using anywhere from 5 up to 360 faceted surfaces to simulate the fuselage cylinder of the Sabreliner. As more facets are used, the outside walls come closer to the curvature of an actual cylinder. We tested the range of 5 to 120 facets to see if there were any trends in accuracy when compared to Sabreliner measurements at TX1. We simulated the fuselage using the fuselage with lossy obstacles configuration (see “c”) from Figure 4.1). The maximum reflections parameter was set to 10. The results are shown in Figure 4.6. We found that as the number of facets increases, the absolute mean error between our simulation capacity and the measured

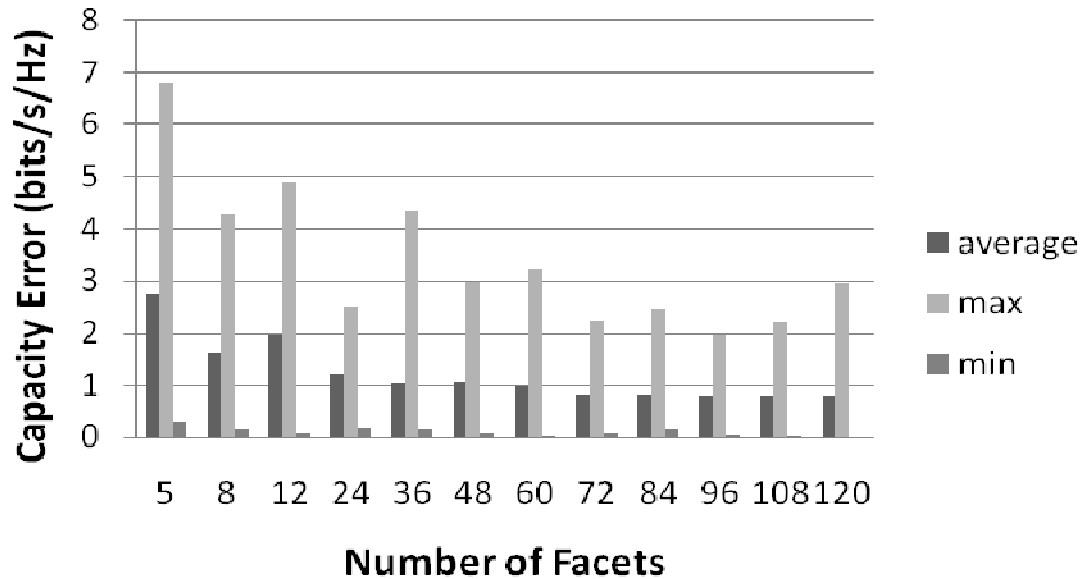


Figure 4.6: Capacity error statistics for varying number of facets for fuselage with lossy obstacles.

capacity decreases to within 1 bit/s/Hz, with minimal change beyond 60 facets, with error less than 1.3 bit/s/Hz for 24 or more facets. All other simulations referenced in this section used 12 facets, a number chosen prior to this study, which is within 2 bits/s/Hz for this fuselage configuration.

4.5.2 Site Specific Obstacles

The site specific obstacles included in this section are: lossy cockpit chairs, lossy back wall, and reflective partial walls 1-5 as depicted in Figure 4.1. The results for the various configurations (see Figure 4.1) showed that for TX1, the fuselage tunnel configuration (with no obstacles) had an average absolute error of 2.1 bits/s/Hz, which decreased by half to about 1.1 bits/s/Hz when endcaps were added to the fuselage (thus increasing the multipath richness), with negligible change when the lossy obstacles were added. This showed that it is especially important to enclose the ends of the fuselage for

greater accuracy. The addition of reflective walls 1 and 2 of the cockpit decreased the error to 1 bit/s/Hz. Adding reflective walls 3 and 4 in the half configuration decreased the average absolute error to 0.7 bits/s/Hz, and reflective wall 5 decreased the error to 0.4 bits/s/Hz. Though the lossy obstacles make a minimal difference in accuracy, the reflective obstacles, namely walls 1-5, make a noticeable difference and are therefore important to include in site-specific simulations. All three transmitter locations had significantly better absolute average capacity error for the cockpit, half and full configurations (improving for each addition of reflective walls) all within 0.5 bits/s/Hz for the full configuration. TX2 in the rear maintenance bay, however, achieved the best absolute value of the average capacity error of about 0.1 bits/s/Hz for both the fuselage with lossy obstacles and the full configuration, suggesting that transmitters located in small cavities throughout the plane are not as sensitive to the internal structure of the fuselage. TX3 had a significant improvement when the walls directly around it were added (walls 3 and 4 and 5) dropping to an average error of 0.2 bits/s/Hz in the half configuration and 0.05 bits/s/Hz in the full configuration. This further validates that the reflective obstacles in the immediate vicinity of the transmitter have the greatest impact on accuracy, whereas reflective obstacles far away have a smaller effect.

4.5.3 Maximum Allowed Reflections

The maximum allowed reflection value was varied from six to 18 in increments of two to evaluate whether allowing more bounces inside the Sabreliner fuselage before it arrived at the transmitter would improve simulation accuracy. We evaluate this for two configurations, b) and f) from Figure 4.1, using 12 facets for the outer walls and all

reflective walls modeled as PEC. The results were that for fewer allowed reflections (6 and 8) the empty fuselage was up to 1 bit/s/Hz more accurate than the full configuration, but above 10 reflections, the full configuration was slightly more accurate than the empty fuselage. This tells us that we need a sufficient number of reflections to enable the signal to accurately move around the reflective partial walls when they are included in the simulation. Both configurations have a mean error within 0.5 bits/s/Hz using above 10 reflections, which is what was used for most simulations in this section.

4.5.4 Electromagnetic Parameters

The small aircraft body of the Diamond DA42 Twin Star is made of carbon fiber reinforced plastic (CFRP) with electrical parameters that vary based on the percent weight of carbon [136]. Because of this, we used measurements on the Twin Star to compare with the simulation of the wall relative permittivity (ϵ_r) and conductivity (σ) set to a range of values approximating glass, composite and metal. Multiantenna measurements (using the same equipment as described in Section 3.3) were taken on the Diamond DA-42 Twin Star for one receiver location, Rx, in the forward luggage compartment while the transmitter was moved to various test locations as shown in Figure 4.7. Only the measurements inside the cabin are used for this analysis.

For composite materials with $\epsilon_r = 3.0$, σ was varied from 0.005 to 0.03 S/m for a mean error of about 6 bits/s/Hz. For composite with ϵ_r varied from 2.5 to 3.6 and $\sigma = 0.001$ S/m, and the error was 6 to 7 bits/s/Hz. For a material between composite and glass, with $\epsilon_r = 2.0$, and σ varied from 0.001 to 0.03, we obtained a mean error of 7

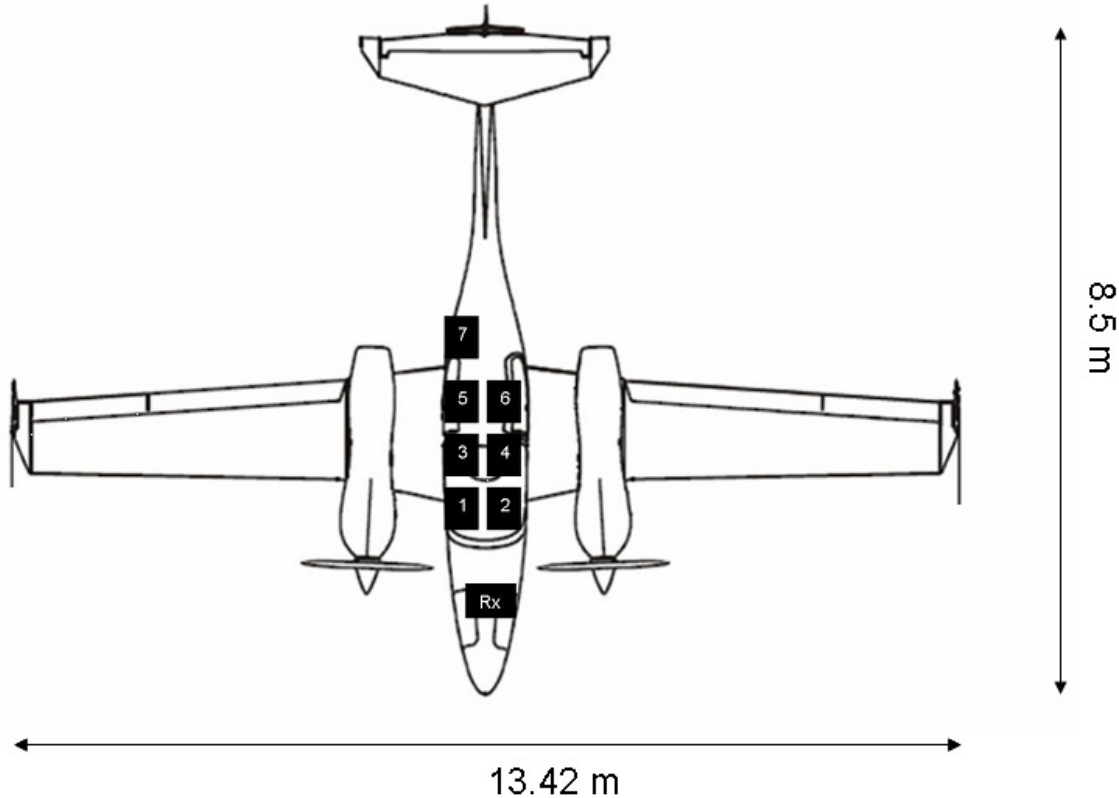


Figure 4.7: Transmitter and receiver locations for multiantenna system measurements on Diamond DA-42 Twin Star.

bits/s/Hz. For glass, with $\epsilon_r = 1.5$ and $\sigma = 0$ [151], we found an error of about 8 bits/s/Hz. And finally, we found that using the values for PEC still gave the most accurate results with a mean error of 0.74 bits/s/Hz. This may be because the amount of carbon fiber was sufficient to provide reasonable electrical shielding, or because other metal structures in the walls effectively provided this shielding instead.

4.6 Conclusion

In order to more accurately simulate multiantenna systems in an intravehicle environment such as aircraft, it was necessary to acquire a more site-specific H matrix than was attainable with the mathematical model for the hyper-Rayleigh environment.

We also did not want the model to require measurements like the K value based Gaussian model (K-G). This was accomplished by adapting a ray tracing software method to a new 3D environment—an aircraft fuselage. This method was validated in [124] and further explored in this paper. It was found that configuring the aircraft with at least 60 facets for the more simplified fuselage with lossy obstacles configuration achieved an average error below 0.82 bits/s/Hz and a max error below 3 bits/s/Hz. If 12 facets were used, the cockpit configuration was required to achieve similar accuracy (within 1 bit/s/Hz), with improving accuracy to 0.7 bits/s/Hz and 0.4 bits/s/Hz as configuration complexity increased to the half and full configurations respectively. Thus, including major site-specific reflective obstacles (especially those in close range to the transmitting antenna), with the maximum allowed reflections set to 10 or more, and using PEC parameters for the walls (regardless of if the aircraft is metallic or composite body) will give an excellent channel model for aircraft. Using the 3D ray tracing software to create the channel matrix for the detailed signal model (DSM) will give a more accurate channel model than other statistical models, achieving an error of within 0.5 to 1 to bit/s/Hz for the Rockwell T-39 Sabreliner (metallic body) and Diamond DA-42 Twin Star (composite body) discussed in this paper.

This improvement over statistical models comes at a cost of time to develop a more detailed model, so is generally only warranted for truly site specific communication systems, such as fixed location sensor networks. Mobile applications such as handheld links will presumably pass through all or most of the locations in the aircraft, thus justifying the use of statistical models in mobile cases as they do not require a detailed physical model of the aircraft. However, this site specific ray tracing model may still be

used to inform and refine the statistical models by precalculating K parameters prior to construction of the aircraft to improve statistical model accuracy. Overall, if it has not been built or cannot be measured easily to find a good K parameter estimate, the 3D ray tracing model is the best estimate of channel capacity within aircraft.

Future work should involve further study of varying sizes of aircraft, tunnels, and buses to evaluate how closely related those environments are. It should also include a rigorous study of the wing and engine compartments, as many sensors will need to be located in those enclosed areas as well. The external wing structure could be modeled with rectangular and triangular surfaces, and the internal cavity would need to have enough randomly placed obstacles to create the expected multipath richness. Ray tracing may need to be combined with other results in order to account for near field scatterers.

4.7 Acknowledgment

Much thanks to Randy Chesley and the Utah State University for allowing us to come and measure their aircraft, as well as my measurement team, James Nagel and Sai Ananthanarayanan. This work was supported by the US Air Force Research Laboratories (AFRL) through a grant from Universal Technologies Corporation and the National Science Foundation under grant ECCS-0823927.

4.8 References

- [122] J. Frolik, "A case for considering hyper-Rayleigh fading channels," *IEEE Transactions on Wireless Communications*, Vol. 6, No. 4, Page(s): 1235–1239, 2007.
- [123] A. Magleby and C. Furse, "Predicted MIMO performance in intravehicle channels," *IEEE Antennas and Propagation Society International Symposium*, San Diego, CA, Page(s): 1-4, 2008.

- [124] S. Y. Lim, Z. Yun, J. M. Baker, N. Celik, H. S. Youn, and M. F. Iskander, "Radio propagation in stairwell: measurement and simulation results," *IEEE Antennas and Propagation Society International Symposium*. Charleston, SC, 2009.
- [125] Z. Yun, Z. Zhang, and M. F. Iskander, "A ray tracing method based on the triangular grid approach and application to propagation prediction in urban environments," *Proceedings of the IEEE International Symposium on Information Theory (ISIT2004)*, Vol. 50, Page(s): 750–758, May 2002.
- [126] C. Takahashi, Z. Yun, M. F. Iskander, et al., "Propagation-prediction and site-planning software for wireless communication systems," *IEEE Antennas and Propagation Magazine*, Vol. 49, No. 2, April 2007.
- [127] Fitzhugh, J. Frolik, J. Covell, R. Ketcham, and T. Meyer, "2.4 GHz multipath environments in airframes," *Proceedings of the 2005 Wireless and Microwave Technology Conference (WAMICON 2005)*, 2005.
- [128] M. Youssef, L. Vahala, and J. H. Beggs. "Electromagnetic propagation of wireless networks in aircraft cabins," *IEEE/ACES International Conference on Wireless Communications and Applied Computational Electromagnetics*, Page(s): 832 – 836, 2005.
- [129] T. T. Evans, "Wireless communication channels in aircraft," Senior Project, University of Utah, Salt Lake City, UT, 2007.
- [130] D. Landon and C. Furse, "The MIMO transmission equation," (Honorable Mention, student paper contest) *IEEE Antennas and Propagation Symposium (APS)*, San Diego, CA, July 7-11, 2008.
- [131] Alyssa Magleby, Cynthia Furse, and Z. Q. Yun, "3D ray tracing for intravehicle MIMO," *IEEE/URSI Antennas and Propagation Symposium*, Charleston, SC, June 1-5, 2009.
- [132] Z. Yun, Software package called "3D ray tracing for radio propagation modeling," last updated Dec. 2009, unpublished.
- [133] Sai Ananthanarayanan, Alyssa Magleby Richards, and Cynthia Furse, "Measurement and modeling of multiantenna systems in small aircraft," Submitted to *Journal of Aerospace Computing, Information, and Communication*, June 2010.
- [134] N. Moraitis and P. Constantinou, "Radio channel measurements and characterization inside aircrafts for in-cabin wireless networks," *IEEE 68th Vehicular Technology Conference-Fall 2008*, Page(s): 1 – 5, 2008.
- [135] A. Kaouris, M. Zaras, M. Revithi, N. Moraitis, and P. Constantinou, "Propagation measurements inside a B737 aircraft for in-cabin wireless networks," *IEEE Vehicular Technology Conference, Spring 2008*. Page(s): 2932 – 2936, 2008.

- [136] [Online] Available: <http://www.carbonfiber.gr.jp/english/tanso/03.html>, [Accessed: Aug 13 2009].
- [137] J. Nagel, A. Magleby, S. Ananthanarayanan, and C. Furse, "Measured multiuser MIMO capacity in aircraft," accepted for publication in *IEEE Antennas and Propagation Magazine*.
- [138] Sai Ananthanarayanan, Alyssa Magleby Richards, and Dr. Cynthia Furse, "Measurement and modeling of multiantenna systems in small aircraft," submitted to *AIAA Journal*, June 2010.
- [139] H.-L. Blocher, K. Beilenhoff, and J. Wenger, "Simulation of the electromagnetic wave propagation in cars," *33rd European Microwave Conference*, Vol. 3, Page(s): 1151 – 1154, 2003.
- [140] M. Heddebaut, V. Deniau, K. Adouane, "In-vehicle WLAN radio-frequency communication characterization," *IEEE Transactions on Intelligent Transportation Systems*, Vol. 5, Issue: 2, Page(s): 114 – 121, 2004.
- [141] Wireless Smoke Detection. [Online] Available: <http://www.securaplane.com/smoke2.html>, [Accessed: June 21 2009].
- [142] Securaplane Technologies, Inc. Press Release, "Securaplane Technologies awarded Boeing 787 contract for wireless emergency lighting," [Online] Available: <http://www.securaplane.com/releases/pr0095.html>. [Accessed: 21st June 2009].
- [143] G.J. Foschini and M.J. Gans, "On limits of wireless communications in a fading environment when using multiple antennas," *Wireless Personal Communications* Vol. 6, Page(s): 311-355, Mar 1998.
- [144] [Online] Available: www.honeywell.com/sites/aero/AircraftSensors.html, [Accessed: June 21 2009].
- [145] [Online] Available: <http://www.aspenflyingclub.com/da42docs.htm>, [Accessed: June 21 2009].
- [146] P. Wertz, V. Cvijic, R. Hoppe, G. Wolfle, and F.M. Landstorfer, "Wave propagation modeling inside vehicles by using a ray tracing approach," *IEEE 55th Vehicular Technology Conference 2002*, Vol. 3, Page(s): 1264 – 1268, 2002.
- [147] D.W.K Wong and G. Chen, "Optical design and multipath analysis for broadband optical wireless in an aircraft passenger cabin application." *IEEE Transactions on Vehicular Technology*, Vol. 57, Issue: 6, Page(s): 3598 - 3606, 2008.

- [148] R. Hoppe, P. Wertz, G. Wolfle, and F. M. Landstorfer, "Fast and enhanced ray optical propagation modeling for radio network planning in urban and indoor scenarios." *MPRG Wireless Personal Communications Symposium 2000, Blacksburg (Virginia, USA)*, Page(s): 14-16, June 2000.
- [149] Zhizhang Chen and Shuiping Luo, "Generalization of the finite-difference-based time-domain methods using the Method of Moments," *IEEE Transactions on Antennas and Propagation*, Vol. 54, Issue: 9, Page(s): 2515 – 2524, 2006.
- [150] Sai Ananthanarayanan, Alyssa Magleby Richards, and Cynthia Furse, "Measurement and modeling of interference for multiantenna system," accepted for publication in *Microwave and Optical Technology Letters*.
- [151] M. F. Iskander, *Electromagnetic fields and waves*. Prospect Heights, IL: Waveland Press, 1992.
- [152] Claude Oestges and Bruno Clerckx, "MIMO wireless communication- from real-world propagation to space-time code design," Elsevier Ltd: 2007.
- [153] Werner Weichselberger, Markus Herdin, Hseyin Ozelik, and Ernst Bonek, "A stochastic MIMO channel model with joint correlation of both link ends," *IEEE Transactions on Wireless Communication*, Vol. 5, No. 1, Page(s): 90-99, Jan 2006.
- [154] D. Palchak and B. Farhang-Boroujeny, "A software defined radio testbed for MIMO systems," *Proceedings of the SDR 06 Technical Conference and Product Exposition*, Orlando, FL, November 2006.
- [155] F. Whetten, A. Soroker, D. Whetten, and J. H. Beggs, "802.11 wireless network performances within aircraft cabins," Embry-Riddle Aeronautical University, 2003.
- [156] Constantine A. Balanis, *Modern antenna handbook*, 2nd ed. New York, NY: Wiley-Interscience, 2008.
- [157] Ramya Bhagavatula, Robert W. Heath Jr., and Sriram Vishwanath, "Optimizing MIMO antenna placement and array configurations for multimedia delivery in aircraft," *IEEE 65th Vehicular Technology Conference, 2007*, April 2007.

CHAPTER 5

MEASUREMENT AND SIMULATION OF THE MULTIAN TENNA COMMUNICATION CHANNEL ON A SHUTTLE BUS³

5.1 Abstract

This paper describes the multiantenna system simulation and measurement of the complex channel found in a 2004 Thomas Bus 110YN. Simulation is done with a site-specific 3D modeling software that uses ray tracing to estimate the location specific capacity in this severe multipath and fading channel. The paper includes an evaluation of which modeling parameters are required for accuracy. The ray tracing software is able to estimate capacity within 1.05 bits/s/Hz for two transmitter locations (one at the front of the bus and one at the back) and is more accurate on average than some statistical models commonly used for wireless environments including Gaussian, hyper-Rayleigh, Weibull and Nakagami. This ray tracing modeling can be used in the design of wireless communication systems inside complex channels, such as buses, to accurately estimate location specific capacity without measurement and can be performed before the vehicle is even built.

³ Content of this chapter is taken from an article coauthored with Sai Ananthanarayanan P.R. and Dr. Cynthia Furse and submitted to *Microwave and Optical Technology letters* [29].

5.2 Introduction

Wireless communication systems are in high demand for both entertainment and safety applications in all forms of public transportation. Multiantenna systems are gaining acceptance for improved data throughput without requiring additional bandwidth. These systems work best in channels with high multipath, and are typically designed for indoor channels. For many users, the ultimate mobile experience is to use their mobile device in a mobile environment—such as airplanes, trains, buses, cars, etc. Demand for higher and higher data rates for entertainment and communication in these vehicles is substantial, as seen in [158]-[160]. The wireless communication systems in these vehicular environments are among the strongest multipath environments available and result in complex fading channels that make traditional wireless communication extremely difficult. But what makes these channels difficult for traditional wireless may make them ideal for multiantenna communication, which thrives on rich multipath channels. The focus of this paper is to understand the channel in a bus, and better understand the wireless parameters in the bus. A major aspect of this work is also analyzing a 3D ray tracing method for site-specific channel prediction. Codes such as this are very important in the initial design of wireless systems, particularly fixed wireless systems for entertainment, sensors, etc. This paper will address what aspects of the bus interior must be modeled in significant detail and which can be simplified in order to achieve good prediction of the site-specific multipath channel.

Prior work to evaluate the channel inside aircraft [161]-[165] has found a wide variation of site-specific K values throughout the aircraft which contribute to an extreme multipath environment. Buses are significantly different from aircraft in one way that is

expected to have a dramatic effect on modeling – the size of the glass windows, which has the potential to reduce the overall multipath and hence the multiantenna channel capacity. Additionally, only limited work has been done to evaluate the complex channel found in other vehicles [166]. This analysis of this bus channel is part of an effort to quantify communication channels in vehicles in order to better design communication systems within them.

This chapter describes the measurement and modeling of a university shuttle bus, the 2004 Thomas Bus 110YN, which is just over 2 m wide, almost 2 m high and about 8.5 m long. It includes the application of a site-specific 3D modeling software designed by Yun in [166] that uses ray tracing to accurately estimate the location specific capacity of a complex channel. Measurements in the shuttle bus confirm the accuracy of the model. This modeling software was previously used to model the complex channel found in aircraft in [162]-[164], indoor environments in [168]-[170], and underground tunnels in [174]. It is now applied to a public transportation bus to enable the design of wireless communication system for buses.

Section 5.3 describes a thorough mapping of the bus made at 915 MHz with a multiantenna measurement test bed. This is then compared with site-specific simulation results in Section 5.4 to evaluate achievable accuracy. The level of modeling detail in both the internal and external vehicle structure required for simulation accuracy is also studied in this section. Section 5.5 looks at the accuracy of other (non-site-specific) statistical modeling methods in comparison to the site-specific ray-tracing model. The conclusion describes the level of accuracy required to model buses as well as when it

would be beneficial to use this 3D ray tracing model instead of statistical models. The complex channel in the shuttle bus is described in detail.

5.3 Bus Measurements and Mapping

This section describes an extensive measurement campaign for a 2004 Thomas Bus 110YN (8.48 m long shuttle bus). Bus measurements were taken with three passengers and our measuring cart made mostly of plastic with a few metal parts as well as metal encased equipment present on the bus. The people and cart moved between measurements, but were stationary during each individual measurement. The front door of the bus was left open for air circulation except for measurements taken within 1.8 m of the door (or 5.5λ at 915 MHz). A few small windows were also slightly open for air circulation. The overall dimensions of the bus are shown in Figure 5.1, with a photo of the rear half of the bus to show detail in Figure 5.2.

Capacity measurements were taken with a 4x4 array of 8.2 cm spaced 0.25λ monopoles at 915 MHz (see antenna setup on left seats and rear shelf of photo in Figure 5.2). Further details of this system can be found in [171] and [172]. Antennas started 0.1 m from the edge of a 38x45.7 cm ground plate, and were centered lengthwise. Data packets were transmitted based on the 4-QAM modulation scheme using differential encoding with 50 kbps of data per antenna. Each packet started with a simple single antenna preamble of 4000 pseudorandom data bits added to allow phase and timing synchronization by the receiver. The packet then included a multiantenna sequence of 4 x 4000 pseudorandom bits to be used as a training sequence for channel estimation. The

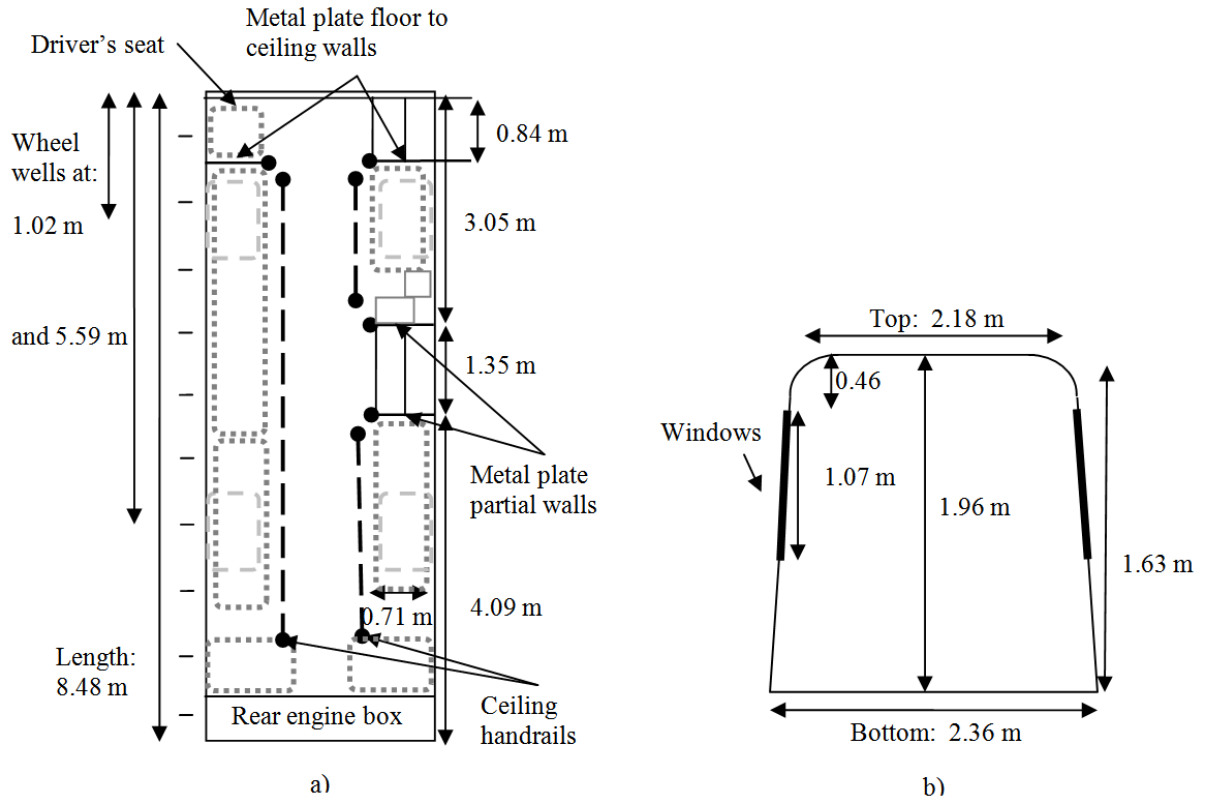


Figure 5.1: Thomas Bus dimensions. a) 8.48 m long, 2.36 m wide, 1.63 m high floor plan dimensions. Short dashed boxes represent seats, and long dashed boxes represent wheel wells. b) Cross-sectional dimensions.



Figure 5.2: Photo of rear half of bus with measurement equipment at location 24 for TX2, marked by large white arrows (see also Figure 5.4).

packet terminated with a small payload of text data used to verify proper packet detection in postprocessing.

Measurements were taken at the receiver locations shown in Figure 5.3 and Figure 5.4 spanning the width of the bus and at 0.914 m increments over the length of the bus. These measurements were taken at various elevations within the bus including seat, cart, floor, stairwell, and on top of the rear engine box, as designated by different colored boxes in the figures.

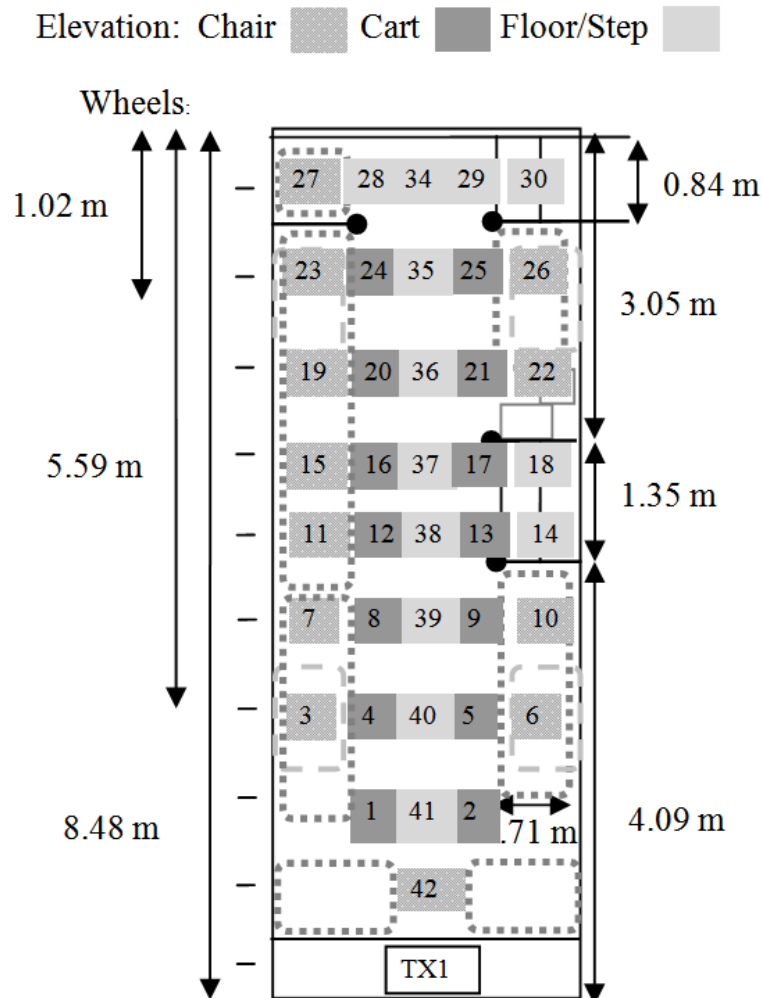


Figure 5.3: TX1 receiver locations.

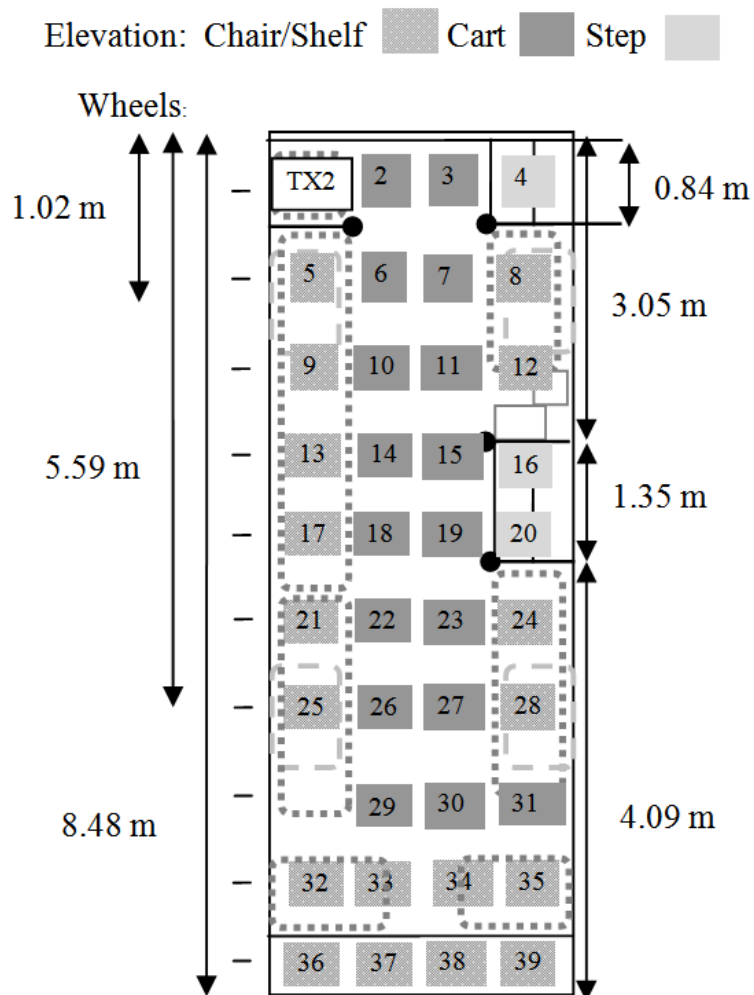


Figure 5.4: TX2 receiver locations.

Capacity was calculated from the measured channel matrix, H , using

$$C = \log_2 \det \left[I + \frac{SNR_r N_r}{\| \mathbf{H} \|_{Frobenius}^2} \mathbf{H} \mathbf{H}^H \right] \quad (5.1)$$

where I is the identity matrix, SNR_r is the signal to noise ratio, and the double bars on the bottom represent taking the Frobenius norm of the channel matrix. This capacity reflects the multipath found in the channel as well as the increase in capacity that results from using a multiantenna system for measurement. More details are given in [173]. The resulting capacity is shown in Figure 5.5 and Figure 5.6. For TX1 at the back of the bus, there was a higher capacity the closer the receiver was to the transmit antenna even with normalized power. The front half of the bus had a more random pattern of high and low spots, with the lowest capacity spots next to plastic covered arm rests with metal supports (which could block many of the impinging rays as they were taller than the antennas) or on the floor next to the front wall. For TX2 in the driver's seat, blocked from the main cabin of the bus by a partial wall, we see a random pattern of high and low capacity locations. Most of the low capacity spots were again located next to either an arm rest with a metal support bar or a metal wall. The site specific capacity ranged from 15 to 22.6 bits/s/Hz. Even with the multiantenna system, this variation could have a serious effect on the reliability of a communication system unless an adaptable code is used to deal with the varying capacity. This would also be essential once people are added to the environment, causing an even greater fluctuation in capacity, as seen in indoor environments when moving people were introduced into a multiantenna system in [176].

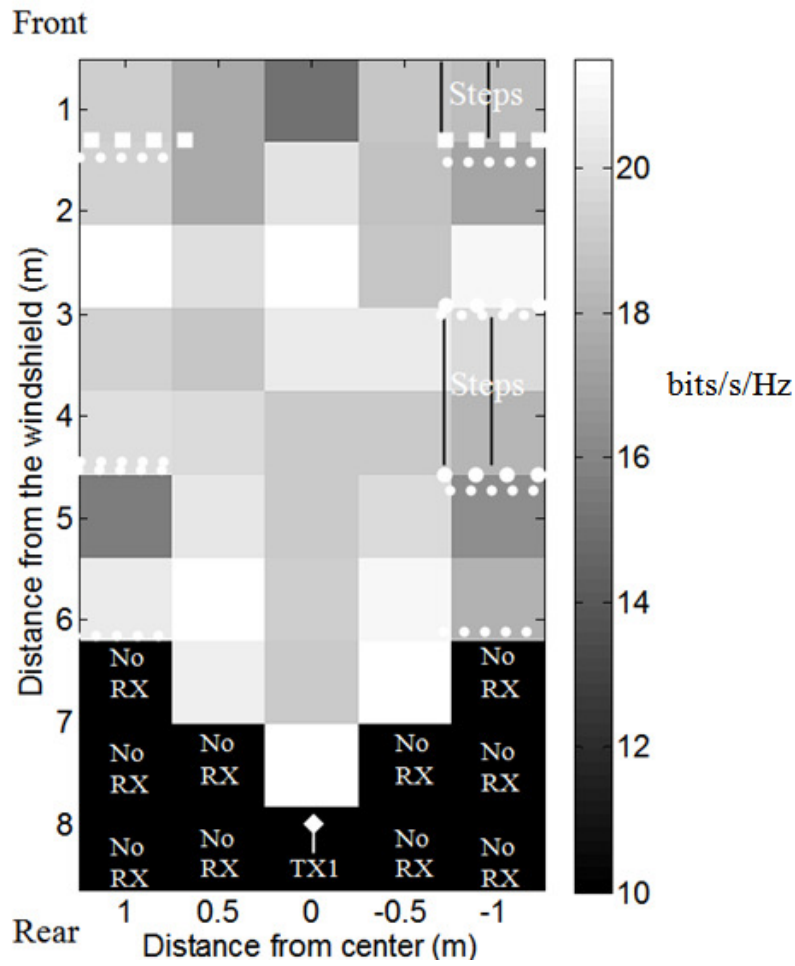


Figure 5.5: TX1 capacity mapping. Floor to ceiling metal dividers are marked by square dotted line, floor to middle metal dividers are marked by large circle dotted line and arm rests with metal support bars are marked by a small circle dotted line. Locations with no recorded capacity are marked by “No RX”, which means no measurement was taken at that location.

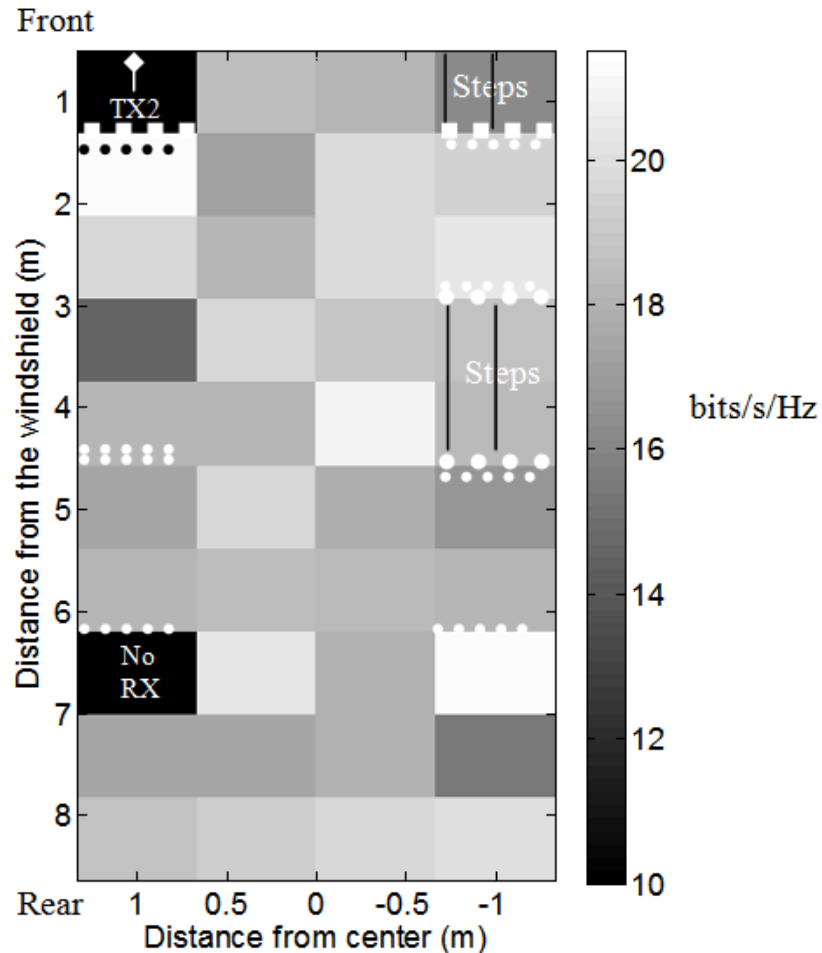


Figure 5.6: TX2 capacity mapping. Floor to ceiling metal dividers are marked by square dotted line, floor to middle metal dividers are marked by large circle dotted line and arm rests with metal support bars are marked by a small circle dotted line. Locations with no recorded capacity are marked by “No RX”, which means no measurement was taken at that location.

The average capacity for TX1 was 19.31 bits/s/Hz and for TX2 was 18.62 bits/s/Hz, which was surprisingly in the same range of average error found in aircraft (which was 18.8 to 20.3 bits/s/Hz).

5.4 Model Accuracy

In this section, measurements are compared to a detailed simulation of the bus using 3D ray tracing software to determine the expected accuracy of the simulation with different levels of site-specific modeling detail. Simulations were created using four different configurations of internal obstacles: 1) empty bus cavity, 2) bus cavity with partially reflective walls, 3) bus cavity with reflective walls and rear engine box, 4) bus cavity with reflective walls, rear engine box and wheel wells. In previous studies, chairs were seen to have a minimal lossy effect (less than 0.1 dB) [163] and were therefore not evaluated in this environment for simplification. Each of these internal configurations was used to simulate the bus for each transmitter for two external configurations: perfect electrical conductor (PEC) for all external walls (no windows) and PEC for external walls along with large windows as located in the actual bus. The electrical properties used for glass windows were $4 < \epsilon_r < 10$, $\sigma = 10^{-12}$ S/m [177]. Maximum reflections for each ray were set to 10, and simulations were run at 915 MHz to compare to measurements. These simulations required 28 to 36 min (depending on number of receive antennas) to run three simulations at a time on an Intel Core 2 Quad processor running at 2.83 GHz with 8 G RAM.

The resulting capacity error is shown in Figure 5.7 and Figure 5.8 for each receiver location. From the graphs, we see that the empty bus had the greatest error for

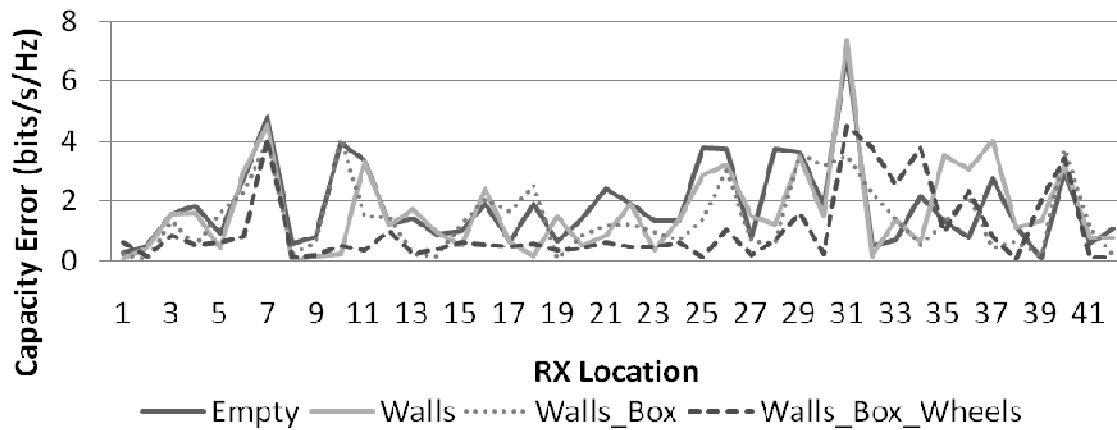


Figure 5.7: Location specific capacity error for TX1 for various internal obstacle configurations.

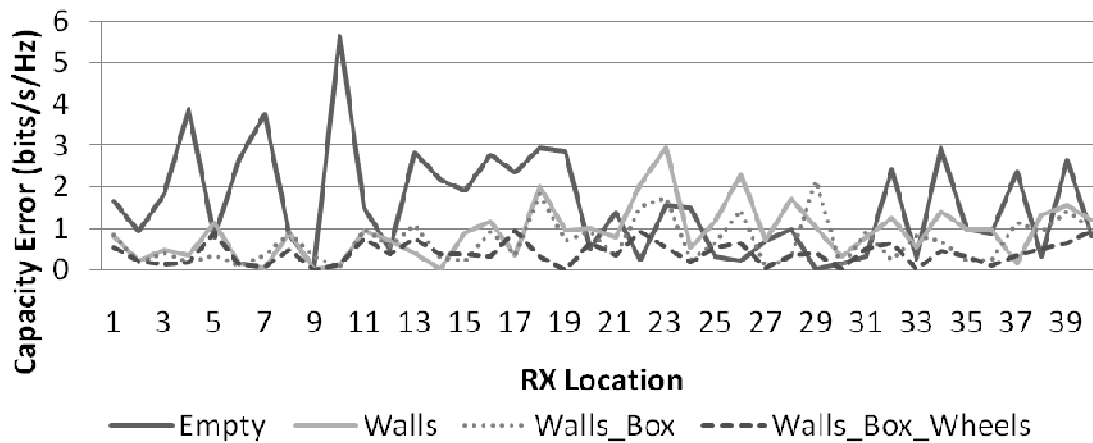


Figure 5.8: Location specific capacity error for TX2 for various internal obstacle configurations.

most receiver locations for both TX1 and TX2, whereas the configuration with wall, rear engine box and wheel wells had the lowest error at most locations.

In general, the average error decreased as the detail of the internal obstacle configuration increased, as shown in Figure 5.9. For TX1 with windows, the simulation went from an error of 1.84 bits/s/Hz for the empty bus, to almost half that at 1.05 bits/s/Hz when walls, engine box and wheel wells were added. For TX2 with windows, the simulation achieved an error of 1.59 bits/s/Hz for the empty bus, decreasing to almost a fourth of that error at 0.41 bits/s/Hz when walls, engine box and wheel wells were added. We found that the more detailed internal obstacle environment gave a smaller improvement in accuracy for the windowless model than in the model with windows, also shown in Figure 5.9. This graph shows that windows are extremely important to the accuracy of the bus model, decreasing error by an average of between 0.33 and 0.74 bits/s/Hz for TX1 and between 0.65 and 1.36 bits/s/Hz for TX2, depending on the

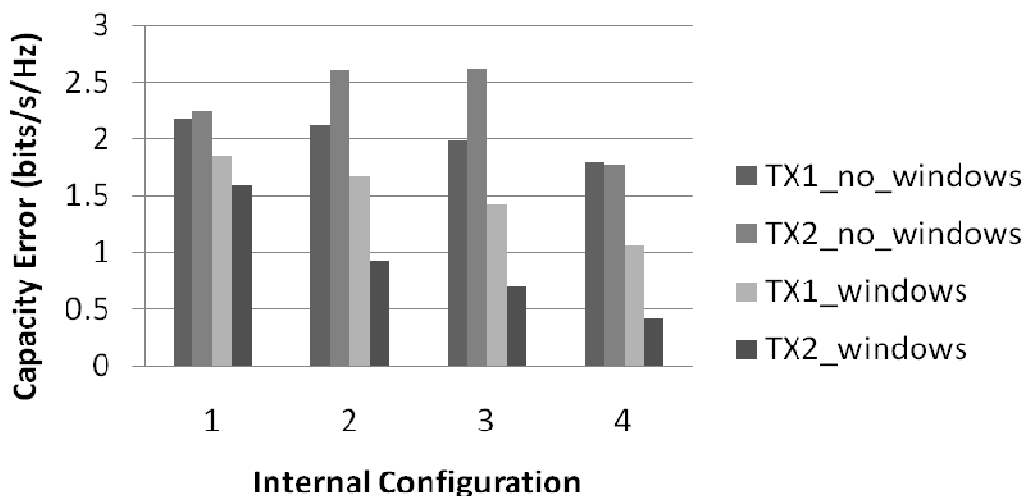


Figure 5.9: Average capacity error for various internal obstacle configurations: 1) empty bus cavity, 2) bus cavity with partially reflective walls, 3) bus cavity with reflective walls and rear engine box, 4) bus cavity with reflective walls, rear engine box as well as wheel wells.

internal configuration used. The combination of windows with a detailed internal obstacle configuration results in average accuracy within 1.05 bits/s/Hz for both transmitters.

Another factor to evaluate is the geometry of the external structure. We have seen that including windows is important, but what about the shape of the outer walls? Since the top of the bus was curved, would a cylinder with windows also result in good accuracy for the bus measurements? What about a simple rectangular box with windows? Were the angles of the outer walls and the beveled edges of the top of the bus important for accuracy? To find the answer, the same internal bus and antenna configurations were simulated in both a cylinder with windows and a simple rectangular box with windows to see the effect of the external geometry on accuracy. An evaluation is made as to whether it is feasible to use different external configurations with similar dimensions to represent multiple vehicular channels, or if a specific external geometry is needed for each vehicle.

The 3D simulations of external geometries for a rectangular box without curved corners and a cylinder with 22 facets to represent curved sides were run with the full internal bus configuration that included walls, a rear engine box and wheels. These were then processed and compared to each receiver location measured on the bus. The resulting capacity error for each external geometry and each transmit antenna are shown in Figure 5.10 and Figure 5.11. Both the external geometries for the rectangular box and the cylinder had greater average error than the bus geometry, with average errors for TX1 of 1.33 bits/s/Hz for the rectangular box and 1.56 bits/s/Hz for the cylinder compared to 1.05 bits/s/Hz for the bus shape and average errors for TX2 of 1.54 bits/s/Hz for the

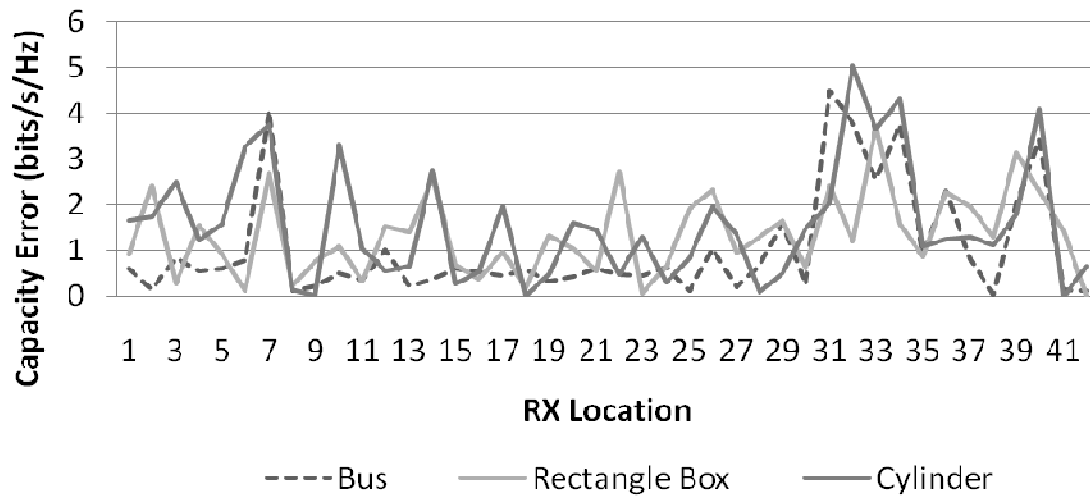


Figure 5.10: Location specific capacity error for TX1 for various external geometries.

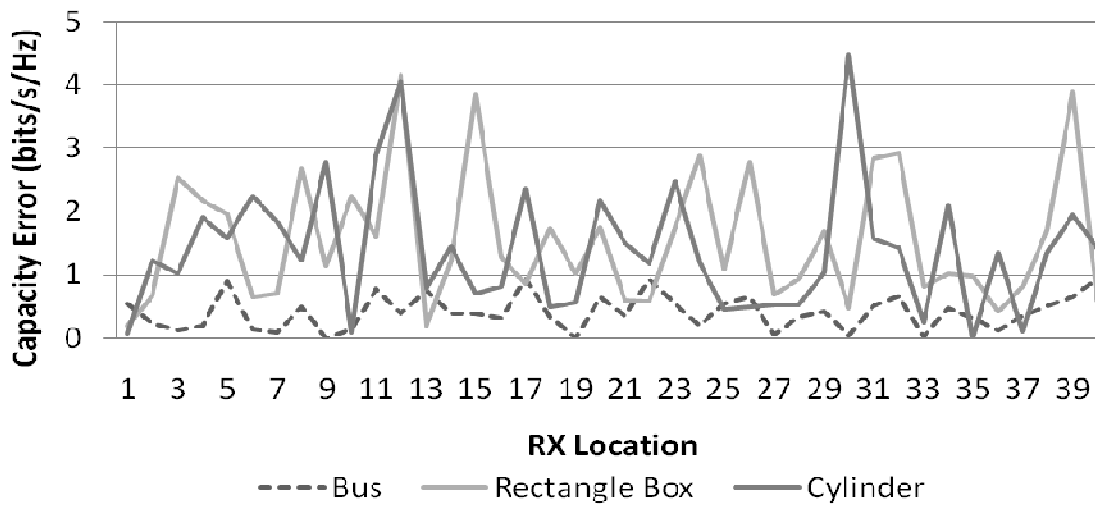


Figure 5.11: Location specific capacity error for TX2 for various external geometries.

rectangular box and 1.39 bits/s/Hz for the cylinder compared to 0.41 bits/s/Hz for the bus shape. The alternate external configurations were all in the same range as the error for the empty bus (see Figure 5.7).

Figure 5.10 and Figure 5.11 show that the basic shape of the external geometry is also important, decreasing the average error for TX1 from 1.33 bits/s/Hz for the rectangle box configuration to 1.05 bits/s/Hz for the bus shape, which differs only by slanted side walls and top corner facets. There was an even greater improvement for TX2 with average error of 1.54 bits/s/Hz for the rectangular box down to 0.41 bits/s/Hz for the bus shape. Thus to use this ray tracing software, it is important to obtain an accurate geometry of the external walls for the complex environment, using angled walls when necessary and facets to account for any curvature in the external surface.

5.5 Other Modeling Techniques

Various channel models based on both statistical modeling as well as 3D ray tracing have been proposed for analyzing wireless systems in aircraft. Statistical models based on Gaussian [178], Weibull [179], hyper-Raleigh [161] and Nakagami-m [182] distributions will be described and then compared with the 3-D ray tracing model [163] in this section. It was previously determined that the most accurate results are obtained using these models to determine the channel matrix and then postprocessing the channel matrix using a detailed signal model (DSM) described in [183]. Additionally, since we found in Sections 5.3 and 5.4 that the best ray tracing model for the bus includes windows along with a detailed configuration of internal obstacles (see configuration 4 in

Figure 5.9), this optimum configuration will be used to compare to the statistical models in this section.

The DSM is based on network theory with additional terms to account for the deleterious effects of imperfect antenna mismatch, coupling between the antennas, polarization and pattern mismatch, loss at the transmitter and receiver, and imperfect antenna efficiency, described in [217]. This model has been used for indoor [175], aircraft [164] and tunnel [174] capacity calculations for single and multiple antenna systems. Various models can be used to create the channel matrix that is then combined with the DSM to include the antenna effects mentioned previously. We will focus on the Gaussian model [178] along with other statistical models that have been used for channels with severe multipath, including Weibull [179], Nakagami [182], and hyper-Rayleigh [158]. The Gaussian model is one of the simplest channel models. It specifies a plane of impinging waves with Gaussian-distributed magnitudes and uniformly distributed angles of arrival (AOAs) and phases. This model is limited because it is based on measured K values. The Weibull distribution was created to model the lifetime of some object that fails based on its weakest link, and thus has been widely used for modeling the fading envelope in wireless communication. Single antenna measurements performed in [181] show that the Weibull model can accurately estimate the path loss in an aircraft channel at 5 GHz. The Weibull model describes the path loss as an exponential decay with uniformly distributed phases. The Weibull model reduces to the Rayleigh model when $\alpha_k = 2$. For this paper, $\alpha_k = 1.5$ is used for the fading parameter and average fading power is $\Omega_k = 1$ based on optimization simulations performed in [183]. The Nakagami-m distribution provides more flexibility and is a better match to most fading

channels, as shown in [182], because it offers one more parameter than the Gaussian and Weibull models. The Nakagami-m model simplifies to the Rayleigh and uniform distribution on the unit circle for the special cases of $m=1$ and $m=\infty$, respectively. The path loss is again modeled as an exponential decay with uniformly distributed phases. For this dissertation, the Nakagami model was simulated with $m=1.4$ also based on optimization simulations performed in [183]. The hyper-Rayleigh model is where the received signal is dominated by two constant amplitude signal components with uniformly distributed angles of arrival over $[0, 2\pi)$, and is also referred to as two-wave with diffuse power (TWDP), as detailed in [161]

All of these models are statistical averages, not site-specific. They were estimated for each receiver site and compared to the site-specific 3D model at that location. The capacity error for each model is shown in Figure 5.12 and Figure 5.13. For TX1, the Gaussian and Weibull models tend to have greater error than the other models. The error from the 3D model is below most of the other models for each location. For TX2, the Weibull model has the worst error at most of the locations. The other models have moderate error, and the 3D model has the smallest error.

The 3D ray tracing model was within 1.0 bit/s/Hz for TX1 at most of the locations except 7, 29, 34, and 36 (and the calibration locations 31-33) for which several of the other models also had the worst accuracy with errors greater than 2 bits/s/Hz. As seen in Figure 5.3, location 7 is next to an arm rest which contains metal bar supports, which were not included in the simulation. This could have caused increased multipath or blocked impinging rays at that location which was not taken into account in the model. Locations 29 and 34 were on the floor at the front of the bus next to the stairwell, which

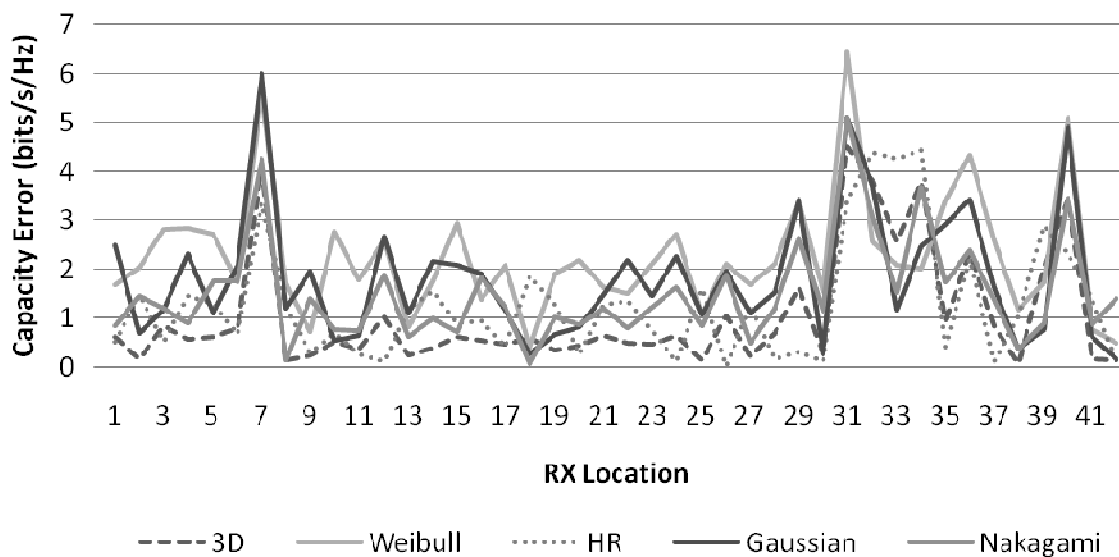


Figure 5.12: Comparison of capacity error at each receiver location for TX1. Locations 31-33 were taken for calibration purposes.

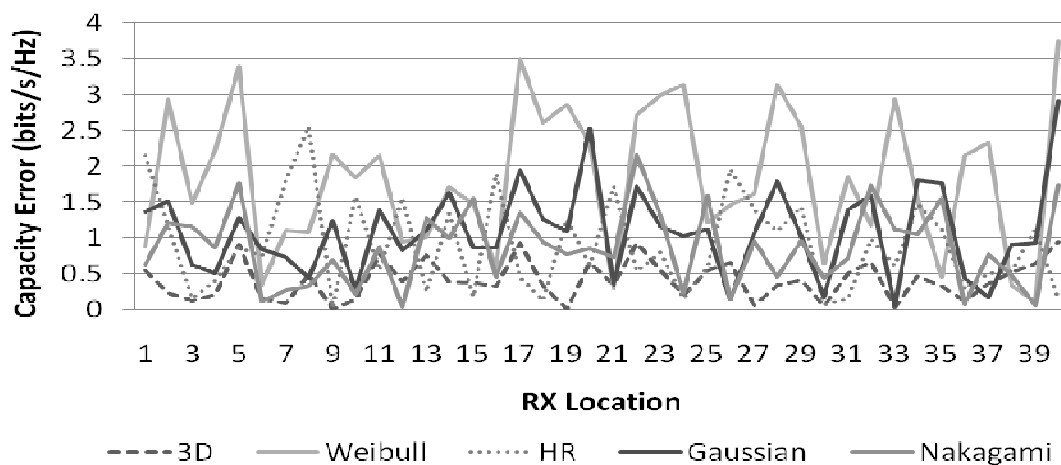


Figure 5.13: Comparison of capacity error at each receiver location for TX2.

was modeled as a flat floor. The stairs could also add to the multipath at those locations. For TX2, the 3D ray tracing model was within 1.0 bits/s/Hz for all locations, and had the minimum average error of 0.41 bits/s/Hz, with the lowest maximum error of 0.94 bits/s/Hz and smallest standard deviation of error of 0.27 bits/s/Hz out of all the models. The 3D model was followed by the Nakagami and hyper-Rayleigh in overall accuracy for average, maximum and standard deviation of the error for TX1 and TX2. Weibull performed the worst with the highest average error for both antennas, shown in Table 5.1.

The 3D ray tracing model outperforms the statistical models, both at location specific comparisons as well as overall average across the channel. This comes at the cost of the additional complexity required to create the 3D model with accurate dimensions. 3D ray tracing modeling could be used for statically deployed wireless networks inside complex channels. This is most useful in situations where the channel of the bus or other vehicle is not easily measurable or not yet built, and vehicle geometry and dimensions are more easily obtained, as we saw that even with the basic vehicle geometry, an average accuracy within 2.5 bits/s/Hz was obtained.

Table 5.1: Statistics on absolute error (bits/s/Hz) of capacity comparisons for various channel models, with the minimum for each category in bold and italics.

	Tx1			Tx2		
Model:	Avg	Max	Std Dev	Avg	Max	Std Dev
3D	<i>1.05</i>	4.51	1.20	<i>0.41</i>	<i>0.94</i>	<i>0.27</i>
Hyper Rayleigh	1.29	<i>4.44</i>	1.21	0.91	2.56	0.66
Nakagami	1.50	5.11	<i>1.08</i>	0.87	2.16	0.55
Gaussian	1.82	6.01	1.34	1.09	2.91	0.63
Weibull	2.26	6.45	1.28	1.82	3.74	1.00

5.6 Conclusion

This paper has described the multiantenna system simulation and measurement of the complex channel found in a 2004 Thomas Bus 110YN. The paper included an evaluation of which modeling parameters are required for accuracy. Section 5.3 described the measurement of the channel inside this shuttle bus. It was found to be rich in multipath with capacity ranging from 15 to 22.6 bits/s/Hz for site-specific locations. Multiantenna systems take advantage of this multipath, but would need to be combined with adaptive coding schemes to adjust to the varying capacity, especially as this variation could potentially increase with the addition of passengers as seen in [176]. Section 5.4 of this paper assessed the level of modeling detail required to accurately model the complex multipath channel inside a bus. Accurately modeling a bus environment requires including windows, which can be a significant source of loss in the actual channel, thus causing the model to overestimate capacity. Including windows reduced error by 0.74 up to 1.36 bits/s/Hz using the full internal bus configuration. We can assume similar results would be seen in other vehicular environments when the windows make up a significant portion of the external surface such as helicopters and automobiles. Internal obstacles also have a notable effect. Adding reflective walls, the rear engine box and wheel wells improved accuracy by up to 1.2 bits/s/Hz when compared with the empty bus cavity. Section 5.5 described how the basic shape of the external geometry is also important, decreasing average error by 0.5 to 1 bits/s/Hz from the simple rectangular configuration to the bus-shaped configuration, which has slanted side walls and curved top corner facets. It was assumed that the seats in the bus did not have a major impact on the channel, because seats have minimal impact on channels in

aircraft. However, our capacity mapping suggests they may indeed be affecting the channel, perhaps because they are made from different materials than aircraft. Future work may address this issue by measuring the actual loss through bus seats and arm rests and simulating with these parameters. Future work could also include comparisons to varying sizes of buses, such as grey-hound sized buses, as well as to smaller vehicles, such as SUVs and cars. This could help determine how size affects the level of detail required to model smaller vehicles.

The measurement of the shuttle bus showed a richly multipath environment that would work well with multiantenna systems, especially when combined with adaptive coding. The ray tracing software is able to estimate capacity within 1.05 bits/s/Hz for two transmitter locations (one at the front of the bus and one at the back) and is more accurate on average than some common statistical models including Gaussian, hyper-Rayleigh, Weibull and Nakagami. This ray tracing modeling can be used in the design of wireless communication systems inside complex channels, such as buses, to accurately estimate location specific capacity and is especially useful for simulating environments that are expensive or difficult to measure, or have not yet been built.

5.7 Acknowledgment

Much thanks to the University of Utah Transportation Services for allowing us to come and measure their bus, as well as my measurement team, James Nagel and Sai Ananthanarayanan. This work was supported by the US Air Force Research Laboratories (AFRL) through a grant from Universal Technologies Corporation and the National Science Foundation under grant ECCS-0823927.

5.8 References

- [158] R. Ketcham, J. Frolik, and J. Covell, "Propagation measurement and statistical modeling for wireless sensor systems aboard helicopters," *IEEE Transactions on Aerospace and Electronic Systems*, Vol. 44, No. 4, Page(s): 1609–1615, 2008.
- [159] Ramya Bhagavatula, Robert W. Heath Jr., and Sriram Vishwanath, "Optimizing MIMO antenna placement and array configurations for multimedia delivery in aircraft," *IEEE 65th Vehicular Technology Conference 2007 (VTC2007-Spring)*, April 2007.
- [160] Charisse Jones, "Buses gussy up for business travelers," USA TODAY, September 21, 2010. [Online] Available: <http://www.theadvertiser.com/article/20100921/BUSINESS/9210317/Buses-gussy-up-for-business-travelers>, [Accessed: August 10 2010].
- [161] J. Frolik, "A case for considering hyper-Rayleigh fading channels," *IEEE Transactions on Wireless Communications*, Vol. 6, No. 4, Page(s): 1235–1239, 2007.
- [162] A. Magleby and C. Furse, "Predicted MIMO performance in intravehicle channels," *IEEE Antennas and Propagation Society International Symposium*, San Diego, CA, Page(s) 1-4, 2008.
- [163] Alyssa Magleby, Cynthia Furse, and Z. Q. Yun, "3D ray tracing for intravehicle MIMO," *IEEE/URSI Antennas and Propagation Symposium*, Charleston, SC, June 1-5, 2009.
- [164] Sai Ananthanarayanan, Alyssa Magleby Richards, and Cynthia Furse. "Measurement and modeling of multiantenna systems in small aircraft," submitted to *Journal of Aerospace Computing, Information, and Communication*, June 2010.
- [165] M. Youssef, L. Vahala, and J. H. Beggs, "Electromagnetic propagation of wireless networks in aircraft cabins," *IEEE/ACES International Conference on Wireless Communications and Applied Computational Electromagnetics*, Page(s): 832 – 836, 2005.
- [166] H.-L Blocher, K. Beilenhoff, and J. Wenger, "Simulation of the electromagnetic wave propagation in cars," *33rd European Microwave Conference*, Vol. 3, Page(s): 1151 – 1154, 2003.
- [167] Z. Yun, Software package called "3D ray tracing for radio propagation modeling," last updated Dec. 2009, unpublished.

- [168] Z. Yun, Z. Zhang, and M. F. Iskander, "A ray tracing method based on the triangular grid approach and application to propagation prediction in urban environments," *Proceedings of the IEEE International Symposium on Information Theory (ISIT2004)*, Vol. 50, Page(s): 750–758, May 2002.
- [169] C. Takahashi, Z. Yun, M. F. Iskander, et al. "Propagation-prediction and site-planning software for wireless communication systems," *IEEE Antennas and Propagation Magazine*, Vol. 49, No. 2, April 2007.
- [170] S. Y. Lim, Z. Yun, J. M. Baker, N. Celik, H.-S. Youn, and M. F. Iskander "Radio propagation in stairwell: measurement and simulation results," *IEEE Antennas and Propagation Society International Symposium*, Charleston, SC, 2009.
- [171] J. Nagel, A. Magleby, S. Ananthanarayanan, and C. Furse, "Measured multiuser MIMO capacity in aircraft," accepted for publication in *IEEE Antennas and Propagation Magazine*.
- [172] D. Palchak and B. Farhang-Boroujeny, "A software defined radio test bed for MIMO systems," *Proceedings of the SDR 06 Technical Conference and Product Exposition*, Orlando, FL, November 2006.
- [173] D. Landon and C. Furse, "The MIMO transmission equation," (Honorable Mention, student paper contest) *IEEE Antennas and Propagation Symposium (APS)*, San Diego, CA, July 7-11, 2008.
- [174] Sai Ananthanarayanan, Alyssa Magleby, and Cynthia Furse, "Measurement and modeling of interference for multiple antenna system," *Microwave and Optical Technology Letters*, Volume 52, Issue 9, Page(s) 2031–2037, September 2010.
- [175] D. Dowdle, "Polarization agile antenna for MIMO," M.S. Thesis, University of Utah, Salt Lake City, UT, 2007.
- [176] K. I. Ziri-Castro, W. G. Scanlon, and N. E. Evans, "Prediction of variation in MIMO channel capacity for the populated indoor environment using a Radar cross-section-based pedestrian model," *IEEE Transactions on Wireless Communications*, Vol. 4, Issue: 3, Page(s): 1186 – 1194, 2005.
- [177] M. F. Iskander, *Electromagnetic fields and waves*, Prospect Heights, IL: Waveland Press, 1992.
- [178] I. Telatar et al., "Capacity of multi-antenna Gaussian channels," *European Transactions on Telecommunications*, Vol. 10, No. 6, Page(s): 585–596, 1999.
- [179] M. Lupupa and M.E. Dlodlo, "Performance of MIMO system in Weibull fading channel-channel capacity analysis," *IEEE EUROCON*, Page(s): 1735-1740, July 2009.

- [180] I.Y. Abualhaol and M.M. Matalgah, "Capacity analysis of MIMO system over ideally independent distributed Weibull fading channels," *IEEE International Conference on Communication*, Page(s): 5003-5008, June 2007.
- [181] D. Matolak and A. Chandrasekaran, "Aircraft intravehicular channel characterization in the 5 GHz band," *Integrated Communications, Navigation and Surveillance Conference, 2008*, Page(s): 1-6, 2008.
- [182] G. Fraidenraich, O. Leveque, and J. Cioffi, "On the MIMO channel capacity for the Nakagami-m channel," *IEEE Transactions on Information Theory*, Vol. 54, No. 8, Page(s): 3752-3757, 2008.
- [183] Sai Ananthanarayanan, "Enabling multiantenna wireless communication in aircraft: Channel modeling, interference & noise analysis, and antenna & detector optimization," PhD Dissertation, University of Utah, Salt Lake City, UT, 2010.

CHAPTER 6

WIRELESS CHANNEL MEASUREMENTS AND MODELING IN A HELICOPTER⁴

6.1 Abstract

This paper describes the measurement of the wireless channel inside a Bell OH-58A helicopter and its modeling using 3D ray tracing software. Modeling accuracy within 1.06 bits/s/Hz of measured capacity was achieved. This modeling is shown as an improvement over other common statistical models both in accuracy and the ability to predict site-specific capacity values within the helicopter.

6.2 Introduction

There is an increasing need for wireless communication systems in aircraft to improve safety and communication systems without increasing weight, as seen in [184] and [185]. Present and proposed systems carry data from smoke detection systems [186], in-flight entertainment systems [187], sensors for wire fault location [188], chemical sensors, moisture sensors, etc. [187]. In order to develop wireless communication systems for a range of vehicles, the severe multipath channel found inside various sizes

⁴ Content of this chapter is taken from an article coauthored with Sai Ananthanarayanan P.R. and Dr. Cynthia Furse and submitted to *IEEE Transactions on Vehicular Technology* [30].

of vehicles must be well defined. This multipath channel is much more complex than usual indoor/outdoor channels, and is unique to each vehicle. Previous work has been done to understand the channel found in narrow body medium length aircraft in [192] and [193], and wide body long aircraft in [194]-[198], as well as buses in [199] and [200]. Underground tunnels, which have channels similar to aircraft of the same size, have also been evaluated in [201] and [202]. All of these studies found a rich multipath environment that varied among different site-specific locations within the channel. This variation was greatly due to internal obstacles, such as walls, seats, etc., thus these obstacles are important to include in the model. The wireless channel in small vehicles, such as helicopters and cars, is also of great interest as seen in [203] and [204], but it is not clear from the previous work if the 3D ray tracing method can be extended to these much smaller cavities. Normally the ray tracer is expected to be used when the walls of the cavity are well in the far field of the source. At 915 MHz, where these tests were performed, the wavelength is 32.8 cm, thus making the distances measurable within a small helicopter only marginally in the far field. This paper evaluates the effectiveness of the ray tracing software despite pushing it beyond its normal limits.

Another reason a helicopter is a particularly interesting wireless channel is its large window surface. Simulations and measurements within a bus (which also has large window surface) showed a strong dependence on proper modeling of the windows. This should come as no surprise, because the windows allow some of the wireless signal to escape, thus reducing the multipath channel within the helicopter. This helps reduce interference in single antenna channels, but limiting the multipath reduces the capacity in multiantenna channels. If this reduced capacity (in the range of 2 bits/s/Hz average in the

bus from [200]) is not accounted for in the model by including windows, the model will overestimate capacity, increasing the error.

As an alternative to site-specific modeling, several statistical models could be used to predict channel performance, including Gaussian [205], Weibull [207], Nakagami [209], and hyper-Rayleigh [190]. These models are limited in their application to aircraft that have already been built and can be measured, because they depend on measured or estimated K values. Additionally, these statistical models are used to obtain average and not site-specific capacity estimates. It will be shown that the 3D ray tracing model has improved accuracy over these statistical models when applied to a helicopter channel.

This paper discusses a measurement campaign to evaluate the complex wireless channel in a Bell OH-58A helicopter. The measurement system uses a 4x4 antenna array to measure the channel capacity at points throughout the helicopter. 3D software was used to simulate the same channel and compared to the measurements to determine which factors are most important for accuracy in the ray tracing simulation. This paper provides an analysis of the wireless channel found in a small vehicle, such as a helicopter and how the configurable parameters of the 3D ray tracing software affect channel modeling accuracy when compared to measured capacity. It then demonstrates the improved accuracy of the 3D ray tracing method over commonly used statistical models at the cost of increased modeling complexity.

6.3 Quantification of the Bell OH-58A Helicopter Wireless Channel

In order to quantify the multiantenna capacity in the wireless channel, we performed a thorough mapping of the Bell OH-58A helicopter, with dimensions shown in

Figure 6.1 and Figure 6.2, photo in Figure 6.3. A multiantenna test bed developed by Palchak [210] and updated by Nagel [211] was used to evaluate the measured channel which was then compared to simulated capacity from 3D ray tracing. Capacity measurements were taken with a 4x4 array of 8.2 cm spaced 0.25λ monopoles at 915 MHz. Antennas started 10 cm from the edge of a 38x45.7 cm ground plate, and were centered lengthwise. Data packets were transmitted based on the 4-QAM modulation

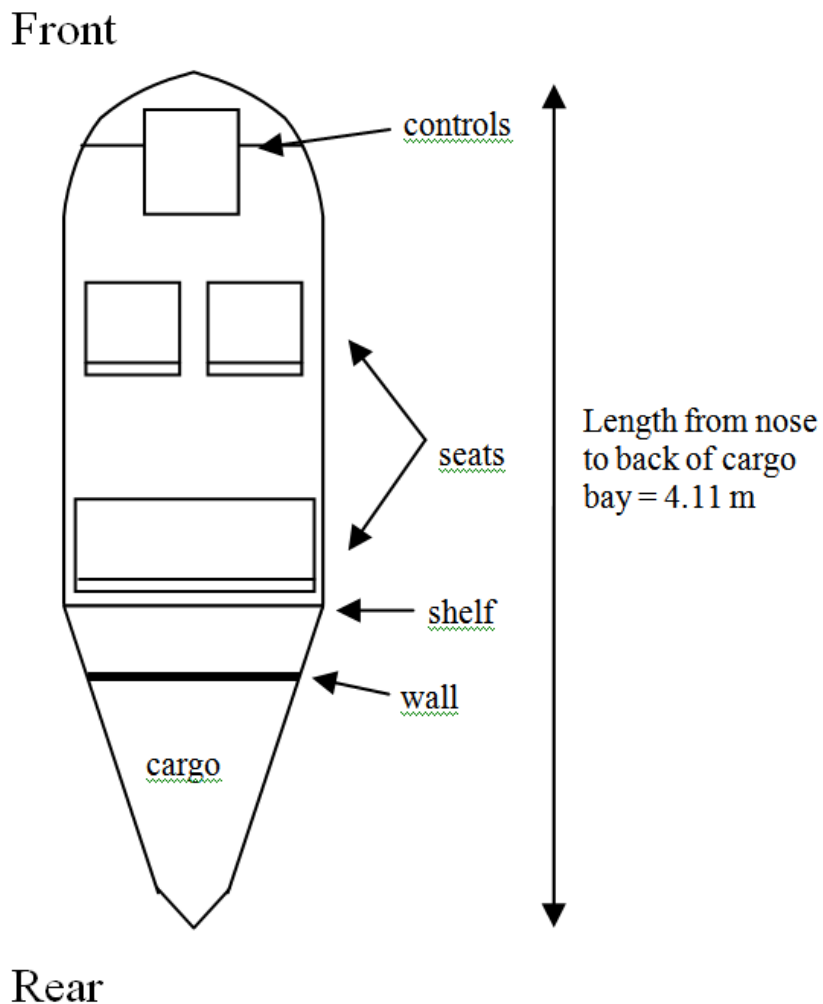


Figure 6.1: Helicopter floor layout

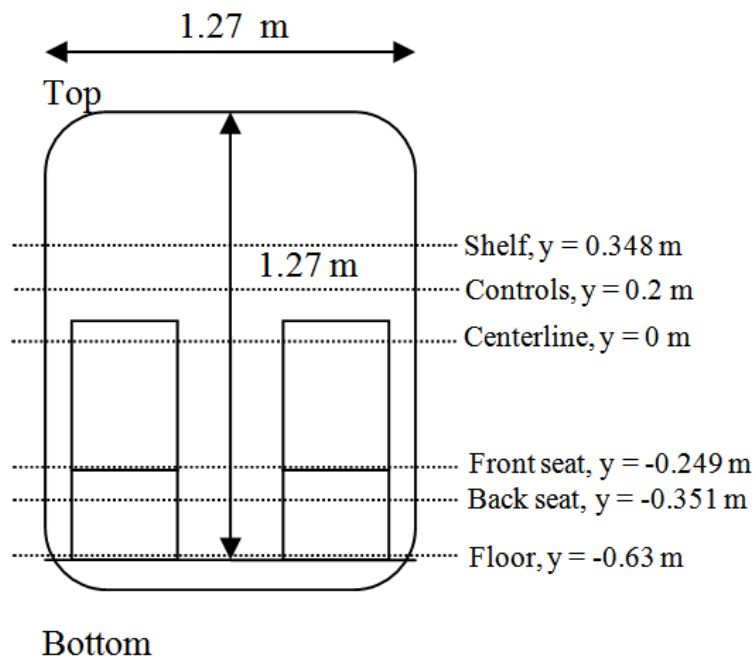


Figure 6.2: Helicopter cross-section with elevations



Figure 6.3: Photo of the Bell OH-58A helicopter

scheme using differential encoding with 50 kbps of data per antenna. Each packet started with a simple single antenna preamble of 4000 pseudorandom data bits added to allow phase and timing synchronization by the receiver. The packet then included a multiantenna sequence of 4×4000 pseudorandom bits to be used as a training sequence for channel estimation. The packet terminated with a small payload of text data used to verify proper packet detection in postprocessing.

We started measurements with the transmit antenna on the dash and moved the receiver to points starting at 0 m from the front of the helicopter, on the floor to either side of the control box (approximately 0.83 m below the transmit antenna), and then continued to the back of the helicopter, repeating every 0.51 m out to 2.04 m, spanning the width of the helicopter at each distance and adding one additional receive location 2.85 m away in the cargo bay as shown in Figure 6.4 (left). We then moved the transmitter to the cargo bay in the rear of the helicopter, and repeated the process, with transmit and receive locations as detailed in Figure 6.4 (right).

The data was postprocessed to obtain a normalized capacity [212] at each received location. The resulting capacity mapping for each transmit antenna is shown in Figure 6.5 and Figure 6.6. The average capacity for TX1 was 20.23 bits/s/Hz. Some signal was lost going from the rear maintenance bay through a wall into the main cabin, dropping the average capacity for TX2 down to 18.06 bits/s/Hz. Comparing this to the higher capacity at the receive location in the rear maintenance bay shows that walls near the transmit antenna have a greater effect on the transmission signal than walls far away from it, which supports previous findings in other aircraft [213].

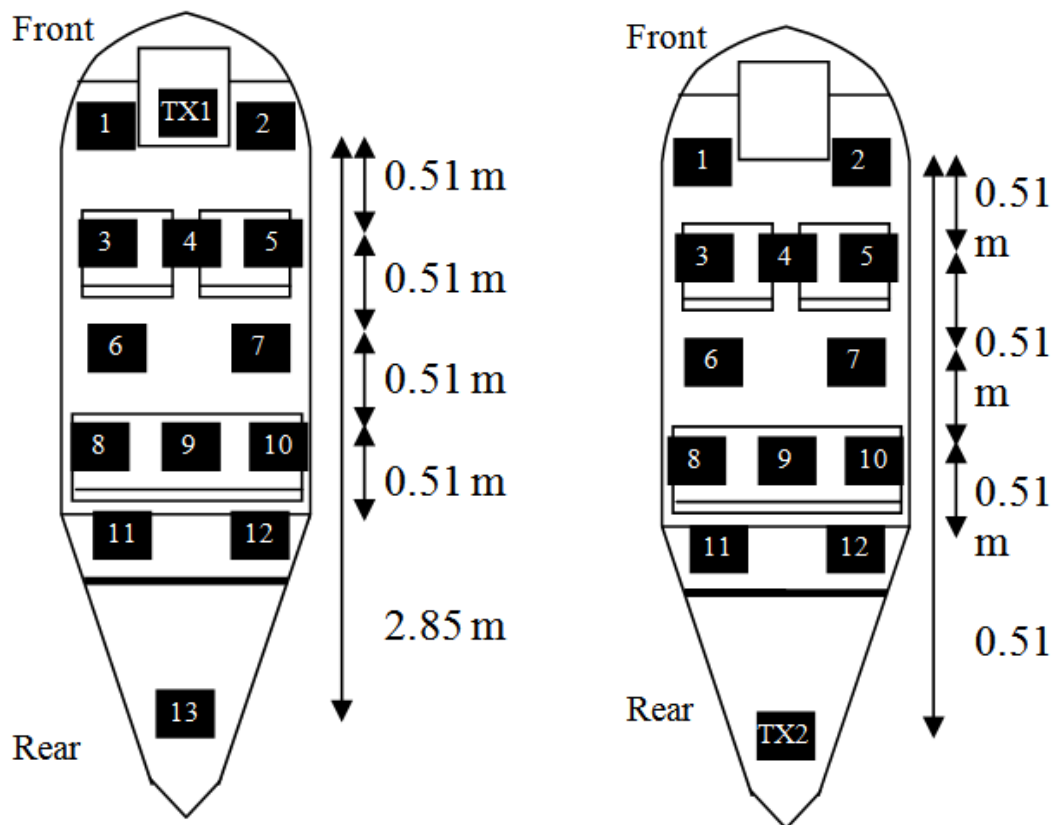


Figure 6.4: Transmit and receive locations and distances for TX1 (left) and TX2 (right)

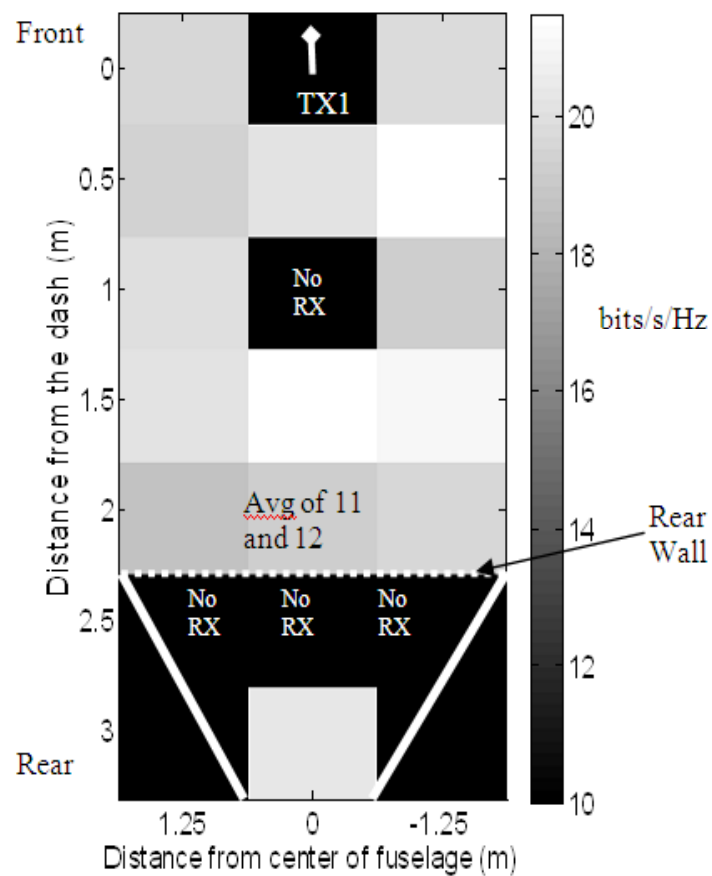


Figure 6.5: Capacity mapping for TX1. The white bars represent internal and external walls of the helicopter as seen in Figure 6.1.

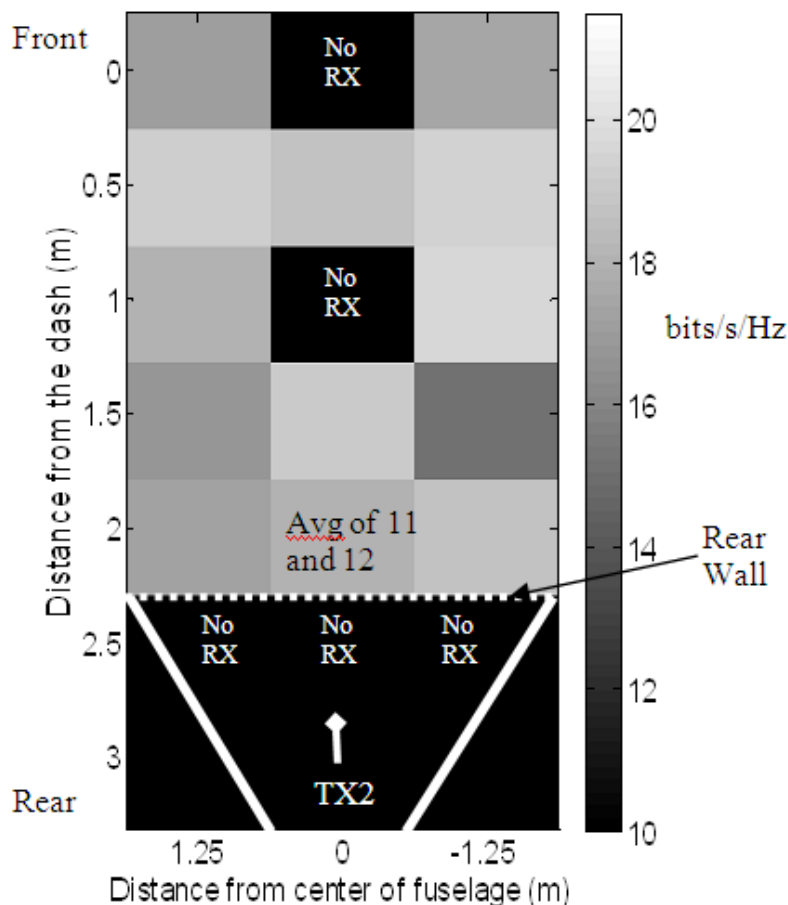


Figure 6.6: Capacity mapping for TX2. The white bars represent internal and external walls of the helicopter as seen in Figure 6.1.

6.4 3D Ray Tracing Modeling

The site-specific capacity mapping from measurements provides information on the complex channel in this particular helicopter with this particular configuration, but it cannot be easily generalized to other helicopters. Channel information would also change if we made changes to this helicopter, such as adding metallic boxes for instrument or luggage storage, for instance. That type of flexibility comes only from simulation and modeling, which is the impetus behind the 3D ray tracing model described in this section. With this model we can evaluate aircraft and vehicles that have not yet

been built. We can also determine how modifications in internal structures of these vehicles might change the communication channel and hence the performance of the communication system. In this section, we will evaluate the parameters necessary to obtain accurate comparisons between the measured capacities from Section 6.3 and those obtained from 3D ray tracing software designed by Yun [214] and adapted to other environments in [192] and [200].

The output of the 3D ray tracing software includes received power, path gains, complex electric field magnitude and phase, and angle of arrival and departure (AOA/AOD) information which is used to create a channel matrix for each transmit to receive location. The channel matrix is combined with a detailed signal model (DSM) which is based on network theory with additional terms to account for the effects of antenna coupling, antenna mismatch, polarization and pattern mismatch, imperfect antenna efficiency, and loss at the transmitter and receiver, as described in [215]. The resulting system matrix, which includes the effect of the antenna system as well as channel effects, is used to calculate site-specific capacity performance within the enclosed environment as detailed in [212].

For the 3D ray tracing analysis, the inside of the helicopter was modeled with 2 rows of lossy seats and a lossy partial wall representing the wall below the shelf between the cabin and cargo areas, with loss set to 0.1 dB for the seats and wall, which was found to be a reasonable estimate in previous measurements. Various configurations of the nose of the helicopter were simulated to evaluate the level of detail required for such a small enclosed space. Prior models for other aircraft had obtained accuracy within 1 bit/s/Hz using a simple flat surface geometry for the front of the aircraft [200], but the

helicopter's more rounded structure did not allow for the simplified flat geometry. The flat front external configuration (*flat front*, shown in Figure 6.7) consists of a flat front wall at the nose of the helicopter with the body modeled as a basic box with faceted edges, narrowing from the rear shelf to the end of the cargo area, with all walls as well as the flat front represented as perfect electrical conductor (PEC). The flat plus glass configuration (*flat plus glass*, shown in Figure 6.8) is the same as the flat front configuration, but includes a glass panel on the top half of the flat front surface to represent the windshield. The angled box configuration (*angled box plus glass*, shown in Figure 6.9) again uses the same body configuration, but replaces the bottom half of the flat front (made of PEC) with an angled box to represent the nose and controls, and moves the glass closer to the seats.

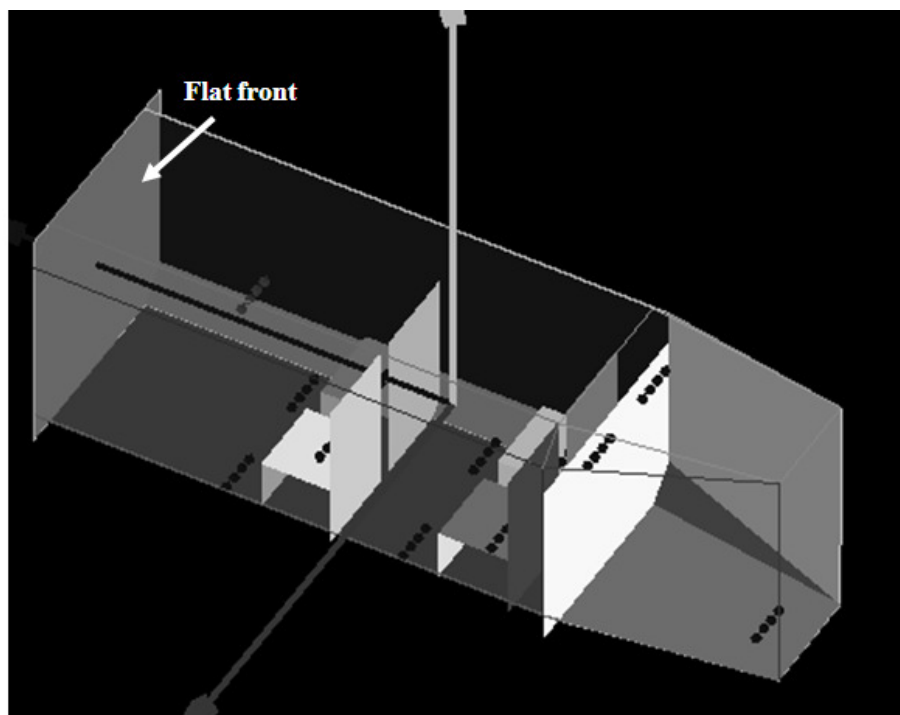


Figure 6.7: Flat front 3D configuration of helicopter

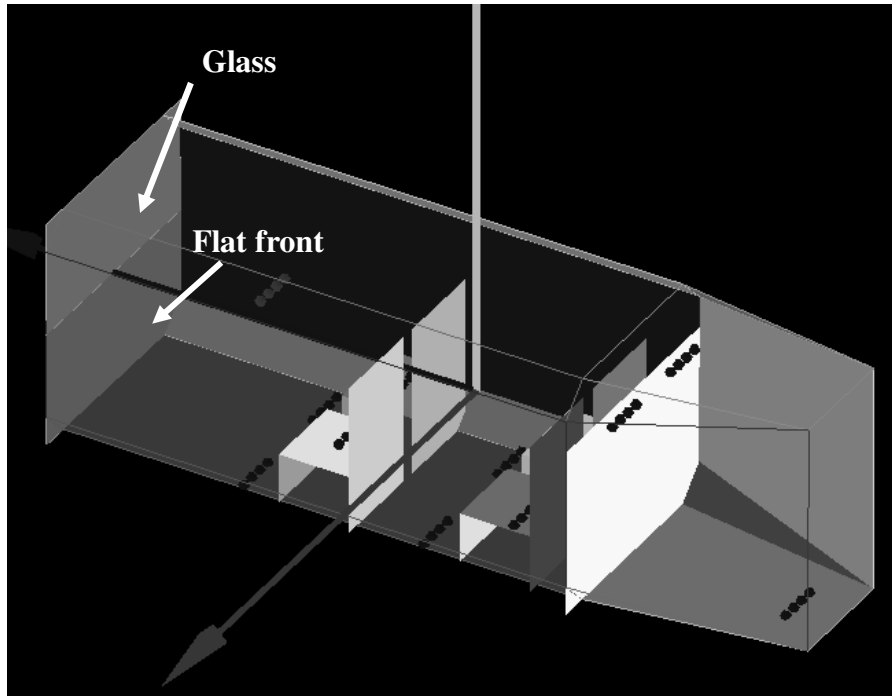


Figure 6.8: Flat front plus glass 3D configuration of helicopter

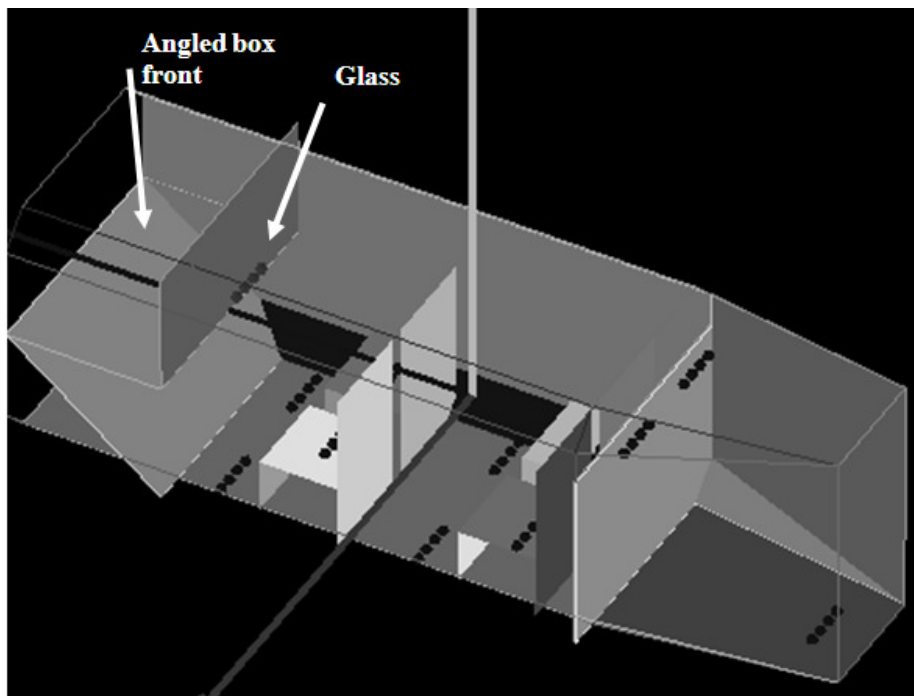


Figure 6.9: Angled box front plus glass 3D configuration of helicopter

The site-specific capacity errors for the three different configurations are shown in Figure 6.10 and Figure 6.11 for TX1 and TX2, respectively. For both TX1 and TX2, it is clear that the simplified models (*flat front* and *flat plus glass*) were not sufficiently detailed, giving average errors in the range of 1.8 to 2.5 bits/s/Hz.

As more detail was added to the model, accuracy improved. For TX1 the average error decreased from 2.19 bits/s/Hz with the PEC flat front model down to 1.06 bits/s/Hz with the angled box configuration to represent the nose combined with a glass windshield. TX1 errors were less than 2 bits/s/Hz for all locations except 5, which had the greatest error. This error could be caused by the close range of less than 1 m between the transmit and receive antennas. For TX2, average capacity error decreased from 2.49 bits/s/Hz for the PEC flat front model down to 0.95 bits/s/Hz for the angled box configuration. This matched expected results that a smaller vehicle would require more detail with obstacles and external geometry making a larger difference as we approach the lower limits of the far field at 915 MHz.

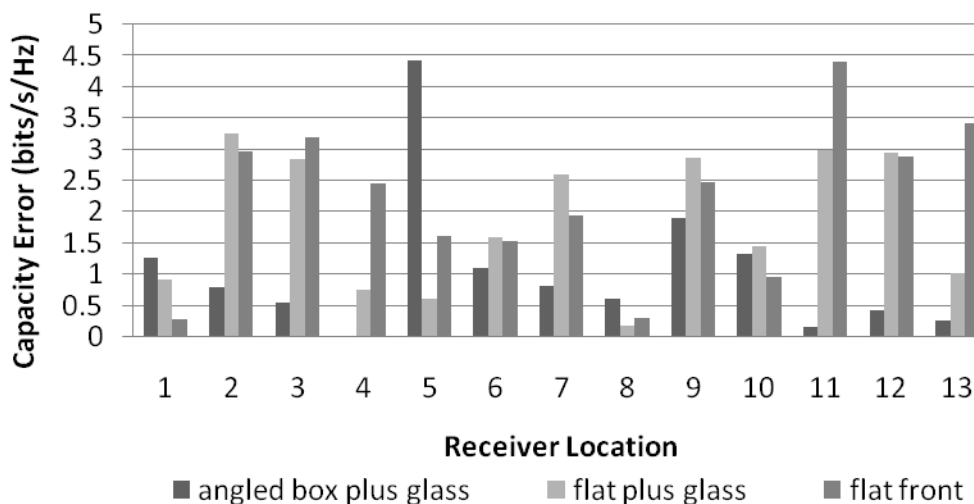


Figure 6.10: Site-specific capacity error in the Bell OH-58A helicopter for TX1.

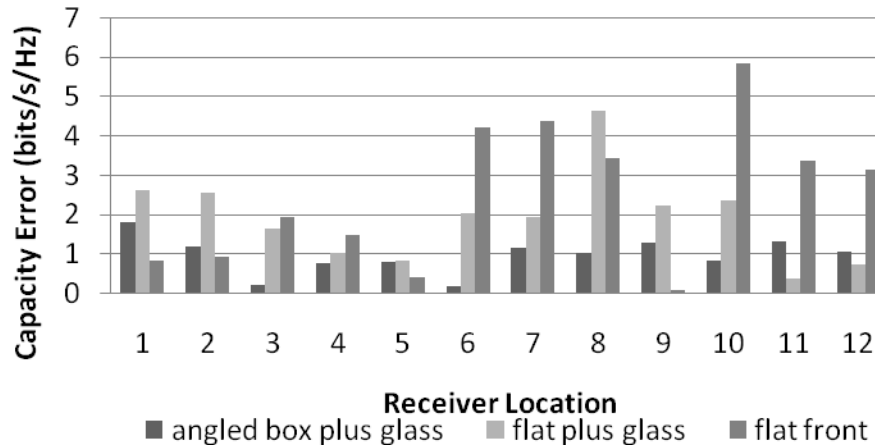


Figure 6.11: Site-specific capacity error in the Bell OH-58A helicopter for TX2.

6.5 Statistical Models

We were able to achieve good capacity estimates within 1.06 bits/s/Hz for both transmit locations using 3D ray tracing with the angled box plus glass configuration, so we wanted to evaluate how this compared with other commonly used statistical models that are not site-specific -- Gaussian [205], Weibull [207], Nakagami [209], and hyper-Rayleigh [190]. The Gaussian model specifies a plane of impinging waves with Gaussian-distributed magnitudes and uniformly distributed angles of arrival (AOAs) and phases. The Weibull distribution was created to model the lifetime of some object that fails based on its weakest link, and thus has been widely used for modeling the fading envelope in wireless communication. The Weibull model has an exponentially decaying path loss with uniformly distributed phases. It reduces to the Rayleigh model for $\alpha_k = 2$. For this paper, $\alpha_k = 1.5$ is used for the fading parameter with average fading power of $\Omega_k = 1$, based on optimization simulations performed in [212]. The Nakagami-m distribution offers more flexibility and a better match to many fading channels, as shown in [209], as it offers the flexibility of one more parameter than the Weibull and Gaussian models.

The Nakagami- m model simplifies to the Rayleigh model for $m=1$ and uniform distribution on the unit circle for $m=\infty$. The path loss is also modeled as an exponential decay with uniformly distributed phases. For this paper, $m=1.73$ and $m=1.4$ were used for the Nakagami model. The hyper-Rayleigh distribution models the received signal dominated by two constant amplitude signal components with uniformly distributed angles of arrival over $[0, 2\pi)$, and is also referred to as two-wave with diffuse power (TWDP), as detailed in [190].

These statistical models were also compared to 3D ray tracing results for other vehicles in [193], [200] and [212]. An estimated K value based on measurements was used for each receive location in order to evaluate each of these statistical models at the locations of interest. The resulting capacity errors are shown in Figure 6.12 and Figure 6.13 for TX1 and TX2, respectively. For TX1, the 3D ray tracing model had an extreme error at location 5 (front passenger seat), but otherwise stayed within 2 bits/s/Hz. For TX2, the 3D ray tracing model was always within 1.8 bits/s/Hz, even when all the other models exceeded that error at locations 8 and 10 (both sides of rear seats).

For TX1, the 3D ray tracing model had the smallest error for 30.8% of the locations, similar to the hyper-Rayleigh model. For TX2, the 3D model had the smallest error of all the models (33.3%) of the locations, similar to the hyper-Rayleigh model and Nakagami-1.4, which means none of the other models had the lowest error at any of the locations. The 3D ray tracing outperformed the statistical models with the best average error for TX1 at 1.06 bits/s/Hz, followed by Nakagami-1.4 at 1.17 bits/s/Hz. The 3D model also had the best average error for TX2 at 0.95 bits/s/Hz, followed by hyper-Rayleigh at 1.23 bits/s/Hz, then Nakagami-1.4 at 2.09 bits/s/Hz, with all other models

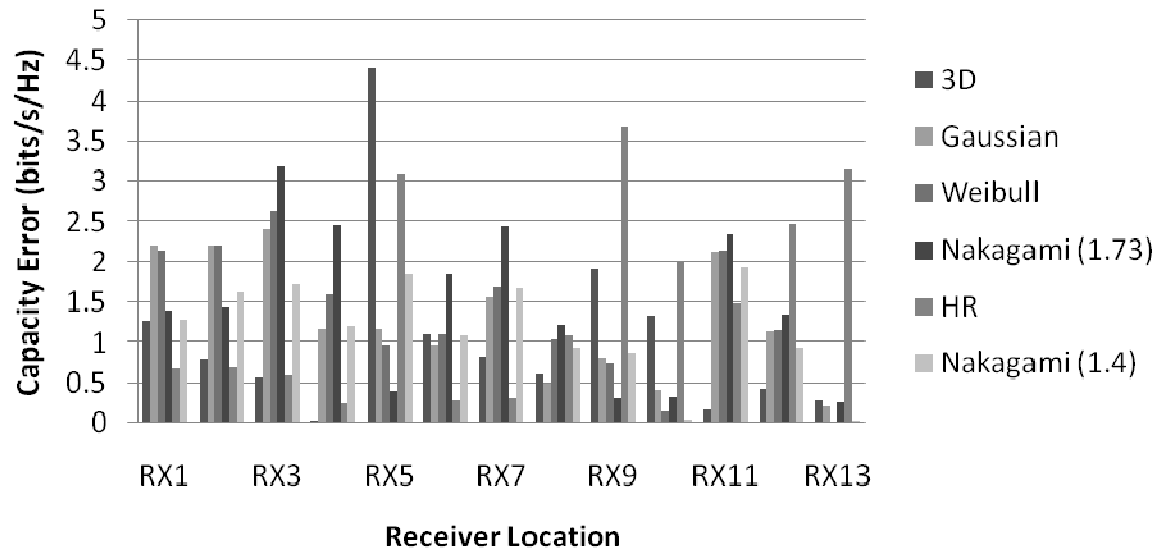


Figure 6.12: Capacity errors for TX1 for 3D ray tracing versus various statistical channel models.

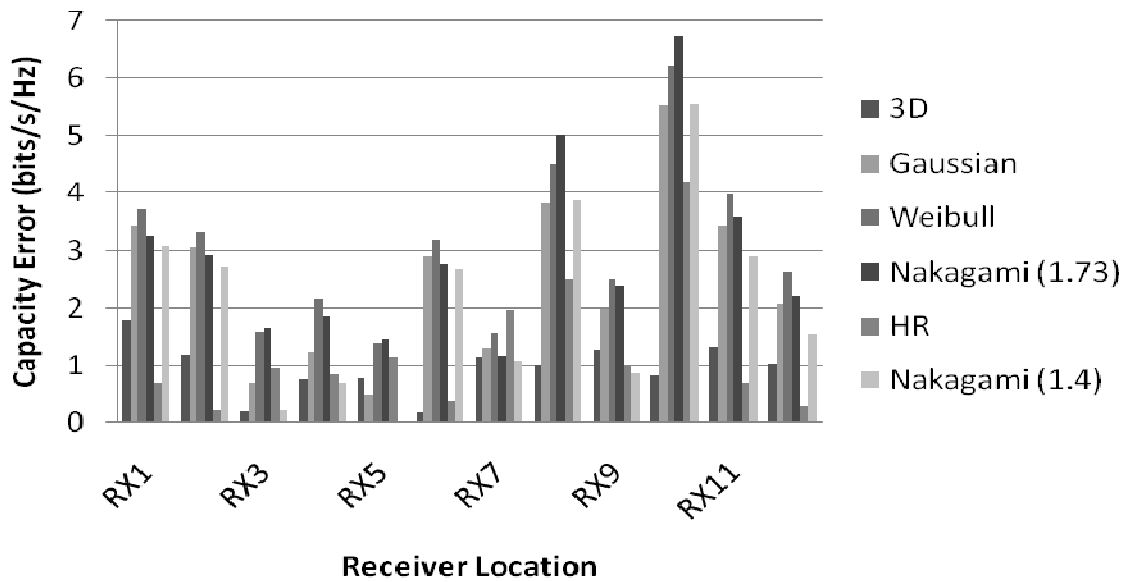


Figure 6.13: Capacity errors for TX2 for 3D ray tracing versus various statistical channel models.

averaging above 2.4 bits/s/Hz. Averaging both transmit locations, the 3D ray tracing method was the most accurate, followed by either the Nakagami-1.4 or the hyper-Rayleigh. The 3D modeling requires more detail in the calculation and processing of data than these statistical models, but does not require measurement to determine the K value. It could therefore be used when the channel is difficult, costly, or impossible to measure (such as before a helicopter is built).

6.6 Conclusion

The helicopter channel was found to have a wide range of site-specific capacities, from 15 to 23 bits/s/Hz based on multiantenna measurements. Despite this strong multipath environment, the 3D ray tracing model was able to achieve an average error within 1.05 bits/s/Hz for the angled box with glass configuration. The variety of configurations simulated showed that as vehicle size or transmission frequency decreases, increased configuration detail is required to maintain accuracy. This is because the space within the vehicle becomes electrically smaller in relation to the wavelength of the signals and small variations in reflective surfaces have a greater impact. It was also seen that the 3D ray tracing model provides a more accurate average and site-specific capacity calculation than other commonly used statistical models, with 0.12 to 3 bits/s/Hz improvement over the statistical models. This type of site-specific analysis is most beneficial for static deployments of wireless systems such as wireless data collection from sensor networks. These results also show that if the improved accuracy is not necessary or the added complexity of the ray tracing method is not desirable, the next best accuracy may be obtained using Nakagami as the statistical model for this channel.

6.7 Acknowledgment

Much thanks to Randy Chesley and the Logan Municipal Airport for allowing us to come and measure their helicopter, as well as my measurement team, James Nagel and Sai Ananthanarayanan. This work was supported by the US Air Force Research Laboratories (AFRL) through a grant from Universal Technologies Corporation and the National Science Foundation under grant ECCS-0823927.

6.8 References

- [184] Susan Karlin. "Take off, plug in, dial up," *IEEE Spectrum*, Page(s): 53-59, August 2001.
- [185] A. Ameti, R. Fontana, E. Knight, and E. Richley, "Ultrawideband technology for aircraft wireless intercommunication systems (AWICS) design," *IEEE Aerospace and Electronic Systems Magazine*, Vol. 19, No. 7, Page(s): 14–18, 2004.
- [186] Wireless Smoke Detection. [Online] Available: <http://www.securaplane.com/smoke2.html>, [Accessed: June 21 2009].
- [187] Securaplane Technologies, Inc. Press Release, "Securaplane Technologies awarded Boeing 787 contract for wireless emergency lighting," [Online] Available: <http://www.securaplane.com/releases/pr0095.html>. [Accessed: 21st June 2009].
- [188] Paul Smith, Cynthia Furse, and Jacob Gunther. "Analysis of spread spectrum time domain reflectometry for wire fault location," *IEEE Sensors Journal*, Vol. 5 No. 6, December 2005.
- [189] [Online] Available: www.honeywell.com/sites/aero/AircraftSensors.html, [Accessed: June 21 2009].
- [190] J. Frolik, "A case for considering hyper-Rayleigh fading channels," *IEEE Transactions on Wireless Communications*, Vol. 6, No. 4, Page(s): 1235–1239, 2007.
- [191] A. Magleby and C. Furse, "Predicted MIMO performance in intravehicle channels," *IEEE Antennas and Propagation Society International Symposium*, San Diego, CA, 2008.

- [192] A. Magleby, C. Furse, and Z. Yun. "3D Ray tracing to find the channel matrix for intravehicle environments," *IEEE Antennas and Propagation Society International Symposium*, Charleston, SC. June 2009.
- [193] Sai Ananthanarayanan, Alyssa Magleby Richards, and Cynthia Furse, "Measurement and modeling of multiantenna systems in small aircraft," submitted to *Journal of Aerospace Computing, Information, and Communication*.
- [194] Fitzhugh, J. Frolik, J. Covell, R. Ketcham, and T. Meyer, "2.4 GHz multipath environments in airframes," *Proceedings of 2005 Wireless and Microwave Technology Conference (WAMICON 2005)*, 2005.
- [195] M. Youssef, L. Vahala, and J. H. Beggs, "Electromagnetic propagation of wireless networks in aircraft cabins," *IEEE/ACES International Conference on Wireless Communications and Applied Computational Electromagnetics*, Page(s): 832 – 836, 2005.
- [196] N. Moraitis and P. Constantinou, "Radio channel measurements and characterization inside aircrafts for in-cabin wireless networks," *IEEE 68th Vehicular Technology Conference-Fall 2008*, 2008.
- [197] A. Kaouris, M. Zaras, M. Revithi, N. Moraitis, and P. Constantinou, "Propagation measurements inside a B737 aircraft for in-cabin wireless networks," *IEEE Vehicular Technology Conference, Spring 2008*. Page(s): 2932 – 2936. 2008.
- [198] D. Matolak and A. Chandrasekaran, "Aircraft intra-vehicular channel characterization in the 5 GHz band," *Integrated Communications, Navigation and Surveillance Conference*, 2008.
- [199] Christopher I. Fitzhugh, "Multipath characterization of enclosed environments," M. S. Thesis, University of Vermont, Burlington, VT, 2006.
- [200] Alyssa Magleby Richards, Sai Ananthanarayanan, and Cynthia Furse, "Complex measurement and simulation of the multiantenna communication channel on a shuttle bus," in preparation for *IEEE Transactions on Vehicular Technology*.
- [201] Sai Ananthanarayanan, Alyssa Magleby, and Cynthia Furse, "Measurement and modeling of interference for multiple antenna system," *Microwave and Optical Technology Letters*, Vol. 52, No. 9, Page(s):2031–2037, September 2010.
- [202] Y. P. Zhang and Y. Hwang. "Theory of the radio-wave propagation in railway tunnels," *IEEE Transactions on Vehicular Technology*, Vol. 47, No. 3, August 1998.
- [203] R. Ketcham, J. Frolik, and J. Covell, "Propagation measurement and statistical modeling for wireless sensor systems aboard helicopters," *IEEE Transactions on Aerospace and Electronic Systems*, Vol. 44, No. 4, Page(s): 1609–1615, 2008.

- [204] H.-L. Blocher, K. Beilenhoff, and J. Wenger, "Simulation of the electromagnetic wave propagation in cars," *33rd European Microwave Conference*, Vol. 3, Page(s): 1151 – 1154, 2003.
- [205] I. Telatar, et al., "Capacity of multiantenna Gaussian channels," *European Transactions on Telecommunications*, Vol. 10, No. 6, Page(s): 585–596, 1999.
- [206] M. Lupupa and M.E. Dlodlo, "Performance of MIMO system in Weibull fading channel-channel capacity analysis," *IEEE EUROCON*, Page(s): 1735-1740, July 2009.
- [207] I.Y. Abualhaol and M.M. Matalgah, "Capacity analysis of MIMO system over ideally independent distributed Weibull fading channels," *IEEE International Conference on Communication*, Page(s): 5003-5008, June 2007.
- [208] D. Matolak and A. Chandrasekaran, "Aircraft intravehicular channel characterization in the 5 GHz band," *Integrated Communications, Navigation and Surveillance Conference*, 2008.
- [209] G. Fraidenraich, O. Leveque, and J. Cioffi, "On the MIMO channel capacity for the Nakagami-m channel," *IEEE Transactions on Information Theory*, Vol. 54, No. 8, Page(s): 3752–3757, 2008.
- [210] D. Palchak and B. Farhang-Boroujeny, "A software defined radio test bed for MIMO systems," *Proceedings of the SDR 06 Technical Conference and Product Exposition*, Orlando, FL, November 2006.
- [211] James R. Nagel, Sai Ananthanarayanan, Alyssa Magleby Richards, and Cynthia Furse, "Measured multiuser MIMO capacity in aircraft," accepted for publication in *IEEE Antenna and Propagation Magazine*.
- [212] Sai Ananthanarayanan, "Enabling multiantenna wireless communication in aircraft: channel modeling, interference & noise analysis, and antenna & detector optimization," PhD Dissertation, University of Utah, Salt Lake City, Utah, 2010. [Online] Available: <http://wwwlib.umi.com/dissertations/>, [Accessed: October 15 2010].
- [213] Alyssa Magleby Richards, Sai Ananthanarayanan, and Cynthia Furse, "3D simulation of the wireless channel in small aircraft," submitted to *IEEE Transactions on Vehicular Technology*.
- [214] Z. Yun, Software package called "3D ray tracing for radio propagation modeling," last updated Dec. 2009, unpublished.
- [215] D. Landon and C. Furse, "The MIMO transmission equation," (Honorable Mention, student paper contest) *IEEE Antennas and Propagation Symposium (APS)*, San Diego, CA, July 7-11, 2008.

CHAPTER 7

COMPLEX CHANNEL MEASUREMENT AND MODELING FOR THE DESIGN OF WIRELESS SYSTEMS⁵

7.1 Abstract

Measurement, along with site specific and statistical modeling are compared for a variety of complex, enclosed channels, including a Beech Baron 58P-metallic body, a Rockwell T-39 Sabreliner-metallic body, a 2004 Thomas Bus 110YN, a Bell OH58 Helicopter and two underground tunnels (one made of cement and the other made of concrete). Average measured capacity was found to be between 18 and 21 bits/s/Hz for most channels using a 4x4 array of antennas, and had no direct relation to the size of the channel. Vehicular channels, whether built or not, can be modeled using 3D ray tracing using a configuration that includes a detailed depiction of the channel geometry, large windows, and reflective objects inside the channel space, especially if they are near the transmitter. 3D ray tracing is site-specific and is able to achieve accuracy within 1.1 bits/s/Hz for all channels studied, which is more accurate than commonly used statistical models.

⁵ Content of this chapter is taken from an article coauthored with Sai Ananthanarayanan P.R. and Dr. Cynthia Furse and in preparation for submission to *IEEE Transactions on Vehicular Technology* [31]

7.2 Introduction

Wireless communication has become an essential part of everyday life. The hunger for more data, more phone calls, more video, and more access in more places is growing massively, challenging the availability of spectral resources and our current infrastructure. Traditional communication systems are nearing their maximum potential and cannot provide the linkages needed for future generations of ‘screaming’ video, voice, and data transmission. Communication in vehicles is particularly challenging because of their extremely high multipath environment, yet this is an area that people spend a great deal of their time and therefore request and require communication capability. In addition, there is significant interest in reducing the number of wires in vehicles to reduce weight, complexity, maintenance, etc. and replace them with wireless systems. Paradigm shifts are needed in order to achieve the anticipated demand for intravehicular communication. A new concept showing great promise for improving communication in complex channels is the use of multiantenna systems which extract multiple effective channels from the rich multipath scattering present in these environments, resulting in better communication as well as increased capacity [216][217][219].

In order to develop wireless communication systems for a range of vehicles and other enclosed spaces, the severe multipath channel found inside various types of these channels must be well defined. This multipath channel is much more complex than usual indoor/outdoor channels, and is unique to each type of channel. Previous work includes measurement of stairwells [220], tunnels [221], aircraft [222], [223], and other indoor environments [223][225]. A characterization of these channels can be made using a

combination of measurement and accurate modeling. A multiantenna test bed was used to measure complex channels in a Beech Baron 58P-small metallic body, a Rockwell T-39 Sabreliner-medium metallic body, a 2004 Thomas Bus 110YN, a Bell OH58 Helicopter and two underground tunnels. To achieve the best accuracy in modeling this variety of complex channels, 3D site-specific ray tracing [219][227][228] has been employed. But the 3D site-specific model requires significantly more complexity than site-averaged statistical models such as Gaussian [229], hyper-Rayleigh [230], Weibull [231], and Nakagami [232].

This paper discusses the measurement, modeling, and statistical analysis of multiantenna channels in 2 underground tunnels, a 2004 Thomas Bus 110YN, and 3 aircraft including a Rockwell T-39 Sabreliner, a Beech Baron 58P, and a Bell OH58 Helicopter. Measurements were made using a multiantenna test bed [233][234] in order to take advantage of the extreme multipath environments found in these channels. 3D ray tracing software [219] combined with a detailed signal model (DSM) that incorporates the effects of antenna polarization, efficiency, radiation pattern, matching, etc. [217] was used for site-specific modeling of the capacity. Gaussian, hyper-Rayleigh, Weibull and Nakagami statistical models were also evaluated. This paper provides an analysis of similarities, differences and trends of the complex channels in these enclosed environments to evaluate design parameters and constraints that may be applied to designing such systems.

Section 7.3 gives an overview of how each channel was measured then shows the site-specific capacity mapping results for each and compares trends found in these measurements for capacity, size, walls, and special locations. Section 7.4 summarizes the

various modeling methods, compares the accuracy of these methods for all complex channels measured, and gives conclusions on how to best use each method. This paper concludes with an overview of how to use this collection of information in the design of wireless multiantenna systems for complex channels.

7.3 Complex Channel Measurement

A thorough mapping of each complex channel using a multiantenna test bed [233][234] was performed previously [235]-[239]. The test bed transmitter and receiver each consisted of a 4x4 array of 0.25λ (0.076 m) spaced monopoles at 915 MHz. Antennas started 0.1 m from the edge, and were centered lengthwise on a 0.38x0.457 m ground plane. Data packets were transmitted using 4-QAM modulation and differential encoding with 50 kbps of data per antenna. Each packet started with a simple single antenna preamble of 4000 pseudorandom data bits added to allow phase and timing synchronization by the receiver. The packet then included a multiantenna sequence of 4 x 4000 pseudorandom bits to be used as a training sequence for channel estimation. The packet terminated with a small payload of text data used to verify proper packet detection in postprocessing [234]. All measurements were normalized using the Frobenius norm of the channel matrix with the SNR was fixed at 20 dB. The capacity was calculated using equation 7.1, which takes into account the increase in capacity due to multiantennas and reflects the richness or poorness of the multipath in the channel.

$$C = \log_2 \det \left[I + \frac{SNR_r N_r}{\| \mathbf{H} \|_{Frobenius}^2} \mathbf{H} \mathbf{H}^H \right] \quad (7.1)$$

7.3.1 Rockwell T-39 Sabreliner

Transmit and receive locations for the Rockwell T-39 Sabreliner are shown in Figure 7.1, with the resulting capacity map for TX1 in Figure 7.2. For TX1 in the cockpit, there was a trend of decreasing capacity as we moved away from the transmitter (to be expected) until the back wall, where there was a hot spot, as shown at the bottom of Figure 7.2. The average capacity over all locations for both TX1 (on the front dash) and TX2 (in the maintenance bay) was 18.8 bits/s/Hz. TX3 was in the center of the fuselage and had the highest average capacity of 20.4 bits/s/Hz.

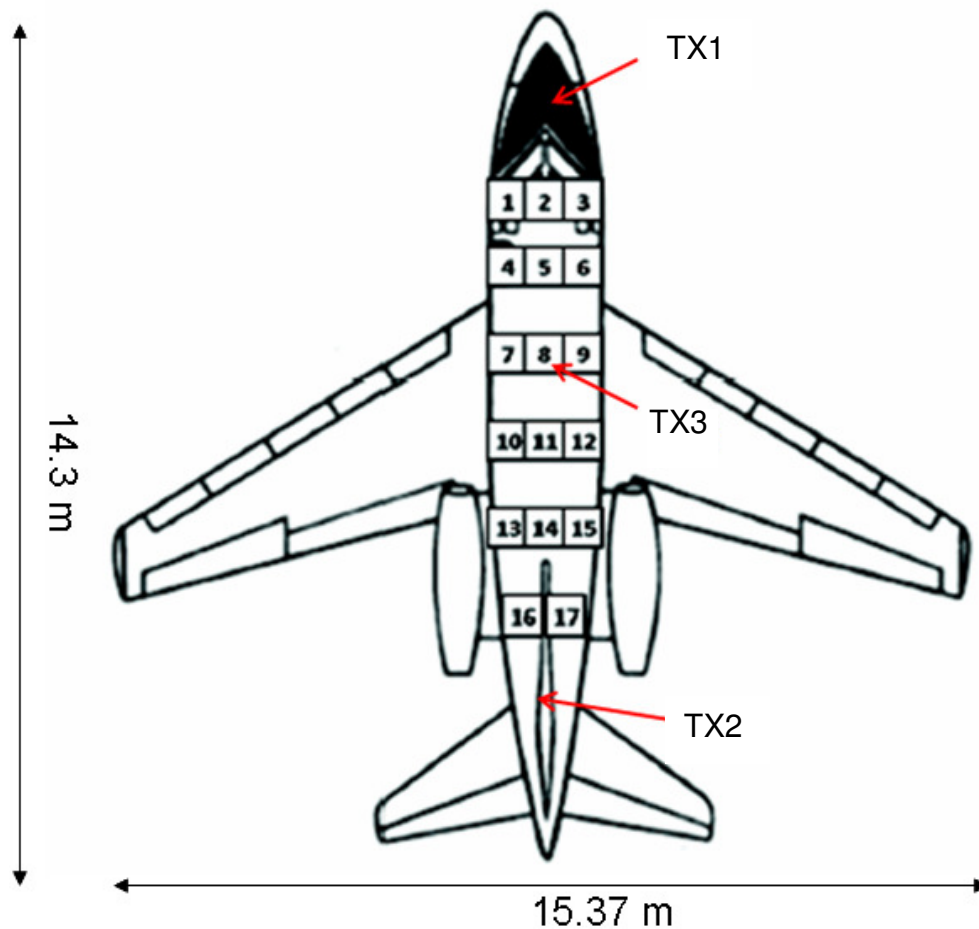


Figure 7.1: Transmitter and receiver locations for multiantenna measurements on Rockwell T-39 Sabreliner (height 2 m).

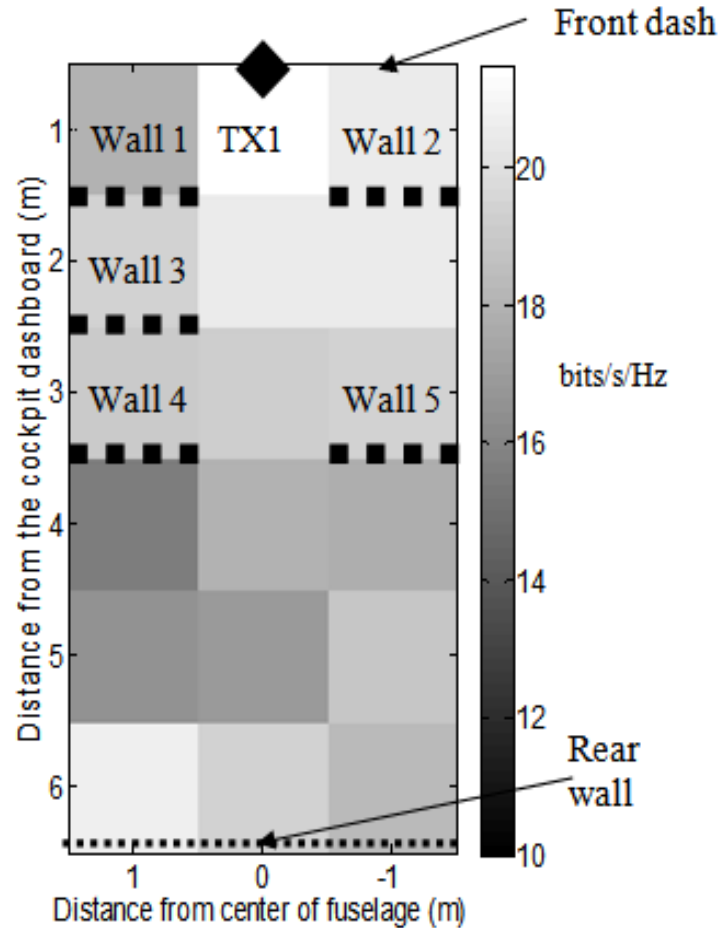


Figure 7.2: Mapped capacity for TX1 on Rockwell T-39 Sabreliner.

7.3.2 Beech Baron 58P

The transmit and receive locations for the Beech Baron 58P are shown in Figure 7.3, with the resulting capacity map for TX1 in Figure 7.4 and TX2 in Figure 7.5. TX1 in the front luggage compartment had an average capacity of 18.36 bits/s/Hz, which was lower than TX2 on the front dash, at 19.12 bits/s/Hz. TX1 had a trend of decreasing capacity as you move away from the transmitter with a hot spot along the back wall as seen at the bottom right of Figure 7.4.

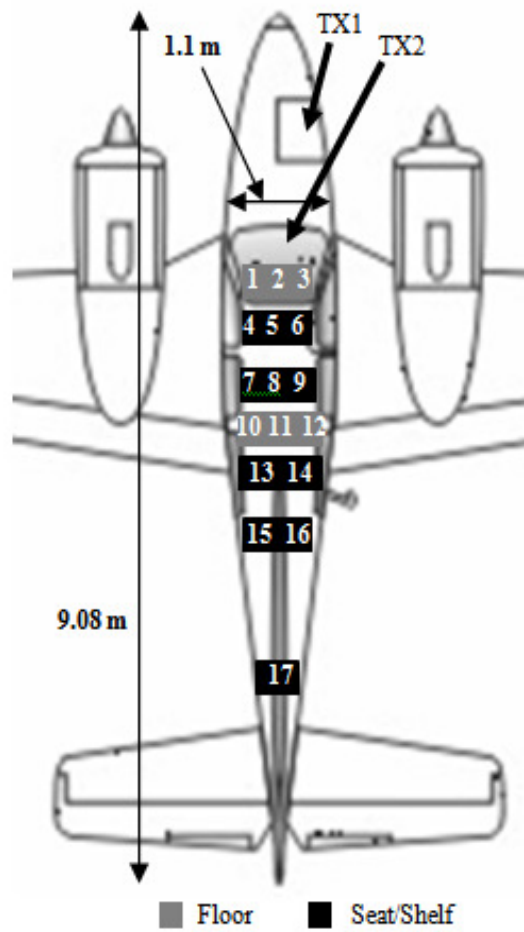


Figure 7.3: Diagram of measurement locations and dimensions for Beech Baron 58P aircraft (height 1.3 m). TX1 was in the front luggage compartment and TX2 was on the dash.

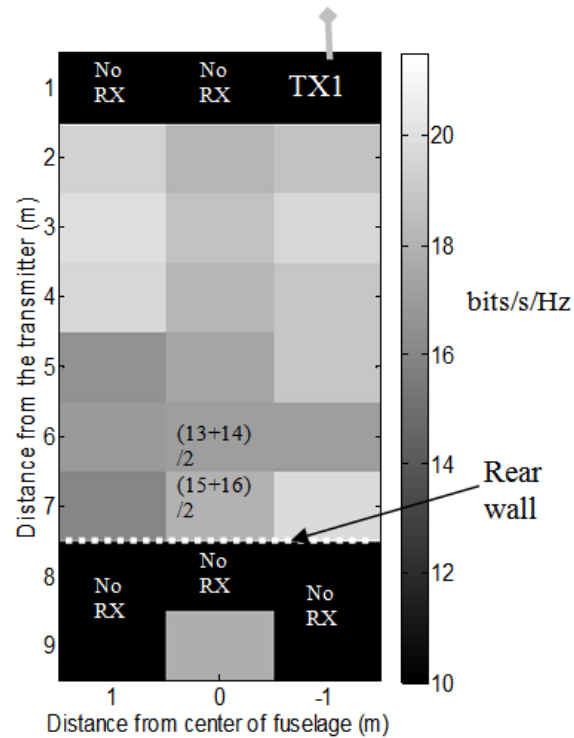


Figure 7.4: Mapped capacity for TX1 on Beech Baron 58P. The center point was averaged from two side measurements on the last two rows as the plane narrowed.

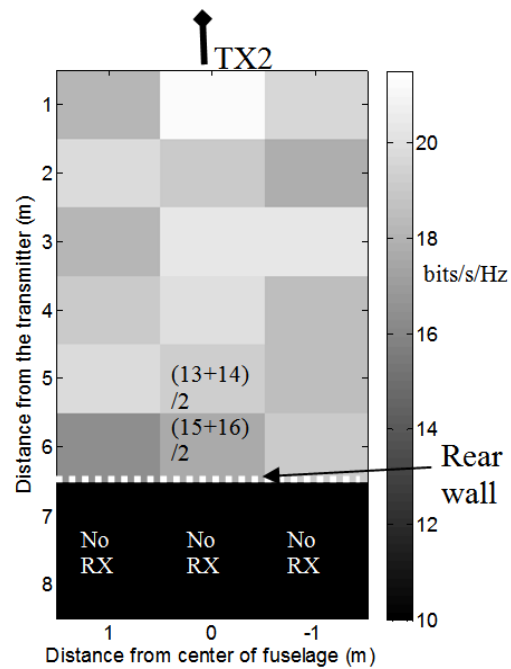


Figure 7.5: Mapped capacity for TX2 on Beech Baron 58P. The center point was averaged from two side measurements on the last two rows as the plane narrowed.

7.3.3 2004 Thomas Bus 110YN

Transmit and receive locations for TX1 in the 2004 Thomas Bus 110YN are shown in Figure 7.6, with the resulting capacity map in Figure 7.7. TX1 on the rear engine box had an average capacity of 19.31 bits/s/Hz, which was higher than the average capacity for TX2 in the driver's seat, at 18.62 bits/s/Hz. TX1 had a trend of decreasing capacity as you move away from the transmitter with a few low capacity spots near walls or arm supports as seen in Figure 7.7.

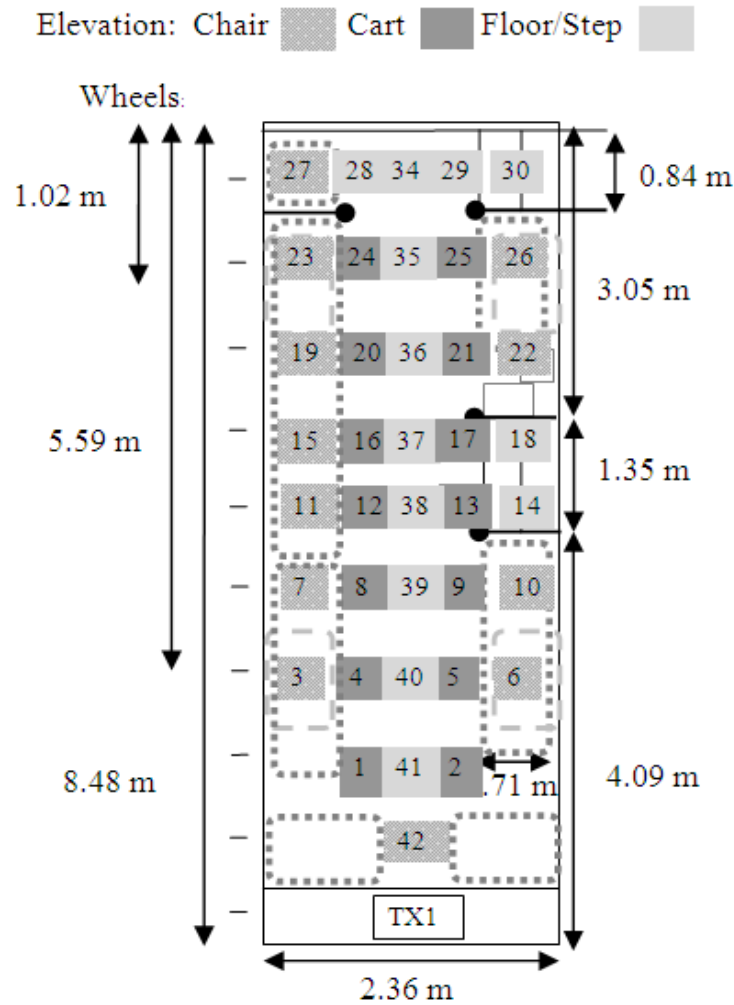


Figure 7.6: Diagram of measurement locations and dimensions for TX1 on 2004 Thomas Bus 110YN (height 1.63 m).

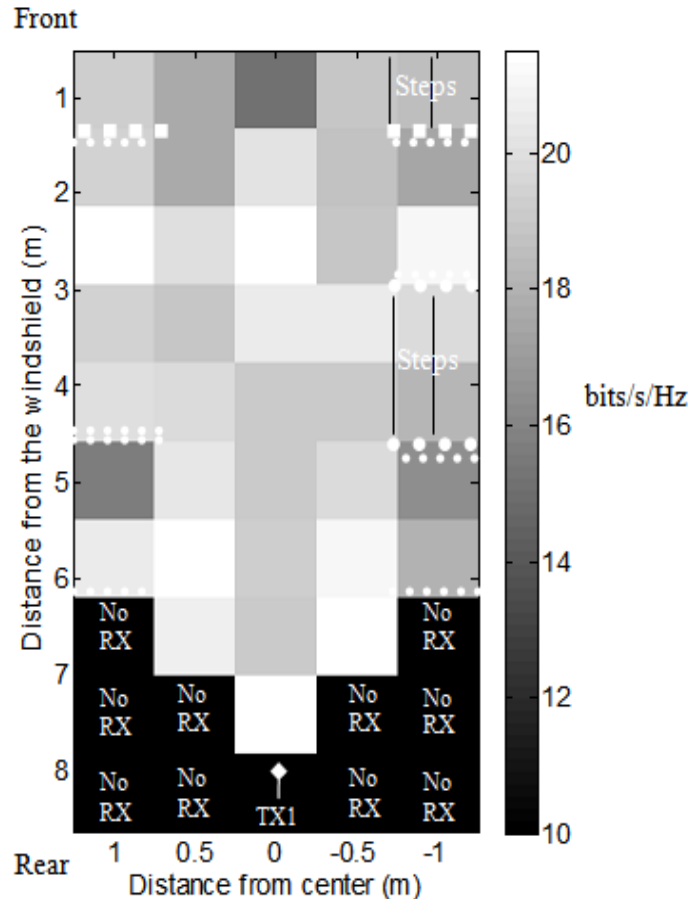


Figure 7.7: Mapped capacity for TX1 on 2004 Thomas Bus 110YN. (Floor to ceiling metal dividers marked by square dotted line, floor to middle metal dividers marked by large circle dotted line and arm rests with metal support bars marked by small circle dotted line, locations with no recorded capacity marked by “No RX”).

7.3.4 Bell OH58 Helicopter

Transmit and receive locations for TX1 in the Bell helicopter are shown in Figure 7.8a). TX1 had a trend of decreasing capacity as you move away from the transmitter with a hot spot in the rear maintenance bay as seen in the resulting capacity map in Figure 7.8b). TX1 on the control dash had an average capacity of 20.23 bits/s/Hz, which was higher than TX2 in the rear maintenance bay, at 18.06 bits/s/Hz. This verified that walls in proximity to the transmitter, such as in the maintenance bay, had a significant

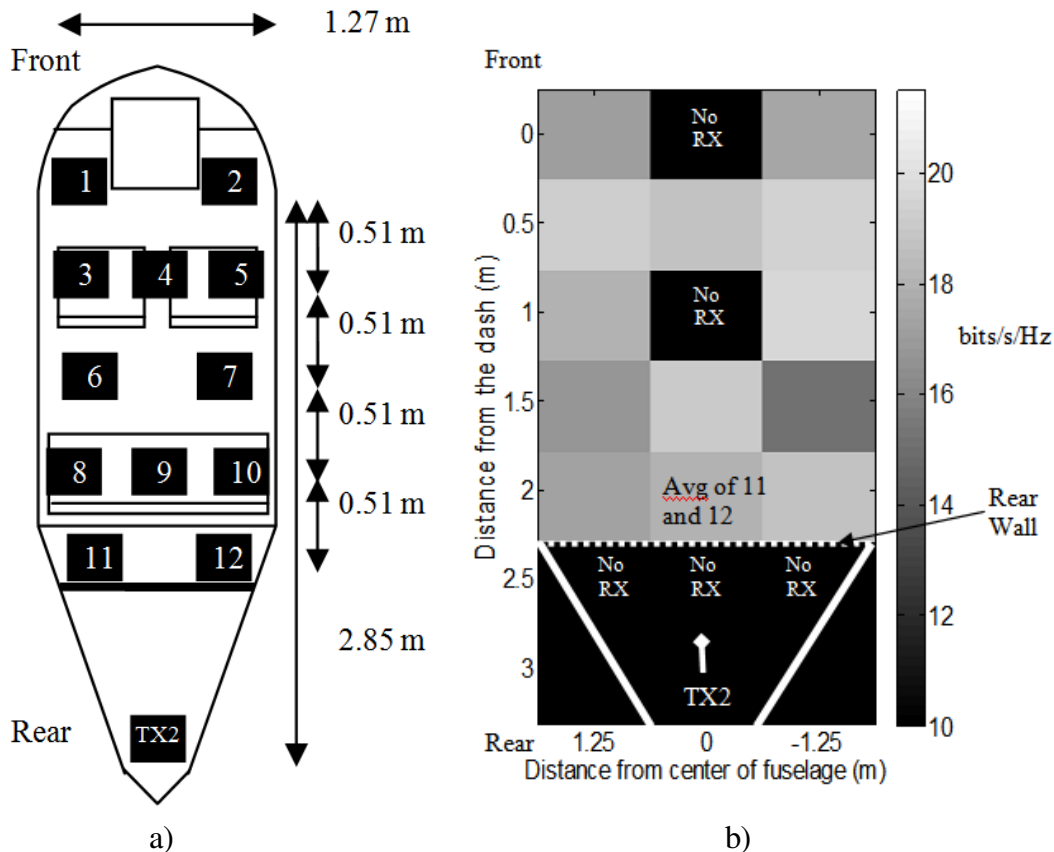


Figure 7.9: TX2 on Bell helicopter. a) Diagram of measurement locations and dimensions for TX2. b) Mapped capacity for TX2.

7.3.5 Underground Cement Tunnel

Tunnels are seen as a similar environment as aircraft fuselage (long narrow, minimal windows), and there is also a great interest for implementing wireless communication systems in them [221], so they are included in this survey of enclosed environments. An underground cement tunnel with permittivity (ϵ_r) of 8.1 F/m and conductivity of 0.0352 S/m was measured. Rather than using several receiver locations for each transmitter location as in other measurements, we used the opposite since the channel would be the same if transmitter and receiver were swapped. Eight transmitter locations were chosen spanning the tunnel, with dimensions 2.64 m x 5.51m x 20m, and

the receiver was placed at the entrance of the tunnel. Transmit and receive locations in the cement tunnel are shown in Figure 7.10, with the resulting capacity received for each transmitter mapped in Figure 7.11. The cement Tunnel had an average capacity of 15.93 bits/s/Hz, which was the lowest of all the channels measured. There was a significant trend of decreasing capacity as the transmitter to receiver distance increased, with an extreme drop in capacity of around 4 bits/s/Hz when measurements started down the hallway past the open ramp area, as seen in Figure 7.11.

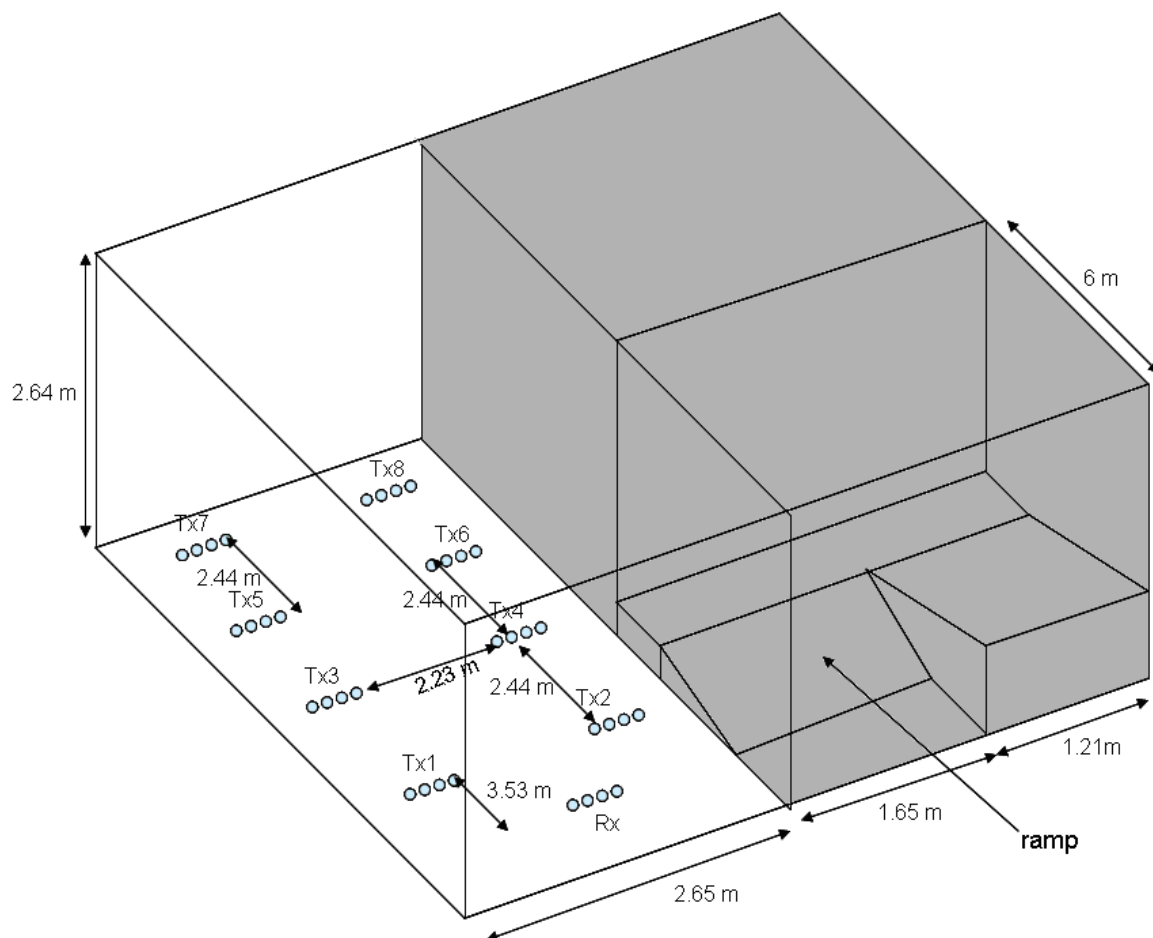


Figure 7.10: Diagram of measurement locations and dimensions (2.64m X 5.51m X 20m) in MEB Tunnel.

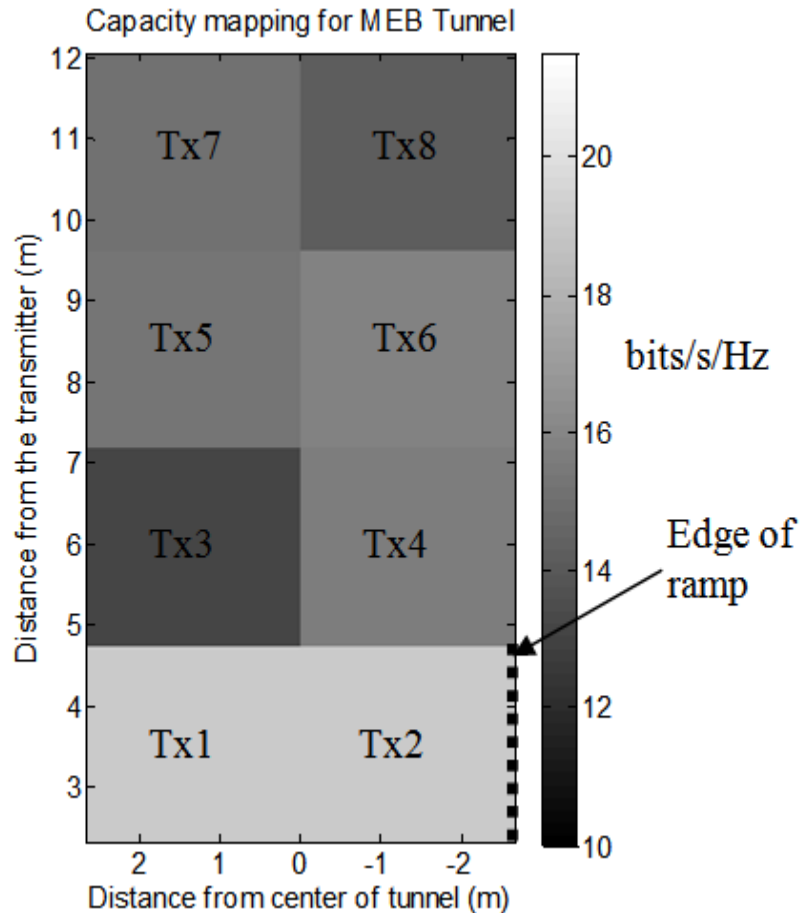


Figure 7.11: Mapped received capacity for Concrete Tunnel.

7.3.6 Basement Concrete Tunnel

A long basement tunnel made of concrete with permittivity (ϵ_r) of 5.1 F/m and conductivity of 0.000152 S/m was measured. Again, multiple transmitter locations were used with a single receiver location. Four transmitter locations were chosen along length of the tunnel with dimensions 4.572m X 3.66m X 50m, and the receiver was placed at the entrance of the tunnel. Transmit and receive locations in the Park Tunnel are shown in Figure 7.12, with the resulting capacity received for each transmitter mapped in Figure 7.13. The concrete tunnel had an average capacity of 18.1 bits/s/Hz. There was a much

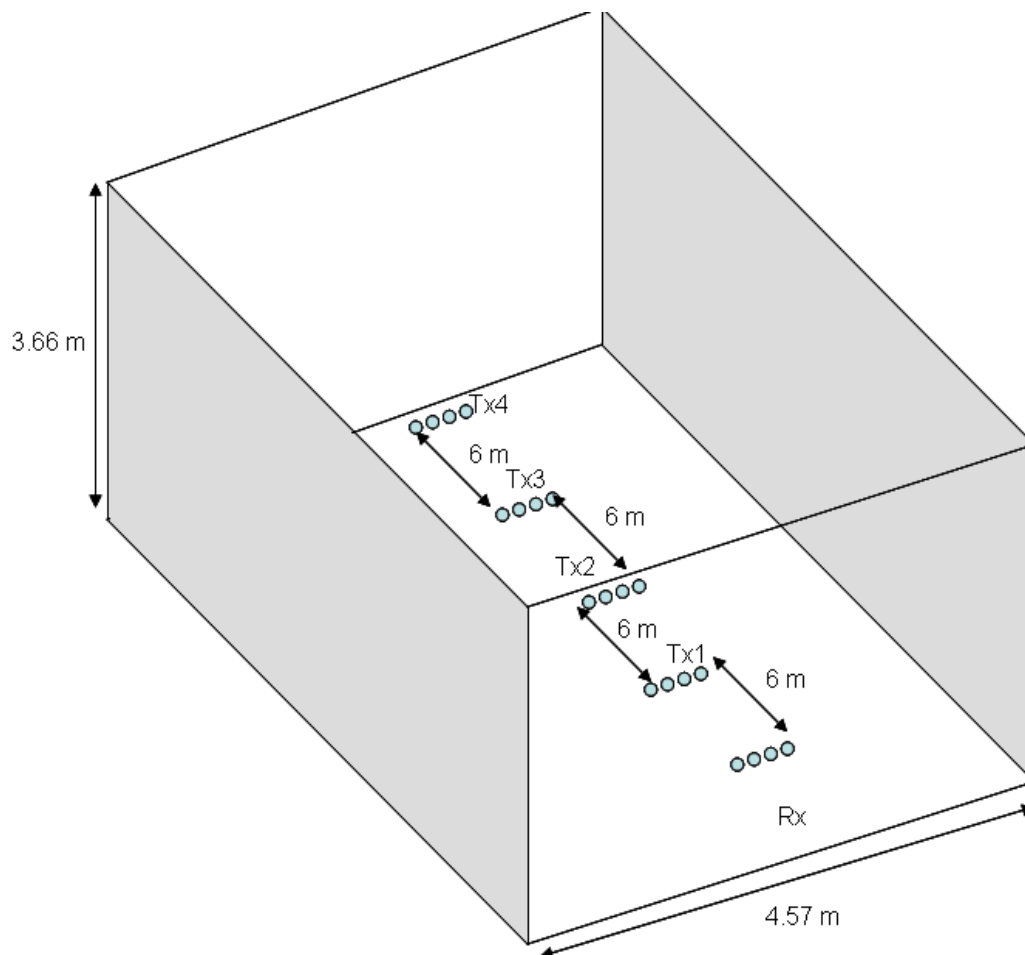


Figure 7.12: Diagram of measurement locations and dimensions (4.572m X 3.66m X 50m) in concrete tunnel.

smaller variation in capacity, from 17.2 to 18.6 bits/s/Hz, which is either due to the decreased number of measurements taken when compared with other channels, or a less multipath rich channel. We will assume the latter due to the low multipath seen when simulating empty fuselages. There was also only a minimal drop in the capacity of approximately 1.4 bits/s/Hz over the range of transmit to receive distances, as seen in Figure 7.13, which is a comparable drop in capacity but over a much greater distance than measurements taken in other channels.

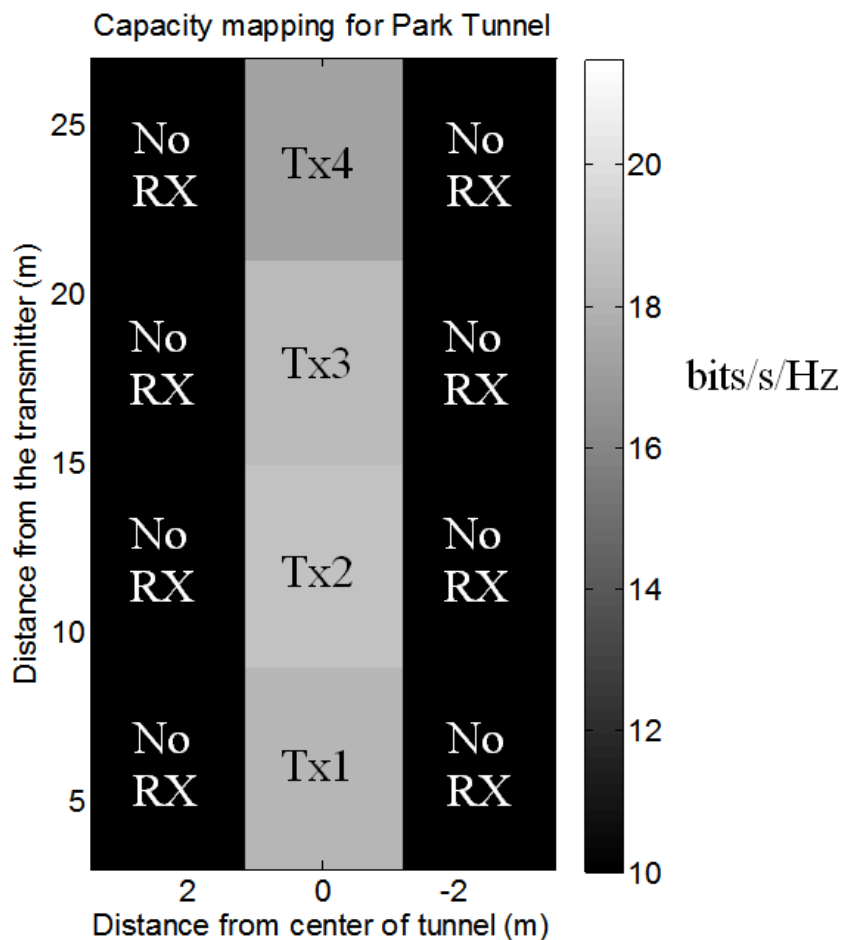


Figure 7.13: Mapped capacity for concrete tunnel.

For the complex channels measured, we compared average capacity and size of the enclosed channel, but found no direct relationship between them. We can see that the capacity is in the range of 18-20 bits/s/Hz for all vehicles over a range of sizes (TX2 in the helicopter had the same average capacity as the large concrete tunnel, of 18.1 bits/s/Hz). The only exception was the cement tunnel with the ramp with an average capacity of 15.9 bits/s/Hz, as much of the signal appears to have stayed in the open area of the ramp and did not travel down the hallway.

We also considered the effect of windows. The bus has the largest portion of its body consisting of windows, helicopter and aircraft have a moderate number of windows, and the tunnels have no windows. We expect the total capacity to drop as the number of windows increases, allowing some of the communication signal to escape the enclosed vehicle or tunnel. To further evaluate the impact of windows on total average capacity, we simulated the Sabreliner with varying percentages (10, 30, 50, and 70%) of external walls made of glass to represent windows. Over the range from 10-70% windows, we saw a decrease of less than 0.8 bits/s/Hz. This suggests that windows do give a slight decrease in overall capacity. For most vehicles, which are less than 50% windows, this decrease is relatively small (less than 1 bits/s/Hz). Though a loss of 0.8 bits/s/Hz would not seem to be a large impact when compared to an average capacity of 18 to 20 bits/s/Hz, it can have a huge impact on accuracy and windows are thus important to include in simulation [236].

Based on observations of a general trend of decreasing capacity with increasing measurement distance, we evaluated both the maximum distance measured as well as average distance measured, as listed in Table 7.1.

The importance of site specific modeling is found most prevalently when evaluating the capacity as a function of distance from the transmitter. In an open environment, we would expect the capacity to decrease further from the transmitter. This effect is seen for most of the points in Figure 7.2, Figure 7.4 , Figure 7.5, Figure 7.7, Figure 7.9, Figure 7.11, and Figure 7.13. However, two significant differences are seen. One is when the measuring point is near the end of the aircraft, with or without walls in front of it as seen for location $(x=-1,y=7)$ in Figure 7.4, for example.

Table 7.1: Average measured capacity for complex channels in relation to transmitter location and distance.

	Avg Capacity (bits/s/Hz)	TX Location	Behind Wall(s)	Avg Meas Distance (m)	Max Meas Distance (m)
Park Tun	18.10	end of tunnel	no	15.00	24
MEB Tun	15.93	end of tunnel	no	7.19	10.9
Sab (TX3)	20.36	center	partial	1.63	2.9
Sab (TX1)	18.88	cockpit	partial	3.11	5.8
Sab (TX2)	18.85	maint bay	yes	4.97	8.2
Baron (TX2)	19.12	dash	no	1.60	4.4
Baron (TX1)	18.36	forward luggage	yes	2.75	5.4
Heli (TX1)	20.23	dash	no	1.16	2.9
Heli (TX2)	18.06	maint bay	yes	1.83	2.9
Bus (TX1)	19.31	rear engine box	no	4.98	8
Bus (TX2)	18.62	drivers seat	partial	4.29	8

Another significant difference is when the receiver is behind a metal wall or otherwise shadowed from the transmitter, such as location (x=1,y=4) in Figure 7.2. This could significantly affect transmitters located in the narrow wings of aircraft or other extended compartments of complex channels, generally requiring the addition of a transmitter in these areas.

7.4 Complex Channel Modeling

Wireless channels have traditionally been modeled using statistical models to represent the average capacity over the channel. This is very effective for mobile deployments where the radios will move randomly covering the entire channel. For fixed location wireless (which is desired for sensor applications), it is important to know what range of error to expect from these statistical models in specific locations in the channel.

As we have seen from the channel measurements in Section 7.3, capacity can vary greatly from location to location. This section compares the site-specific 3D ray tracing model with site-averaged statistical models that have been used for wireless applications, including Gaussian [229], hyper-Rayleigh [230], Weibull [231], and Nakagami [232]. We will evaluate which statistical models work best in these channels and when it would be better to use the site-specific.

The Gaussian model is one of the simplest channel models. It is based on a plane of impinging waves with Gaussian-distributed magnitudes and uniformly distributed angles of arrival (AOAs) and phases. This model is limited because it is based on measured K values. The hyper-Rayleigh model has a received signal dominated by two constant amplitude signal components with uniformly distributed angles of arrival over $[0, 2\pi)$, and is also referred to as two-wave with diffuse power (TWDP), as detailed in [230]. The Weibull distribution has been widely used for modeling the fading envelope in wireless communication because it was created to model the lifetime of some object that fails based on its weakest link. Single antenna measurements performed in [231] show that the Weibull model can accurately estimate the path loss in an aircraft channel at 5 GHz. The Weibull model describes the path loss as an exponential decay with uniformly distributed phases. The Weibull model reduces to the Rayleigh model when $\alpha_k = 2$. For this paper, $\alpha_k = 1.5$ is used for the fading parameter and average fading power is $\Omega_k = 1$ based on optimization simulations performed in 0. The Nakagami-m distribution provides more flexibility and is a better match to most fading channels, as shown in [232], because it offers one more parameter than the Gaussian and Weibull models. The Nakagami-m model simplifies to the Rayleigh and uniform distribution on the unit circle

for the special cases of $m=1$ and $m=\infty$, respectively. The path loss is again modeled as an exponential decay with uniformly distributed phases. The Nakagami model was simulated with $m=1.4$ also based on optimization simulations performed in 0.

These statistical models were run to compare against the 3D ray tracing simulation for the following channels: Beech Baron 58P [241], a Rockwell T-39 Sabreliner [240][235], 2004 Thomas Bus 110YN [236], and Bell OH58 Helicopter [237]. Details about how these channels were modeled with the 3D ray tracer can be found in their references.

As we can see from Table 7.2, the 3D ray tracing method had the most accurate average capacity with the smallest error and also resulted in the smallest error for more site-specific locations than the statistical models. The ray tracing model was followed by Nakagami 1.4, then Gaussian and hyper-Rayleigh, with Weibull performing the worst. It is recommended to use the 3D ray tracing for optimum accuracy within 1.1 bits/s/Hz or less for all complex channels evaluated, but this comes at the cost of increased complexity in modeling. If the increased complexity is not desirable, Nakagami 1.4 is recommended, and was still able to achieve accuracy within 2.1 bits/s/Hz for all channels evaluated. Other analysis was performed for the statistical models to evaluate their usefulness. It was found that for each complex channel, hyper-Rayleigh almost consistently underestimates when run for site-specific locations, resulting in an average estimation 1-3 bits/s/Hz below measured capacity that could be used as a lower bound of achievable capacity. The other statistical modeling techniques overestimate average capacity by 1-3 bits/s/Hz and could therefore be used as an upper bound of achievable capacity.

Table 7.2: Average error, maximum error and percent of locations error was best (minimum) for complex channels simulated with various modeling techniques.

	Error	3D	Gaussian	HR	Weibull	Nak 1.4
Sab (TX1)	<i>avg</i>	0.41	0.72	1.98	0.86	0.59
	<i>max</i>	1.21	2.67	2.74	2.61	2.45
	<i>% best</i>	41.18%	23.53%	0.00%	0.00%	29.41%
Sab (TX2)	<i>avg</i>	0.58	0.79	3.47	0.75	0.78
	<i>max</i>	1.53	2.67	4.60	1.82	1.71
	<i>% best</i>	45.45%	9.09%	0.00%	27.27%	0.00%
Sab (TX3)	<i>avg</i>	0.29	0.75	1.34	1.28	0.95
	<i>max</i>	1.02	1.67	3.47	2.48	1.81
	<i>% best</i>	55.56%	11.11%	11.11%	11.11%	11.11%
Baron (TX1)	<i>avg</i>	0.26	1.09	2.39	1.35	0.64
	<i>max</i>	0.99	2.81	3.36	4.15	1.86
	<i>% best</i>	70.59%	0.00%	0.00%	17.65%	5.88%
Baron (TX2)	<i>avg</i>	0.69	0.85	2.33	1.42	1.15
	<i>max</i>	1.41	2.60	3.16	3.15	3.67
	<i>% best</i>	18.75%	18.75%	0.00%	12.50%	18.75%
Heli (TX1)	<i>avg</i>	1.06	1.30	1.52	1.35	1.17
	<i>max</i>	4.43	2.41	3.69	2.63	1.93
	<i>% best</i>	30.77%	7.69%	30.77%	7.69%	7.69%
Heli (TX2)	<i>avg</i>	0.95	2.49	1.23	3.06	2.09
	<i>max</i>	1.79	5.53	4.19	6.21	5.56
	<i>% best</i>	33.33%	0.00%	33.33%	0.00%	33.33%
Bus (TX1)	<i>avg</i>	1.04	1.79	1.27	2.21	1.47
	<i>max</i>	4.51	6.01	4.44	6.45	5.11
	<i>% best</i>	50%	0%	36%	5%	10%
Bus (TX2)	<i>avg</i>	0.41	1.07	0.89	1.78	0.85
	<i>max</i>	0.94	2.91	2.56	3.74	2.16
	<i>% best</i>	50.00%	5.00%	27.50%	5.00%	12.50%

7.5 Conclusion

The extensive measurements that have been performed show a common trend of decreasing capacity with increasing measurement distance, with exceptions near reflective objects that increase multipath. Measurement of every channel to find these exceptions is often difficult, costly, time consuming or just impossible. Due to these special circumstances for site-specific locations within complex channels, it is recommended that 3D ray tracing be used for modeling as it is more accurate than commonly used statistical models and able to achieve accuracy within 1.1 bits/s/Hz for all channels studied without being based on measurement. This variety of complex channel simulation showed that our 3D ray tracing is adaptable to various environments and gives a more accurate depiction than statistical models that average channel variations

The design requirements for modeling different complex channels include a detailed depiction of the channel geometry, including height, width, length, basic shape (square, cylindrical, slanted walls, etc.), large windows, and reflective objects inside the channel space, especially if they are near the transmitter. Additionally, since more detail was required with the smaller vehicles evaluated and because of electrical size in relation to frequency, we expect that more detail will also be required for lower frequencies.

3D ray tracing is the most accurate model for estimating average channel capacity and is capable of site-specific modeling for statically deployed wireless systems. This modeling comes at the cost of greater complexity in developing the 3D model. If the increased complexity of the site-specific model is not desirable, Nakagami 1.4 is the next

most accurate model, and hyper-Rayleigh could be used as a lower bound on achievable capacity.

Future work should include measurement on large aircraft and small cars to further evaluate how the size of a vehicle affects the level of detail required for accuracy at different frequencies. The small car would require a higher frequency test bed in order to maintain the far-field assumptions.

7.6 Acknowledgment

Much thanks to Randy Chesley, Utah State University, Logan Municipal Airport, and University of Utah Transportation Services for allowing us to come and measure their vehicles, as well as my measurement team, James Nagel and Sai Ananthanarayanan. This work was supported by the US Air Force Research Laboratories (AFRL) through a grant from Universal Technologies Corporation and the National Science Foundation under grant ECCS-0823927.

7.7 References

- [216] G.J. Foschini and M.J. Gans, "On limits of wireless communications in a fading environment when using multiple antennas," *Wireless Personal Communications*, Vol. 6, Page(s): 311-355, Mar 1998.
- [217] M.A. Jensen and J.Wallace, "A review of antennas and propagation for MIMO wireless communications," *IEEE Transactions on Antennas and Propagation*, Vol. 52, Page(s): 2810-2824, Nov 2004.
- [218] D. Landon and C. Furse, "The MIMO transmission equation," (Honorable Mention, student paper contest) *IEEE Antennas and Propagation Symposium (APS)*, San Diego, CA, July 7-11, 2008.
- [219] A. Magleby and C. Furse, "Predicted MIMO performance in intravehicle channels," *IEEE Antennas and Propagation Society International Symposium*, San Diego, CA, Page(s) 1-4, 2008.

- [220] S. Y. Lim, Z. Yun, J. M. Baker, N. Celik, H.-S. Youn, and M. F. Iskander “Radio propagation in stairwell: measurement and simulation results,” *IEEE Antennas and Propagation Society International Symposium*, Charleston, SC, 2009.
- [221] D. G. Dudley, M. Lienard, S. F. Mahmoud, and P. Degauque, “Wireless propagation in tunnels,” *IEEE Antennas and Propagation Magazine*, Vol. 49, Issue: 2, Page(s):11, April 2007.
- [222] M. Youssef, L. Vahala, and J. H. Beggs. “Electromagnetic propagation of wireless networks in aircraft cabins,” *IEEE/ACES International Conference on Wireless Communications and Applied Computational Electromagnetics*, Page(s): 832 – 836, 2005.
- [223] Fitzhugh, J. Frolik, J. Covell, R. Ketcham, and T. Meyer, “2.4 GHz multipath environments in airframes,” *Proceedings of the 2005 Wireless and Microwave Technology Conference (WAMICON 2005)*, 2005.
- [224] J. Koivunen, P. Almers, V.-M. Kolmonen, J. Salmi, A. Richter, F. Tufvesson, P. Suvikunnas, A. Molisch, and P. Vainikainen, “Dynamic multi-link indoor MIMO measurements at 5.3 GHz,” *Proceedings of the 2nd European Conference on Antennas and Propagation (EuCAP 2007)*, Edinburgh, 2007.
- [225] V. R. Anreddy and M. A. Ingram, “Capacity of measured Ricean and Rayleigh indoor MIMO channels at 2.4 GHz with polarization and spatial diversity,” *IEEE Wireless Communications Networking Conference 2006*, Vol. 2, Page(s): 946-951, 2006.
- [226] Z. Yun, Software package called “3D ray tracing for radio propagation modeling,” last updated Dec. 2009, unpublished.
- [227] C. Takahashi, Z. Yun, M. F. Iskander, et al., “Propagation-prediction and site-planning software for wireless communication systems,” *IEEE Antennas and Propagation Magazine*, Vol. 49, No. 2, April 2007.
- [228] Alyssa Magleby, Cynthia Furse, and Z. Q. Yun, “3D Ray tracing for intravehicle MIMO,” *IEEE/URSI Antennas and Propagation Symposium*, Charleston, SC, June 1-5, 2009.
- [229] I. Telatar et al., “Capacity of multiantenna Gaussian channels,” *European Transactions on Telecommunications*, Vol. 10, No. 6, Page(s): 585–596, 1999.
- [230] J. Frolik, “A case for considering hyper-Rayleigh fading channels,” *IEEE Transactions on Wireless Communications*, Vol. 6, No. 4, Page(s): 1235–1239, 2007.
- [231] M. Lupupa and M.E. Dlodlo, “Performance of MIMO system in Weibull fading channel-channel capacity analysis,” *IEEE EUROCON*, Page(s): 1735-1740, July 2009.

- [232] G. Fraidenraich, O. Leveque, and J. Cioffi, "On the MIMO channel capacity for the Nakagami-m channel," *IEEE Transactions on Information Theory*, Vol. 54, No. 8, Page(s): 3752–3757, 2008.
- [233] D. Palchak and B. Farhang-Boroujeny, "A software defined radio test bed for MIMO systems," *Proceedings of the SDR 06 Technical Conference and Product Exposition*, Orlando, FL, November 2006.
- [234] James R. Nagel, Sai Ananthanarayanan, Alyssa Magleby Richards, and Cynthia Furse, "Measured multiuser MIMO capacity in aircraft," accepted for publication in *IEEE Antenna and Propagation Magazine*.
- [235] Alyssa Magleby Richards, Sai Ananthanarayanan, and Cynthia Furse, "3D simulation of the wireless channel in small aircraft," submitted to *IEEE Transactions on Vehicular Technology*.
- [236] Alyssa Magleby Richards, Sai Ananthanarayanan, and Cynthia Furse, "Wireless channel measurements and modeling in a helicopter," submitted to *Microwave and Optical Technology Letters*.
- [237] Alyssa Magleby Richards, Sai Ananthanarayanan, and Cynthia Furse, "Complex measurement and simulation of the multiantenna communication channel on a shuttle bus," in preparation for *IEEE Transactions on Vehicular Technology*.
- [238] Sai Ananthanarayanan, Alyssa Magleby Richards, and Cynthia Furse. "Measurement and modeling of multiantenna systems in small aircraft," submitted to *Journal of Aerospace Computing, Information, and Communication*, June 2010.
- [239] Sai Ananthanarayanan, Alyssa Magleby, and Cynthia Furse, "Measurement and modeling of interference for multiple antenna system," *Microwave and Optical Technology Letters*, Volume 52, Issue 9, pages 2031–2037, September 2010.
- [240] [Online] Available:
http://en.wikipedia.org/wiki/File:T-39_SABRELINER_3siteview_NAVY.png
- [241] [Online] Available:
<http://www.pilotfriend.com/aircraft%20performance/Beech/Baron.htm#r>,
[Accessed: January 13 2009]
- [242] Z. Yun, Z. Zhang, and M. F. Iskander, "A ray tracing method based on the triangular grid approach and application to propagation prediction in urban environments," *Proceedings of the IEEE International Symposium on Information Theory (ISIT2004)*, Vol. 50, Page(s): 750–758, May 2002.

CHAPTER 8

CONCLUSION AND FUTURE WORK

8.1 Contributions

The purpose of this research was to quantify complex channels in aircraft and vehicular environments, evaluate their relationship to other environments (indoor, outdoor, etc. that have already been extensively characterized and for which wireless systems are already prevalent), evaluate MIMO in aircraft, provide design constraints for how to accurately model these complex channels, and provide information to assist in predicting antenna type and location are best to enable communication in aircraft/cars/buses/ships/trains/etc. and other extreme channels. The results of these contributions are described in more detail in the following sections.

8.1.1 3D Ray Tracing Model

In order to quantify the complex channels in vehicles, a 3D ray tracing model was used to simulate their site-specific characteristics. This is described in Chapter 3 of this dissertation, was presented at [243] and [244], and has been submitted for publication in [245]. Angle of arrival and departure information from 3D ray tracing were combined with antenna gain patterns modeled in CST®, then this and other outputs of the 3D simulation were combined with multiantenna effects (polarization loss, mismatch,

radiation efficiency, etc.) using a detailed signal model described in [246]. This site-specific modeling technique provides capacity mapping information that can be used to determine hot spots and dead spots to fully characterize the channel and to optimize the location of antenna arrays for wireless communication in these channels. This model provides an accurate estimate of complex channel capacity (for example, an average error within 0.58 bits/sec/Hz in the Sabreliner channel [245]). This is, to our knowledge, the first full site-specific characterization of the inside of small/medium sized aircraft, and the first time a model has been available to accurately predict the channel in these environments prior to building the aircraft or other vehicle. Details of the 3D simulation and how specific parts of the model affected the accuracy is given below. Not surprisingly, fully modeling the shape and size of the fuselage, windows, and walls is very important. Seats were less important, except in the bus where they had a significant contribution.

8.1.2 Quantification of Vehicular Channels

Three vehicular channels (small/medium aircraft, helicopter, and bus) were characterized using the site-specific 3D ray tracing software, non-site specific statistical models, and multiantenna measurement at 915 MHz. Each environment was also evaluated to determine what level of detail is required in the 3D modeling to obtain accuracy in simulation.

The small/medium aircraft channel (Diamond DA42 Twin Star-composite body [245], Beech Baron 58P-metallic body [249], and Rockwell T-39 Sabreliner-metallic body [245]) was found to be rich in multipath with capacity ranging from 15.4 to 20.2

bits/s/Hz for the Twin Star, 16.1 to 21.1 bits/s/Hz for the Beech Baron, and 15.6 to 21.8 bits/s/Hz for the Sabreliner, depending on location. Seats did not appear to have a significant effect on the channel, but partial walls between different segments of the cabin increased multipath. Key factors in configuring the aircraft model included a tradeoff between using 60 or more facets (increasing facets improves the smoothness of fit to the actual fuselage shape) for a simplified fuselage containing only lossy obstacles or 12 facets with a more detailed configuration including lossy and some reflective obstacles for accuracy within 0.8 to 1 bit/s/Hz. Average error was reduced to 0.4 bits/s/Hz as internal configuration complexity increased to include all the walls within the fuselage. Thus, including major site-specific reflective obstacles (especially those in close range to the transmitting antenna), with the maximum allowed reflections set to 10 or more, and using PEC parameters for the walls (regardless of if the aircraft is metallic or composite body) will give an excellent channel model for these aircraft.

The bus channel was also found to be rich in multipath with a slightly wider range in capacity from 15 to 22.6 bits/s/Hz depending on the location [247]. Accurately modeling a bus environment requires including windows. Windows are a source of loss in the actual channel, and not modeling them properly can cause the model to overestimate capacity by an average of 1-2 bits/s/Hz. Including windows reduced error by 0.74 up to 1.36 bits/s/Hz, depending on the internal configuration used. We can assume similar results would be seen in other vehicular environments such as helicopters and automobiles when the windows make up a significant portion of the external surface. Internal obstacles also have a notable effect in the bus as they did in the aircraft. Adding reflective walls, the rear engine box and wheel wells improved accuracy by up to 1.2

bits/s/Hz when compared with the empty bus cavity. As with the aircraft channel, the number and angle of facets used to accurately represent the shape of the bus had a significant impact on the accuracy of the simulation. Average error decreased by 0.5 to 1 bits/s/Hz when going from the simple rectangular configuration to the more bus-shaped configuration, which has slanted side walls and curved top corner facets. Unlike aircraft, where the seats did not have a major impact on the channel, our capacity mapping suggests they may indeed be affecting the bus channel. Both seats have a metal frame, but the frame of the bus seats are more exposed and the seats are made of mostly of thick, hard plastic which is more reflective than the soft fabric and cushioning in aircraft seats.

The helicopter channel was found to have the widest range of site-specific capacities of the vehicles we measured, from 15 to 23 bits/s/Hz [248]. The variety of configurations we simulated showed that as vehicle size or transmission frequency decreases, increased configuration detail is required to maintain accuracy. This is because the space within the vehicle becomes electrically smaller in relation to the wavelength of the signals, and small variations in reflective surfaces have a greater impact. The 3D ray tracing model was able to achieve an average error within 1.05 bits/s/Hz for a detailed configuration that included the front windshield and nose of the helicopter as well as facets for the curved sides and an angled tailpiece.

Overall, these vehicular channels have a rich multipath environment with a wide range of Ricean K values, from -150 to 8 dB. This is mostly in the negative range, below -3 dB, which is characteristic of Rayleigh fading or worse [257]. This is an extremely diverse environment, especially when compared to the -5 to 35 dB range characteristic of the Ricean channel commonly found in indoor/outdoor environments [257][258][259].

Multiantenna systems take advantage of the extreme multipath found in these vehicular channels, but would need to be combined with adaptive coding schemes to adjust to the varying capacity, especially as this variation could potentially increase with the addition of passengers as seen in [252]. This type of site-specific analysis is most beneficial for static deployments of wireless systems such as wireless data collection from sensor networks. This ray tracing modeling can be used in the design of wireless communication systems inside complex channels, such as buses, to accurately estimate location specific capacity and is especially useful for simulating environments that are expensive or difficult to measure, or have not yet been built.

8.1.3 Comparison to Statistical Models

Prior to this work, vehicular channels were mainly described by statistical models, without a real understanding of the expected accuracy of these channels. Statistical channel models provide estimates for the average capacity in a channel, which is probably best suited for mobile deployments where the radios will move randomly throughout the entire channel. For fixed location wireless (which is desired for sensor applications), it is important to know what range of error to expect from these statistical models in specific locations in the channel. A comparison of the site-specific 3D modeling to various common statistical models provided these details. The Gaussian [253], hyper-Rayleigh [254], Weibull [255], and Nakagami [256] statistical models were evaluated for each of the vehicular channels. These were compared to site-specific measurements and the detailed 3D ray tracing simulation. The 3D ray tracing model had the lowest average error and the lowest site specific error for the highest percentage of

receive locations for 9 transmit locations for the complex channels analyzed (aircraft, bus, helicopter and tunnel compared in Chapter 7 [249]). It also had the lowest maximum error for 7 of the transmit locations. This was followed in accuracy by the Nakagami 1.4, with the Gaussian and hyper-Rayleigh coming in third. The hyper-Rayleigh performed best in open areas that were less rich in multipath with fewer internal walls (such as the helicopter), which is understandable as it is based on a receive signal made up of only two rays. The 3D ray tracing model was able to achieve excellent accuracy within 0.4 to 1.05 bits/s/Hz for all the channels modeled.

This improvement over statistical models comes at a cost of time to develop a more detailed model, so is generally only warranted for truly site specific communication systems, such as fixed location sensor networks. As mentioned previously, mobile applications such as handheld links will presumably pass through all or most of the locations in the aircraft, thus justifying the use of statistical models in mobile cases as they do not require a detailed physical model of the aircraft. These results also show that if the improved accuracy is not necessary or the added complexity of the ray tracing method is not desirable, the next best accuracy may be obtained using Nakagami 1.4 as the statistical model for these channels. However, this site specific ray tracing model may still be used to inform and refine the statistical models by precalculating Ricean K parameters prior to construction of the aircraft to improve statistical model accuracy. Overall, if it has not been built or cannot be measured easily to find a good K parameter estimate, the 3D ray tracing model is the best estimate of channel capacity in vehicular channels.

8.2 Future Work

The most pressing question remaining is an evaluation of the sections of the aircraft that are even more enclosed than those evaluated here. The wings, engine compartment, and other maintenance bays are of significant interest in the development and deployment of fixed-location wireless systems for sensors and safety systems. This dissertation work has shown the importance of true site-specific modeling and the level of accuracy that can be expected. The ray tracing model is not suitable, however, for locations where the scatterers are dominantly in the near field. For these small, enclosed spaces that would be in the near field for the frequency of interest, more advanced 3D field models (FDTD, FEM, etc.) would be better suited [260].

Future work should involve further study of varying sizes of aircraft, tunnels, buses and cars to evaluate how larger and smaller environments affect the channel and modeling. It should also include a rigorous study of the wing and engine compartments that are large enough to be in the far field at the frequency of interest, as many sensors will need to be located in those enclosed areas as well. The external wing structure could be modeled with rectangular and triangular surfaces, and the internal cavity would need to have enough randomly placed obstacles to create the expected multipath richness.

For future measurement flexibility of the MIMO test bed, the number of transmit and receive channels could be increased to at least 8x8, but preferably 16x16, and should include automatically-controlled polarization agile antenna configurations. The packet data rate should be increased to a minimum of 5-10 Mbps (to test fast-fading channels). The bandwidth frequency should be tunable to a range of 2.0-2.5 GHz to reduce the required antenna size, while increasing the transmission range to 2-18 GHz, and

removing the pilot signal. Additional detector algorithms could be programmed on the test bed to perform a validation and evaluation of which adaptive algorithms are best suited to this environment, especially with moving passengers. The performance of MIMO combined with other multiple access methods could also be evaluated to explore all possible options.

8.3 References

- [243] A. Magleby and C. Furse, "Predicted MIMO performance in intravehicle channels," *IEEE Antennas and Propagation Society International Symposium*, San Diego, CA, Page(s): 1-4, 2008.
- [244] Alyssa Magleby, Cynthia Furse, and Z. Q. Yun, "3D Ray tracing for intravehicle MIMO," *IEEE/URSI Antennas and Propagation Symposium*, Charleston, SC, June 1-5, 2009.
- [245] Alyssa Magleby Richards, Sai Ananthanarayanan, and Cynthia Furse, "3D simulation of the wireless channel in small aircraft," submitted to *IEEE Transactions on Vehicular Technology*.
- [246] D. Landon, C. Furse, "The MIMO transmission equation," (Honorable Mention, student paper contest) *IEEE Antennas and Propagation Symposium (APS)*, San Diego, CA, July 7-11, 2008.
- [247] Alyssa Magleby Richards, Sai Ananthanarayanan, and Cynthia Furse, "Measurement and simulation of the multiantenna communication channel on a shuttle bus," in preparation for *IEEE Transactions on Vehicular Technology*.
- [248] Alyssa Magleby Richards, Sai Ananthanarayanan, and Cynthia Furse, "Wireless channel measurements and modeling in a helicopter," submitted to *Microwave and Optical Technology Letters*.
- [249] Alyssa Magleby Richards, Sai Ananthanarayanan, and Cynthia Furse, "Complex channel measurement and modeling for the design of wireless systems," in preparation for *IEEE Transactions on Vehicular Technology*.
- [250] Sai Ananthanarayanan, Alyssa Magleby Richards, Cynthia Furse, "Measurement and modeling of multiantenna systems in small aircraft," submitted to *Journal of Aerospace Computing, Information, and Communication*, June 2010.

- [251] Sai Ananthanarayanan, Alyssa Magleby, and Cynthia Furse, "Measurement and modeling of interference for multiple antenna system," *Microwave and Optical Technology Letters*, Vol. 52, Issue: 9, pages 2031–2037, September 2010.
- [252] K. I. Ziri-Castro, W. G. Scanlon, and N. E. Evans, "Prediction of variation in MIMO channel capacity for the populated indoor environment using a Radar cross-section-based pedestrian model," *IEEE Transactions on Wireless Communications*, Vol. 4, Issue: 3, Page(s): 1186 – 1194, 2005.
- [253] I. Telatar et al., "Capacity of multiantenna Gaussian channels," *European Transactions on Telecommunications*, Vol. 10, No. 6, Page(s): 585–596, 1999.
- [254] J. Frolik, "A case for considering hyper-Rayleigh fading channels," *IEEE Transactions on Wireless Communications*, Vol. 6, No. 4, Page(s): 1235–1239, 2007.
- [255] M. Lupupa and M.E. Dlodlo, "Performance of MIMO system in Weibull fading channel-channel capacity analysis," *IEEE EUROCON*, Page(s): 1735-1740, July 2009.
- [256] G. Fraidenraich, O. Leveque, and J. Cioffi, "On the MIMO channel capacity for the Nakagami-m channel," *IEEE Transactions on Information Theory*, Vol. 54, No. 8, Page(s): 3752–3757, 2008.
- [257] A. Bohdanowicz, G.J.M. Janssen, and S. Pietrzyk, "Wideband indoor and outdoor multipath channel measurements at 17 GHz," *IEEE 50th Vehicular Technology Conference, Fall 1999*, Volume: 4, Page(s): 1998 – 2003, 1999.
- [258] C. Oestges, D. Vanhoenacker-Janvier, and B. Clerckx, "Channel characterization of indoor wireless personal area networks," *IEEE Transactions on Antennas and Propagation*, Vol. 54, Issue: 11, Part: 1, Page(s): 3143 – 3150, 2006.
- [259] Y. Sun, P. Hafezi, A. Nix, and M. Beach, "Indoor channel characterization measurements with directional antennas for future high frequency ATM wireless access systems," *The 8th IEEE International Symposium on Personal, Indoor and Mobile Radio Communications*, Vol. 1, Page(s): 184 - 188, 1997.
- [260] H. L. Blocher, K. Beilenhoff, and J. Wenger, "Simulation of the electromagnetic wave propagation in cars," *33rd European Microwave Conference*, Vol. 3, Page(s): 1151 – 1154, 2003.

APPENDIX

3D RAY TRACING TUTORIAL

Tutorial for Fuselage software adapted from initial user manual created by ZQ Yun (“User Manual for Fuselage Ray Tracing.pdf”):

3/24/09

<http://www-ee.eng.hawaii.edu/~zqyun/rtplayground.html>

Just check item III and download the programs. An updated input format explanation is also there. You can ignore the wall thickness (put any values for it, but don't leave it blank) right now because I have not implemented the slab reflection coefficient in Python yet.--ZQ

A general purpose 3D ray tracer with limited functions (VPython interface, [Visual 3](#)).

- Download the Python [program](#) and the required [module](#).
- Sample input files can be downloaded for [a rectangular room](#) and [a ground](#).
- A snapshot of the room can be found [here](#).
- Take a look at the explanation of the [input file format](#). Note that RefGroup, TxGroup, RxGroup, and FreqGroup are required; other groups are optional.
- The output file has three columns. The first column is the computation index in which frequency changes the first, rx the second and the tx the last. The second column is the path gain and the third column is the mean path gain (all in dB).

User Manual for a General Purpose 3D Ray Tracer with Limited Functions (Testing Version 5)

I. Overview:

1. Installation of Python
2. Installation of VPython
3. Copy wisrt*.pyc and zqyfunctions.pyc to a directory
4. Create an input file
 - a. Use Matlab
 - b. Use File Format
5. Run the ray tracing program
 - a. Ray trajectories
 - b. Output results

II. Detailed Instructions:

1. Installation of Python:

Go to http://www.vpython.org/win_download25.html, click on [Python-2.5.1.ms](#) and save it to your computer. Double click it to install.

2. Installation of VPython:

Go to http://www.vpython.org/win_download25.html, click on [VPython-Win-Py2.5.-3.2.11.exe](#) and save it to your computer. Double click it to install.

Note: If the above doesn't work, you need two installs. For the first one go to http://sourceforge.net/project/showfiles.php?group_id=1369&package_id=175103 Click on `numpy-1.2.0-win32-superpack-python2.5.exe`, save it and double click it to install. For the second one, go to <http://prdownloads.sourceforge.net/scipy/scipy-0.6.0.win32-py2.5.exe?download> and save the file and install it.

3. Copy `wisrt*.pyc` and `zqyfunctions.pyc` to a directory:

Create a directory and copy `wisrt*.pyc` and `zqyfunctions.pyc` to it.

4. Create an input file

In the same directory as the `*.pyc` files, create an input file. The input file to the ray tracing engine is a description of the site to be tested, the electric parameters of materials at the site, the antenna locations, and frequencies of interest. This file must adhere to the format from <http://www-ee.eng.hawaii.edu/~zqyun/rtplayground/inputformat.htm>. This can be accomplished in two ways: use Matlab program “.m” to create the input file or use the file format directly.

a. Use Matlab

Create an antenna file as follows (this example is the diamond MIMO file):

```
% setup file for Diamond DA42 mimo antenna simulation

ng_tx_group = 1;
ne_tx_group = 1;
coord_tx_group = [0.2 0 3.6]; % Rx1 on diamond
repeat_tx_group = [1 1 4];
step_tx_group = [1 1 0.08]; % Rx1 was aligned with the plane and
started towards the tail of the fuselage and went towards the nose

ng_rx_group = 7;
ne_rx_group = [1 1 1 1 1 1 1];
coord_rx_group = [-0.4 -0.2 1.9; 0.2 -0.2 1.9; 0.2 -0.4 2.4; -0.2 -0.2
0.8; 0.2 -0.2 0.8; -0.4 -0.2 0.2; -0.2 -0.4 2.4]; %tx1 thru tx7 on
diamond
repeat_rx_group = [4 1 1;4 1 1;1 1 4;1 1 4;1 1 4;4 1 1;1 1 4]; % repeat
each location 4 times across the seat
step_rx_group = [0.08 1 1;0.08 1 1;1 1 -0.08;1 1 0.08;1 1 0.08;0.08 1
1;1 1 -0.08]; % at 8 cm separation

% FreqGroup: Frequency (or range) to test
ng_freq_group = 1;
start_stop_freqs = [0.915];
num_freqs = length(start_stop_freqs);
freq_repeat = 1;
freq_step = 0;
```

Then open ‘`create_geo_input.m`’ and change line 70 to be the appropriate output filename ie.:

```
fid = fopen('testDA42_mimob', 'wt'); % switch to above input file lines
when finished with coding
```

And change line 147 to load the appropriate antenna file:

```
% Load tx/rx location info:
    TxRxGroupDA42_mimob;
```

Then run 'create_geo_input.m' from the Matlab command prompt. It will ask:
 "What type of environment? (f = fuselage, b = bus, t = tunnel, d = divided room):"
 and choose the appropriate environment for the antenna input file you entered in the code, then it will ask one of the following:

```
'Which Fuselage (b = beech baron, d = diamond DA42, c = configure your own): '  

  'Which Bus (d = default, c = configure your own): '  

  'Which Tunnel (d = default, c = configure your own): '-this function not fully coded yet!
```

For each type of environment, follow the other prompts given to create the appropriate input file.

b. Use File Format

The file contains five top level groups: TransGroup/endTransGroup, RefGroup/endRefGroup, TxGroup/endTxGroup, RxGroup/endRxGroup, and FreqGroup/endFreqGroup. All dimensions are processed according to the coordinate system shown in Figure A.1.

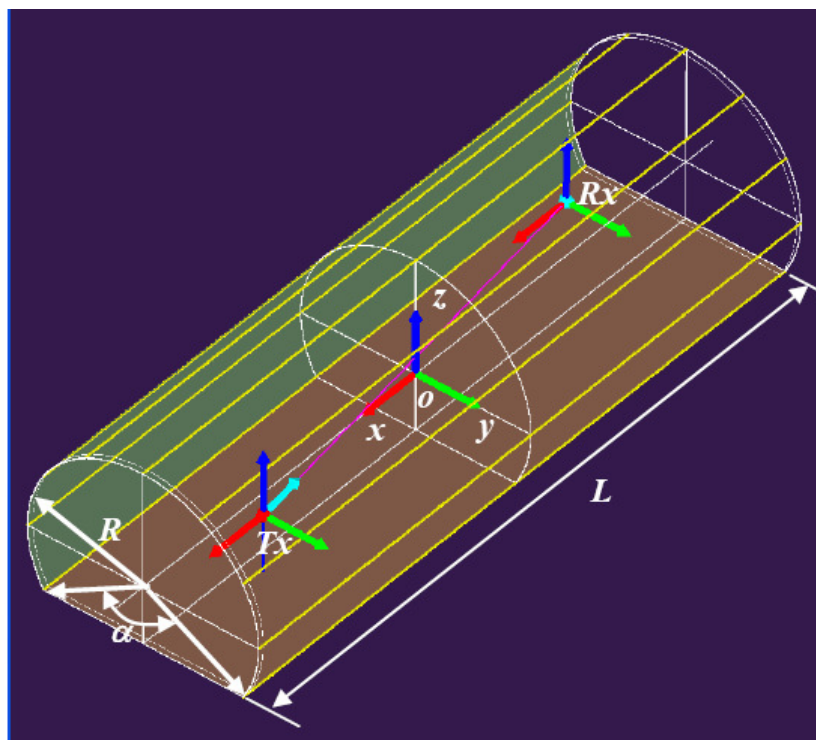


Figure A.1: 3D Ray tracing coordinate system and parameters

1. `TransGroup`: Description of transmission objects, e.g., chairs, walls, people
 - a. The group starts with ‘`TransGroup`’ on a single line
 - b. The next line is the number of subgroups, ng ; e.g., a section of seats in coach. A distinction of a subgroup is that the elements in it can be generated by repeating a set of primitives and have the same parameters (`dBLoss`, or for `RefGroup`, relative permittivity, conductivity, and thickness); e.g., the seats in a section can be generated by repeating a chair
 - c. Then each subgroup will have the following format:
 - i. The subgroup starts with ‘`Group`’ on a single line
 - ii. The next line is ‘`dBLoss`’ which indicates the following line will give the loss in dB for the objects in this subgroup
 - iii. The loss value in dB
 - iv. The number of elements in this subgroup, ne . Note that each element is a set of polygons (primitives) with 3 or 4 vertices on a common plane. For a polygon with 4 vertices, the outer perimeter should be convex; otherwise it should be decomposed into 2 triangles
 - v. In each of the following ne lines, one or more polygons (primitives) is defined which has 3 or 4 vertices (vertices). One vector has three decimal numbers corresponding to three coordinates (x, y, z). A white space is used as the delimiter between coordinate values while a semicolon is used as the delimiter between vectors. Currently, only one polygon (either 3 or 4 vertices) on each line. Also, the last “;” on each line is optional.
 - vi. The elements in the subgroup can be repeated to generate more elements. For example when one chair is built, we can repeat it in x, y, z direction several times. The next ‘`Repeat`’ line achieves this capability.
 - vii. The subsequent two lines give the number of repetitions and the repetition step, in x, y , and z directions.
 - viii. The subgroup is ended with ‘`endGroup`’
 - ix. The group is ended with ‘`endTransGroup`’
 - x. Two restrictive rules are used for listing the vertices of a planar polygon, i.e., the vertices should be listed clockwise or counterclockwise and the polygon primitive perimeter should be convex.
2. `RefGroup`: Description of reflection objects, e.g., fuselage walls
 - a. This group is similar to `TransGroup`; the difference is that the `epsilon_r`, `sigma`, and thickness of walls will be entered here, instead of `dBLoss`. Note that

for PEC, set $\sigma = -1$; for half space material (e.g., a ground) interface, set $\text{thick} = -1$ (Currently, thickness is not actually implemented in the code).

- b. Three restrictive rules are used for listing the vertices of a planar polygon for this group. First the polygon perimeter should be convex. Second, the vertices should be listed counterclockwise. A polygon is two sided: the positive side and the negative side, corresponding to positive normal direction and negative normal direction. The positive normal direction is defined by right hand rule when the vertices are traversed. Thus the third rule can then be stated as: only positive side will reflect.
3. TxGroup: Description of transmit antennas
 - a. Starts with TxGroup on one single line
 - b. The number of groups
 - c. 'Group' on a single line
 - d. Number of arrays of antennas, nt
 - e. One line lists the location of the first antenna in each array, i.e., nt vectors
 - f. 'Repeat'
 - g. A line each for repetition times (NxM and orientation) and steps (antenna spacing) in the x, y, and z directions
 - h. 'endGroup'
 - i. 'endTxGroup'
 4. RxGroup: Description of receive antennas; the same as TxGroup
 5. FreqGroup: Description of frequency;
 - a. Starts with FreqGroup on a single line
 - b. The number of groups
 - c. 'Group' on a single line
 - d. Next line is the number of Frequencies
 - e. Next line is the frequency to test for a single frequency, or the start and stop frequencies separated by a space
 - f. 'Repeat'
 - g. Number of frequencies in sweep (1 for single freq)
 - h. Size of steps in sweep (0 for single freq)
 - i. 'endGroup'
 - j. 'endFreqGroup'
 6. Flags are optional and each flag has a line to separate it from other groups with a '#', then a line with the flag name, and a line with what the flag is set to.
 - a. '#'
 - b. 'dispRays' sets whether the rays are displayed on the 3D plot
 - c. by default set to '1'
 - d. '#'
 - e. 'stepManual' sets whether the program pauses between antenna pairs
 - f. by default set to '0', but set to '1' to step through each antenna pair manually

- g. '#'
- h. 'maxRefLevel' sets the max number of reflections for the rays to bounce before arriving at the receiver.
- i. by default set to '2'
- j. '#'
- k. 'aoaOutput'
- l. by default set to '0', but set to '1' to output AoA and AoD info.
 - i. Note that AoD is automatically calculated when aoaOutput tag is set to 1. The output file will be *_aoa.m. Please see Output Results section for further details.

7. Other rules:

- a. No blank lines inside each (sub)group
- b. Only '#' is used to separate groups
- c. All the tag names and delimiter symbols should be followed exactly as stated above

An example of the input file is as follows. *****

```

TransGroup
  3
Group
dBLoss
0.10
  1
-0.65 -0.50 4.80; 0.65 -0.50 4.80; 0.65 0.50 4.80; -0.65 0.50 4.80;
Repeat
1 1 1
0.0000 0.0000 0.0000
endGroup
Group
dBLoss
0.10
  1
-0.65 -0.50 1.30; 0.65 -0.50 1.30; 0.65 0.50 1.30; -0.65 0.50 1.30;
Repeat
1 1 1
0.0000 0.0000 0.0000
endGroup
Group
dBLoss
0.10
  2
0.01 -0.40 2.10; 0.53 -0.40 2.10; 0.53 0.20 2.10; 0.01 0.20 2.10;
0.01 -0.40 2.10; 0.01 -0.40 2.60; 0.53 -0.40 2.60; 0.53 -0.40 2.10;
Repeat
2 1 3
-0.5360 0.0000 0.8200
endGroup
endTransGroup
#
RefGroup

```

```

12
Group
Epsilon $\rho$ ,sigma,thickness
-1.00 -1.00 -1.00
  1
0.55 0.00 0.00; 0.55 0.00 5.40; 0.47 0.32 5.40; 0.47 0.32 0.00;
Repeat
1 1 1
0.00 0.00 0.00
endGroup
Group
Epsilon $\rho$ ,sigma,thickness
-1.00 -1.00 -1.00
  1
0.47 0.32 0.00; 0.47 0.32 5.40; 0.26 0.53 5.40; 0.26 0.53 0.00;
Repeat
1 1 1
0.00 0.00 0.00
endGroup
Group
Epsilon $\rho$ ,sigma,thickness
-1.00 -1.00 -1.00
  1
0.26 0.53 0.00; 0.26 0.53 5.40; -0.00 0.60 5.40; -0.00 0.60 0.00;
Repeat
1 1 1
0.00 0.00 0.00
endGroup
Group
Epsilon $\rho$ ,sigma,thickness
-1.00 -1.00 -1.00
  1
-0.00 0.60 0.00; -0.00 0.60 5.40; -0.26 0.53 5.40; -0.26 0.53 0.00;
Repeat
1 1 1
0.00 0.00 0.00
endGroup
Group
Epsilon $\rho$ ,sigma,thickness
-1.00 -1.00 -1.00
  1
-0.26 0.53 0.00; -0.26 0.53 5.40; -0.47 0.32 5.40; -0.47 0.32 0.00;
Repeat
1 1 1
0.00 0.00 0.00
endGroup
Group
Epsilon $\rho$ ,sigma,thickness
-1.00 -1.00 -1.00
  1
-0.47 0.32 0.00; -0.47 0.32 5.40; -0.55 -0.00 5.40; -0.55 -0.00 0.00;
Repeat
1 1 1
0.00 0.00 0.00
endGroup
Group
Epsilon $\rho$ ,sigma,thickness

```

```

-1.00 -1.00 -1.00
  1
-0.55 -0.00 0.00; -0.55 -0.00 5.40; -0.47 -0.32 5.40; -0.47 -0.32 0.00;
Repeat
1 1 1
0.00 0.00 0.00
endGroup
Group
Epsilonr,sigma,thickness
-1.00 -1.00 -1.00
  1
-0.47 -0.32 0.00; -0.47 -0.32 5.40; -0.26 -0.53 5.40; -0.26 -0.53 0.00;
Repeat
1 1 1
0.00 0.00 0.00
endGroup
Group
Epsilonr,sigma,thickness
-1.00 -1.00 -1.00
  1
-0.26 -0.53 0.00; -0.26 -0.53 5.40; 0.00 -0.60 5.40; 0.00 -0.60 0.00;
Repeat
1 1 1
0.00 0.00 0.00
endGroup
Group
Epsilonr,sigma,thickness
-1.00 -1.00 -1.00
  1
0.00 -0.60 0.00; 0.00 -0.60 5.40; 0.26 -0.53 5.40; 0.26 -0.53 0.00;
Repeat
1 1 1
0.00 0.00 0.00
endGroup
Group
Epsilonr,sigma,thickness
-1.00 -1.00 -1.00
  1
0.26 -0.53 0.00; 0.26 -0.53 5.40; 0.47 -0.32 5.40; 0.47 -0.32 0.00;
Repeat
1 1 1
0.00 0.00 0.00
endGroup
Group
Epsilonr,sigma,thickness
-1.00 -1.00 -1.00
  1
0.47 -0.32 0.00; 0.47 -0.32 5.40; 0.55 0.00 5.40; 0.55 0.00 0.00;
Repeat
1 1 1
0.00 0.00 0.00
endGroup
endRefGroup
#
TxGroup
  4
Group

```

```
    1
-0.30 0.00 4.08;
Repeat
1 1 1
1.0000 1.0000 1.0000
endGroup
Group
    1
0.30 0.00 3.07;
Repeat
1 1 1
1.0000 1.0000 1.0000
endGroup
Group
    1
-0.30 0.00 2.16;
Repeat
1 1 1
1.0000 1.0000 1.0000
endGroup
Group
    1
0.30 0.00 0.01;
Repeat
1 1 1
1.0000 1.0000 1.0000
endGroup
endTxGroup
#
RxGroup
    1
Group
    1
-0.20 0.00 5.38;
Repeat
1 1 1
1.0000 1.0000 1.0000
endGroup
endRxGroup
#
FreqGroup
    1
Group
    1
0.915
Repeat
    1
0.0000
endGroup
endFreqGroup
#
dispRays
1
#
stepManual
1
#
```

```
maxRefLevel
2
#
```

5. Run the ray tracing program:

Double click on fuselage*.pyc to run the ray tracing program. You are prompted to enter the name of the input file as seen in Figure A.2. After you enter the filename, it will load the file and display a summary of key parameters in the command window, as shown in Figure A.3.



Figure A.2: Input file prompt

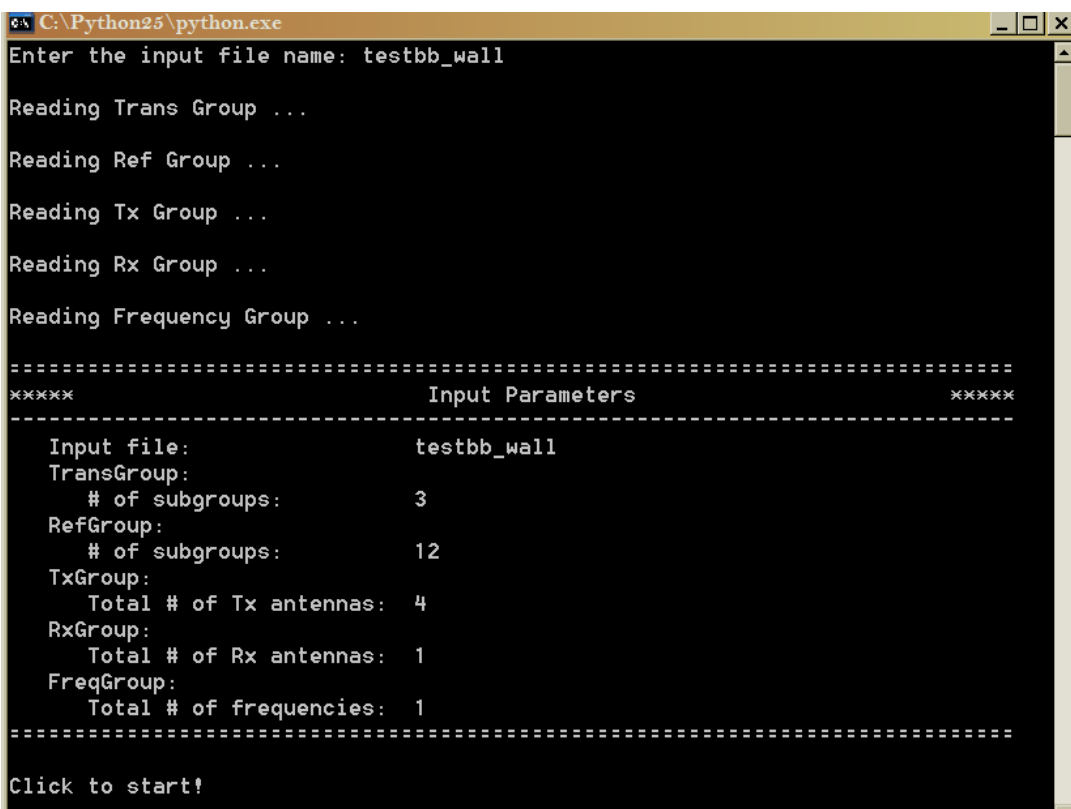


Figure A.3: Display of loaded input file

a. Ray trajectories

At the same time another window will open with the front view (-x direction) of the 3D model, which can be rotated by holding down the right-click on the mouse or touchpad and dragging to get the view seen in Figure A.4. To zoom in or out, click both left and right buttons and move up (zoom in) or down (zoom out). To run the simulation, left click your mouse inside this window. You will see the rays appearing, as shown in the two different angles seen in Figure A.5 a and b.

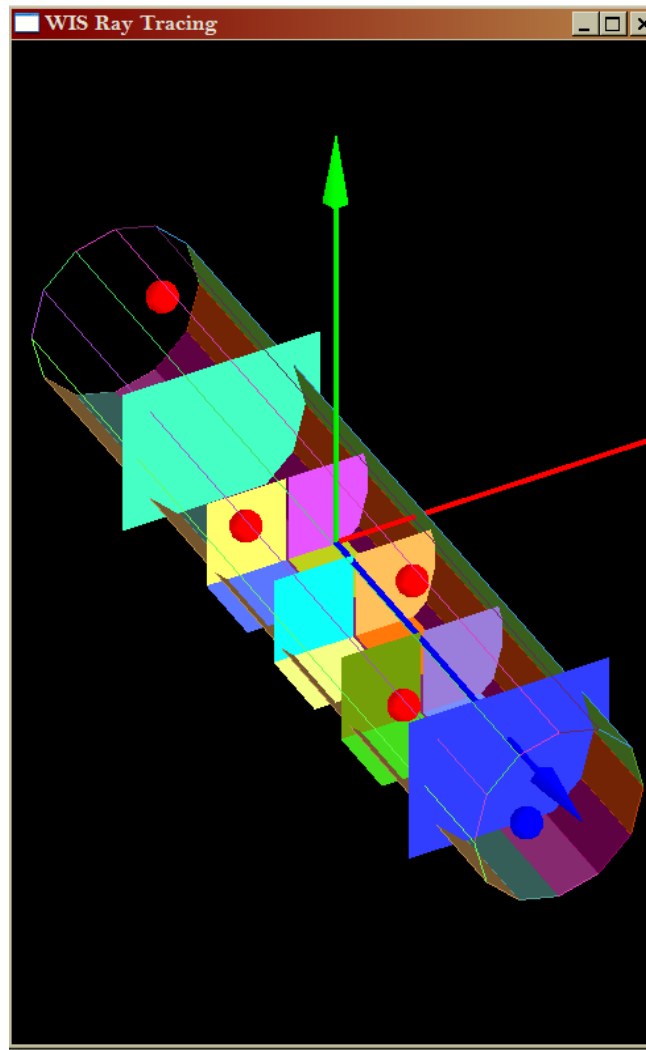
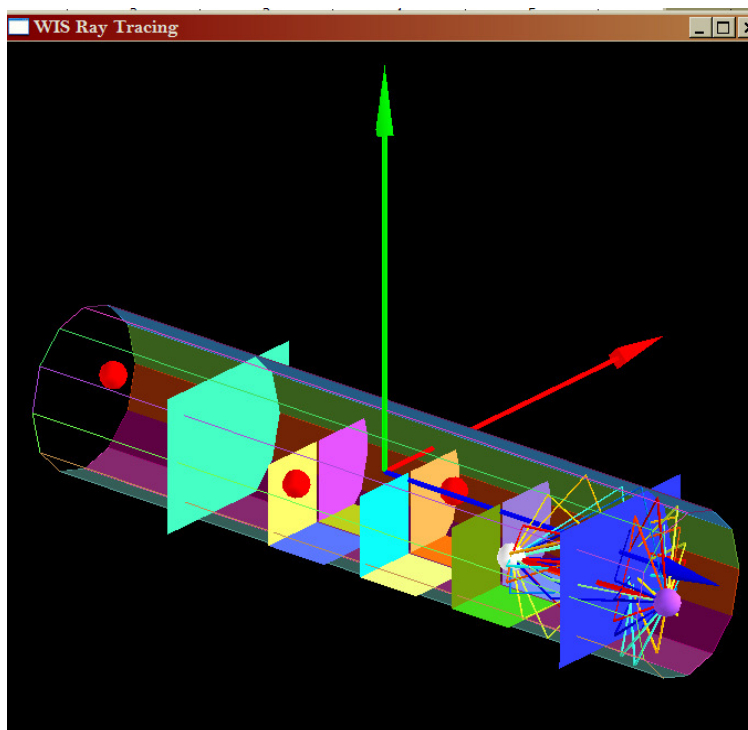
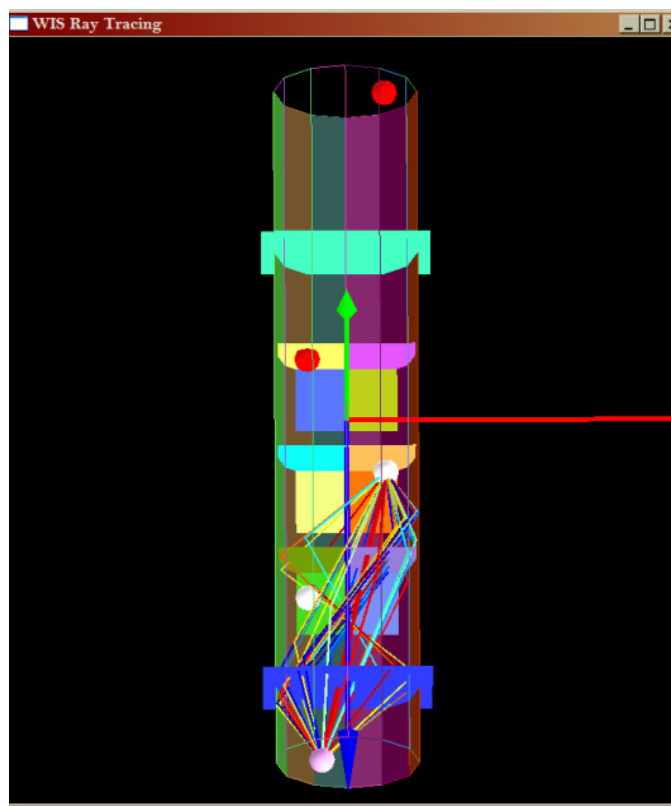


Figure A.4: Screen capture of 3D configuration with seats as well as front and rear walls.



a)



b)

Figure A.5: Ray trajectories between transmit and receive antennas. a) Side view. b) Top view.

Based on flags in the input file, left clicking in the drawing window will either run one antenna pair or run through all antenna pairs. If it only runs a single antenna pair, you must click on the drawing for each antenna pair until the simulation is complete. After the simulation is done, some statistics will show up in the window, such as the total simulation time, total number of rays received, and the output file information, as seen in Figure A.6.

a. Output results

The output results are stored in a file '<input filename>_out.m'. This file stores the output as a variable named pwr. It contains a line of data for each antenna pair. The first column in the output file is the computation index which can be determined by $(tx_index-1)*nrx*nfreq+(rx_index-1)*nfreq+freq_index$. It also outputs the complex E-fields (in V/m) at Rx locations: the 2nd column in the output file is the real part and the 3rd column the imaginary part of the received fields. The 4th column is instantaneous power and 5th is average power. Note that the fields are calculated using the complex sum and the power calculated based on these fields should be the same as values in the fourth column in the output file. All the powers calculated are real numbers.

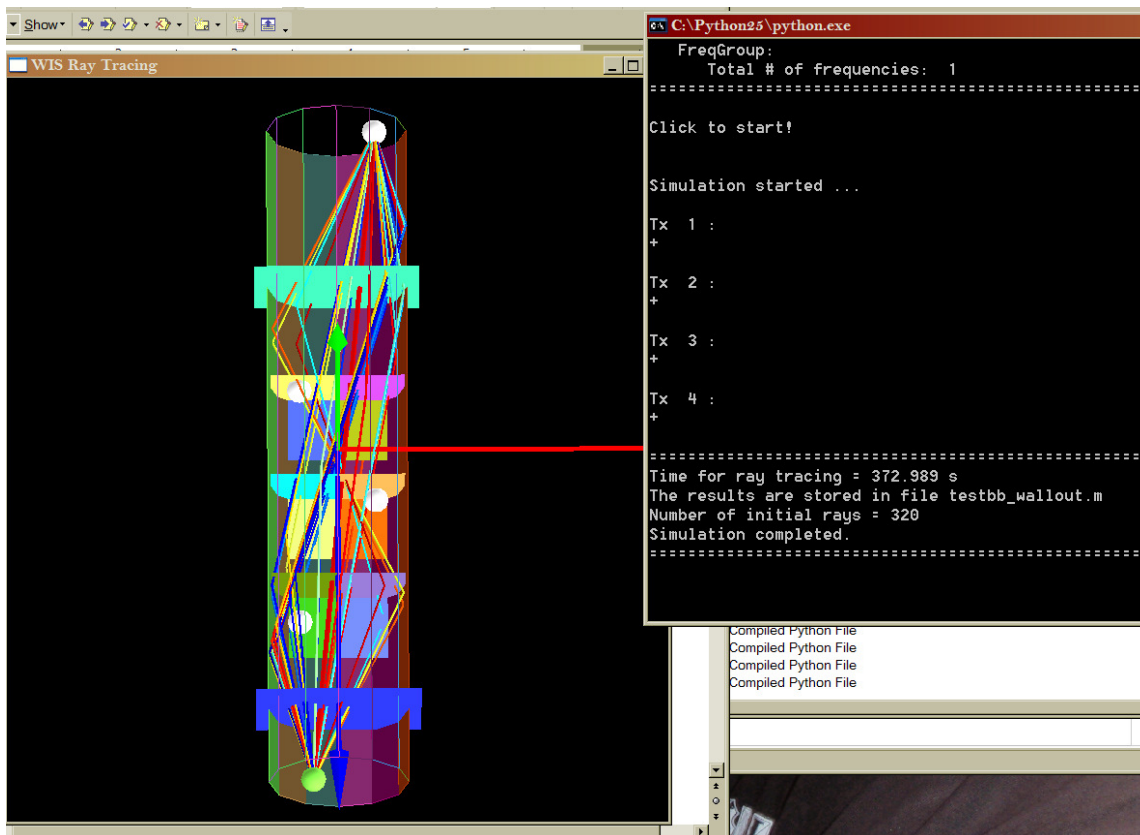


Figure A.6: Completed simulation with output statistics

If the appropriate flag is set, this program will also output a file '`<input filename>_aoa.m`' which includes all the angles of arrival and departure. This file is a little bit complicated. The first line of the file has 3 numbers, `nTx`, `nRx`, `nFreq`, i.e., the number of Tx's, Rx's, and frequencies, respectively. The following lines will be composed of `nTx*nRx` blocks (tx/rx pairs). All the blocks have the same structure. Each block starts with one integer (on one line), `nRays`, the number of rays for the Tx/Rx pair.

So in this block data, there will be `nRays` groups of data, each with the same structure. For each group (i.e., each ray for the Tx/Rx pair), the first 4 lines represents `aoa_theta`, `aoa_phi`, `aod_theta`, `aod_phi`, all in degrees. The subsequent `nFreq` lines are the complex fields for each frequency. There two numbers on each of these lines: the 1st is the real part and the second the imaginary part of the e-field. Note that the `nTx*nRx` blocks are arranged, in terms of Matlab language, as follows:

```
for i=1:nTx
    for j=1:nRx
        ...
    end
end
```

The AoA and AoD values are in degrees and a standard spherical coordinate system is used. In the 3D gui of the program, the blue arrow is x, the red arrow is y, the green one is z. This is different from the system for geometry definition (where x,y,z correspond to red, green, blue arrows). When all the AoA/AoD/efield values are known, it's easy to enforce an antenna radiation pattern even without ray tracing.

Matlab:

To convert this to a graph, it is next loaded into matlab for processing. Here's some sample Matlab code that was used for comparison. (after running `fuselage_test_b_ver3`, I renamed each output file to '`fldresults_xm`', where x was the distance (1 through 8), in order to run Matlab and compare data)

```
% This file loads the output of frequency swept fuselage tests into
arrays for processing.
% The output results are loaded from 'fldresults_xm' where x ranges
from 1 to 8. Running the file
% will give a variable 'pwr' which is an MxN array of received power.
Here M is the number of
% rays, N=number of frequency points.

% created 10/23/2008 by Alyssa Magleby
% use with fuselage_test_b

clear all
close all

%Set properties for good figures
```

```

set(0,'DefaultAxesFontSize',16)
set(0,'DefaultLineLineWidth',2)
set(0,'DefaultTextFontSize',16)

step = .0830e9/300;
freq = 2.4e9:step:2.483e9;
freq_index = 1:length(freq);

%bus-2400MHz-OO-Aisle_Center-Vertical-lm
bus_2400MHz_OO_Aisle_Center_Vertical_mag(1,:) = [ -44.5377383313356 -
44.3872428552547 -44.2405713457173 -44.0369365147423 -43.9759597509417
-43.7189444140294 -43.6287022486194 -43.5847438584444 -43.4524552861311
-43.4524552861311 -43.4524552861311 -43.4524552861311 -43.3466244282805
-43.2667000825079 -43.3124154302839 -43.3465210778334 -43.3465210778334
-43.3465210778334 -43.3465210778334 -43.3465210778334 -43.4055858583623
-43.4788096501467 -43.6203997627007 -43.7149309716663 -43.7874829855443
-43.9283151948195 -44.0695263557341 -44.2108064169468 -44.3695527037227
-44.5732219848467 -44.7305730405865 -44.8810685166674 -45.0398148034433
-45.259176127455 -45.4454308582393 -45.7008098130721 -46.061433973222 -
46.329835084392 -46.6063664307353 -46.862365488251 -47.0945250426309 -
47.3923638061555 -47.6060925307992 -47.8177714715749 -48.0378390236419
-48.2265741651571 -48.2676559678872 -48.3820821379232 -48.5020203318057
-48.5057753980511 -48.6204254940559 -48.6204254940559 -48.6204254940559
-48.6204254940559 -48.5058787484982 -48.3824094143391 -48.2677593183343
-48.0706183404534 -47.932628268474 -47.7126985170032 -47.6240066082999
-47.4021304234083 -47.1918122635197 -46.9977201238288 -46.8036624342869
-46.5303177267297 -46.3467673326451 -46.1450272598673 -46.0481017655435
-45.957015571482 -45.8070885228603 -45.7188961413181 -45.6395229979301
-45.5515028671332 -45.551330616388 -45.471957473 -45.471957473 -
45.471957473 -45.3837650914578 -45.3837650914578 -45.3837650914578 -
45.3043919480698 -45.3043919480698 -45.3043919480698 -45.2252255055761
-45.2250188046819 -45.2250188046819 -45.1192912972784 -45.1192912972784
-45.1192912972784 -45.2250188046819 -45.2250188046819 -45.2250188046819
-45.2250188046819 -45.2250188046819 -45.1476609950128
-45.2225900691746 -45.2249154542348 -45.2249154542348 -45.2249154542348
-45.3042541474737 -45.3042885976227 -45.3042885976227 -45.3836617410107
-45.3836617410107 -45.3836617410107 -45.3836617410107 -45.3043919480698
-45.3043919480698 -45.2250188046819 -45.0696486325119 -44.9869682748161
-44.90752623113 -44.7575991825083 -44.6080510855261 -44.4644800894022 -
44.3216669965572 -44.0816528081962 -43.9322597368846 -43.8581402412252
-43.7170324307577 -43.6112015729071 -43.4789130005938 -43.4416896145562
-43.3277629716812 -43.328882601525 -43.328882601525 -43.328882601525 -
43.328882601525 -43.328882601525 -43.328882601525 -43.4522485852369 -
43.4522485852369 -43.5845371575502 -43.5845371575502 -43.7168257298635
-43.7403379565832 -43.8929865669791 -43.9637643981816 -44.1048722086491
-44.2459800191165 -44.4409678626825 -44.6069659058313 -44.7574958320612
-44.9851079667679 -45.2215393396289 -45.4673928282522 -45.6107743485563
-45.8248820248394 -46.1040143574353 -46.3186043358049 -46.6004065549514
-46.8914414140406 -47.1911749357624 -47.4707206701468 -47.7120267390969
-48.0086941975541 -48.2651755571563 -48.6077478392092 -48.7261530014594
-48.9708696351644 -49.0005312134878 -49.0965610039366 -49.0965610039366
-49.0966643543837 -49.0966643543837 -49.0966643543837 -48.9731950202246
-48.8571841433327 -48.7554528532178 -48.7262563519065 -48.6116062559017
-48.4881369217426 -48.3734868257378 -48.2588367297329 -48.2588367297329
-48.147132121471 -48.1441866337281 -48.0384591263246 -48.0384591263246
-48.030191090555 -47.9330761204115 -47.932628268474 -47.932628268474 -

```

```

47.8179781724692 -47.8179781724692 -47.7121473146185 -47.6189424363911
-47.6063164567679 -47.5421875043301 -47.5004855989173 -47.605954730203
-47.6062131063208 -47.6062131063208 -47.6062131063208 -47.7119406137243
-47.7119406137243 -47.9160232966368 -48.0353069376875 -48.144083283281
-48.2587333792858 -48.4878957706993 -48.7259635256397 -48.9715241879962
-49.2173776766195 -49.475426518003 -49.7403653891945 -50.063146060624 -
50.3038320268913 -50.6097838005148 -51.0456815363169 -51.2397564509332
-51.5497561170689 -51.8129897058829 -52.1494470864812 -52.4119744472399
-52.7196142781663 -52.9960939492862 -53.2151279968819 -53.5185304594765
-53.7229404188048 -53.9471419887566 -54.1673301163452 -54.2822730386169
-54.395441778213 -54.3969231346217 -54.3969231346217 -54.3969231346217
-54.3714644744812 -54.3776827263829 -54.282376389064 -54.1722737127324
-54.1677262930591 -54.0829961514955 -54.0618954352085 -53.9472453392037
-53.8459619010263 -53.7394075900459 -53.5244903352604 -53.4181944003977
-53.2158514500118 -53.1095210650001 -52.8414300051715 -52.6244629665181
-52.4392589652795 -52.1834321585091 -51.9561645252928 -51.6085797465545
-51.4426850538528 -51.3144960492753 -51.2221007495503 -51.0633544627743
-50.9839813193864 -50.9046081759984 -51.0081653240124 -51.010439033849
-51.1673939128749 -51.2838870918534 -51.5745085491541 -51.7417640227429
-51.9978836557801 -52.3593862947304 -52.7285196416931 -53.045616038531
-53.520700818866 -54.0024172528911 -54.5218221499659 -55.0124783976669
-55.5242009115058 -56.0878570250224 -56.4936970057871 -56.842797591083
-57.0868941221054 -57.2454337079871 -57.2456404088813 -56.9060136145713
-56.6610730548975 -56.2449497046444 -55.8153563461166 -55.413030280554
-55.1371362619678 -54.767434487546 -54.3009794695455 -53.9592856662931
-53.7355836235025 -53.5239219078012 -53.3373743507501 -53.2741066520383
-53.1184264285269 -52.9155495008308 -52.8184862059109 -52.7218363127794
-52.6567083060194 -52.6244629665181 -52.6244629665181 -52.5274513468217
-52.5274513468217 -52.4392589652795 -52.4392589652795 -52.4392589652795
];

```

```

%bus-2400MHz-OO-Aisle_Center-Vertical-2m

```

```

bus_2400MHz_OO_Aisle_Center_Vertical_mag(2,:) = [ -59.864850790237 -
60.0403053992973 -60.2166384871581 -60.4204627939527 -60.7118766046814
-60.7674791452318 -60.7733356705686 -60.7733356705686 -60.7361122845309
-60.6587889250109 -60.5353195908518 -60.2184987952062 -59.9797075871361
-59.7770201352597 -59.7592266332806 -59.65339577543 -59.65339577543 -
59.7584859550762 -59.8649541406841 -60.0827479829144 -60.3142357593881
-60.6633535697586 -60.9235210953081 -61.2652148985605 -61.4171400558265
-61.6594624041733 -61.7874791580056 -61.8252192962788 -61.9274156634057
-61.9287592192183 -61.907968542727 -61.9287592192183 -61.9286041935476
-61.9989858480361 -62.0656985616519 -62.3242813803455 -62.6721762104251
-63.0330070714692 -63.4131472410501 -63.8140436254276 -64.3184799327446
-64.7741865042446 -65.1622674331792 -65.4673924032257 -65.778735625174
-65.957859175107 -65.9950136608465 -66.1025842512237 -66.0032472464671
-66.1089058535725 -66.1089747538706 -66.2988812004531 -66.4148059519724
-66.4530283923322 -66.6902004433975 -66.936587909331 -66.9790821681717
-67.0193716174739 -67.0703233879039 -66.8632607670995 -66.6314284891354
-66.329455707726 -65.9125572291195 -65.4802078586686 -64.9754615000103
-64.5157587112216 -64.1485717976797 -63.8621704836364 -63.6567097947623
-63.4533505649797 -63.2256695299749 -63.0944144621328 -62.9807289703011
-62.9815040986545 -62.9034745110791 -62.9075913038894 -62.7577159304912
-62.7560106481138 -62.7905469225263 -62.6782911118797 -62.6782911118797
-62.6782911118797 -62.6098558908119 -62.6955678616232 -62.6827868563294
-62.762676751953 -62.9074879534423 -62.8723143512725 -63.0308539371542
-63.1897035743772 -63.3636940521033 -63.4569333804799 -63.5647106717512
-63.7055773311754 -63.704733302524 -63.7808853569767 -63.7934596613763
-63.8906263067433 -64.1327247291214 -64.3005314050948 -64.6700092535479

```

```

-65.06747778480959 -65.5571694916238 -65.888390449568 -66.4405057631562
-67.0259171457915 -67.546407222561 -68.1710745500273 -68.3302859138152
-68.4436269041566 -68.4098657580975 -68.1990136208987 -67.8117767206155
-67.3149366711618 -66.6833448637386 -65.9973562709813 -65.1715861984945
-64.440071733781 -63.5537727494311 -62.9051108931585 -62.1536670172254
-61.4295421094809 -60.8158471544838 -60.2060795164773 -59.7418637581645
-59.2390121577034 -58.8075240409784 -58.4080573377861 -58.1099257479947
-57.8470883358946 -57.5197257946429 -57.2663621735288 -57.037354807786
-56.8046785011704 -56.5068397376458 -56.2935071897161 -56.0116705204206
-55.6756782168343 -55.4005937767506 -55.1204623898325 -54.7572544685047
-54.5028917930685 -54.1677435181337 -53.8414489315021 -53.5284693274745
-53.2449101507269 -53.0214492589795 -52.827202093618 -52.569170477309 -
52.3959379028618 -52.3422473455831 -52.2540549640409 -52.2540549640409
-52.2540549640409 -52.342143995136 -52.4391556148324 -52.5273479963746
-52.6984446615813 -52.8183828554638 -53.111174672154 -53.2151452219565
-53.4179876995035 -53.6251019955314 -53.7827114273891 -53.9560990275069
-54.2781217956575 -54.5115732306265 -54.8722318409254 -55.2361115401595
-55.6259494266952 -56.0259501071976 -56.4961774165179 -57.0237469989152
-57.5074443165101 -57.9813577917777 -58.5612227004176 -59.0377027117886
-59.6172920192362 -60.119936918803 -60.5115834381633 -60.9133410762668
-61.2934984709222 -61.6503675648267 -61.8518492614867 -61.9992097740049
-61.954424580253 -61.9288281195164 -61.6818205509002 -61.3284309220487
-61.0380161656422 -60.5536987453646 -59.9842550068093 -59.5724379251862
-59.1430168174036 -58.5982910607845 -58.1105114005284 -57.7132667319491
-57.3241867486923 -56.956724233958 -56.727975244333 -56.4348044760033 -
56.2069339651788 -55.9643532407143 -55.8698220317487 -55.7640083989726
-55.7640083989726 -55.7571528193137 -55.7639050485255 -55.7639050485255
-55.7638361482274 -55.8330809477977 -56.0108437168436 -55.993463616653
-56.1167262499178 -56.2433649977885 -56.3274061363714 -56.4783666894643
-56.6985720421274 -57.0051094682846 -57.2879107417533 -57.6440391574534
-58.0107954441323 -58.5722639731849 -59.0063530761623 -59.545997435798
-60.1650493889708 -60.6540348044433 -61.1412632623149 -61.52286756323 -
62.0375527898863 -62.4576206822045 -62.6940520550655 -62.9074879534423
-62.9105712417813 -62.9075913038894 -62.7809181058696 -62.537872304393
-62.3496539151134 -62.0395164483816 -61.6944637555978 -61.3283792468252
-60.9167688660963 -60.5532336683526 -60.0862618981165 -59.7532323073477
-59.3945890307676 -59.0364625064232 -58.6814192704178 -58.2580958390153
-58.0006843253891 -57.8075051146478 -57.6749581662167 -57.471495585987
-57.2977290342296 -57.0868941221054 -56.9526418912968 -56.7342451714583
-56.5060129340688 -56.2935244147906 -56.0307214528397 -55.7672294879079
-55.500619784488 -55.2437766983209 -54.8879583339621 -54.5295045332018
-54.1815752529732 -53.9563057284012 -53.7356869739496 -53.4876459008622
-53.3123635425471 -53.1095210650001 -52.9537202659671 -52.8184862059109
-52.8183828554638 -52.7214745862145 -52.7164448644547 -52.5133095606408
-52.514739241826 -52.6061871624524 -52.6765515918664 -52.7037327594589
-52.9142748453164 -52.915291124713 -53.0123027444094 -53.1093143641058
-53.1093143641058 -53.2150935467329 -53.2402593806066 -53.3103826589773
-53.3293474660238 -53.3123118673235 -53.3122601921 -53.4180910499506 -
53.5238702325777 -53.6278407823801 -53.7355836235025 -53.9502080520211
-54.1744612971964 -54.4009193519103 -54.6323899033095 -54.8225547260098
];
%bus-2400MHz--OO-Aisle_Center-Vertical-3m
bus_2400MHz_OO_Aisle_Center_Vertical_mag(3,:) = [ -50.6240289371428 -
50.7795541349835 -50.9306180385235 -51.0897088267899 -51.4079248534716
-51.5016981591582 -51.8243065798425 -52.0810807657115 -52.3595929956247
-52.7204066315942 -53.0280809126697 -53.3210794302542 -53.5945791634821
-53.9238709130801 -54.1764766309153 -54.5240269595045 -54.767434487546

```

-55.1086459887118 -55.3929630687382 -55.658177541122 -56.0224706421446
-56.3659386280725 -56.7846974147272 -57.1907096462371 -57.5371575700571
-57.913025921157 -58.3506806145601 -58.7781208387729 -59.2333967834099
-59.689000044627 -60.110463127817 -60.6403236451255 -61.0378955901206
-61.5493769529162 -62.1167881326781 -62.6664919358335 -63.3697400532598
-63.9486920329501 -64.4882847173623 -64.8643942195056 -65.367986498171
-65.6235721538982 -65.8882009737483 -65.7826629421645 -65.5836444311609
-65.1694675143285 -64.486717235581 -63.9188582038816 -63.2820299738042
-62.7232830065258 -62.2387761104285 -61.6882455036961 -61.2956688303118
-61.0380161656422 -60.7910774973241 -60.4301432858329 -60.200205766066
-60.0855384449867 -59.9797075871361 -59.8573751078953 -59.8649541406841
-59.6537575019949 -59.5490634990626 -59.4855890994566 -59.4416307092816
-59.4434048919572 -59.5469103647476 -59.5411744149325 -59.6563412631729
-59.8558593013376 -60.0690540486711 -60.3016614549886 -60.5351128899576
-60.7908363462808 -61.1409876611225 -61.3974001204266 -61.6551561355433
-61.9635538697486 -62.1779543722985 -62.3812963770066 -62.5198032012216
-62.5293458925056 -62.4578101580242 -62.3872562527905 -62.221998887846
-62.0883839847947 -61.7876514087508 -61.4394637524044 -61.1628979559119
-61.0411683542794 -60.8968050047276 -60.7733356705686 -60.53897130665 -
60.4246484870611 -60.3156482154988 -60.3058126979479 -60.1912659523902
-60.2128489707637 -60.1912659523902 -60.1912659523902 -60.1912659523902
-60.1901463225464 -60.0960974156674 -60.0854350945396 -59.9707849985347
-59.8177229863504 -59.6536024763242 -59.5474615671322 -59.2494505528625
-59.1341975792494 -58.9477533726454 -58.847262287896 -58.6567185135562
-58.6567185135562 -58.6567185135562 -58.831294643816 -58.9476500221983
-59.2337585099748 -59.4116590796169 -59.6532407497593 -59.8649541406841
-60.1679259764156 -60.3168367456407 -60.5440182534844 -60.6479199029888
-60.6592884521719 -60.616225765872 -60.5338726845921 -60.305916048395 -
60.0854350945396 -59.7636707025068 -59.4571505014241 -59.2387882317346
-58.8509484538432 -58.4519123775139 -58.0511710188071 -57.6899784311981
-57.3531593240349 -57.035666750483 -56.7384136394921 -56.5068397376458
-56.363733818534 -56.1520721028328 -56.0109470672907 -55.8698392568233
-55.7640083989726 -55.6317198266594 -55.4996896304639 -55.3594258486479
-55.1900516908931 -55.1379458404703 -54.9156390287157 -54.8910071721522
-54.6456359856154 -54.5297629093196 -54.4059490736702 -54.2912989776653
-54.1766488816605 -54.0619987856556 -54.0508024872177 -53.9472453392037
-53.8414144813531 -53.8414144813531 -53.7355836235025 -53.7355836235025
-53.7355836235025 -53.7355836235025 -53.8390718712184 -53.841311130906
-53.841311130906 -53.841311130906 -53.841311130906 -53.9120028367359 -
53.9387533774653 -53.8414144813531 -53.8414144813531 -53.7367032533462
-53.7355836235025 -53.6297527656518 -53.4533680025675 -53.4181944003977
-53.3123635425471 -53.2223108529568 -53.1108646208126 -53.0145936793206
-53.0125094453037 -52.9154978256073 -52.9154978256073 -52.8184862059109
-52.7214745862145 -52.7214745862145 -52.7214745862145 -52.8269437175002
-52.827202093618 -52.827202093618 -52.827202093618 -52.9233869097374 -
52.9241103628673 -52.9241103628673 -52.9241103628673 -52.9241103628673
-52.9241103628673 -52.9241103628673 -52.9220605789994 -52.9218194279561
-52.8593785328213 -52.9234041348119 -52.827202093618 -52.828063347344 -
52.7216640620342 -52.7214745862145 -52.827202093618 -52.6422564684972 -
52.6244629665181 -52.624359616071 -52.5274513468217 -52.5274513468217 -
52.5288465778578 -52.5274513468217 -52.5274513468217 -52.5274513468217
-52.5274513468217 -52.5450725980556 -52.544986472683 -52.4479748529866
-52.3610915771079 -52.3597824714444 -52.2715900899022 -52.1745784702058
-52.0869372910483 -52.0157632831318 -51.9981937071215 -51.9188205637335
-51.9188205637335 -51.8794440433809 -51.9187172132864 -51.9187172132864
-51.9187172132864 -51.9187172132864 -51.8923628492708 -51.980555230813
-52.0665255777421 -52.1608328607389 -52.2537621377741 -52.342143995136

```

-52.5273479963746 -52.7201310304019 -52.8726590652761 -52.8977559988517
-53.0998233480453 -53.3624885094002 -53.5236635316834 -53.6296494152047
-53.7354630479808 -53.7354802730553 -53.9333791542151 -53.9471419887566
-53.9471419887566 -53.9471419887566 -54.0346625923925 -54.0617920847614
-54.0617920847614 -54.167622942612 -54.2821869132443 -54.342371323617 -
54.5293150573821 -54.8890435136569 -55.1340874237778 -55.5251827407534
-55.9650766938441 -56.3524513947234 -56.8426425654124 -57.3918296163322
-57.9885750980016 -58.5617050025041 -59.1399679792136 -59.6126929243393
-60.291240284904 -60.8934977904198 -61.5621751832845 -62.487781787689 -
63.47700059222956 -64.6524741276865 -65.9192405580333 -67.9608080653622
-70.5941946830478 -75.1479187335908 -81.9304468514948 -77.5552951485001
-71.9931980104842 -68.1805138908642 -65.5808195189396 -63.5805921904586
-61.9840517084273 -60.8361382922683 -59.8975095315268 -59.1380732210164
-58.558122187004 -58.0948882579388 -57.7500250409747 -57.4134987600783
];
%bus-2400MHz-OO-Aisle_Center-Vertical-4m
bus_2400MHz_OO_Aisle_Center_Vertical_mag(4,:) = [ -57.6573541400573 -
57.647604747879 -57.5689206074719 -57.4808315763768 -57.4839493148649 -
57.4015617834359 -57.3224986913893 -57.322188640048 -57.4004766037412 -
57.4014584329888 -57.4014584329888 -57.3289236441853 -57.2181491899474
-57.2163577821974 -57.2163577821974 -57.2131022431131 -57.1546058900433
-57.1381559438768 -57.2162544317502 -57.2163577821974 -57.2956275751382
-57.4587318057677 -57.6391989115133 -57.9012267451109 -57.9962230310884
-58.3272372881385 -58.6971457634545 -59.0197886342879 -59.3440506621261
-59.8392371044258 -60.1860639798851 -60.561363903526 -60.9565243380883
-61.3684964453821 -61.6800291431501 -62.0043256211373 -62.3327733420839
-62.3874285035357 -62.2498690584193 -62.0346762024415 -61.5856012846317
-61.1684788800564 -60.7122383312463 -60.1066736114227 -59.4584079318641
-58.858493036483 -58.2083842739507 -57.681228093342 -57.2477935431963 -
56.7883491305255 -56.4005782529322 -56.0474125500495 -55.7658859320953
-55.4159585432224 -55.1750314259117 -54.8912655482699 -54.6685797848759
-54.3605782273846 -54.1124854790736 -53.8915049980571 -53.7855707897594
-53.5739607492817 -53.3711871720327 -53.1694643243295 -53.0712124992677
-52.923869211824 -52.8679738450067 -52.7699114957646 -52.6937422162373
-52.6831660204821 -52.6831660204821 -52.6831660204821 -52.6831660204821
-52.7800742897314 -52.8372787622122 -52.8770859094278 -52.9740975291242
-53.0711091488206 -53.168120768517 -53.2651323882134 -53.370963246064 -
53.4679748657604 -53.6210368779447 -53.7854674393122 -53.8912982971629
-54.1481586084045 -54.3322085296502 -54.45583288948 -54.7828164790923 -
55.064325871972 -55.5418566128887 -55.8132032118016 -56.1878141324617 -
56.5453550042724 -56.8543211659369 -57.2426087957658 -57.7258238112741
-58.2184264923959 -58.6958711079401 -59.2336723846022 -59.8994387398731
-60.5765564192526 -61.3154948910842 -62.164553264322 -63.0232060040673
-63.7661062430386 -64.5418891492684 -65.1905682306155 -65.4189899438246
-65.6208850422731 -65.6215395951048 -65.5013430251046 -65.3177065056473
-65.0220553265868 -64.7819894630021 -64.4619992536448 -64.183762624924
-63.9276946671103 -63.4059988351243 -63.2401558176462 -62.9516702695859
-62.7093651463137 -62.4948612933167 -62.398073599589 -62.3577841502869
-62.4162460532076 -62.5074183726417 -62.7423339389449 -63.034126701313
-63.5914439874062 -64.1896019251863 -65.2088095845321 -66.1789257814961
-67.4306547217869 -68.8473654258299 -70.4418905741423 -72.074586487591
-73.1864133726307 -73.0176593175587 -71.9636914578315 -70.2241139569865
-68.7725224770406 -67.3109060037242 -65.937189085683 -64.6171454998461
-63.6253773842105 -62.6813227249952 -61.828371484916 -61.0116790267012
-60.3141668590901 -59.6346721194268 -59.0886028069951 -58.6648831988787
-58.2470028910245 -57.9668026038083 -57.7311291342263 -57.6356333210876
-57.6308619754456 -57.6307586249985 -57.736486132402 -57.8951807439544

```

```

-57.9922440388743 -58.1350915818683 -58.3127854506162 -58.4866553528207
-58.6184099478238 -58.8036139490624 -58.9878533461279 -59.0946488081516
-59.2886720475444 -59.416068698694 -59.4915145250914 -59.7031762407927
-59.8090070986433 -60.0116601003706 -60.1283772053178 -60.2826449727185
-60.5842388024885 -60.806941790957 -61.0464909023061 -61.3412636025661
-61.5994157943967 -62.0466476292329 -62.4562943514665 -62.9076257540384
-63.2175048446525 -63.6541260335843 -63.988740331209 -64.439210480055 -
64.8174042162151 -65.3953743666578 -65.8792094848489 -66.4555949284357
-66.9701423544958 -67.7238599402656 -68.5698005750153 -69.4472286459874
-70.7377312290226 -72.1808307472301 -73.9115717848464 -76.0497202850087
-78.4807295021593 -83.0365550117938 -88.1254276775229 -91.0998018704056
-87.428552837669 -82.4467340100814 -80.934630843347 -79.5400371349877 -
78.2910642066201 -77.4182180054703 -77.0410060985577 -76.1196713126342
-75.5200320184455 -74.9230109355838 -73.9829697187316 -73.6215532051539
-73.1358577789146 -72.4213616878268 -71.8123691781737 -71.3368882211248
-70.8205149371655 -70.2985607290617 -69.4786644069863 -68.9612920687049
-68.2677933434568 -67.4879280945658 -66.8737852876312 -66.2800369689283
-65.8679098359638 -65.5152264351676 -65.1973549099764 -64.8272741839151
-64.6447400692271 -64.5455064149176 -64.5448690871604 -64.4567456059163
-64.3749609520955 -64.488474193182 -64.5378068066072 -64.6036065912734
-64.7211504997976 -64.7994729136399 -64.8489777778102 -64.8541969753898
-64.8416915712883 -64.8518888154041 -64.8141142269818 -64.6166631977596
-64.4764166410181 -64.4950713967232 -64.3511558991089 -64.4258782723765
-64.3493472662843 -64.4386592776703 -64.8248798985568 -65.2969330657762
-65.9747914233601 -66.8092257083304 -68.0190804924632 -69.5935556540344
-71.6892271204305 -74.7391677152323 -79.0553752132196 -83.983951335466
-80.1793630008704 -75.0838242313021 -72.8460459001163 -70.6053393062622
-69.2620935450469 -68.2140855611036 -67.2435387372766 -66.6536143851171
-66.0508573524402 -65.4261038996014 -64.7233725344107 -63.9880513282282
-63.1793857547398 -62.5387163330445 -61.8795988565383 -61.2499362574613
-60.7255877639993 -60.1554894726122 -59.7987065040803 -59.385890368135
-58.9372116270392 -58.6987476953849 -58.5302175662816 -58.3382785609057
-58.2412152659858 -57.9729347303375 -57.9597919984787 -57.8867232323651
-57.8652091142896 -57.7984275003758 -57.7102351188336 -57.6318610297678
-57.4791435190738 -57.3751040689733 -57.1809258039098 -56.9782383520335
];
%bus-2400MHz-OO-Aisle_Center-Vertical-5m
bus_2400MHz_OO_Aisle_Center_Vertical_mag(5,:) = [ -55.4163719450109 -
55.4258457359968 -55.6816036424692 -55.8135821634411 -56.0178887723223
-56.2011807902892 -56.4122224033077 -56.7016897806156 -56.9809771388821
-57.2427121462129 -57.5685761059815 -57.879333675396 -57.9854918096625
-58.3252391794941 -58.5125101896751 -58.6707052740664 -58.7948980613553
-58.8331721769386 -58.7950014118024 -58.7950014118024 -58.6755110698575
-58.5626696066772 -58.5221562314063 -58.5403975853229 -58.2425415967238
-58.1423777883903 -58.1227756535866 -58.0541854068481 -58.0071781784831
-58.054082056401 -58.054082056401 -58.1407069561618 -58.1422744379432 -
58.2392860576396 -58.4156708207239 -58.6008748219625 -58.9006255687588
-59.1723166691621 -59.3838405842672 -59.4915145250914 -59.6955972080039
-59.8089726484942 -59.8898271482909 -59.9148379564939 -59.9003172186736
-59.876546615836 -59.678837210496 -59.5411571898579 -59.4917212259857 -
59.3168522694591 -59.2882414206814 -59.1132863387822 -58.9242583710002
-58.8920130314988 -58.697989792106 -58.6009781724096 -58.4161186726614
-58.2468478653538 -58.0586467011488 -57.8872744347497 -57.7677496426557
-57.5156090018326 -57.2948696718593 -57.0069870014073 -56.7127655035319
-56.4307393584166 -56.1374652396398 -55.8754201809677 -55.5798551272798
-55.2944873177076 -55.0468596464087 -54.8289796788058 -54.5654188135759
-54.4470136513257 -54.2177134593161 -54.0030890307974 -53.89140164761 -

```

53.7855707897594 -53.6797399319087 -53.5739090740581 -53.3710665965111
-53.2652357386605 -53.0720737529937 -52.9742008795713 -52.7801776401785
-52.5950253141635 -52.420294158233 -52.2158497487556 -52.0319548531806
-51.8764124302654 -51.8806153484482 -51.7210422580954 -51.6248574419759
-51.5454842985879 -51.4572919170458 -51.3779187736578 -51.2985456302698
-51.2191724868819 -51.2191724868819 -51.2191724868819 -51.2111628272301
-51.1878573014046 -51.1397993434939 -51.1397993434939 -51.1397993434939
-51.1158048146876 -51.1042984649083 -51.1026793079034 -51.0604262001059
-51.1396959930468 -51.1396959930468 -51.2190691364347 -51.2984422798227
-51.4538124519927 -51.5453809481408 -51.712946473071 -51.9478620393742
-52.1357359271633 -52.2157463983085 -52.3921139363184 -52.5773351626315
-52.6959125756269 -52.7713584020243 -52.7713584020243 -52.7703765727766
-52.7202688309981 -52.5953525905793 -52.4098385379994 -52.2361753366892
-52.0484392494962 -51.8806153484482 -51.7130498235181 -51.5454842985879
-51.2988556816112 -51.2191724868819 -51.1397993434939 -50.98151813373 -
50.981053056718 -50.9146159442945 -50.9808635808983 -50.9809497062709 -
50.9809497062709 -51.0603228496588 -51.0603228496588 -51.0644396424691
-51.1396959930468 -51.1386969387246 -51.1396959930468 -51.0756187158325
-50.9546986927024 -50.9546986927024 -50.8753255493145 -50.8157956917735
-50.8047716440807 -50.8047716440807 -50.725570751438 -50.7253985006928
-50.7253985006928 -50.7253985006928 -50.883128508072 -50.9103958010371
-50.9103958010371 -50.9809497062709 -50.9809497062709 -51.0603228496588
-51.136853855751 -51.1396959930468 -51.2078211627732 -51.2190691364347
-51.2190691364347 -51.2984422798227 -51.2984422798227 -51.2984422798227
-51.3710804190734 -51.3778154232107 -51.4571885665986 -51.5422287595037
-51.6247196413797 -51.7097942844338 -51.6865921090554 -51.8524523516081
-51.9383365731646 -52.0305423970699 -52.1187347786121 -52.2157463983085
-52.3113455618943 -52.4354522238106 -52.5770940115882 -52.6740711811356
-52.7712895017262 -52.8682838963481 -52.9624361536742 -53.0708507727028
-53.168120768517 -53.2638921828479 -53.2651323882134 -53.370963246064 -
53.4679576406859 -53.4679748657604 -53.573805723611 -53.67951600594 -
53.784864561704 -53.8823068082634 -53.997111929939 -54.1117792510183 -
54.2176101088689 -54.4456700955132 -54.5586149091405 -54.6847885799992
-54.6899905525042 -54.6939523196438 -54.9231491612064 -54.835215155782
-54.8174216538029 -54.8174216538029 -54.694055670091 -54.581885984817 -
54.5794055740861 -54.4559362399271 -54.4559362399271 -54.3605782273846
-54.3412861439222 -54.4470136513257 -54.4469103008786 -54.3323635553209
-54.3323635553209 -54.4240870771397 -54.4465830244627 -54.4469103008786
-54.4863212713803 -54.660397874479 -54.6850297310425 -54.9229080101631
-55.0466184953655 -55.2252080679884 -55.4258457359968 -55.6815347421711
-55.8138922147824 -56.1310919620674 -56.2365955435022 -56.4464141762298
-56.5986838349862 -56.8123953345553 -56.9776699245743 -57.1367090376171
-57.2956275751382 -57.5357106637974 -57.7042407929006 -57.841765787868
-58.119709590322 -58.530958244486 -58.8912034529964 -59.2882241956069 -
59.8080424944702 -60.3507012421469 -60.9434849566767 -61.5726824787417
-62.2803229901706 -62.8829249971768 -63.6580705756494 -64.4270840275929
-65.114226700343 -65.6204371903356 -66.1497292801848 -66.2109127448797
-66.3882621121372 -66.0534755637673 -65.7291963108546 -65.2419678529831
-64.5429915540377 -63.9165844940449 -63.0942938866112 -62.2908647357768
-61.6009660511035 -60.8537767685768 -60.253706847525 -59.5122879649625
-59.0699997265135 -58.6808508429587 -58.3983423957568 -58.2541168468012
-58.3241367747249 -58.2601111727342 -58.4155674702768 -58.5519556103258
-58.7918492231653 -58.9846667073417 -59.2079553483439 -59.5863902355473
-59.8090070986433 -59.809162124314 -60.019824785693 -60.1354222607965 -
60.3635166975897 -60.60284188297 -60.9620191368602 -61.46635209373 -
62.174095955606 -63.0487507895804 -64.166503100255 -65.4640679638434] ;
%bus-2400MHz-OO-Aisle_Center-Vertical-6m

```
bus_2400MHz_OO_Aisle_Center_Vertical_mag(6,:) = [ -62.3655009836718 -  
62.6870758998849 -62.9609545847522 -63.2637541697385 -63.5073856237488  
-63.5039061586958 -63.5926841927716 -63.4771900681153 -63.2663551559911  
-63.1076433193642 -63.0282357258272 -62.8793077315276 -62.7019239141211  
-62.7481387890581 -62.799779562469 -62.9187359271038 -63.1578544115898  
-63.394526935494 -63.7336025274194 -63.9582863994577 -64.2572964680497  
-64.5951146295351 -64.7942709411348 -65.0268611223778 -65.0405206064721  
-64.9587015025024 -64.8185410711335 -64.6250173589017 -64.4199011715181  
-64.1615422787932 -63.8466851416429 -63.487249511635 -63.1104165563619  
-62.7772491649969 -62.5849484330561 -62.3994171554016 -62.4335572531001  
-62.2103719625451 -62.2255817033462 -62.1551483736341 -62.1550277981124  
-62.1615561013555 -62.1231614102505 -62.0844738928787 -61.9451402650868  
-61.8379141762 -61.5995191448438 -61.3438473637441 -61.194437067358 -  
60.9663943057883 -60.841064663581 -60.7077770369456 -60.6029452334172 -  
60.4760997846522 -60.3785197374966 -60.4736021488468 -60.479372548811 -  
60.479372548811 -60.60284188297 -60.7174919789749 -60.9466888205374 -  
61.0097670434295 -61.1904753002184 -61.1936274888555 -61.2663517534788  
-61.3170968230146 -61.3170968230146 -61.3464655750711 -61.4687463790883  
-61.572958079934 -61.5786251294511 -61.7178554067959 -61.9400416430288  
-62.0019657859281 -62.0843705424316 -62.1549244476653 -62.2256506036443  
-62.4359687635329 -62.3673440666454 -62.4371400686003 -62.4312835432635  
-62.4372434190474 -62.4316280447539 -62.3722015376601 -62.3666895138137  
-62.4371400686003 -62.440343932461 -62.4665432708059 -62.5080212502499  
-62.7136886400182 -62.8825977207609 -63.0279256744858 -63.1046461563977  
-63.2661484550968 -63.3455215984848 -63.3297089800755 -63.2998234757833  
-63.217987146739 -63.0565365232634 -63.031508489986 -62.9574751196992 -  
62.8814264156936 -62.816212283561 -62.8075480710775 -62.7207681456459 -  
62.6900730628514 -62.6576210224558 -62.5218529850895 -62.4159187767917  
-62.2961356085799 -62.1828290683876 -61.8383792532121 -61.5797447592949  
-61.3542857589032 -61.0827152340215 -60.8233572869745 -60.5762463679112  
-60.2145542531412 -59.9151652329098 -59.7039341440715 -59.4960102695411  
-59.385890368135 -59.1884393389128 -59.183047890588 -59.2327594556526 -  
59.2875524177006 -59.1921082797855 -59.2886720475444 -59.3593293032253  
-59.2887753979915 -59.394502905395 -59.394502905395 -59.2887753979915 -  
59.2887753979915 -59.1921771800836 -59.1917637782951 -59.0948210588968  
-59.1400024293627 -59.191660427848 -59.2886720475444 -59.394502905395 -  
59.4916523256876 -59.7879063823563 -59.9137183266501 -60.119041214928 -  
60.2411497682 -60.3557998642048 -60.5792435308777 -60.5210227790002 -  
60.5477560946552 -60.4801304520899 -60.4794758992581 -60.3648258032533  
-60.2501757072484 -60.0991462538574 -60.029694753393 -59.9150446573881  
-59.8404600847167 -59.8092137995375 -59.914941306941 -60.0206688143445  
-60.0207721647916 -60.1353189103493 -60.2411153180509 -60.3595204803011  
-60.5529408420857 -60.7085693903735 -60.8620620294209 -61.0701581546965  
-61.1935241384084 -61.3170968230146 -61.4486963923471 -61.5437443535482  
-61.5728547294869 -61.7051433018002 -61.8374318741135 -62.1494296488935  
-62.4369505927806 -62.8059633642216 -63.1250750947784 -63.6431019858916  
-64.3960616683825 -65.1589085436478 -65.894849852513 -66.8641564709746  
-67.8650366510312 -68.9422239112113 -70.2183952322459 -71.618845465942  
-73.0836658031191 -74.5987661328201 -76.3668683570701 -77.9981173642592  
-80.4626293513511 -83.7018735151272 -88.1996160734804 -91.070760394765  
-85.8772970765507 -81.4692627062974 -78.3679741643517 -75.9117818882529  
-74.4210205888486 -73.2849752490339 -72.1962816390745 -71.7138762020686  
-71.2823364101201 -71.0799073343615 -71.1223843681278 -71.0865906632753  
-71.6439596245921 -71.9578004823457 -73.2113208303865 -74.0994628977101  
-74.7928754975855 -75.5104032017888 -76.9689536118407 -78.0457619203814  
-77.86855035372 -77.79606724014 -78.8992815879198 -78.181374932077 -  
78.9075323986148 -80.053034304341 -81.9386804371153 -83.9108481192033 -
```

```

89.2555992669264 -101.337766062386 -90.2230972525633 -83.3215094195775
-79.9897838307037 -78.0744933446806 -76.2644480639745 -75.118274380342
-74.4300982031207 -73.9107449812694 -74.0291156933706 -74.3427670753045
-75.1423205843719 -75.6565579590907 -76.8822942619308 -77.697643164333
-78.4550985912736 -77.78566329513 -76.9839222015986 -75.9094737282672 -
74.616818010917 -73.798196344356 -73.1332567926621 -72.5565612977339 -
72.7252120023588 -72.9589045883711 -72.9563208271931 -73.258345283826 -
74.218918789506 -75.2824293405172 -76.5038765998019 -77.8364083646658 -
79.9652553245873 -80.9435189817993 -81.494790266736 -81.2621828604185 -
80.3749537220445 -78.7162823962197 -78.3072213265198 -76.6823972721267 -
76.7328322903212 -76.2690471588713 -75.8521659053393 -75.287028435414
-74.5837803179877 -73.4830463809389 -73.0050505630101 -71.942935243035
-71.2598232377225 -70.5386265926464 -69.797311060531 -69.3506648782285
-69.2239572300597 -68.9581915552913 -68.7038805550786 -68.5058783234717
-68.2845705660393 -67.7563981060338 -67.1132482736077 -66.2233664737576
-65.3217888483085 -64.2695607211079 -63.48204753913 -62.7736835745712 -
62.0186224329889 -61.3784180883056 -60.8913102059558 -60.603668686547 -
60.4794758992581 -60.4778911924023 -60.5068120925213 -60.7174919789749
-61.0773926859949 -61.4657836662709 -61.8078736462372 -62.1197508454956
];

```

```

%bus-2400MHz-OO-Aisle_Center-Vertical-7m

```

```

bus_2400MHz_OO_Aisle_Center_Vertical_mag(7,:) = [ -59.9703888218208 -
60.0853317440924 -60.191162601943 -60.3058126979479 -60.413779465039 -
60.3060193988421 -60.1913693028373 -60.0855384449867 -59.8606134219051
-59.65339577543 -59.3459626453978 -59.0678121420495 -58.6596295511501 -
58.4627986246105 -58.0953361098763 -57.8400088302669 -57.510355354104 -
57.3264260083799 -57.1663706159405 -56.9285095618944 -56.7980985227038
-56.7100267166832 -56.6381809308605 -56.675766043463 -56.5488172442509
-56.4785733903585 -56.4772126094715 -56.3990968965235 -56.3285429912897
-56.2319447733818 -56.1239780062907 -55.9800108334529 -55.9052195598872
-55.7641117494198 -55.6582808915691 -55.5259923192559 -55.501119311649
-55.4994312543461 -55.3766164730188 -55.4535092056759 -55.375961920187
-55.375961920187 -55.375961920187 -55.375961920187 -
55.375961920187 -55.2702344127835 -55.2702344127835 -55.2702344127835 -
55.3936003964955 -55.3936003964955 -55.5247004386669 -55.6576091136629
-55.7639567237491 -55.9720700740992 -56.1706579582398 -56.4715800101034
-56.6967289591538 -57.0556306118516 -57.4837426139707 -57.9597747734042
-58.4770782113876 -59.0123474020952 -59.6485727545644 -60.2941513224979
-60.8929121378861 -61.6328324389654 -62.4087014705678 -63.0175045044012
-63.6264453388308 -64.2173515202379 -64.6704398804109 -64.9599417078678
-65.2569364427409 -65.2524579233657 -65.3616821208967 -65.3382732446241
-65.1980266878826 -65.0686319280887 -64.8743330875036 -64.7781138212351
-64.5851757615371 -64.4957087244804 -64.4068617901065 -64.2156117877114
-64.1577010871753 -63.9659171074701 -63.7719799934499 -63.6044144685197
-63.3895144388087 -63.1681550061528 -62.9075913038894 -62.5723741286565
-62.3217320693166 -62.0362609092973 -61.7875480583037 -61.4678506752133
-61.2672130072048 -61.0203776893338 -60.8968050047276 -60.6588061500854
-60.6586855745637 -60.4207556202196 -60.3061916495873 -60.0984228007276
-59.9707849985347 -59.7595883598455 -59.5652550691114 -59.3446190895852
-59.04536786995 -58.754970338618 -58.568526132014 -58.2039746548736 -
57.9536426468751 -57.6922693661093 -57.5214310770203 -57.3514712667319
-57.1232734794915 -56.8536493880306 -56.7253225828569 -56.5524000597511
-56.4070893311007 -56.257989086056 -56.060383031163 -56.0006292476533 -
55.7778918090357 -55.6317198266594 -55.4897852126149 -55.2436733478738
-54.9967519046302 -54.7103850407359 -54.5116765810737 -54.1726526643718
-53.9472453392037 -53.6387442545512 -53.4675270138229 -53.3210794302542
-53.1190982064332 -53.0212597831598 -53.0212253330108 -53.0212253330108

```

```

-53.0212253330108 -53.1181336022601 -53.226393195618 -53.4159034654866
-53.5238185573541 -53.7354802730553 -53.9433180222131 -53.9977148075472
-54.0873713204235 -54.2903343734922 -54.405845723223 -54.5293150573821
-54.5293150573821 -54.6438790280143 -54.6497011032021 -54.767434487546
-54.7675378379931 -54.890903821705 -55.1201006632676 -55.2435699974266
-55.3755485183986 -55.3758585697399 -55.4987939265889 -55.499327903899
-55.6316164762122 -55.726819463084 -55.7639050485255 -55.9402898116099
-56.0108437168436 -56.1448547966089 -56.2212652271794 -56.2930248876296
-56.4201114874378 -56.4341671482461 -56.5816999115095 -56.7340212454895
-56.8045751507233 -56.9378283272097 -57.0073487279722 -57.2231961367818
-57.4116384520301 -57.59840993505 -57.8333771765768 -58.0040948901441 -
58.1878175349739 -58.2700155905832 -58.3654941786473 -58.446383128593 -
58.3657870049141 -58.3354536486845 -58.230587395007 -58.1221555509038 -
57.9423602230645 -57.6033363063627 -57.3626331150208 -57.0341681689998
-56.7083386593803 -56.4345633249601 -56.1530883822294 -55.8723541177032
-55.6318231771065 -55.4336314696799 -55.262431454026 -55.2436733478738
-55.1202040137147 -55.2424675926574 -55.2435699974266 -55.3758585697399
-55.3937898723152 -55.6210919556805 -55.8696153308545 -56.0310659543301
-56.1869873288847 -56.3983906684681 -56.6522710418178 -56.8484301904511
-57.0868941221054 -57.3923119184187 -57.5395863055644 -57.6601446021295
-57.8365293652139 -58.1098223975476 -58.2949402734135 -58.3826503528692
-58.5681471803746 -58.7529033296756 -58.8506384025019 -59.0446616418947
-59.3406917725947 -59.5473582166851 -59.8644029382995 -60.191162601943
-60.5351128899576 -60.7785376430736 -61.1431924706611 -61.5224886115906
-61.7874447078565 -62.0343833761747 -62.0579989533415 -62.1385606268714
-62.2108714897061 -62.1403175844724 -61.9293104216029 -61.6906225639799
-61.4172606313481 -61.1616233003975 -60.7872879809297 -60.3558687645029
-59.9729725829988 -59.7144586646032 -59.4420096609211 -59.157968182087
-58.9773805008197 -58.8419225147948 -58.9454796628088 -58.9394164365777
-59.0443343654788 -59.1409498084612 -59.4251979881896 -59.6235274962124
-59.9631026152988 -60.3055370967556 -60.6409781979572 -60.9141851049183
-61.2415648712446 -61.5493425027672 -61.681717200453 -61.9026632313205
-61.9821914003792 -61.8582053139845 -61.6654395050317 -61.4173812068698
-61.1614854998013 -60.7910774973241 -60.3783130366024 -59.8708278910954
-59.5387456794251 -59.151543229291 -58.8251280671378 -58.6316043549061
-58.4620579464062 -58.2788003785883 -58.0931485254122 -58.0040948901441
-57.9069454698515 -57.7483369836717 -57.6058856173917 -57.5878165142202
-57.3548646064123 -57.0079516055804 -56.7231005482439 -56.4062280773747
-56.1204985412377 -55.8301871352783 -55.5259923192559 -55.1391343706121
-54.8910071721522 -54.644068503834 -54.4067242020235 -54.2912989776653
];
%bus-2400MHz-OO-Aisle_Center-Vertical-8m
bus_2400MHz_OO_Aisle_Center_Vertical_mag(8,:) = [ -61.3175963501757 -
61.3173035239088 -61.3170968230146 -61.2685048877938 -61.2808897163736
-61.1945748679541 -61.1938341897498 -61.1938341897498 -61.0767036830141
-61.0703648555907 -60.8234261872726 -60.6000858710468 -60.2501757072484
-60.0350862017177 -59.8146052478623 -59.5998257936729 -59.3861487442528
-59.1849598738597 -58.9890935514933 -58.8920130314988 -58.7077736344334
-58.6011676482293 -58.5224662827477 -58.6165151896266 -58.415774171171
-58.415774171171 -58.4067999073461 -58.3275817896289 -58.2393894080867
-58.1423777883903 -57.9835626013163 -57.8866198819179 -57.7984275003758
-57.6320505055875 -57.5426695939034 -57.535831239319 -57.569023957919 -
57.569023957919 -57.5697129608998 -57.6325328076741 -57.6528583956076 -
57.736486132402 -57.7895738120725 -57.81585927579 -57.81585927579 -
57.81585927579 -57.6421099491072 -57.5437719986727 -57.4641232540924 -
57.3764131746368 -57.2961960025974 -57.2163577821974 -57.057628720496 -
56.8991235847633 -56.7753097491139 -56.6785392804607 -56.5368802676086

```

-56.5284572061683 -56.4500142168045 -56.4490840627804 -56.5548115701839
-56.5548115701839 -56.611861016994 -56.7040151656757 -56.7727604380849
-56.7841978875662 -56.8545623169802 -56.8996920122225 -56.9809254636586
-57.0838625089899 -57.1632356523778 -57.3107339654922 -57.3219819391537
-57.3979789679358 -57.4013550825417 -57.4807282259297 -57.4807282259297
-57.5689206074719 -57.6482937508598 -57.6482937508598 -57.6482937508598
-57.569023957919 -57.4913560969085 -57.4808315763768 -57.3254614042068
-57.3044468132924 -57.235925466852 -56.9786173036729 -56.8383018466333
-56.7489381600238 -56.7075807561014 -56.5551216215252 -56.4137037597164
-56.3431498544826 -56.1777891390911 -56.1314881387814 -56.0609342335477
-56.0607275326534 -56.0608308831005 -56.0608308831005 -56.201938693568
-56.2700466382199 -56.3785473826212 -56.438370066429 -56.6077097740347
-56.6340813631247 -56.7046352683585 -56.7046352683585 -56.7047386188056
-56.7047386188056 -56.6341847135718 -56.5548115701839 -56.4841026392795
-56.40819173587 -56.3431498544826 -56.2725959492489 -56.2020420440152 -
56.1316431644521 -56.0202486075315 -55.9552067261442 -55.8876499838769
-55.8531653846879 -55.7083025079751 -55.5759794855128 -55.5454222033144
-55.3364992744618 -55.1720514880198 -55.0467218458126 -54.696708331567
-54.4499591390686 -54.2177134593161 -53.9125023638969 -53.6433605745226
-53.3723068018765 -53.0712124992677 -52.8771892598749 -52.6762759906741
-52.4979620192435 -52.4097696377013 -52.3215772561591 -52.2245656364627
-52.2255991409339 -52.321473905712 -52.3389745814243 -52.4978586687964
-52.5946980377476 -52.683062670035 -52.7800742897314 -52.8130086322135
-52.8683700217207 -52.9653816414171 -53.0618937339524 -53.0623932611135
-53.1594048808099 -53.2652357386605 -53.2652357386605 -53.276914339185
-53.3622473583569 -53.3622473583569 -53.4679748657604 -53.3710665965111
-53.2652357386605 -53.1688614467213 -53.0712124992677 -52.8780505136009
-52.7809010933083 -52.5981258275771 -52.4979620192435 -52.3242299176352
-52.2245656364627 -52.0488354262101 -51.9492055951867 -51.7925263173532
-51.7130498235181 -51.6248574419759 -51.5454842985879 -51.5454842985879
-51.4573780424184 -51.457894794654 -51.4396534407373 -51.4396534407373
-51.5190265841253 -51.6072189656675 -51.6072189656675 -51.6865921090554
-51.7747844905976 -51.828233896833 -51.9311020418662 -51.9423500155278
-51.9423500155278 -52.0305423970699 -52.1149797123668 -52.2242039098978
-52.2244622860156 -52.2244622860156 -52.321473905712 -52.321473905712 -
52.321473905712 -52.3275199068685 -52.4083571815907 -52.3228863618227 -
52.4087533583047 -52.4093906860619 -52.4096490621797 -52.4967045888036
-52.4978586687964 -52.5938367840216 -52.5948702884928 -52.683062670035
-52.5775246384512 -52.6739333805394 -52.7800742897314 -52.692140284307
-52.5774385130786 -52.5774385130786 -52.4894528324307 -52.3928373894482
-52.39223451184 -52.3040421302978 -52.2450117999179 -52.2158497487556 -
52.1188381290592 -52.2245656364627 -52.2245656364627 -52.2195359147029
-52.2244622860156 -52.2244622860156 -52.3203026006447 -52.4096662872542
-52.4978069935728 -52.5948702884928 -52.7800742897314 -52.9737530276338
-53.1666394121083 -53.3645727434171 -53.4679748657604 -53.6793954304183
-53.7854674393122 -53.8912982971629 -53.89140164761 -54.0060517436148 -
54.0060517436148 -54.1118826014654 -54.1118826014654 -54.1118826014654
-54.1036145656959 -54.0061550940619 -54.0012631728983 -53.8915049980571
-53.7837966070838 -53.8465647786345 -53.7855707897594 -53.6820136417454
-53.5848297713038 -53.4680782162075 -53.4658045063709 -53.3710665965111
-53.2652357386605 -53.1682241189641 -53.0712124992677 -52.9742008795713
-52.8771892598749 -52.7801776401785 -52.6830798951095 -52.4892461315364
-52.39223451184 -52.304214381043 -52.3040421302978 -52.3040421302978 -
52.3040421302978 -52.3040421302978 -52.3921311613929 -52.4891427810893
-52.6290620614149 -52.7713584020243 -52.9641414360516 -52.9512398552362
-53.1505856426557 -53.3531869691594 -53.5618687469687 -53.6709206937545
-54.004932113771 -54.1117792510183 -54.2264293470232 -54.3186351709285

```
-54.341079443028 -54.341079443028 -54.2516468561204 -54.3217701344911 -
54.2177134593161 -53.8945021610236 -53.7859841915478 -53.679946632803 -
53.5951131407922 -53.5740124245052 -53.4681815666546 -53.4681815666546
-53.4681815666546 -53.4674408884503 -53.4680782162075 -53.4680782162075
];
```

```
cd sim_vs_bus_ver3_sweep
```

```
fldresults_1m
```

```
freq_pwr(1,:) = pwr
```

```
fldresults_2m
```

```
freq_pwr(2,:) = pwr
```

```
fldresults_3m
```

```
freq_pwr(3,:) = pwr
```

```
fldresults_4m
```

```
freq_pwr(4,:) = pwr
```

```
fldresults_5m
```

```
freq_pwr(5,:) = pwr
```

```
fldresults_6m
```

```
freq_pwr(6,:) = pwr
```

```
fldresults_7m
```

```
freq_pwr(7,:) = pwr
```

```
fldresults_8m
```

```
freq_pwr(8,:) = pwr
```

```
for dist = 1:8,
```

```
    figure(dist)
```

```
    handle = figure(dist);
```

```
    set(handle, 'Color', [1 1 1]);
```

```
    plot(freq, freq_pwr(dist, :))
```

```
    hold on
```

```
    plot(freq, bus_2400MHz_OO_Aisle_Center_Vertical_mag(dist, :), 'r-.')
```

```
    legend('Sim power', 'Bus power')
```

```
    title(['Magnitude Received Power along center at ' num2str(dist) 'm  
swept 2.4 to 2.483 GHz'])
```

```
    xlabel('Frequency')
```

```
    ylabel('Magnitude Rx Power')
```

```
    hold off
```

```
end
```